

การสังเคราะห์ โครงสร้างผลึกและการประเมินความเป็นพิษต่อเซลล์ของสารเชิงซ้อน
โลหะแทรนซิลันของ 6-ดีออกซีโคเลทอรีแอสีทิลและซิฟเบสเพื่อเป็นสารต้านมะเร็งชนิดใหม่

นางสาวฉัตรตรี ภูรัต

วิทยานิพนธ์นี้เป็นส่วนหนึ่งของการศึกษาตามหลักสูตรปริญญาวิทยาศาสตรดุษฎีบัณฑิต

สาขาวิชาเคมี ภาควิชาเคมี

คณะวิทยาศาสตร์ จุฬาลงกรณ์มหาวิทยาลัย

ปีการศึกษา 2554

ลิขสิทธิ์ของจุฬาลงกรณ์มหาวิทยาลัย

บทคัดย่อและแฟ้มข้อมูลฉบับเต็มของวิทยานิพนธ์ตั้งแต่ปีการศึกษา 2554 ที่ให้บริการในคลังปัญญาจุฬาฯ (CUIR)

เป็นแฟ้มข้อมูลของนิสิตเจ้าของวิทยานิพนธ์ที่ส่งผ่านทางบัณฑิตวิทยาลัย



The abstract and full text of theses from the academic year 2011 in Chulalongkorn University Intellectual Repository (CUIR) are the thesis authors' files submitted through the Graduate School.

SYNTHESIS, CRYSTAL STRUCTURES AND CYTOTOXICITY EVALUATION
OF TRANSITION METAL COMPLEXES OF
6-DEOXYCLITORIACETAL AND SCHIFF BASE
AS NOVEL ANTICANCER AGENTS

Miss Chuttree Phurat

A Dissertation Submitted in Partial Fulfillment of the Requirements
for the Degree of Doctor of Philosophy Program in Chemistry
Department of Chemistry
Faculty of Science
Chulalongkorn University
Academic Year 2011
Copyright of Chulalongkorn University

ฉัตรตรี ภูริต : การสังเคราะห์ โครงสร้างผลึก และการประเมินความเป็นพิษต่อเซลล์ของ สารเชิงซ้อนโลหะแทรนซิชันของ 6-ดีออกซีคลอโรริแอซีทัลและชิฟเบส เพื่อเป็นสารต้าน มะเร็งชนิดใหม่ (SYNTHESIS, CRYSTAL STRUCTURES AND CYTOTOXICITY EVALUATION OF TRANSITION METAL COMPLEXES OF 6-DEOXYCLITORIACETAL AND SCHIFF BASE AS NOVEL ANTICANCER AGENTS) อ.ที่ปรึกษาวิทยานิพนธ์ หลัก: รศ.ดร. นงนุช เหมืองสิน, 189 หน้า

สารประกอบโลหะ Fe(III), Co(II), Ni(II), และ Cu(II) ของ 6-ดีออกซีคลอโรริแอซีทัล (L) ได้ ถูกสังเคราะห์ เสนอโครงสร้างโมเลกุลจากการวิเคราะห์ด้วยวิธีทางสเปกโทรสโกปีได้ดังนี้ $FeL(H_2O)_4Cl_2$ (1), $CoL(NO_3)(H_2O)_2 \cdot 2H_2O$ (2), $NiL(CH_3COO) \cdot 4H_2O$ (3), และ $CuL_2 \cdot 2H_2O$ (4) สารทุกตัวไม่มีความเป็นพิษต่อเซลล์ปกติของตับ (CH), ผิวหนัง (CCD) และ เยื่อหุ้มผิวหนัง (HS27) เมื่อทดสอบ ความเป็นพิษต่อเซลล์มะเร็งของ L ให้ฤทธิ์ที่ตีมากที่สุดต่อ BT474 (IC_{50} 0.003 μM), มีฤทธิ์ตีต่อ CHAGO, KATO, HepG2, SW620 (IC_{50} 0.136-0.216 μM), และมีฤทธิ์ปานกลางต่อ KB, NCI-H187, MCF7 (IC_{50} 0.654-0.764 μM) สาร 1 2 และ 3 ให้ฤทธิ์ที่ตีกับ KB, CHAGO, KATO3 (IC_{50} 0.002 - 0.007 μM) สาร 4 มีฤทธิ์ที่ตีต่อทุกเซลล์มะเร็ง ยกเว้น KB ศึกษาความสามารถการยึดจับกับ DNA โดยเทคนิค UV-Vis, ฟลูออเรสเซนซ์ และ T_m พบว่าสารประกอบทุกตัว จับกับ CT-DNA แบบแทรกสอด

อีกส่วนหนึ่งของงานวิจัยนี้คือ การสังเคราะห์และทดสอบความเป็นพิษต่อเซลล์ของสารประกอบ โลหะ Ni(II), Cu(II) และ Zn(II) ของชิฟเบส 2-[(4-คลอโรเบนซิลอิมิโน)-เมธิล]พีนอล (A) และ 2-[(4-เมธอกซีเบนซิลอิมิโน)-เมธิล]พีนอล (B) โครงสร้างผลึกของสารประกอบ NiA_2 (A1), CuA_2 (A2), NiB_2 (B1), CuB_2 (B2) มีรูปร่างสี่เหลี่ยมแบนราบ ส่วน ZnA_2 และ ZnB_2 (A3 และ B3) มีรูปร่างทรงสี่หน้า สารทุกตัว ไม่มีความเป็นพิษต่อเซลล์ปกติของลิงแอฟริกันสีเขียว (vero) สารประกอบโลหะ Cu(II) และ Zn(II) มี ฤทธิ์ยับยั้งที่ตีมากที่สุดต่อทุกเซลล์มะเร็ง โดยเฉพาะอย่างยิ่งสารประกอบ Cu(II) (B2) ให้ฤทธิ์ต่อ KATO3 ที่ ค่า IC_{50} 25 nM และฤทธิ์ต่อ BT474 ให้ค่า IC_{50} 1.45 nM ค่าคงที่การยึดจับ DNA (K_b) ของสารประกอบ โลหะ Cu(II) และ Zn(II) มีค่ามาก ศึกษาความสามารถการยึดจับกับ CT-DNA โดยเทคนิค UV-Vis, ฟลูออเรสเซนซ์ และ T_m ระบุว่าสารเหล่านี้จับกับ DNA แบบแทรกสอด ส่วนสารประกอบ Ni(II) มีค่าคงที่ การยึดจับ DNA น้อย แสดงว่าจับกับ DNA แบบผูกพันร่อง และไม่มีฤทธิ์ยับยั้งต่อทุกเซลล์มะเร็ง

ภาควิชา.....เคมี..... ลายมือชื่อนิสิต.....
 สาขาวิชา.....เคมี..... ลายมือชื่อ อ.ที่ปรึกษาวิทยานิพนธ์หลัก.....
 ปีการศึกษา2554.....

5073815623 : MAJOR CHEMISTRY

KEYWORDS: 6-DEOXYCLITORIACETAL / TRANSITION METAL COMPLEXES / CYTOTOXICITY / DNA BINDING AFFINITY

CHUTTREE PHURAT: SYNTHESIS, CRYSTAL STRUCTURES AND CYTOTOXICITY EVALUATION OF TRANSITION METAL COMPLEXES OF 6-DEOXYCLITORIACETAL AND SCHIFF BASE AS NOVEL ANTICANCER AGENTS. THESIS ADVISOR: ASSOC. PROF. NONGNUJ MUANGSIN, 189 pp.

The Fe(III), Co(II), Ni(II), and Cu(II) complexes with 6-deoxyclitoriacetal (**L**) have been synthesized. The proposed molecular structures based on spectroscopic methods, EA, and TGA are as follow: $\text{FeL}(\text{H}_2\text{O})_4\text{Cl}_2$ (**1**), $\text{CoL}(\text{NO}_3)(\text{H}_2\text{O})_2 \cdot 2\text{H}_2\text{O}$ (**2**), $\text{NiL}(\text{CH}_3\text{COO}) \cdot 4\text{H}_2\text{O}$ (**3**), and $\text{CuL}_2 \cdot 2\text{H}_2\text{O}$ (**4**). All complexes are non-cytotoxic to normal cell lines of human liver cell (CH), skin fibroblast (CCD), and foreskin fibroblast (HS27). **L** showed strong cytotoxicity against BT474 (IC_{50} 0.003 μM), good activity against CHAGO, KATO, HepG2, SW620 (IC_{50} 0.136-0.216 μM), and moderate against KB, NCI-H187, and MCF7 (IC_{50} 0.654-0.764 μM). Complexes **1**, **2** and **3** exhibited strong cytotoxicity to cell lines of KB, CHAGO, and KATO3 with IC_{50} in the range of 0.002 μM to 0.007 μM . Only **4** has strong cytotoxicity for all tested cell lines except KB. All complexes and free ligand can bind with CT-DNA by intercalation mode observed with UV-Vis, fluorescent, and T_m techniques.

Another part of this project is to synthesis and cytotoxic evaluation of Ni(II), Cu(II) and Zn(II) with two Schiff base ligands: 2-[(4-chlorobenzylimino)-methyl]-phenol (**A**) and 2-[(4-methoxybenzylimino)-methyl]-phenol (**B**). The X-ray crystal structures of complexes NiA_2 (**A1**), CuA_2 (**A2**), NiB_2 (**B1**), and CuB_2 (**B2**) are square planar, while ZnA_2 and ZnB_2 complexes (complexes **A3** and **B3**) showed tetrahedral geometry. All complexes are non-cytotoxic to normal kidney cell line of an African green monkey (vero cell). The potent cytotoxic activities have shown for Cu(II) and Zn(II) complexes against all tested cancer cell lines, especially Cu(II) complexes (**B2**) against KATO3 (IC_{50} 25 nM) and BT474 (IC_{50} 1.45 nM). DNA binding studies revealed the strong binding constant (K_b) of Cu(II) and Zn(II) complexes. By UV-Vis, fluorescent and T_m , the binding mode of Cu(II) and Zn(II) complexes were confirmed to be intercalation. However, Ni(II) complexes were found to bind with CT-DNA by groove binding mode and it is inactive to all tested cancer cells.

Department:.....Chemistry..... Student's Signature:.....

Field of Study:...Chemistry..... Advisor's Signature:.....

Academic Year:.....2011.....

ACKNOWLEDGEMENTS

I wish to sincerely thank and express my deepest gratitude to Associate Professor Dr. Nongnuj Muangsin, my thesis advisor, for her kindness, guidance, suggestions and assistance throughout the course of this research. I am also grateful to thesis examiners: Associate Professor Dr. Warinthorn Chavasri, Professor Dr. Thawatchai Tuntulani, Associate Professor Dr. Orawon Chailapakul and Associate Professor Dr. Sujittra Youngme for their valuable comments and suggestions. I would like to thank the Research Centre for Bioorganic Chemistry (RCBC); Department of Chemistry, Chulalongkorn University for the use of facilities, equipment, glassware, and chemicals; the Organic Synthesis Research Unit (OSRU) for a generous use of UV-visible Spectrophotometer; Associate Professor Dr. Nattaya Ngamrojnavanich, and Miss Songchan Puthong for initiating a generous support of the cytotoxicity test equipment. Assist. Prof. Kuakarun Krusong for initiating a generous support of the gel electrophoresis equipments. I would like to thank the 90th Anniversary Chulalongkorn University Fund (Ratchadaphisek Somphot Endowment Fund), Center of Excellence on Petrochemical and Materials Technology for financial support. Finally, I would like to thank my parents who had encouraged me with sincere and my best friends for their love, understanding encouragement and social support throughout my study period.

CONTENTS

	Page
Abstract in Thai.....	iv
Abstract in English.....	v
Acknowledgements.....	vi
Contents	vii
List of Tables	xii
List of Figures	xiii
List of Abbreviations.....	xvii
CHAPTER I Introduction.....	1
1.1 Introduction.....	1
1.2 Objectives.....	3
CHAPTER II BACKGROUND AND LITERATURE REVIEWS.....	5
2.1 Cancer and the cell cycle.....	5
2.2 Anticancer drugs.....	8
2.2.1 DNA-target anticancer drugs.....	8
2.1.1.1 Drugs interfering with DNA synthesis.....	8
2.2.1.2 Drugs interact directly with DNA.....	9
2.3 Metal complex as anticancer agents binding to DNA	11
2.4 Chromone based-structures as anticancer agents.....	13
2.4.1 Coumarin.....	14
2.4.2 Flavonoid.....	15
2.4.3 Rotenoids.....	19
2.5 Schiff Base.....	20

	Page
2.5.1 Schiff bases transition metal complexes.....	21
2.5.2 Biological activities of Schiff bases transition metal complexes.....	21
2.6 Drug-DNA interaction.....	24
2.7 The study of drugs-DNA interaction.....	28
2.7.1 Titration with UV absorption spectroscopy.....	29
2.7.2 Ethidium bromide (EB) displacement study by fluorescence spectroscopy.....	30
2.7.3 Thermal denaturation.....	31
2.8 Cytotoxicity test by MTT assays.....	32
2.9 DNA cleavage.....	34
2.9.1 DNA hydrolysis.....	34
2.9.2 Photochemical cleavage of DNA.....	35
2.9.3 Oxidative DNA cleavage.....	38
 CHAPTER III EXPERIMENTAL	 39
Part I Metal complexes of 6-deoxyclitoriacetal	39
1. Materials.....	39
2. Preparation of 6-deoxyclitoriacetal (L)	39
3. Synthesis of Metal complexes.....	40
3.1 Synthesis of 6-Deoxyclitoriacetal Iron(III) complex (1).....	40
3.2 Synthesis of 6-Deoxyclitoriacetal Cobalt (II) complex (2).....	41
3.3 Synthesis of 6-Deoxyclitoriacetal Nickel(II) complex (3).....	41
3.4 Synthesis of 6-Deoxyclitoriacetal Copper(II) complex (4).....	42
4. Characterization of complexes.....	43

	Page
5. Stoichiometric study (Job's Plot)	43
6. Evaluation of cytotoxic activity	43
7. The DNA-Binding studies.....	44
7.1 Titration with UV absorption spectroscopy.....	44
7.2 Ethidium bromide (EB) displacement study by fluorescence spectroscopy.....	45
7.3 DNA melting temperature.....	45
8. DNA cleavage activity.....	46
Part II Metal complexes of Schiff bases.....	47
1. Preparation of Schiff base.....	47
1.1 2-[(4-Chlorobenzylimino)-methyl]-phenol (A).....	47
1.2 2-[(4-Methoxybenzylimino)-methyl]-phenol (B).....	47
2. Synthesis of Metal complexes	48
2.1 Synthesis of NiA ₂ (A1)	48
2.2 Synthesis of CuA ₂ (A2)	49
2.3 Synthesis of ZnA ₂ (A3)	48
2.4 Synthesis of NiB ₂ (B1)	49
2.5 Synthesis of CuB ₂ (B2)	50
2.6 Synthesis of ZnB ₂ (B3)	50
3. Characterization of complexes.....	50
3.1 Spectroscopic method.....	50
3.2 Single crystal X-ray crystallographic method.....	51
4. Evaluation of cytotoxic activity	51
5. The DNA-Binding experiments.....	52
5.1 Titration with UV absorption spectroscopy.....	52

	Page
5.2 Ethidium bromide (EB) displacement study by fluorescence spectroscopy.....	53
5.3 DNA melting temperature.....	53
6. DNA cleavage activity.....	54
CHAPTER IV RESULTS AND DISCUSSION	55
Part I Metal complexes of 6-deoxyclitoriacetal.....	55
1. Molecular Structure Elucidation of 6-deoxyclitoriacetal (L) and complexes 1 to 4	55
1.1 6-deoxyclitoriacetal (L)	55
1.2 Fe(III)-6deoxyclitoriacetal complex (1)	55
1.3 Co(II)-6deoxyclitoriacetal complex (2)	57
1.4 Ni(II)-6deoxyclitoriacetal complex (3)	58
1.5 Cu(II)-6deoxyclitoriacetal complex (4)	59
1.6 Stoichiometric study (Job Plot)	70
1.7 Summary of molecular structures.....	73
2. Bioassay	78
3. DNA binding studies.....	81
3.1 DNA-binding study by UV-Vis spectroscopic method.....	81
3.2 Ethidium bromide (EB) displacement study by fluorescence spectroscopic method.....	85
3.3 DNA melting temperature.....	90
4. DNA cleavage activity.....	91
Part II Metal complexes of Schiff bases.....	93
1. Crystal Structures.....	93

	Page
2. Bioassay	105
3. DNA binding experiments	108
3.1 Titration with UV absorption spectroscopy.....	108
3.2 Fluorescence Emission spectra.....	114
3.3 DNA melting temperature	121
4. DNA cleavage activity.....	122
CHAPTER IV CONCLUSION	125
REFERENCES	127
APPENDICES	
APPENDIX A.....	142
APPENDIX B.....	168
VITA	189

LIST OF TABLES

Table		Page
4.1	The selected vibration frequencies of 6-deoxyclitriacetal and 6-deoxyclitriacetal-metal complexes.....	62
4.2	Physical Properties and percentages of C and H of 6-deoxyclitriacetal-metal complexes.....	64
4.3	TGA data of 6-deoxyclitriacetal-metal complexes.....	64
4.4	The proposed molecular structure, optimized geometry and MM2 minimization energy of 6-deoxyclitriacetal-metal complexes.....	76
4.5	Inhibition of cell growth and toxicity to normal cell lines by 6-deoxyclitriacetal and metal complexes.....	80
4.6	The binding constant (K_b) and the change of absorption spectra.....	85
4.7	The Stern-Volmer quenching constant (K_{sv}), the apparent binding constant (K_{app}), and DNA melting temperature (T_m).....	89
4.8	Crystal data and refinement parameters of Schiff base metal complexes...	99
4.9	Selected bond distances and bond angles for (a) A1 , (b) A2 , (c) A3 , (d) B1 , (e) B2 , and (f) B3	100
4.10	Toxicity test against normal cell lines and the inhibition of cell growth (IC_{50}) against cancer cell lines.....	107
4.11	The binding constant (K_b) and the absorption spectra change.....	112
4.12	Stern-Volmer quenching constant (K_{sv}), the apparent binding constant (K_{app}), and DNA melting temperature (T_m).....	119
4.13	DNA cleavage reaction conditions and %NC.....	124

LIST OF FIGURES

Figure		Page
2.1	Cell division of normal and cancer cell.....	5
2.2	The cell cycle.....	6
2.3	Examples of alkylating agents.....	9
2.4	Chemical structure of the Co (III) bleomycin in DNA strands.....	10
2.5	Chemical structure of (a) doxorubicin (b) intercalation of doxorubicin- d(CGATCG) ₂	11
2.6	Examples of transition metal complexes bind to DNA.....	12
2.7	The structure of chromone.....	13
2.8	Structures of bis-coumarin complexes with M = Ce(III), La(III), Nd(III) and Zr(IV)	14
2.9	The most probable structural formula of Ln (III) complexes.....	15
2.10	Chemical structures of the test compounds: (a) cisplatin, (b) cis- [Pt(AF) ₂ Cl ₂].....	16
2.11	Structure formula of the ligand 3-aminoflavone and molecular structure and labeling scheme of [Cu(3-af) ₂ (NO ₃) ₂].....	17
2.12	Structure of the 6-hydroxy chromone-3-carbaldehyde thiosemicarbazone Ni(II) complex.....	18
2.13	Chemical structures of 6-deoxyclitriacetate.....	19
2.14	Chemical structure of (a) rotenoid structure, (b) 6-deoxyclitriacetate, and (c) doxorubicin HCl.....	20
2.15	Deoxyribonucleic acid (DNA) and hydrogen bonding of nitrogenous bases.....	24
2.16	Intercalation of a planar ligand in the double helix.....	26
2.17	Chemical structures of (a) doxorubicin HCl (b) daunorubicin HCl and (c) ethidium bromide.....	27
2.18	Chemical structure of Hoechst 33258.....	27
2.19	Oxidation of MTT in living cell.....	33
2.20	Proposed reaction mechanism for the hydrolysis of DNA.....	35
2.21	Type I and II photochemical cleavage of DNA. Both processes start...	36

Figure	Page
2.22 Different reaction pathways of guanine with singlet oxygen.....	37
3.1 Synthesis of 6-deoxyclitoriacetal metal complexes.....	41
3.2 Synthesis reaction of Schiff base and metal complexes.....	48
4.1 ¹ H NMR spectrum for 6-deoxyclitoriacetal (L) (a), Fe complex (1) (b), Co(II) complex (2) (c), Ni(II) complex (3) (d), and Cu(II) complex (4) (e).....	60
4.2 Magnified ¹ H NMR spectrum at 8.00-3.00 ppm for 6- deoxyclitoriacetal (L) (a), Fe complex (1) (b), Co(II) complex (2) (c), Ni(II) complex (3) (d), and Cu(II) complex (4) (e).....	61
4.3 IR spectrum of L (a), 1 (b), 2 (c), 3 (d), and 4 (e).....	63
4.4 TGA thermogram of 6-deoxyclitoriacetal.....	65
4.5 TGA thermogram of 6-deoxyclitoriacetal metal complexes 1 (a), 2 (b), 3 (d), and 4 (e).....	66
4.6 Job's plot of the complex formation of ligand (L) with metal ion Fe(III) (a), Co(II) (b), Ni(II) (c), and Cu(II) (d) monitored with UV- Vis spectrophotometer.....	72
4.7 Propose reaction mechanism of 6-deoxyclitoriacetal-metal complexes.	75
4.8 Electronic absorption spectra for DNA binding study of L (a), 1 (b), 2 (c), 3 (d), 4 (e).....	84
4.9 Emission spectra of (a) L , (b) 1 , (c) 2 , (d) 3 , (e) 4 , (f) Stern-Volmer plot of L and metal complexes (1-4).....	88
4.10 Stern-Volmer plot of metal complexes (1-4) with the electrostatic effect test using EB-DNA systems.....	89
4.11 Normalized melting temperature curve (T _m) (a) and derivatives melting temperature curve (b).....	90

Figure	Page
<p>4.12 Cleavage of pUC19 DNA incubate in the dark (a) lane 1: Marker, lane 2: pUC19 DNA; lane 3: pUC19 DNA + H₂O₂ (250 μM); lane 4: pUC19 DNA + H₂O₂ (250 μM) + Doxorubicin (100 μM); lane 5: pUC19 DNA + H₂O₂ (250 μM) + L (100 μM); lane 6: pUC19 DNA + H₂O₂ (250 μM) + 1 (100 μM); lane 7: pUC19 DNA + H₂O₂ (250 μM) + 2 (100 μM); lane 8: pUC19 DNA + H₂O₂ (250 μM) + 3 (100 μM)); lane 9: pUC19 DNA + H₂O₂ (250 μM) + 4 (100 μM). Under UV-A (b) lane 1: pUC19 DNA; lane 2: pUC19 DNA + H₂O₂ (250 μM); lane 3: pUC19 DNA + H₂O₂ (250 μM) + L (100 μM); lane 4: pUC19 DNA + H₂O₂ (250 μM) + 1 (100 μM); lane 5: pUC19 DNA + H₂O₂ (250 μM) + 2 (100 μM); lane 6: pUC19 DNA + H₂O₂ (250 μM) + 3 (100 μM); lane 7: pUC19 DNA + H₂O₂ (250 μM) + 4 (100 μM).....</p>	91
<p>4.13 Propose mechanistic pathway for the photo-induced nuclease activity of the complexes.....</p>	92
<p>4.14 Crystal structure of (a) NiA₂ (A1), (b) CuA₂ (A2), (c) ZnA₂ (A3), (d) NiB₂ (B1), (e) CuB₂ (B2), (f) ZnB₂ (B3).....</p>	96
<p>4.15 Electronic absorption spectra of (a) 4Cl-BMP (A), (b) NiA₂ (A1), (c) CuA₂ (A2), (d) ZnA₂ (A3), (e) 4OMe-BMP (B), (f) NiB₂ (B1), (g) CuB₂ (B2), (h) ZnB₂ (B3).....</p>	110
<p>4.16 Emission spectra of (a) 4Cl-BMP (A), (b) NiA₂ (A1), (c) CuA₂ (A2), (d) ZnA₂ (A3), (e) 4OMe-BMP (B), (f) NiB₂ (B1), (g) CuB₂ (B2), (h) ZnB₂ (B3).....</p>	116
<p>4.17 Stern-Volmer plot of (a) Schiff base (A) and metal complexes (A1-3), (b) Schiff base (B) and metal complexes (B1-3).....</p>	117
<p>4.18 Stern-Volmer plot of metal complexes with the electrostatic effect test using EB-DNA systems (a) NiA₂ (A1), (b) CuA₂ (A2), (c) ZnA₂ (A3), (d) NiB₂ (B1), (e) CuB₂ (B2), (f) ZnB₂ (B3).....</p>	118
<p>4.19 Normalized melting temperature curve (T_m).....</p>	121

Figure	Page
<p>4.20 Cleavage of pUC19 DNA incubation in the dark (a) and 15 min irradiated under UV-A 365 nm (b) lane 1: pUC19 DNA; lane 2: pUC19 DNA + A (100 μM); lane 3: pUC19 DNA + A1 (100 μM); lane 4: pUC19 DNA + A2 (100 μM); lane 5: pUC19 DNA + A3 (100 μM); lane 6: pUC19 DNA + B (100 μM); lane 7: pUC19 DNA + B1 (100 μM); lane 8: pUC19 DNA + B2 (100 μM); lane 9: pUC19 DNA + B3 (100 μM).....</p>	123
<p>4.21 Propose mechanistic pathway for the photo-induced nuclease activity of the complexes.....</p>	124

LIST OF ABBREVIATIONS

δ	chemical shift
μL	microliter
μmol	micromole
$[\alpha]_{\text{D}}$	specific rotation
A	adenine
aq	aqueous
br	broad
c	concentration
C	cytosine
calcd	calculated
CDCl_3	deuterated chloroform
d	doublet
D_2O	deuterium oxide
DCM	dichloromethane
DMAP	4-dimethylaminopyridine
DMF	N,N'-dimethylformamide
DMSO-d_6	deuterated dimethylsulfoxide
DNA	deoxyribonucleic acid
equiv	equivalent (s)
g	gram
G	guanine
h	hour
J	coupling constant
Lys	lysine
M	multiplet
MALDI-TOF	matrix-assisted laser desorption/ionization-time of flight
MeOH	methanol
mg	milligram
MHz	megahertz
min	minute
mL	milliliter

CHAPTER I

INTRODUCTION

1.1 Introduction

At present, cancer is a leading cause of death. Therefore, taking care of cancers are important. Cancers can be treated by surgery, chemotherapy, radiation, or combination of these treatments, depending on the type and the stage of cancer. The development strategies for anticancer drugs are considered based on (i) good intrinsic properties, saline solubility, and stable enough to reach the cellular target; (ii) ability to transport in blood and through membranes, (iii) an efficient DNA-binding but slow reactivity with proteins, and (iv) ability to inhibit the tumors as well as the other cancer drugs [1]. These requirements may be overcome by using metal complexes as an anticancer drug. One of the most widely used metal complexes as anticancer drugs is cisplatin. The proposed mechanism on the activity of transition metal complexes toward cytotoxic activity is that positively charged metal ion favorably bind to a negatively charged biomolecules. The formation of this opposite charged particles gives a transition metal-proteins/nucleic acid complex which then inhibits enzymes controlling nucleic acid biosynthesis. The examples of ligand coordinated metal complex and show the greater biological activity are flavonoid and rotenoid. Flavonoid is a group of phenolic compounds which present a basic structure with two aromatic rings linked through three carbons that usually form an oxygenated heterocyclic [2]. Rotenoid is a class of plant secondary metabolites that derived from isoflavones. Rotenoid has been used as insecticides and fish poison in South America and East Africa [3]. Many transition

metal flavonoid and rotenoid complexes have been reported to have antitumor activities and can inhibit DNA topoisomerase enzyme [3-6]. Therefore, this work we are interested in a rotenoid compound named 6-deoxyclitoriacetal.

6-Deoxyclitoriacetal, a rotenoid compound, was isolated from the dried roots of *Stemona collinsae* Craib. It has a strong cytotoxic activity against various types of human carcinoma [7]. The knowledge from the structure-based search revealed that 6-deoxyclitoriacetal shares some similarities to a well known anticancer drug (doxorubicin) and natural compounds such as coumarins and flavonoids. The transition metal complexes of these compounds can enhance and accelerate their anticancer efficacy.

Another example is transition metal of Schiff base. These metal Schiff base complexes have gained more interested from scientists in their role of industrial chemistry, agriculture and especially pharmaceutical used as antimicrobial, antifungal, antiviral, antitumor, and enzymatic agents [8]. There is an increase in the number of complexes with therapeutic value, for example, cobalt (III) Schiff base complexes, potential antiviral agents, cis-dichlorodiamineplatinum (II) is an anti-cancer agent and copper (II) schiff base complex is an antitubercular agent [9]. In recent years metal complexes of Schiff bases have attracted considerable attention due to their remarkable antibacterial, antitumor and anticancer activity. In particular, Merck company has successfully developed an antibacterial drug cilastatin using chiral copper (II). Several research papers have synthesized and characterized on transition metal complexes of Schiff base derived from salicylaldehyde [10-14].

In order to discover and develop new anticancer drugs candidate and their anticancer mechanism, we focus on the investigation of the transition metal complexes of 6-deoxyclitoriacetal and Schiff base of 2-[(4-chlorobenzylimino)-methyl]-phenol and 2-[(4-methoxybenzylimino)-methyl]-phenol. The dissertation is divided into 2 main parts;

Part I Metal complexes of 6-deoxyclitoriacetal, where M are Fe(III), Co(II), Ni(II), and Cu(II).

Part II Metal complexes of Schiff base 2-[(4-chlorobenzylimino)-methyl]-phenol and 2-[(4-methoxybenzylimino)-methyl]-phenol, where M are Ni(II), Cu(II), and Zn(II).

The synthesis, characterization, crystal structure determination, DNA-binding affinity, cytotoxicity, and DNA cleavage activity of these metal complexes are studied.

1.2 Objectives of this research

1. To synthesis the transition metal complexes of 6-deoxyclitoriacetal and Schiff base of 2-[(4-chlorobenzylimino)-methyl]-phenol and 2-[(4-methoxybenzylimino)-methyl]-phenol.
2. To test the cytotoxic activities against cancer cell MTT assays of the transition metal complexes of 6-deoxyclitoriacetal and Schiff base of 2-[(4-chlorobenzylimino)-methyl]-phenol and 2-[(4-methoxybenzylimino)-methyl]-phenol.

3. To study the DNA binding affinity of the transition metal complexes of 6-deoxyclitoriacetal and Schiff base of 2-[(4-chlorobenzylimino)-methyl]-phenol and 2-[(4-methoxybenzylimino)-methyl]-phenol using UV-Visible, fluorescence spectroscopy, and DNA melting temperature.
4. To investigate the DNA cleavage mechanism of the transition metal complexes of 6-deoxyclitoriacetal and Schiff base of 2-[(4-chlorobenzylimino)-methyl]-phenol and 2-[(4-methoxybenzylimino)-methyl]-phenol.

CHAPTER II

BACKGROUND AND LITERATURE REVIEWS

2. Background and literature reviews

2.1 Cancer and the Cell Cycle

Cancer is a disease caused by unregulated proliferation of cells (Fig. 2.1). According to World Health Organization (WHO), it is the second major cause of death following cardiovascular diseases [15]. In Thailand, the rate of people dying from cancer is still increasing every year and it is the first leading cause of death [16].

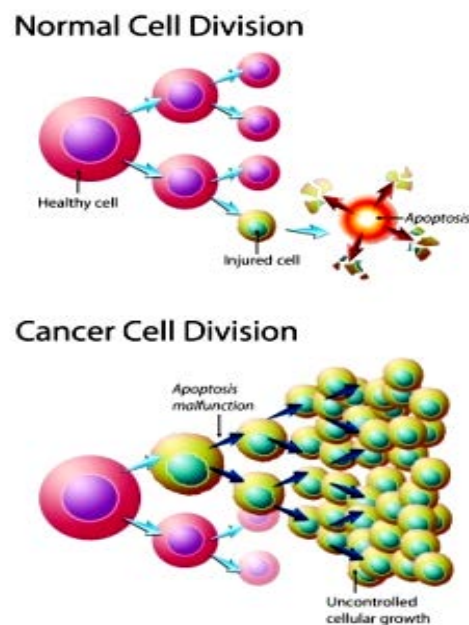


Figure 2.1 Cell division of normal and cancer cell.

The cell division process in both normal cell and cancer cell occur as an orderly progression through four different stages, known collectively as the “cell cycle” (Fig. 2.2).

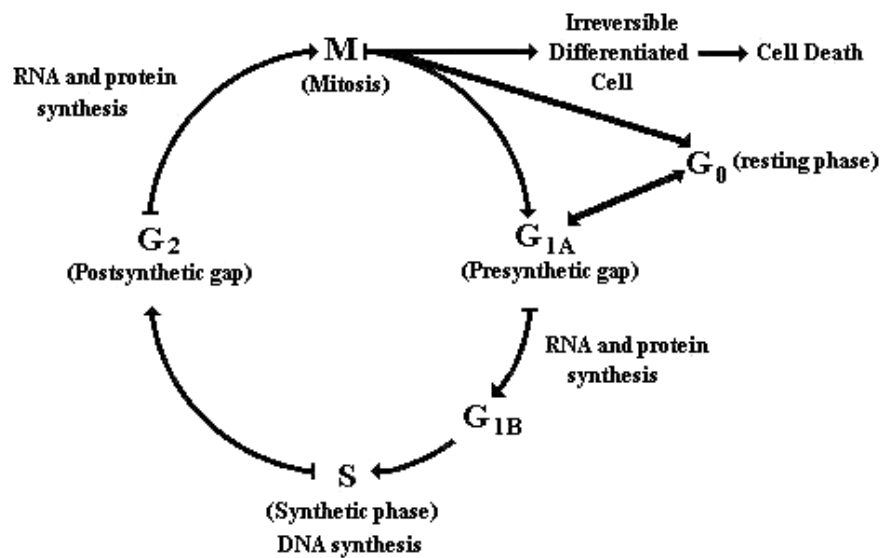


Figure 2.2 The cell cycle.

The Cell Cycle

- The cell cycle consists of four stages: G₁, S, G₂, and M.
- G₁ and G₂ are 'gap' phases in which the cell grows and prepares to divide.
- S is the synthesis phase in which the chromosomes (DNA) are copied (replicated).
- M is the mitotic phase in which the cell physically divides into two daughter cells.
- Most cells are NOT actively dividing. These cells are in a resting state (G).

Mitosis (M phase)

- Mitosis in normal cells produces two cells with identical genetic content.
- Mitosis has four sub-phases:
 - *Prophase* - Chromosomes condense, the nuclear membrane breaks down, and spindle fibers form
 - *Metaphase* - The replicated chromosomes line up in the middle of the cell
 - *Anaphase* - Chromosomes separate and the cell becomes elongated, with distinct ends (poles)
 - *Telophase* - Nuclear envelopes re-form at the two poles and new cell membranes are formed to create two independent cells

DNA Synthesis (S phase)

- Humans have 46 chromosomes, 23 from each parent.
- Each chromosome is comprised of a single piece of DNA containing millions of nucleotides.
- A pair of homologous chromosomes has the same genes, but can have different versions of those genes.
- In many cancer cells the number of chromosomes is altered so that there are either too many or too few chromosomes in the cells. These cells are said to be aneuploid.
- Errors may occur during the DNA replication resulting in mutations and possibly the development of cancer.

- Cells have mechanisms to correct errors due to faulty DNA replication.
- Many chemotherapy agents target the S phase of the cell cycle. [17-18]

As cancer is developed from the mutation of DNA during the cell cycle, therefore, DNA is target for many anticancer drugs.

2.2 Anticancer drugs

Anticancer drugs used for treatment of cancer in cancer chemotherapy have originated from a variety of sources, including dyestuffs, chemical warfare agents, natural products from plants, microbes, and fungi. The key issue of anticancer drugs in chemotherapy is killing the tumor cells without causing too much harm to healthy cells. Anticancer agents can be divided into two main categories based on their mode of action: DNA- or mitotic-target anticancer agents [19]. In this work we focus on DNA-target anticancer agents.

2.2.1 DNA-target anticancer drugs

DNA-target anticancer drugs are divided into two classes including drugs interfering with DNA synthesis and drugs interacting directly with DNA.

2.2.1.1 Drugs interfering with DNA synthesis

Drugs interfering with DNA synthesis are dealing with inhibition of a number of different enzymes involved in the synthesis of DNA. These inhibitors, which are called antimetabolites, block more or less crucial steps in DNA synthesis. The actions

of these drugs include inhibition of, e.g. tetrahydrofolate synthesis, purine and pyrimidine synthesis, DNA/RNA polymerases and ribonucleotide reductase [20].

2.2.1.2 Drugs interact directly with DNA

Drugs that can interact directly with DNA have many sorts as the following details:

Alkylating agents

Alkylating agents is the compounds that undergo the reaction in which an alkyl group becomes covalently linked to some cellular constituent, preferably the DNA molecule. Nitrogen mustards, aziridines, nitrosoureas, triazenes, hydrazine, and methanesulphonate ester are the alkylating agents. These drugs lead to DNA cross-linking which is believed to inhibit to cell growth and result in the antitumor activity [20].

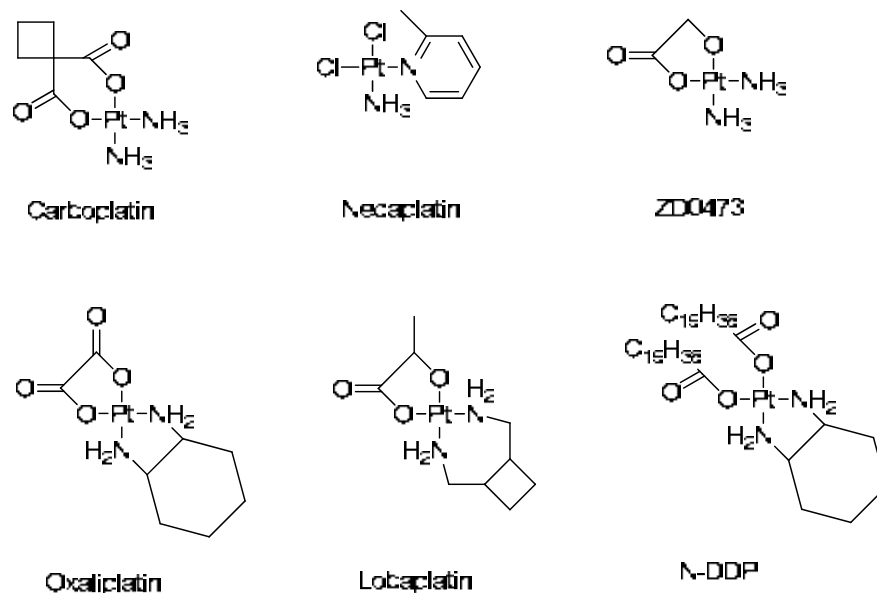


Figure 2.3 Examples of alkylating agents.

Groove binding agent

Compounds cause degradation of DNA, for example, bleomycin. Bleomycin is a group of related glucopeptide antibiotics isolated from *Streptomyces verticillus*. Metal ion and O₂ in bleomycin act as cofactors that bind in the minor groove of DNA with specific DNA sequences, leading to sequence selectivity in DNA cleavage [17].

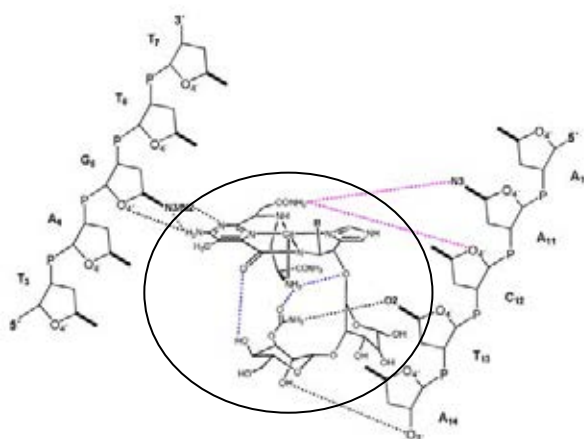


Figure 2.4 Chemical structure of the Co (III) bleomycin in DNA strands.

Intercalating agents

They bind reversibly to double-stranded DNA by intercalation, inserting between adjacent base pairs of DNA. Such compounds have to be rather planar and most often aromatic ring systems, which are held between the flat base pairs ring by van der Waals and π - π interactions. The DNA intercalation has various biological consequences e.g. inhibition of DNA replication and transcription, probably due to prevention of DNA/RNA polymerase activity. Intercalating agents such as daunorubicin, daunomycin, doxorubicin, and adriamycin are anthracycline antibiotics isolated from various *Streptomyces* species [17].

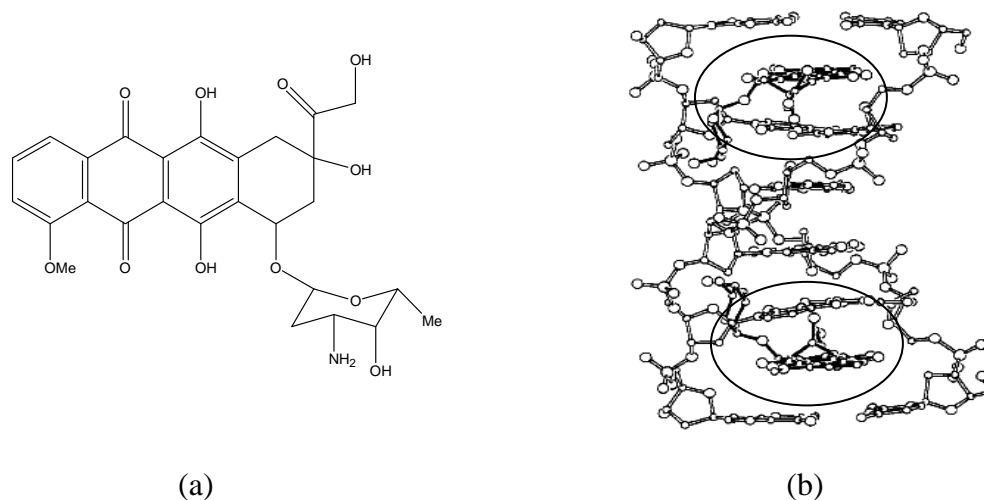


Figure 2.5 Chemical structure of (a) doxorubicin (b) intercalation of doxorubicin- $d(\text{CGATCG})_2$.

As mention in previous part, we categorized drugs that directly interact with DNA into 3 groups of alkylating agents, groove binding agents, and intercalating agents. It is interesting that many effective anticancer agents are metal complexes.

2.3 Metal complex as anticancer agents binding to DNA

It is known that the DNA incapable of replication or repair and recognizable by proteins known as high mobility group proteins (HMG) that bind to bend DNA and the cell may thus targets for death. Metal complex as anticancer drugs include cisplatin ($\text{cis}-(\text{NH}_3)_2\text{PtCl}_2$) (Fig. 2.6a), ruthenium(II) polypyridyl complex $[\text{Ru}(\text{bpy})_2(\text{appo})]^{2+}$ as topoisomerase II inhibitor [20] (Fig 2.6b), palladium(II) complex of 3-(1-aminoethyl)-4-hydroxychromen [21] (Fig 2.6c), zirconium(IV) complexes of warfarin, coumachlor and niffcoumar [22] (Fig 2.6d), and copper(II) complex of coumarin-3-carboxylic acid (CcaH) [23] (Fig 2.6e).

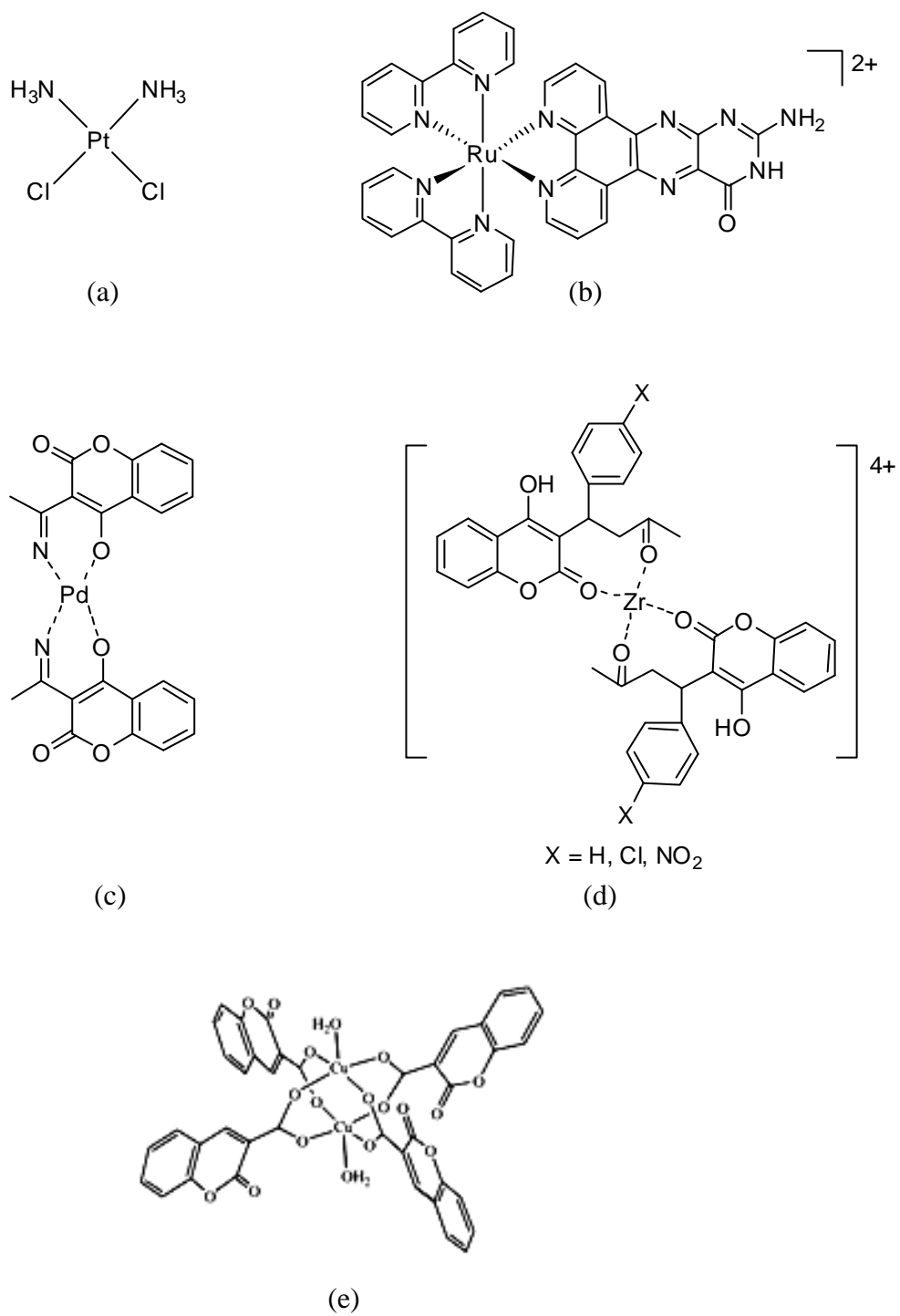


Figure 2.6 Examples of transition metal complexes bind to DNA.

As mention above, each chemotherapeutic agent has different activity to cell. For example, alkylating agents will be active to every stage of cell cycle and not specific to cancer cell. It can crosslink with DNA strands of the normal cells and lead to abnormal cell growth. For antimetabolic agents, it is specific to the synthetic phase of DNA. Examples of antimetabolites are folic acid antagonists, purine antagonists, and pyrimidine antagonists. These agents will obstruct DNA synthesis by changing folic acid to tetrahydrofolate, and inhibiting purine and pyrimidine formation. For intercalating agents such as actinomycin, bleomycin, and doxorubicin, these compounds will intercalate between the space of DNA pairs and stop RNA/DNA replication and transcription.

In order to discover and develop of new anticancer agents for the direct target, we have to understand the mechanism of the candidate compounds. Two interesting class of transition metal complexes as anticancer agent are the metal complexes of i) 6-deoxyclitoriacetal which is a chromone based-structures, and ii) Schiff base. This reveals the higher biological activity than other ligands.

2.4 Chromone based-structures as anticancer agents

Chromone (or 1, 4-benzopyrone) is a derivative of benzopyran with a substituted keto group on the pyran ring. Derivatives of chromone are collectively known as chromones. The examples of well known chromone-based structures that have anticancer activity include coumarin, flavonoids, and rotenoid.

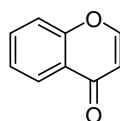


Figure 2.7 The structure of chromone [24].

2.4.1 Coumarin

Coumarin ligands have the remarkable biological significance such as antitumor, anti-inflammatory, antioxidant, antiallergic, antiviral, and anticarcinogenic activities [25]. It is an appropriate ligand for synthesis of coordination compound. This ligands show topoisomerases II inhibition [26].

In 2006, Kostova and Momekov synthesized bis-coumarin complexes of Ce(III), La(III), Nd(III) and Zr(IV) that exhibited the metal coordinate ligand through hydroxyl group. These compounds have demonstrated cytotoxic activity on human chronic myeloid leukemia (LAMA-84) and the acute pro-myelocyte leukemia (HL-60) cancer cell lines. From this experiment, they found that the presence of phenolic, hydroxyl and carboxylic groups on the coumarin nucleus are necessary for antimicrobial activity and cytotoxicity [27-28].

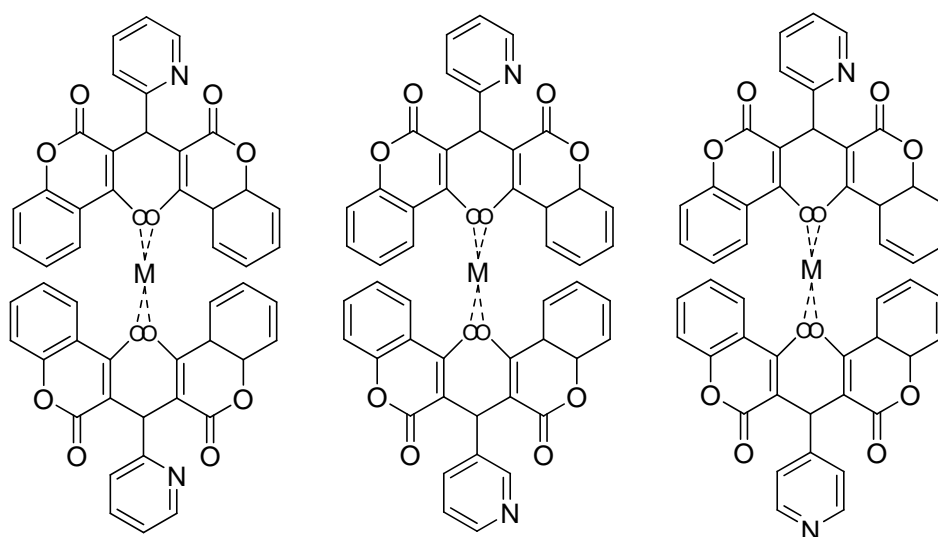


Figure 2.8 Structures of bis-coumarin complexes with M = Ce(III), La(III), Nd(III) and Zr(IV).

A number of lanthanide complexes (Ce(III), La(III), and Nd(III)) have been synthesized and their cytotoxicity was tested by Kostova et al. in 2007 [29]. These compounds have demonstrated good anti-proliferative activity on various cancer cell lines (human leukemic cell line (HL-60), T-cell leukemia-derived (SKW-3), and pre-B cell leukemia-derived (Reh)) and presented interesting metalorganic compounds with antitumor activity. Coumarin derivatives can coordinate a transition metal via oxygen of the carbonyl group on the lactone ring.

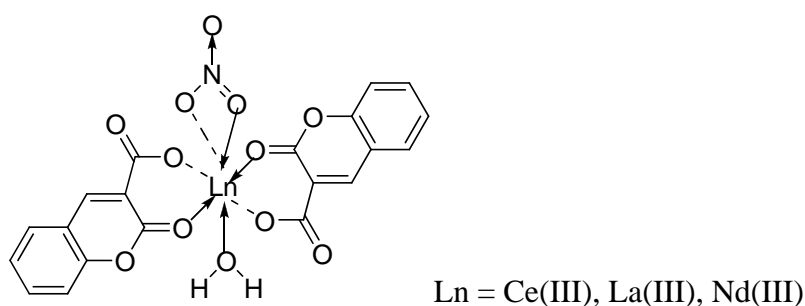


Figure 2.9 The most probable structural formula of Ln (III) complexes [29].

2.4.2 *Flavonoid*

Flavonoid is another example of ligand capable of coordinating metal and shows the greater biological activity. It is a group of phenolic compounds which present a basic structure with two aromatic rings linked through three carbons that usually form an oxygenated heterocyclic [30]. Many transition metal-flavonoid complexes have been reported to have antitumor activities and can inhibit DNA topoisomerase enzyme. The examples of these complexes are as follows:

In 2006, Kosmider et al. studied cytotoxic activities of cis-bis(3-aminoflavone)dichloroplatinum(II) (the cis-Pt(II) complex of 3-aminoflavone) in comparison with cisplatin. They examined the effect of both tested compounds on cell viability and induction of apoptosis and necrosis. The cis-Pt(II) complex of 3-aminoflavone showed a weaker genotoxic effect in normal lymphocytes in comparison with cisplatin, which was a stronger inducer of apoptosis and necrosis [31].

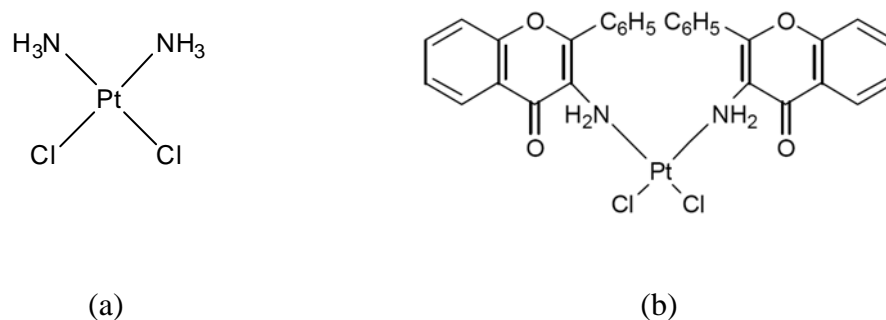


Figure 2.10 Chemical structures of the test compounds: (a) cisplatin, (b) cis-[Pt(AF)₂Cl₂].

In 2009, Zurowska et al. synthesized novel metal complexes of 3-aminoflavone. The complexes of general formula $[M(3\text{-af})_2(\text{H}_2\text{O})_2](\text{NO}_3)_2 \cdot n\text{H}_2\text{O}$, where $M = \text{Co(II)}$, Ni(II) , and Zn(II) , and $n = 0, 2, 0$, respectively, and $[\text{Cu}(3\text{-af})_2(\text{NO}_3)_2]$ compound were prepared and studied. These compounds exhibited significant antitumor activity against the development of leukemia L1210 cells in mice. Cytotoxicity was tested by measuring the inhibitory effect on L1210 cell proliferation [32].

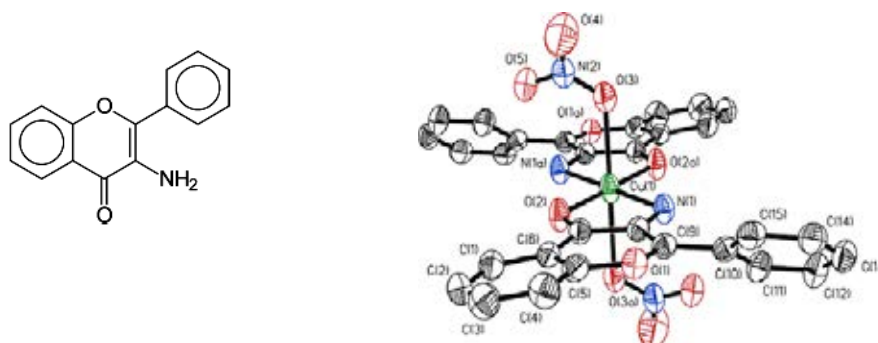


Figure 2.11 Structure formula of the ligand 3-aminoflavone and molecular structure and labeling scheme of [Cu(3-af)₂(NO₃)₂].

In 2009, a new ligand L, 6-hydroxy chromone-3-carbaldehyde thiosemicarbazone, and its Ni(II) complex have been synthesized and characterized by Wang et al. Ni(II) complex and ligand L were subjected to biological tests in vitro using THP-1, Raji and Hela cancer cell lines. The ligand showed cytotoxic activity in vitro against three human cancer cell lines (Hela, IC₅₀ > 300 μM; Raji, IC₅₀ = 240.2 μM; Thp-1, IC₅₀ > 300 μM), while the Ni(II) complex exhibited different cytotoxic activity in vitro against three human cancer cell lines (Hela, IC₅₀ = 181 μM; Raji, IC₅₀ = 97 μM; Thp-1, IC₅₀ = 89 μM). The IC₅₀ values of Ni(II) complex against three cell lines were lower than that of ligand. The interactions of Ni(II) complex and ligand L with calf thymus DNA were investigated. The experimental results indicated that Ni(II) complex bound to DNA by intercalative mode via the ligand L [5].

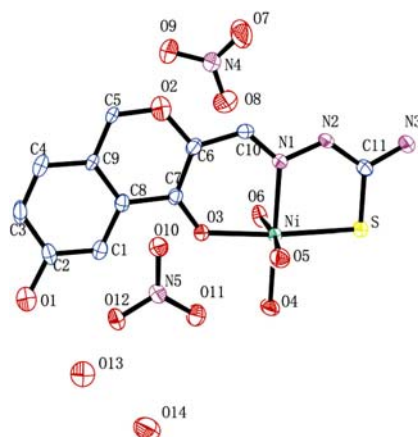


Figure 2.12 Structure of the 6-hydroxy chromone-3-carbaldehyde thiosemicarbazone Ni(II) complex.

From the literatures above, it can be concluded that the transition metal-coumarin and flavonoid complexes with antitumor activities and DNA topoisomerase inhibitory activity should bear (i) the planar moiety to intercalate with DNA strands, and (ii) the carbonyl group to coordinate with the metal and form intermolecular interaction with DNA strands. In addition, not only the noble metal complexes have strong anticancer activities, but also the first row transition metal complexes of chromone-based structure inhibited various human cell lines. From the advantages of metal-chromone-based drugs with the good bioactivities, it is interesting to discovery the new group of transition metal-chromone-based drug. In this work, we focus on a rotenoid compound bearing chromone structure and they have been reported to have various anticancer activities [5, 26-32].

2.4.3 Rotenoids

Rotenoid compounds are a class of plant secondary metabolites that derived from isoflavones. These compounds have long been used as insecticides and fish poison in South America and East Africa [33].

6-Deoxyclitoriacetal is a rotenoid compound isolated from the dried roots of *Stemona collinsae* Craib. The four fused ring structure of 6-deoxyclitoriacetal is shown in Fig.2.13.

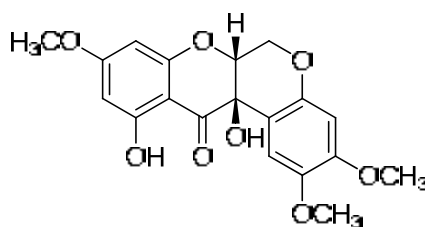


Figure 2.13 Chemical structure of 6-deoxyclitoriacetal.

6-Deoxyclitoriacetal becomes more interesting because of its various bioactivities such as antimicrobial, antiviral, insecticide and antifeedant properties. One of the most interesting bioactivities of this compound is that it has cytotoxic activity against various types of human carcinoma [34]. The molecular structure of 6-deoxyclitoriacetal adopts a roof-shaped conformation. It is similar to the structure of known anticancer drug; doxorubicin (Fig. 2.14). The previous work of P. Chimsook [34], studied the structure activity-relationship of 6-deoxyclitoriacetal on cytotoxicity based on X-ray structure. The results revealed that the bent shape and functional groups of 6-deoxyclitoriacetal are important factors for stabilizing the intercalation of DNA. The proposed anticancer mechanism of 6-deoxyclitoriacetal is via DNA intercalation or topoisomerase II inhibitory activity.

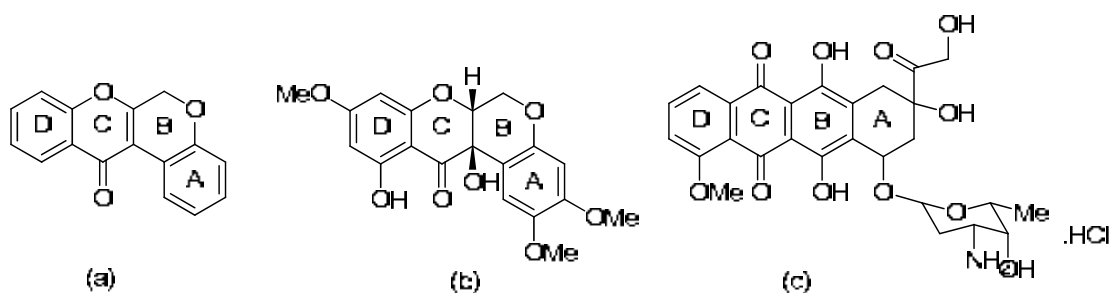
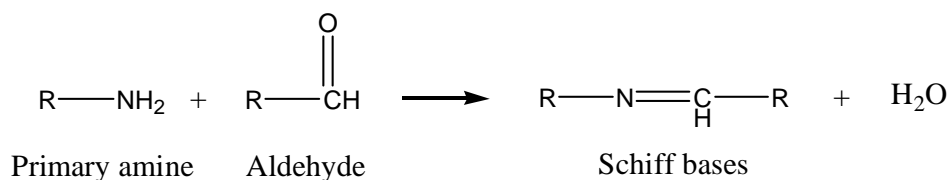


Figure 2.14 Chemical structures of (a) rotenoid structure, (b) 6-deoxyclitriacetate, and (c) doxorubicin HCl.

2.5 Schiff base

Schiff bases are condensation products of primary amines and aldehydes or ketones ($\text{RCH}=\text{NR}'$, where R and R' represent alkyl and/or aryl substituents). They are usually formed according to the following scheme:



where R may be aliphatic or aromatic group. Schiff bases of aliphatic aldehydes are unstable and readily to polymerize while those of aromatic aldehydes, having an effective conjugation system, are more stable. Schiff bases are generally bi- or tri-dentrate ligands capable of forming very stable complexes with transition metals [35].

Schiff bases and their metal complexes can be used as catalysts (in various biological systems, polymers and dyes), include some used as antimicrobial, antifungal, antiviral, anti tumor and enzymatic agents [36].

2.5.1 Schiff bases transition metal complexes

Among the transition metals V, Cr, Mn, Fe, Co, Ni, Cu, and Zn, these present at trace quantities but play vital roles at the molecular level in living system. Metal-Schiff base complexes have been known since the mid nineteenth century. It occupied a central place in the development of coordination chemistry and has being developed till in the present [37]

At the beginning, Ettlings prepared complexes from the condensation of salicylaldehyde with primary amines and reacted with cupric acetate, and isolated a dark green crystalline [38]. Delepine prepared complexes by reacting metal acetate, salicylaldehyde and primary amine in alcohol and demonstrated a 2:1 stoichiometry [39]. Rahman (1994), Metal (M = Ni, Cu, Pd and Pt) complexes of the schiff base of 2-aminobenzaldehyde with S-methyldithiocarbazate were prepared and characterized. The magnetic and spectral evidence suggests a square-planar structure for mono-ligated complexes and an octahedral structure for *bis-chelated* complexes. The copper (II) complexes have shown high antifungal activities [40].

2.5.2 Biological activities of Schiff bases transition metal complexes

Transition metal schiff base complexes have been found to play a vital role in medicine, biological systems and industries. The field of medicine has witnessed an increase in the number of complexes with therapeutic value, for example, cobalt (III)

Schiff base complexes are potential antiviral agents, cis-dichlorodiamineplatinum (II) is an anti-cancer agent and copper (II) schiff base complex is an antitubercular agent [9]. The use of atom transfer radical cyclisation mediated by copper (II) schiff base complexes to furnish nitrogen heterocycles most of which are biologically active molecules and also the use of copper schiff base catalyst in carbon based radical cyclisation reactions were recently investigated [41]. The complex compound formed by schiff base derived from benzoin and 2-amino benzoic acid with cobalt (II) salt has been reported [42]. This paper reports the preparation and characterization of two new complex compounds formed by iron (II) and nickel (II) metal ions with the schiff base.

In recent years metal complexes of schiff bases have attracted considerable attention due to their remarkable antifungal, antibacterial, antitumor and anticancer activity. In particular, Merck company has successfully developed an antibacterial drug cilastatin using chiral copper (II). Several research papers have been synthesized and characterized on transition metal complexes of Schiff base derived from salicylaldehyde [11-13, 43-45].

For example, Xishi *et al.* (2003) reported the synthesis and characterization of Mn (II), Co (II) and Cu (II) complexes with a novel schiff base ligand derived from 2, 2' – bis(*p*-methoxyphenylamine) and salicylaldehyde [43].

Zhong *et al.* (2007), synthesized mononuclear complexes of Cu(II), Ni(II), and Mn(II) with a new Schiff base ligand derived from indoline-2,3-dione and 2-hydroxybenzohydrazide. The complexes have been structurally characterized by X-ray crystallography. Founded the Cu(II) complex had the novel highest antitumor activity [44].

Elzahany *et. al* (2008), prepared Schiff bases from the N-amino rhodanine and each of 2-formylindole and salicylaldehyde, respectively. The Cr(III), Co(II), Ni(II) and Ag(I) complexes of the ligands were prepared and characterized. Tetrahedral geometrical structure was proposed for Ag(I) complex, whereas Cr(III), Co(III), Ni(II) and Cu (II) have octahedral configurations. The free ligands, and their metal complexes were screened for their antimicrobial activities. The results indicated that the ligands do not have any activity, whereas their complexes showed more activity against the same organisms under identical experimental conditions [45].

Shaker *et al.* (2009), prepared metal Schiff bases complexes by condensation of *p*-amino-2,3-dimethyl-1-phenyl-3-pyrazoline-5-on with salicylaldehyde and reacted with ethanolic solution of metal salts to give complexes with general formula [M(L)(Q)] where Q=8- hydroxyquinoline, L=*o*hydroxybenzylidene-1-phenyl-2,3-dimethyl-4-amino-3-pyrazolin-5-on and M=Fe(II), Co(II), Ni(II) and Cu(II) ions [46].

As we have known that Schiff base are usually formed by condensation of primary amine with carbonyl compound. In this experiment, we synthesized 2 new Schiff base structures from condensation reaction of 4-methoxybenzylamine with salicylaldehyde, and 4-chlorobenzylamine with salicylaldehyde. In addition, the metal complexes of those Schiff base were synthesized. All compounds were characterized by ¹H NMR spectroscopy, UV-Vis spectroscopy, and X-Ray crystallography. The cytotoxic activity of these compounds was tested and the DNA binding affinities were also studied.

2.6 Drug-DNA interaction

In general, the major target for many anticancer drugs is deoxyribonucleic acid (DNA). DNA is the genetic material that stores genetic information. It is a long polymer made from repeating units called nucleotides. Chemically, DNA consists of two long polymers of simple units called nucleotides, with a backbone made of sugars and phosphate groups joined by phosphodiester bonds. DNA is double helix stabilized by hydrogen bonds between the bases attached to the two strands (Fig. 2.16). The four bases found in DNA are adenine (A), cytosine (C), guanine (G), and thymine (T) [47-49].

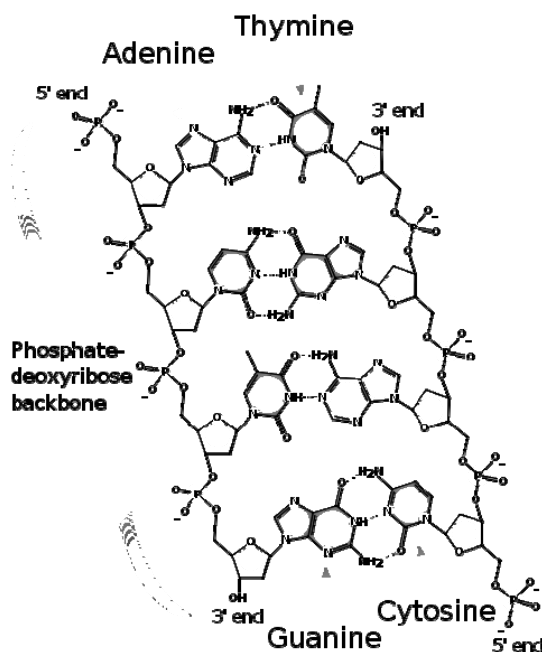


Figure 2.15 Deoxyribonucleic acid (DNA) and hydrogen bonding of nitrogenous bases.

The binding of small organic and inorganic molecules to DNA can interfere with the numerous processes, including transcription and replication, a major step in cell growth and division. Such interference by the anticancer drug can retard or prevent cell growth. Many of the anticancer agents in clinical use are known to

interact strongly with DNA (e.g. adriamycin, cis-platin, mitoxantrone). The exact mechanism of action remains unresolved in most cases. There is a wide range of studies of the drug-DNA interactions. The major objective of such studies has been to determine the structure of the drug-DNA complex, with the objective being to use this information in the design of new derivatives [50].

The interaction of the anticancer drugs with DNA occurs principally by three different ways [51]. The first one is through control of transcription factors and polymerases; in which drug interacts with proteins that bind to DNA. The second is through RNA binding either to the DNA double helix to form nucleic acid triple helix structures or to exposed DNA single strand forming DNA-RNA hybrids that may interfere with transcriptional activity. The third type of interaction involves the binding of small aromatic ligand molecules to DNA double helical structures.

The binding of small molecules to DNA involves electrostatic interaction with the negatively charged nucleic acid sugar-phosphate structure, intercalation of planar 5 aromatic ring systems between base pairs and minor and major grooves binding interaction. DNA helix is shown associated and interacted with proteins, such as Topoisomerase I and II. Blocking proteins from binding to DNA is the way of interfering with protein-DNA complexes. Topoisomerase are nuclear enzymes regulating the topoisomerase logical state of DNA by breaking and rejoining of DNA strands [52]. Topoisomerase I generates single-strands breaks [53], and topoisomerase I introduces double-stranded breaks [54].

The cytotoxicity of topoisomerase I and II is due to stabilization of the enzyme-DNA covalent cleavage intermediates, which are referred to as cleavage complexes. Compounds that block access of topoisomerase to DNA do not show

clinical efficacy; however, compounds that trap an intermediate in which the protein is covalently bound to DNA result in potent cytotoxicities [53-54]. Clinically effective drugs that are believed to show their cytotoxicities through this mechanism include SN-38 (topoisomerase I), and doxorubicin and mitoxantrone (topoisomerase II). In addition, two principal modes for binding of small molecules to DNA are intercalation binding and minor groove binding [55].

The first mode is DNA-intercalation. Intercalating drugs should have planar, heteroaromatic ring systems which insert themselves between two adjacent base pairs in a DNA helix. The drug-DNA complex is stabilized by π - π and van der Waals interactions between the DNA base and the drug molecule. Intercalating drugs also cause structural perturbations in the DNA to accommodate the binding, such as the unwinding of the helix and a lengthening of the DNA, thereby, inhibits the ability of enzymes such as topoisomerase II to interact with DNA (Fig. 2.17). This enzyme cleaves double stranded DNA to reduce the strain that comes from local unwinding. The formation of drug-DNA-enzyme complex leads to breakage of the DNA backbone and inhibits DNA replication and transcription of the target DNA [56]. Intercalators include ethidium bromide, doxorubicin and its derivatives (Fig. 2.17).

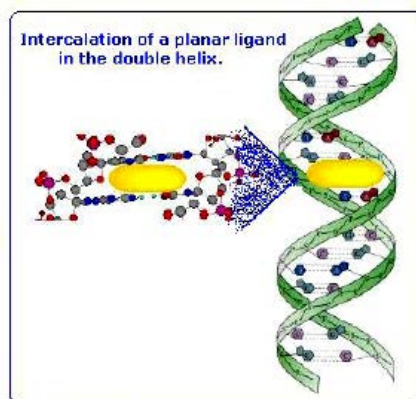


Figure 2.16 Intercalation of a planar ligand in the double helix [56].

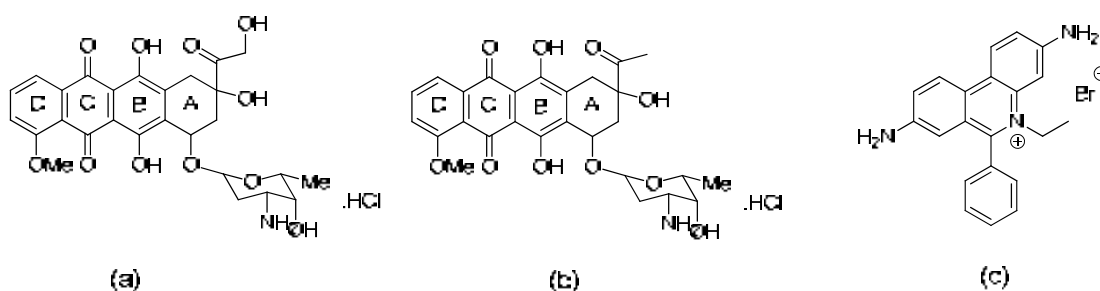


Figure 2.17 Chemical structures of (a) doxorubicin HCl (b) daunorubicin HCl and (c) ethidium bromide.

The second mode is a minor groove binding. These drugs consist of several aromatic rings (e.g. benzene or pyrrole). The drug-DNA binding is stabilized by hydrophobic interactions, as well as van der Waals interactions and hydrogen bonding. The drug-DNA binding preference is to the A-T base pairs. Minor groove binders do not induce significant structural changes to the DNA. Drugs in this category include Hoechst 33258 (Fig. 2.19).

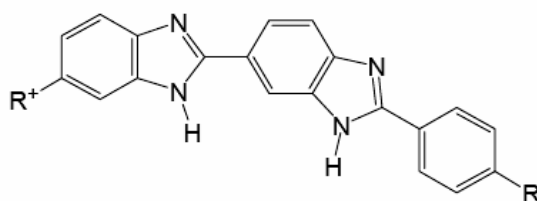


Figure 2.18 Chemical structure of Hoechst 33258 [57].

2.7 The study of drugs-DNA interaction

The numerous biological experiments performed so far suggest that DNA is the primary intracellular target of anticancer drugs because the interaction between small molecules and the DNA can cause DNA damage in cancer cells, blocking the division of cancer cells and resulting in cell death [58-61]. The interaction of transition metal complexes, containing multidentate aromatic ligands, with DNA has gained much attention, owing to their possible applications as new therapeutic agents and their photochemical properties that make them potential probes of DNA structure and conformation [62-67].

It is necessary to understand the binding properties in developing new potential DNA targeting antitumor drugs. Basically, metal complexes interact with double helix DNA in either non-covalent or covalent way. The non-covalent way includes intercalation, groove binding and external static electronic effects. The intercalation is one of the most important DNA binding modes. It was reported that the intercalating ability appeared to increase with the planarity of ligands [68-69]. In the case of covalent binding, the labile ligand of the complexes is replaced by a nitrogen base of DNA such as guanine N7. In addition, the coordination geometry and ligand donor atom type also play the key roles in determining the binding extent of complexes to DNA [70-71]. The metal ion type and its flexible valence, which are responsible for the geometry of complexes, also affect the intercalating ability of metal complexes to DNA [72-73].

There are several methods that are commonly used to study the DNA binding such as titration with UV absorption spectroscopy, ethidium bromide displacement

study by fluorescence spectroscopy, thermal denaturation study, and viscosity experiments.

2.7.1 Titration with UV absorption spectroscopy

Titration with UV absorption spectroscopy is an effective method to examine the binding mode of DNA with metal complexes [74]. In the intercalative binding mode, the π^* orbital of the intercalating ligand can couple with the π orbital of the DNA base pairs, thus, decreasing $\pi \rightarrow \pi^*$ transition energy and resulting in the bathochromism. On the other hand, the coupling π orbital is partially filled by electrons, thus, decreasing the transition probabilities and concomitantly resulting in hypochromism [75]. In general, the binding of an intercalative molecule to DNA is accompanied by hypochromism (blue-shift) and/or significant bathochromism (red-shift) in the absorption spectra due to strong stacking interaction between the aromatic chromophore of the ligand and DNA base pairs with the extent of hypochromism and red-shift commonly consistent with the strength of intercalative interaction [76]. Therefore, in order to obtain evidence for the possibility of binding of each compound to CT DNA, spectroscopic titration of a solution of the compounds with CT DNA should be performed [76].

Calculation of binding constant (K_b)

The fixed concentration and volume of complexes were titrated with increasing amount of CT DNA. The calculation of the binding constants to CT DNA (K_b) is as the following equation.

$$\frac{[DNA]}{(\varepsilon_a - \varepsilon_f)} = \frac{[DNA]}{(\varepsilon_b - \varepsilon_f)} + \frac{1}{(\varepsilon_b - \varepsilon_f) K_b}$$

When

$$\varepsilon_a = A_{\text{obs}} / [\text{cpd}]$$

ε_f = Extinction coefficient of free compound

ε_b = Extinction coefficient of the compound in fully bound form

K_b = Binding constant

Plot $\frac{[DNA]}{(\varepsilon_a - \varepsilon_f)}$ vs $[DNA]$ we got an intercept = $\frac{1}{(\varepsilon_b - \varepsilon_f) K_b}$ or $\frac{\text{slope}}{K_b}$

$$\text{Then } K_b = \frac{\text{slope}}{\text{intercept}}$$

2.7.2 Ethidium bromide (EB) displacement study by fluorescence spectroscopy

EB (3,8-Diamino-5-ethyl-6-phenyl-phenanthridiniumbromide) is a phenanthridine fluorescence dye and is indicator for intercalation. In order to investigate the interaction modes between complexes and CT DNA, the EB fluorescence displacement experiments need to be studied. Generally, the fluorescence intensity of CT DNA is very low [72, 73, 75], and EB in Tris-HCl buffer is not intense because the quenching by the solvent molecules. Addition of CT DNA to EB can enhance the fluorescence intensity of EB because of EB intercalate to DNA. Therefore, EB was used to identify the intercalation modes of complexes to DNA.

The EB fluorescence intensity can be quenched by addition of another molecule because the available binding sites of DNA for EB were decreased.

Intercalation mode of compound binding to DNA can be determined by the classical Stern-Volmer equation [74-78]

$$I_0/I = 1 + K_{sv}[Q]$$

Where I_0 = fluorescence intensity in the absence of quencher
 I = fluorescence intensity in the presence of quencher
 Q = concentration of the quencher
 K_{sv} = linear Stern-Volmer quenching constant

Plot I_0/I vs $[Q]$, K_{sv} value is given by the slope.

2.7.3 Thermal denaturation

The strands of a double-helix quickly dissociate by heating of DNA solution, then the hydrogen bonds between the base pairs are loosened. The unwinding of the double-helix is called *melting* and it occurs rather suddenly at the certain temperature. The melting temperature (T_m value) is defined as that temperature at which half of the helical structure is lost. The melting of DNA can be easily detected by measuring the absorption at λ 260 nm. The dissociation process of the base pairs brings about an increase in absorption. This is called the hyperchromic effect. Alteration of secondary DNA structure upon rising of the temperature results in change of light absorption. The consequence is a sigmoidal temperature dependence. The melting point coincides with the inflection point of the sigmoidal curve. It strongly depends on the base

composition in the studied DNA. Large number of G-C base pairs increases T_m of DNA, while DNA with mainly A-T composition has lower melting point. The nature of base pair interaction can serve as an explanation for that phenomenon. G-C base pairs have three connecting hydrogen bonds compared to A-T base pairs which have two hydrogen bonds only. Thus, breaking down of stronger G-C interactions requires more energy. Measurement of DNA absorption upon changing of temperature allows the precise determination of its base composition.

2.8 Cytotoxicity test by MTT assays

The MTT assays for measuring the activity of enzymes that reduce MTT or close dyes (XTT, MTS, WSTs) to formazan dyes, giving a purple color. A main application allows to assess the viability (cell counting) and the proliferation of cells (cell culture assays). It can also be used to determine cytotoxicity of potential medicinal agents and toxic materials, since those agents would stimulate or inhibit cell viability and growth.

MTT (3-(4,5-Dimethylthiazol-2-yl)-2,5-diphenyltetrazolium bromide, a yellow tetrazole), is reduced to purple formazan in living cells [79] A solution (usually either dimethyl sulfoxide, an acidified ethanol solution, or a solution of the detergent sodium dodecyl sulfate in diluted hydrochloric acid) is added to dissolve the insoluble purple formazan product into a colored solution. The absorbance of this colored solution can be quantified by measuring at a certain wavelength (usually between 500 and 600 nm) by a spectrophotometer. The absorption maximum is dependent on the solvent employed.



Figure 2.19 Oxidation of MTT in living cells.

MTT Assays significance

These reductions take place only when reductase enzymes are active, and therefore conversion is often used as a measure of viable (living) cells. However, it is important to keep in mind that other viability tests (such as the CASY cell counting technology) sometimes give completely different results, as many different conditions can increase or decrease metabolic activity. Changes in metabolic activity can give large changes in MTT or MTS results while the number of viable cells is constant. When the amount of purple formazan produced by cells treated with an agent is compared with the amount of formazan produced by untreated control cells, the effectiveness of the agent in causing death, or changing metabolism of cells, can be deduced through the production of a dose-response curve [80-83].

2.9 DNA Cleavage

Cleavage of DNA is an essential process in all living systems. For example, topoisomerase enzymes resolve topological problems of DNA in replication, transcription and other cellular transactions by cleaving one or both strands of the DNA [84]. Another example are restriction enzymes (or restriction endonucleases), which protect the cell against virus infection by cleavage of the foreign DNA [85, 86] or by degrading cellular DNA during apoptosis (programmed cell suicide) of the affected cell [87]. Finally, the activity of many anticancer drugs rely on their ability to introduce extended damage to the DNA in the (affected) cells (*e.g.* bleomycin) [88], which can trigger apoptosis [89], leading to the cell death [90]. In general, there are 3 different types of DNA cleavage: i) DNA hydrolysis, ii) photochemical cleavage, and iii) oxidative cleavage.

2.9.1 DNA hydrolysis

The half life of a typical phosphate diester bond of DNA in neutral water under ambient conditions (25°C) is estimated to be in the order of tens to hundred billions of years [91, 92]. This means that a catalyst has to accelerate this reaction 10¹⁷-fold to achieve an effective hydrolysis of the phosphate backbone of DNA within an acceptable timeframe (*i.e.* a couple of minute). The hydrolysis reaction is facilitated by the presence of metal ions, acting as Lewis acids. These Lewis acids can activate the phosphate group towards nucleophilic attack, activate water or hydroxide as nucleophile or increase the leaving group ability of the departing alcohol. The general accepted mechanism of the DNA hydrolysis reaction is a nucleophilic attack at the DNA phosphate backbone, to form a five coordinate intermediate, which can be

stabilized by the catalyst (Fig. 2.20) [93-96]. Subsequent cleavage of either the 3'-PO (as most often seen in enzymatic systems) or the 5'-PO results in a strand scission.

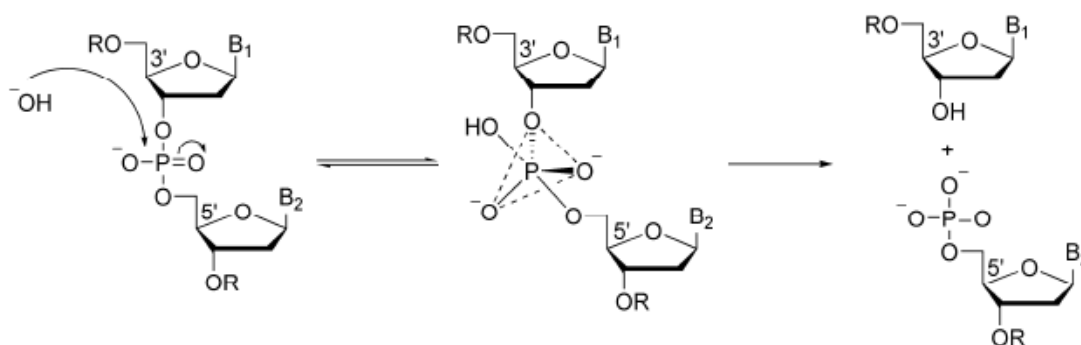


Figure 2.20 Proposed reaction mechanism for the hydrolysis of DNA.

In nature, many enzymes are capable of catalyzing this hydrolysis reaction of a phosphate bond, for example phosphatases [93-101], all via similar mechanisms. Many researches have conducted to mimic the function of these enzymes and to develop “artificial nucleases” for the hydrolysis of phosphate esters and the hydrolysis of DNA with relative simple systems, such as metal ions or metal complexes [102-108].

2.9.2 Photochemical cleavage of DNA

Photochemical cleavage of DNA can be subdivided in two categories: i) direct UV-induced DNA damage and ii) DNA cleavage via the generation of reactive (oxygen) species, by photochemical means. The former involves a direct UV-promoted dimerization reaction between two pyrimidine residues (*i.e.* thymine and cytosine) to form mutagenic and cytotoxic DNA lesions [109]. The focus of this paragraph is on the latter, as much overlap exists between this type of photochemical

DNA cleavage and oxidative cleavage of DNA. In both photochemical and oxidative DNA cleavage often similar reduced oxygen species are generated as reactive intermediates. In photochemical DNA cleavage these intermediates are generated by organic compounds or metal complexes (Fig. 2.21) [110-114].

It is important to note here that most DNA-cleaving agents are not directly responsible for the DNA damage observed, but they generate highly reactive intermediates, which cause DNA damage (*e.g.* sugar or nucleobase modification) [115]. In turn, the damaged DNA can undergo auto-oxidation reactions leading to strand scission. Alternatively, labile sites are generated in the DNA, which require further treatment (such as alkaline workup) to effect strand scission.

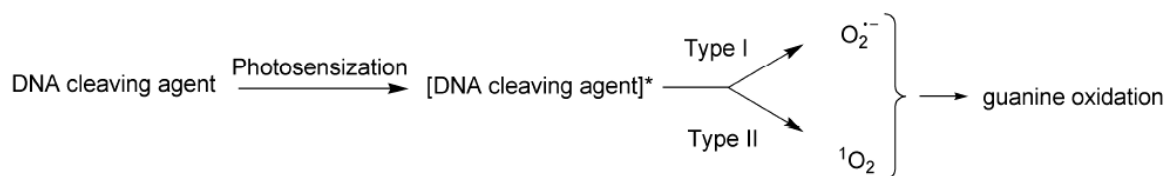


Figure 2.21 Type I and II photochemical cleavage of DNA. Both processes start with the photosensitization of the DNA cleavage agent and result in the oxidation of guanine bases.

DNA damage initiated by photosensitization can be divided in two major types; a one electron process (Type I process, Fig. 2.21), and a pathway involving singlet oxygen (Type II process, Fig. 2.21) [116, 117]. In the first type (Type I process), the cleaving agent is excited and generates sequentially a superoxide radical from molecular oxygen via an electron transfer step. Superoxide itself is a rather poor oxidant [118], and it can be further reduced (leading to H_2O_2 and $\cdot OH$) or it can

function as a reductant. The DNA damage observed via this pathway is mainly guanine oxidation, formed via guanine radical cations [117, 118]. This results in the formation of base labile sites in the DNA. In a Type II process, the photo excited compound generates singlet oxygen, which only modifies guanine residues, in contrast to superoxide. Two pathways can be distinguished (Fig. 2.22) [116, 118]. A Diels-Alder reaction with singlet oxygen results in the formation 4,8-dihydro-4-hydroxy-8-oxo-dG, and after further reduction in 8-oxo-dG. A [2+2] cycloaddition with singlet oxygen results after a cascade of reactions in the formation of cyanuric acid. The modified residues are base labile positions in the DNA and alkaline workup is required to initiate strand breaks.

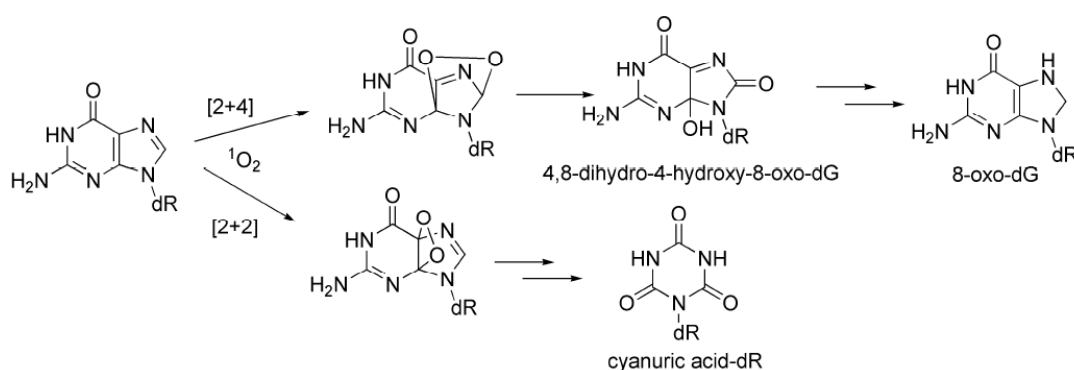


Figure 2.22 Different reaction pathways of guanine with singlet oxygen.

2.9.3 Oxidative DNA cleavage

The reactive intermediates (often reduced oxygen species) in oxidative DNA cleavage are generated via redox active metal complexes. The interaction of these intermediates with the sugar moiety or with nucleobases can result in direct strand cleavage or in the formation of labile sites in the DNA. Besides these oxygen based intermediates, also metal bound active intermediates are known, *e.g.* intermediates in the catalytic cycle of iron bleomycin (*vide infra*) [47-53].

CHAPTER III

EXPERIMENTAL

Part I Metal complexes of 6-deoxyclitoriacetal

1. Materials

All organic solvents were reagent grade purchased from Aldrich Chem. Co and commercial sources. pUC19 plasmid DNA was purchased from MBGen. Co. and purity check by agarose gel electrophoresis, DNA concentration was determined using UV spectroscopy. Calf thymus DNA (CT DNA) and ethidium bromide (EB) were obtained from Sigma Chemical Co. All measurements were carried out using doubly distilled water.

2. Preparation of 6-deoxyclitoriacetal (L)

6-deoxyclitoriacetal (L) was extracted from dried root of *Stemona collinsae* Craib using reference method [7]. Yield: 3.5%. ^1H NMR (400 MHz, CDCl_3): δ 11.50 (s, 1H, $\text{C}^{11}\text{-OH}$), 6.67 (s, 1H, $\text{C}^1\text{-H}$), 6.49 (s, 1H, $\text{C}^4\text{-H}$), 6.06 (s, 1H, $\text{C}^{10}\text{-H}$), 5.97 (s, 1H, $\text{C}^8\text{-H}$), 4.61 (dd, 1H, $J = 18\text{Hz}$, $\text{C}^6\text{-H}$), 4.48 (dd, 1H, $J = 12\text{Hz}$, $\text{C}^6\text{-H}$), 4.58 (s, 1H, $\text{C}^{6a}\text{-H}$), 3.82 (s, 3H, $\text{C}^9\text{-OCH}_3$), 3.75 (s, 3H, $\text{C}^2\text{-OCH}_3$), 3.77 (s, 3H, $\text{C}^3\text{-OCH}_3$). ^{13}C NMR (100 MHz, CDCl_3): δ 195.0 (s, C^{12}), 169.1 (s, C^9), 164.4 (s, C^{11}), 161.7 (s, C^{7a}), 151.4 (s, C^3), 148.4 (s, C^{4a}), 144.4 (s, C^2), 109.3 (d, C^1), 108.3 (s, C^{1a}), 101.2 (d, C^4), 95.6 (d, C^{10}), 100.1 (s, C^{11a}), 94.6 (d, C^8), 75.6 (d, C^{6a}), 67.0 (s, C^{12a}), 63.7 (t, C^6), 56.4 (q, Ome^2), 55.9 (q, Ome^3), 55.8 (q, Ome^9). IR (KBr, cm^{-1}): 3477m, 1635s, 1510s,

1453s, 1351m, 1225m. UV-vis (MeOH): λ_{max} 290 nm (ϵ 13950 M⁻¹cm⁻¹), 361 nm (ϵ 5745 M⁻¹cm⁻¹). MS (MALDI) m/z for C₁₉H₁₉O₈: calc. 374.11, found 373.79.

3. Synthesis of Metal complexes

3.1 Synthesis of 6-Deoxyclitoriacetal Iron(III) complex (I)

To a 10 mL EtOH solution containing 0.0374 g (0.10 mmol) of 6-deoxyclitoriacetal placed in a two-necked, round bottomed flask provided with a magnetic stirrer, reflux condenser and CaCl₂ guard tube, was added excess amount of 1 mM NaOH and stirred for 30 min. The flask was heated 60°C on a water-bath until dissolved, then 0.0270 g (0.10 mmol) of FeCl₃·6H₂O in 10 mL EtOH was added dropwisely to the mixture solution, stirred and refluxed for 6 h. as shown in Fig. 3.1. The mixture was cooled to room temperature and allowed the product to precipitate, then filtered and washed with 1:3 EtOH-H₂O several times. The red brown solid product was air dried. Yield: 36%. ¹H NMR (400 MHz, CDCl₃) : δ 11.52 (s, 1H, C¹¹-OH), 6.68 (s, 1H, C¹-H), 6.50 (s, 1H, C⁴-H), 6.06 (s, 1H, C¹⁰-H), 5.97 (s, 1H, C⁸-H), 4.48 (s, 2H, C⁶-H), 4.57 (s, 1H, C^{6a}-H), 4.10 (s, 3H, C⁹-OCH₃), 3.76 (s, 6H, C²-OCH₃, C³-OCH₃). ¹³C NMR (100 MHz, CDCl₃) : δ 195.0 (s, C¹²), 169.1 (s, C⁹), 164.4 (s, C¹¹), 161.7 (s, C^{7a}), 151.4 (s, C³), 148.4 (s, C^{4a}), 144.2 (s, C²), 109.4 (d, C¹), 108.4 (s, C^{1a}), 101.3 (d, C⁴), 95.6 (d, C¹⁰), 100.1 (s, C^{11a}), 94.6 (d, C⁸), 75.7 (d, C^{6a}), 67.0 (s, C^{12a}), 63.7 (t, C⁶), 56.5 (q, OMe²), 55.9 (q, OMe³), 55.8 (q, OMe⁹). IR (KBr, cm⁻¹): 3425m, 1617m, 1509m, 1409m, 1375m, 1222m. UV-vis (MeOH): λ_{max} 293 nm (ϵ 15085 M⁻¹cm⁻¹), 342 nm (ϵ 5000 M⁻¹cm⁻¹). MS (MALDI) m/z for [FeC₁₉H₁₈O₈(H₂O)₄]Cl₂: calc. 501.04, found 505.56.

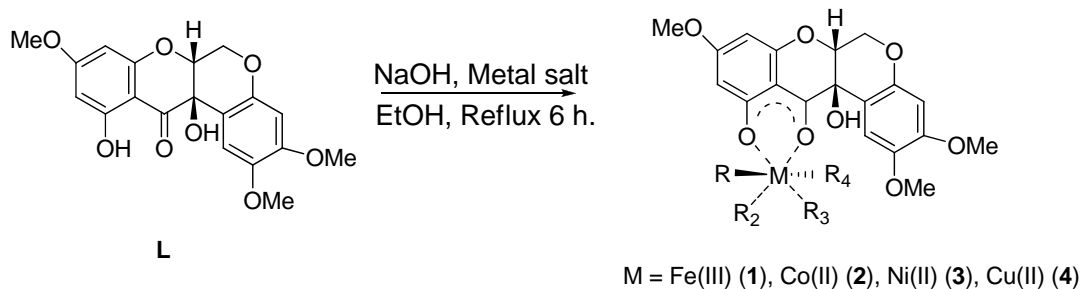


Figure 3.1 Synthesis of 6-deoxyclitoriacetal metal complexes.

3.2 Synthesis of 6-Deoxyclitoriacetal Cobalt (II) complex (2)

Synthesis by the same method as 3.1 but use metal salt as $\text{Co}(\text{NO}_3)_2 \cdot 6\text{H}_2\text{O}$ 0.0219 g (0.10 mmol). The yellow-green solid powder was obtained. Yield: 40%. ^1H NMR (400 MHz, CDCl_3): δ 11.52 (s, 1H, C^{11} -OH), 6.67 (s, 1H, C^1 -H), 6.57 (s, 1H, C^4 -H), 6.02 (s, 2H, C^{10} -H, C^8 -H), 4.55 (s, 3H, C^6 -H, C^{6a} -H), 4.09 (s, 3H, C^9 - OCH_3), 3.76 (s, 6H, C^2 - OCH_3 , C^3 - OCH_3). ^{13}C NMR (100 MHz, CDCl_3): δ 195.0 (s, C^{12}), 169.1 (s, C^9), 164.4 (s, C^{11}), 161.7 (s, C^{7a}), 151.4 (s, C^3), 148.4 (s, C^{4a}), 144.1 (s, C^2), 109.4 (d, C^1), 108.4 (s, C^{1a}), 101.2 (d, C^4), 95.6 (d, C^{10}), 100.1 (s, C^{11a}), 94.6 (d, C^8), 75.7 (d, C^{6a}), 67.0 (s, C^{12a}), 63.7 (t, C^6), 56.4 (q, OMe^2), 55.9 (q, OMe^3), 55.80 (q, OMe^9). IR (KBr, cm^{-1}): 3424m, 1618m, 1509m, 1411m, 1382m, 1222m, 478w. UV-vis (MeOH): λ_{max} 292 nm (ϵ 13445 $\text{M}^{-1}\text{cm}^{-1}$), 360 nm (ϵ 3690s $\text{M}^{-1}\text{cm}^{-1}$). ESI-MS m/z for $\text{Co}(\text{C}_{19}\text{H}_{18}\text{O}_8)\text{NO}_3(\text{H}_2\text{O})_2 \cdot 2\text{H}_2\text{O}$: calc. 566.12, found 567.07.

3.3 Synthesis of 6 - Deoxyclitoriacetal Nickel(II) complex (3)

Synthesis by the same method as 3.1 but use metal salt as $\text{Ni}(\text{CH}_3\text{COO})_2 \cdot 4\text{H}_2\text{O}$ 0.0249 g (0.10 mmol). The green solid powder was obtained. Yield: 42 %. ^1H NMR

(400 MHz, CDCl₃): δ 6.68 (s, 1H, C¹-H), 6.47 (s, 1H, C⁴-H), 5.91 (s, 2H, C¹⁰-H, C⁸-H), 4.42 (s, 3H, C⁶-H, C^{6a}-H), 3.89 (s, 3H, C⁹-OCH₃), 3.72 (s, 6H, C²-OCH₃, C³-OCH₃). ¹³C NMR (100 MHz, CDCl₃): δ 195.0 (s, C¹²), 169.1 (s, C⁹), 164.4 (s, C¹¹), 161.7 (s, C^{7a}), 151.4 (s, C³), 148.4 (s, C^{4a}), 144.1 (s, C²), 109.4 (d, C¹), 108.4 (s, C^{1a}), 101.2 (d, C⁴), 95.6 (d, C¹⁰), 100.1 (s, C^{11a}), 94.6 (d, C⁸), 75.6 (d, C^{6a}), 66.9 (s, C^{12a}), 63.7 (t, C⁶), 56.4 (q, OMe²), 55.9 (q, OMe³), 55.8 (q, OMe⁹). IR (KBr, cm⁻¹): 3445m, 1622m, 1509m, 1422m, 1365m, 1223m, 478w. UV-Vis (MeOH): λ_{max} 292 nm (ϵ 17310 M⁻¹cm⁻¹), 363 nm (ϵ 8640 M⁻¹cm⁻¹). MS (MALDI) m/z for Ni(C₁₉H₁₈O₈)CH₃COO·4H₂O: calc. 544.90, found 544.78.

3.4 Synthesis of 6 - Deoxyclitoriacetal Copper(II) complex (4)

Synthesis by the same method as 3.1 but use metal salt as CuCl₂·2H₂O 0.0170 g (0.10 mmol). The green solid powder was obtained. Yield: 46%. ¹H NMR (400 MHz, CDCl₃): δ 11.56 (s, 1H, C¹¹-OH), 6.70 (s, 1H, C¹-H), 6.50 (s, 1H, C⁴-H), 6.02 (s, 1H, C¹⁰-H), 5.96 (s, 1H, C⁸-H), 4.47 (s, 2H, C⁶-H), 4.57 (s, 1H, C^{6a}-H), 3.93 (s, 3H, C⁹-OCH₃), 3.76 (s, 3H, C³-OCH₃), 3.66 (s, 3H, C²-OCH₃). ¹³C NMR (100 MHz, CDCl₃): δ 195.0 (s, C¹²), 169.7 (s, C⁹), 164.4 (s, C¹¹), 161.7 (s, C^{7a}), 151.4 (s, C³), 148.4 (s, C^{4a}), 144.1 (s, C²), 109.5 (d, C¹), 108.4 (s, C^{1a}), 101.2 (d, C⁴), 95.6 (d, C¹⁰), 100.2 (s, C^{11a}), 94.6 (d, C⁸), 75.6 (d, C^{6a}), 67.0 (s, C^{12a}), 63.7 (t, C⁶), 56.4 (q, OMe²), 55.9 (q, OMe³), 55.9 (q, OMe⁹). IR (KBr, cm⁻¹): 3420m, 1618m, 1508m, 1420m, 1377m, 1224m, 475w. UV-Vis (MeOH): λ_{max} 292 nm (ϵ 14750 M⁻¹cm⁻¹), 365 nm (ϵ 4850 M⁻¹cm⁻¹). MS (MALDI) m/z for Cu(C₁₉H₁₈O₈)₂·2H₂O: calc. 845.88, found 848.07.

4. Characterization of complexes

^1H NMR spectra were recorded on a Varian Mercury+ 400 NMR Spectroscope. The spectra were processed with the MestRe-C2.3a software. IR was performed using a FT-IR spectrometer (Nicolet 6700). IR spectra were obtained on KBr pellets in the region from 4000 cm^{-1} to 400 cm^{-1} . Absorption spectra were recorded on the CARY 100 Bio UV-Visible spectrophotometer (Varian Ltd.). Samples were measured over the region of 200-600 nm. The percentages of C, H, and N were determined with CHNS/O ANALYSER (Perkin Elmer PE2400 SeriesII). The gaseous product freed by pyrolysis in high-purity oxygen and were chromatographically separated by frontal analysis with quantitatively detected by thermal conductivity detector. Thermogravimetric analysis (TGA) was performed using a Perkin Elmer Pyris1 under N_2 flow, measure from 30-800°C with heating rate 10 °C/min. TGA data were analyzed with Pyris Manager software v4.0.

5. Stoichiometric study (Job's Plot)

UV-Vis measurements can be used in spectrophotometric titration to study equilibrium and elucidation of the structures of complexes in aqueous solution. The concentration ratio of metal ion (C_M) and ligand (C_L) were varied and complexes solution was measured and plot between absorption intensity and molar ratio of C_M to C_M+C_L .

6. Evaluation of cytotoxic activity

The test for normal cell line (vero cell) was determined using GFP-based assay and cancer cell lines of oral cavity carcinoma (KB), small cell lung carcinoma (NCI-

H187), human breast carcinoma (MCF7) were tested using REMA assays. This was performed by the National Center for Genetic Engineering and Biotechnology (BIOTEC), National Science and Technology Development Agency (NSTDA), Bangkok, Thailand. There are also test for normal cell lines of skin fibroblast (CCD) and foreskin fibroblast (HS27) and the cytotoxicity assay tested against human breast carcinoma (BT 474), lung carcinoma (CHAGO), hepato-carcinoma (Hep-G2), gastric carcinoma (KATO III), and colon carcinoma (SW 620) were examined using MTT assay. Cells were cultured at 37°C under a humidified atmosphere of 5% CO₂ in RPMI 1640 medium supplemented with 5% fetal serum and dispersed in replicate 96-well plates with 5x10³ cells/well and incubated for 24 h. Compounds, of which the final concentration is 0 – 50 µg/mL, were then added. After 72-h exposure to the toxins, cells viability were determined by the 3 - (4, 5 - dimethylthiazol - 2 - yl) - 2, 5 - diphenyltetrazolium bromide (MTT) cytotoxicity assay measuring the absorbance at 540 nm with an Titertek Multiskan[®] MCC/340 MK II Serial RS-232C reader. Each test was performed in triplicate. The % cell viability and IC₅₀ were calculated.

7. The DNA-Binding studies

7.1 Titration with UV absorption spectroscopy

DNA stock solution was prepared in Tris-HCl buffer solution (pH 7.2). The solution of Calf Thymus DNA (CT DNA) gave a ratio of UV absorbance at 260 nm and 280 nm of 1.90, indicating that the DNA was sufficiently free of protein contamination. The DNA concentration was determined by the UV absorbance at 260

nm and using $\epsilon = 6600 \text{ M}^{-1} \text{ cm}^{-1}$ [21, 44, 75]. Each complex was dissolved in DMSO and diluted in Tris-HCl buffer to make its concentration to 20 μM .

The fixed concentration (20 μM) and volume of complexes were titrated with increasing amount of CT DNA (2-20 μM). The absorption spectra were recorded on the CARY 100 Bio UV-Visible spectrophotometer (Varian Ltd.).

7.2 Ethidium bromide (EB) displacement study by fluorescence spectroscopy

Ethidium bromide (EB) displacement study was used in order to proof the intercalation mechanism. The experiments were performed in Tris-HCl buffer solution (pH 7.2). 2 μM EB was added to 30 μM CT-DNA in Tris-HCl buffer solution and stored in the dark for 1 hour. Then the solution of each complex at 5, 10, 15, 20, 25, and 30 μM were titrated to the DNA-EB mixture. The mixture were shaken and kept in the dark at room temperature for 15 minutes before measurement of fluorescence spectra. The emission spectra were recorded using Perkin Elmer LS45 luminescence spectrometer.

7.3 DNA melting temperature

Thermal denaturation studies were carried out in tris-(hydroxymethyl) aminomethane-HCl (Tris-HCl) buffer solution (pH 7.2) containing 60 μM of CT DNA and 20 μM of the compounds. Melting curves were recorded on the CARY 100 Bio UV-Visible spectrophotometer (Varian Ltd.) equipped with a thermoelectric cell temperature controller and a stirrer unit at 260 nm. The temperature was increased at a

rate of $1^{\circ}\text{C min}^{-1}$ from 20-90 $^{\circ}\text{C}$. The melting temperature (T_m) was determined by differentiation of the melting curves.

8. DNA cleavage activity

The 100 μM of compounds are used for study the cleavage of pUC19 DNA (5 μL , 0.5 μg) using agarose gel electrophoresis. A 16 μL mixture was irradiated with monochromatic UV-A light (365 nm) for 15 min. in the dark at room temperature follow by addition of 4 μL GelRed. Electrophoresis was carried out in 0.8% agarose gel at 50 V for 1 h. in 1X TBE buffer. The bands were visualized by UV light and photographed to determine the extent of DNA cleavage from intensities of the bands using GeneTools software v5.04.

PART II Metal complexes of Schiff base 2-[(4-chlorobenzylimino)-methyl]-phenol and 2-[(4-methoxybenzylimino)-methyl]-phenol

1. Preparation of Ligands

1.1 2-[(4-chlorobenzylimino)-methyl]-phenol (A)

To a stirred ethanol solution of salicylaldehyde (2.50 ml, 2.86 g, 0.02 mol) was added 4-chlorobenzylamine (2.80 ml, 2.88 g, 0.02 mol). The reaction mixture was refluxed for 1 h. and then the mixture was allowed to stand at room temperature for a week to give yellow crystals suitable for X-ray diffraction analysis. Yield: 84%. ¹H NMR (400 MHz, CDCl₃) : 13.25 (s,1H), 8.44 (s,2H), 7.35-7.23 (m,4H), 6.96 (d,1H), 6.90 (t,1H), 4.77 (s,1H). IR (KBr, cm⁻¹): 3483m, 1633m, 1085m, 758m. UV-vis (MeOH): λ nm (ϵ , mol⁻¹ cm⁻¹ L): 277 (18800), 395 (7200).

1.2 2-[(4-methoxybenzylimino)-methyl]-phenol (B)

B was synthesized by the same procedure as 2.2.1 with salicylaldehyde (2.50 ml, 2.86 g, 0.02 mol) and 4-methoxybenzylamine (2.80 ml, 2.88 g, 0.02 mol). After a week, it gives yellow needle crystals suitable for X-ray diffraction analysis. Yield: 79%. ¹H NMR (400 MHz, CDCl₃): 13.46 (s,1H), 8.41 (s,1H), 7.31-7.22 (m, 4H), 6.95 (d,2H), 6.88 (d,2H), 4.75 (s,1H), 3.81 (s,1H). IR (KBr, cm⁻¹): 3415m, 1630m, 1247m, 765m. UV-Vis (MeOH): λ_{max} 271nm (ϵ 10535 M⁻¹cm⁻¹), 395 nm (ϵ 1935 M⁻¹cm⁻¹).

2. Synthesis of Metal Schiff base complexes

2.1 Synthesis of NiA_2 (**A1**)

To a 10 mL ethanol solution containing 0.2440 g (0.10 mmol) of 2-[(4-chlorobenzylimino)-methyl]-phenol (**A**) was added 0.0249 g (0.10 mmol) of $Ni(CH_3COO)_2 \cdot 4H_2O$ which was dissolved in 10 mL EtOH. The mixture solution was refluxed for 4 h., cooled to room temperature. The green needle crystals were obtained, around 2 weeks. The reaction scheme is shown in Fig. 3.2. Yield: 56%. 1H NMR (400 MHz, $CDCl_3$): 7.48 (d,2H), 7.34 (d,2H), 7.26 (s,2H), 7.06-6.97 (dd,1H), 6.40 (d,1H), 4.78 (s,1H). IR (KBr, cm^{-1}): 3419m, 1638m, 1413m, 1017m. UV-vis (MeOH): λ , nm (ϵ , $mol^{-1} cm^{-1} L$): 263 (8350).

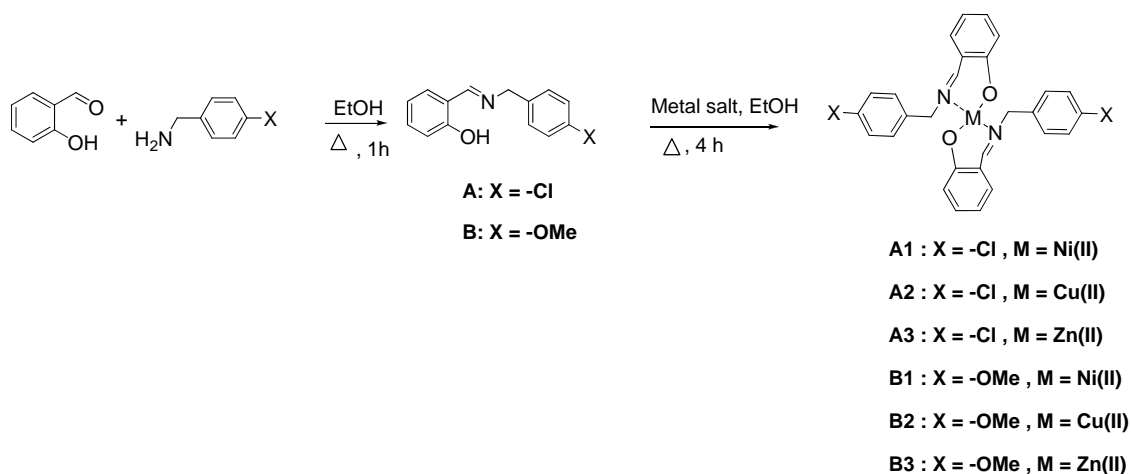


Figure 3.2 Synthesis of Schiff base and metal complexes.

2.2 Synthesis of CuA_2 (**A2**)

Complex **A2** was synthesized by the same procedure as 2.3.1 with **A** (0.2440 g, 0.10 mmol) and $\text{Cu}(\text{CH}_3\text{COO})_2 \cdot \text{H}_2\text{O}$ (0.0199 g, 0.10 mmol). The green needle crystals were obtained in 2 weeks. Yield: 63%. ^1H NMR (400 MHz, CDCl_3): 7.82 (s, 1H), 7.25 (s, 2H), 5.63 (s, 1H). IR (KBr, cm^{-1}): 3449m, 1618m, 1000m. UV-vis (MeOH): λ , nm (ϵ , $\text{mol}^{-1} \text{cm}^{-1} \text{L}$): 251 (42150), 278 (36900), 311 (22250), 385 (17600).

2.3 Synthesis of ZnA_2 (**A3**)

Complex **A3** was synthesized by the same procedure as 2.3.1 with **A** (0.2440 g, 0.10 mmol) and $\text{Zn}(\text{CH}_3\text{COO})_2$ (0.0183 g, 0.10 mmol). The yellow needle crystals were obtained, around 10 days. Yield: 66%. ^1H NMR (400 MHz, CDCl_3): 8.43 (s, 1H), 7.32 (t, 1H), 7.28 (d, 2H), 7.17 (d, 1H), 6.93 (dd, 2H), 4.79 (s, 2H). IR (KBr, cm^{-1}): 3415m, 1618m, 1537m, 1344m, 1089m, 759m. UV-Vis (MeOH): λ , nm (ϵ , $\text{mol}^{-1} \text{cm}^{-1} \text{L}$): 275 (24350), 386 (10600).

2.4 Synthesis of NiB_2 (**B1**)

To a 10 mL ethanol solution containing 0.2400 g (0.10 mmol) of 2-[(4-Methoxy-benzylimino)-methyl]-phenol (**B**) was added 0.0249 g (0.10 mmol) of $\text{Ni}(\text{CH}_3\text{COO})_2 \cdot 4\text{H}_2\text{O}$ which was dissolved in 10 mL EtOH. The mixture solution was refluxed for 4 h., cooled to room temperature. The green needle crystals were obtained, around 10 days. Yield: 63%. ^1H NMR (400 MHz, CDCl_3): 7.49 (d, 1H), 7.26 (d, 1H), 7.22 (d, 1H), 7.07 (d, 1H), 6.91 (d, 1H), 6.40 (d, 2H), 6.30 (t, 2H), 5.50 (s, 1H), 3.82 (s, 3H). IR (KBr, cm^{-1}): 3448m, 1606m, 1511m, 1325m, 1248m, 759m. UV-Vis (MeOH): λ_{max} 266nm (ϵ 14850 $\text{M}^{-1}\text{cm}^{-1}$).

2.5 Synthesis of CuB_2 (**B2**)

Complex **B2** was synthesized by the same procedure as 2.3.4 with **B** (0.2400 g, 0.10 mmol) and $\text{Cu}(\text{CH}_3\text{COO})_2 \cdot \text{H}_2\text{O}$ (0.0199 g, 0.10 mmol). The green needle crystals were obtained after 2 weeks. Yield: 75%. ^1H NMR (400 MHz, CDCl_3): 7.39 (s,1H), 7.26 (s,4H), 5.52 (s,1H), 4.12 (s,3H). IR (KBr, cm^{-1}): 3463w, 1619m, 1512w, 758w. UV-Vis (MeOH): λ_{max} 264nm (ϵ 97750 $\text{M}^{-1}\text{cm}^{-1}$), 384 nm (ϵ 12050 $\text{M}^{-1}\text{cm}^{-1}$).

2.6 Synthesis of ZnB_2 (**B3**)

Complex **B3** was synthesized by the same procedure as 2.3.4 with **B** (0.2400 g, 0.10 mmol) and $\text{Zn}(\text{CH}_3\text{COO})_2$ (0.019 g, 0.10 mmol). The yellow needle crystals were obtained after 2 weeks. Yield: 65%. ^1H NMR (400 MHz, CDCl_3) : 8.03 (s,1H), 7.26 (d,2H), 7.22 (t,2H), 6.96-6.87 (m,4H), 6.71 (d,2H), 4.76 (s,4H), 3.78 (s,3 H). IR (KBr, cm^{-1}): 3448m, 1616m, 1512m, 1325m, 1248m, 759m. UV-Vis (MeOH): λ_{max} 270nm (ϵ 91209 $\text{M}^{-1}\text{cm}^{-1}$), 375 nm (ϵ 12658 $\text{M}^{-1}\text{cm}^{-1}$).

3. Characterization of complexes

3.1 Spectroscopic method

^1H and ^{13}C NMR spectra were recorded on a Varian Mercury+ 400 NMR Spectroscope. The spectra were processed with the MestRe-C2.3a software. Mass spectra (MS) were recorded on a Water's Micromass Quattamicro API ESCi mass spectrometer using the electrospray (ES) ionization mode and matrix-assisted laser desorption ionization (MALDI-MS) IR was performed using a FT-IR spectrometer (Nicolet 6700). IR spectra were obtained on KBr pellets in the region from 4000 cm^{-1}

to 400 cm^{-1} . Absorption spectra were recorded on the CARY 100 Bio UV-Visible spectrophotometer (Varian Ltd.). Samples were measured over the region of 200-600 nm.

3.2 Single crystal X-ray crystallographic method

All X-ray data collected by Bruker SMART APEX II CCD area-detector diffractometer, with Mo $K\alpha$ radiation source ($\lambda = 0.7107\text{ \AA}$) at 296 K. The crystal structures were solved by the directed method with SHELXS-97 [119]. The full matrix least squares procedures using SHELXL-97 on F^2 anisotropic for all non-hydrogen atom was used to refine the crystal structures [119]. Hydrogen atoms were placed in their calculated positions and refined following the riding model. The crystal data and structural refinement parameters are summarized in Table 4.8. The selected bond distances and bond angles are listed in Table 4.9.

4. Evaluation of cytotoxic activity

The test for normal cell line (vero cell) was determined using GFP-based assay and cancer cell lines of oral cavity carcinoma (KB), small cell lung carcinoma (NCI-H187), human breast carcinoma (MCF7) were tested using REMA assays. This was performed by the National Center for Genetic Engineering and Biotechnology (BIOTEC), National Science and Technology Development Agency (NSTDA), Bangkok, Thailand. There are also test for normal cell lines of skin fibroblast (CCD) and foreskin fibroblast (HS27) and the cytotoxicity assay tested against cancer cell lines of human breast carcinoma (BT474), lung carcinoma (CHAGO), hepatocarcinoma (Hep-G2), gastric carcinoma (KATO III), and colon carcinoma (SW 620)

were examined using MTT assay. Cells were cultured at 37°C under a humidified atmosphere of 5% CO₂ in RPMI 1640 medium supplemented with 5% fetal serum and dispersed in replicate 96-well plates with 5x10³ cells/well and incubated for 24 h. Compounds, of which the final concentration is 0 – 50 µg/mL (except **B2** used 0-100µg/mL), were then added. After 72-h exposure to the toxins, cells viability were determined by the 3 - (4, 5 - dimethylthiazol - 2 - yl) - 2, 5 - diphenyltetrazolium bromide (MTT) cytotoxicity assay measuring the absorbance at 540 nm with an Titertek Multiskan[®] MCC/340 MK II Serial RS-232C reader. Each test was performed in triplicate. The % cell viability and IC₅₀ were calculated [80-83].

5. The DNA-Binding experiments

5.1 Titration with UV absorption spectroscopy

DNA stock solution was prepared in Tris-HCl buffer solution (pH 7.2). The solution of Calf Thymus DNA (CT DNA) gave a ratio of UV absorbance at 260 nm and 280 nm of 1.90, indicating that the DNA was sufficiently free of protein contamination. The DNA concentration was determined by the UV absorbance at 260 nm and using $\epsilon = 6600 \text{ M}^{-1} \text{ cm}^{-1}$ [21, 44, 75]. Each complex was dissolved in DMSO and diluted in Tris-HCl buffer to make its concentration to 20 µM.

The fixed concentration (20 µM) and volume of complexes were titrated with increasing amount of CT DNA (2-20 µM). The absorption spectra were recorded on the CARY 100 Bio UV-Visible spectrophotometer (Varian Ltd.).

5.2 Ethidium bromide (EB) displacement study by fluorescence spectroscopy

Ethidium bromide (EB) displacement study was used in order to proof the intercalation mechanism. The experiments were performed in Tris-HCl buffer solution (pH 7.2). 10 μM EB was added to 50 μM CT-DNA in Tris-HCl buffer solution and stored in the dark for 1 hour. Then the solution of each complex at 10, 20, 30, 40, 50, and 60 μM were titrated to the DNA-EB mixture. The mixture were shaken and kept in the dark at room temperature for 15 minutes before measurement of fluorescence spectra. The emission spectra were recorded using Perkin Elmer LS45 luminescence spectrometer.

5.3 DNA melting temperature

Thermal denaturation studies were carried out in tris-(hydroxymethyl) aminomethane-HCl (Tris-HCl) buffer solution (pH 7.2) containing 60 μM of CT DNA and 20 μM of the compounds. Melting curves were recorded on the CARY 100 Bio UV-Visible spectrophotometer (Varian Ltd.) equipped with a thermoelectric cell temperature controller and a stirrer unit at 260 nm. The temperature was increased at a rate of 1°C min^{-1} from 20-90 $^\circ\text{C}$. The melting temperature (T_m) was determined by differentiation of the melting curves.

6. DNA cleavage activity

The 100 μM of compounds are used for study the cleavage of pUC19 DNA (2 μL , 0.2 μg) using agarose gel electrophoresis. A 16 μL mixture was irradiated with monochromatic UV-A light (365 nm) for 15 min. in the dark at room temperature follow by addition to 4 μL of GelRed. Electrophoresis was carried out in 1% agarose gel at 50 V for 1 h. in TBE buffer. The bands were visualized by UV light and photographed to determine the extent of DNA cleavage from intensities of the bands using GeneTools software v5.04.

CHAPTER IV

RESULTS AND DISCUSSIONS

Part I Metal complexes of 6-deoxyclitriacetal

1. Molecular Structure Elucidation of 6-deoxyclitriacetal (**L**) and complexes **1** to **4**

1.1 6-deoxyclitriacetal (**L**)

The ^1H NMR spectrum of 6-deoxyclitriacetal (**L**) (Fig. 4.1a, 4.2a) showed H-bonded hydroxyl signal at δ 11.50, two aromatic singlets (H-1 and H-4) at δ 6.67 and 6.49, two meta-coupled proton signals (H-10 and H-8) at δ 5.97 and 6.06, a pair of nonequivalent methylene proton signals (H-6) at δ 4.61 and 4.48, a methine proton (H-6a) at δ 4.58, and three methoxy singlets (OMe-2, OMe-3, and OMe-9) at δ 3.75, 3.77, and 3.82. The IR spectrum of 6-deoxyclitriacetal (**L**) consists of ν_{OH} stretching around 3477 cm^{-1} , $\nu_{\text{C=O}}$ stretching at 1635 cm^{-1} , $\nu_{\text{C=C}}$ stretching 1510 cm^{-1} , $\nu_{\text{C-C}}$ stretching 1453 cm^{-1} , $\nu_{\text{C-OH}}$ stretching at 1351 cm^{-1} , and $\nu_{\text{C-O-C}}$ stretching at 1225 cm^{-1} .

1.2 Fe(III)-6-deoxyclitriacetal complex (**1**)

The ^1H NMR spectra of 6-deoxyclitriacetal Fe(III) complex (**1**) showed resonance shifts relative to the uncoordinated ligand. Because of the metal complexes coordination through hydroxyl and carbonyl group on the ligand's ring, the H-bonded hydroxyl (11-OH) signals were shifted downfield of 0.03 ppm (Fig. 4.1b). Chemical

shifts to higher ppm were observed as a result of an increase in charge delocalization upon complexation through the hydroxyl and carbonyl oxygen atoms with metal ion. Moreover, the broad spectrum at OMe-9, 2 and 3 including the change in coupling constant at aromatic H-10 and 8 are effect from metal coordination (Fig. 4.2b). The broad signal appeared at chemical shift 3.40-3.60 ppm in complex spectra indicating a present of water molecules in complex [13].

Considering the changes in absorption frequencies between IR spectrum of the free and coordinated ligand (Fig. 4.3), a broad band characteristic for ν_{OH} stretching is shift to frequency at 3300-3450 cm^{-1} . It is indicated that there are coordinated water molecules in complex. The characteristic stretching frequency of the carbonyl group ($\nu_{\text{C=O}}$ 1635 cm^{-1}) and $\nu_{\text{C-O}}$ 1225 cm^{-1} in ligand decreased to 1617 cm^{-1} and 1199 cm^{-1} , respectively, in the complex. This suggests that there is the coordination of metal ion through the carbonyl oxygen atom of ligand. Furthermore, the increase vibration frequency of $\nu_{\text{C-OH}}$ in metal complexes appeared to be the increase in bond order of C11-OH. This can be considered as associated with the antisymmetric and symmetric stretching modes of the C-O group at the chelating site. The bonds related to the $\nu_{\text{C=C}}$ and $\nu_{\text{C-O-C}}$ are slightly shift upon complexation indicating that the π bond electrons in C=C and the oxygen in the ring B and C are not involved in the chelation with metal.

Mass spectrum result from MS (MALDI) found m/z for $\text{FeC}_{18}\text{H}_{18}\text{O}_8(\text{H}_2\text{O})_4\text{Cl}_2$: 505.56 (calc. 501.04) (see Appendix A). Elemental analysis with CHNS/O ANALYSER (Perkin Elmer PE2400 SeriesII) to determine percentages of C, H, and N. The gaseous product freed by pyrolysis in high-purity oxygen and were chromatographically separated by frontal analysis with quantitatively detected by thermal conductivity detector. The molecular formula of Fe complex is given in Table 4.2, found (calc.) C

45.54% (45.54%), H 4.98 % (5.08%). However, these results did not confirm the water molecules composition. Therefore, thermogravimetric analysis (TGA) was performed in order to examine the number of water molecules in the complexes.

Thermogravimetric analysis (TGA) was performed under the flow of nitrogen to confirm the number of water molecules in the complexes. The decomposition data are given in Table 4.3 and the thermogram shown in Fig. 4.5, which showed the temperature values for decomposition from 30-800°C along with the corresponding weight loss values. For the Fe(III) complex (**1**), the weight loss of 13% occurs at 30-300°C is attributed to the liberation of four moles of hydrated water molecules (calculated weight 14.37%).

1.3 Co(II)-6-deoxyclitoriacetal complex (2)

The ¹H NMR spectra of Co(II)-6-deoxyclitoriacetal complex (**2**) showed the downfield shift of 11-OH signal of 0.03 ppm and the change in coupling constant at aromatic H-10 and 8 (Fig. 4.1c and 4.2c) are effect from metal coordination through the hydroxyl and carbonyl oxygen. The broad signal which is corresponding to water molecules in complex appeared at chemical shift 3.40-3.60 ppm.

IR spectrum of Co complex (Fig. 4.3), there is a broad band characteristic for ν_{OH} stretching shift to frequency at 3424 cm^{-1} . It is indicated the coordinated water was observed. The characteristic stretching frequency of the carbonyl group ($\nu_{\text{C=O}}$) decreased from 1635 cm^{-1} in free ligand to 1618 cm^{-1} in the complex. This suggests that there is the coordination of metal ion through the carbonyl oxygen atom of

ligand. The vibration frequencies of $\nu_{\text{C-OH}}$ and $\nu_{\text{C-O}}$ in metal complexes increase because the increasing in bond order of C11-OH.

ESI-MS m/z for $\text{CoC}_{19}\text{H}_{18}\text{O}_8(\text{NO}_3)(\text{H}_2\text{O})_2 \cdot 2\text{H}_2\text{O}$: calc. 566.12, found 567.07. The molecular formula of Co(II) complex is given in Table 4.2, found (calc.) C 40.08 % (40.30 %), H 4.93 % (4.42 %).

TGA analysis of Co(II) complex (**2**) data is given in Table 4.3 and the thermogram in Fig. 4.5. The first step occurs at 30-200°C with the weight loss of 11.50% is attributed to the liberation of four moles of hydrated water molecules (calculated weight 12.70%). The second decomposition stage, resulting from the decomposition of nitrate ion (NO_3^-) from 200°C to 280°C with the weight loss of 11.00% (calculated 10.95%).

1.4 Ni(II)-6-deoxyclitoriacetal complex (3)

The H-bonded hydroxyl (11-OH) signal in ^1H NMR spectra for complex **3** was not found. The disappearance of the exchangeable hydrogen peak because the coordinated hydroxy oxygen atom and deprotonated (11-OH) of the metal ion to ligand (Fig. 4.1d). In addition, chemical shift at 2.31 ppm found indicated the composition of acetate (CH_3COO^-) coordinated with metal complex **3**.

The coordinated water was observed in IR spectrum of Ni(II) complex (Fig. 4.3) at a broad band for ν_{OH} stretching at 3445 cm^{-1} . The characteristic stretching frequency of the carbonyl group ($\nu_{\text{C=O}}$) decreased from 1635 cm^{-1} in free ligand to 1622 cm^{-1} in the complex. In addition, $\nu_{\text{C-O}}$ 1225 cm^{-1} in ligand decreased to 1617 cm^{-1}

and 1199 cm^{-1} in the complex. This indicated the coordination of metal ion through the carbonyl oxygen atom of ligand.

MS (MALDI) m/z for $\text{NiC}_{19}\text{H}_{18}\text{O}_8(\text{CH}_3\text{COO})\cdot 4\text{H}_2\text{O}$: calc. 544.90, found 544.78.

The molecular formula of Ni(II) complex is given in Table 4.2, found (calc.) C 43.64 % (46.28 %), H 4.77 % (5.01 %).

From TGA of Ni(II) complex (**3**) (Fig. 4.5), the first step weight loss occurs at 30-200°C of 10.00% is attributed to the liberation of four moles of hydrated water molecules (calculated weight 10.00%). The second decomposition stage, resulting from the decomposition of nitrate ion (CH_3COO^-) from 200°C to 280°C with the weight loss of 10.00% (calculated 11.00%).

1.5 Cu(II)-6-deoxyclitoriacetal complex (4)

The similar ^1H NMR results as complexes **1** to **3** are also found in complex **4**. IR spectrum of Cu complex (Fig. 4.3), the coordinated water molecules were observed from a broad band of ν_{OH} stretching at 3420 cm^{-1} . The indication of the coordination of metal ion through the carbonyl oxygen atom of ligand can be observed from the decrease stretching frequency of the characteristic carbonyl group ($\nu_{\text{C=O}}$) from 1635 cm^{-1} in free ligand to 1618 cm^{-1} in the complex and $\nu_{\text{C-O}}$ from 1225 cm^{-1} in ligand to 1200 cm^{-1} in the complex.

MS (MALDI) m/z for $\text{Cu}(\text{C}_{19}\text{H}_{18}\text{O}_8)_2\cdot 2\text{H}_2\text{O}$: calc. 845.88, found 848.07. The molecular formula of Cu(II) complex is given in Table 4.2, found (calc.) C 53.71% (53.90 %), H 4.56 % (4.72%).

TGA of Cu(II) complex (**4**) (Fig. 4.5) show the first step weight loss of 4.00% at 30-200°C. It is attributed to the liberation of two moles of hydrated water molecules (calculated weight 4.25%).

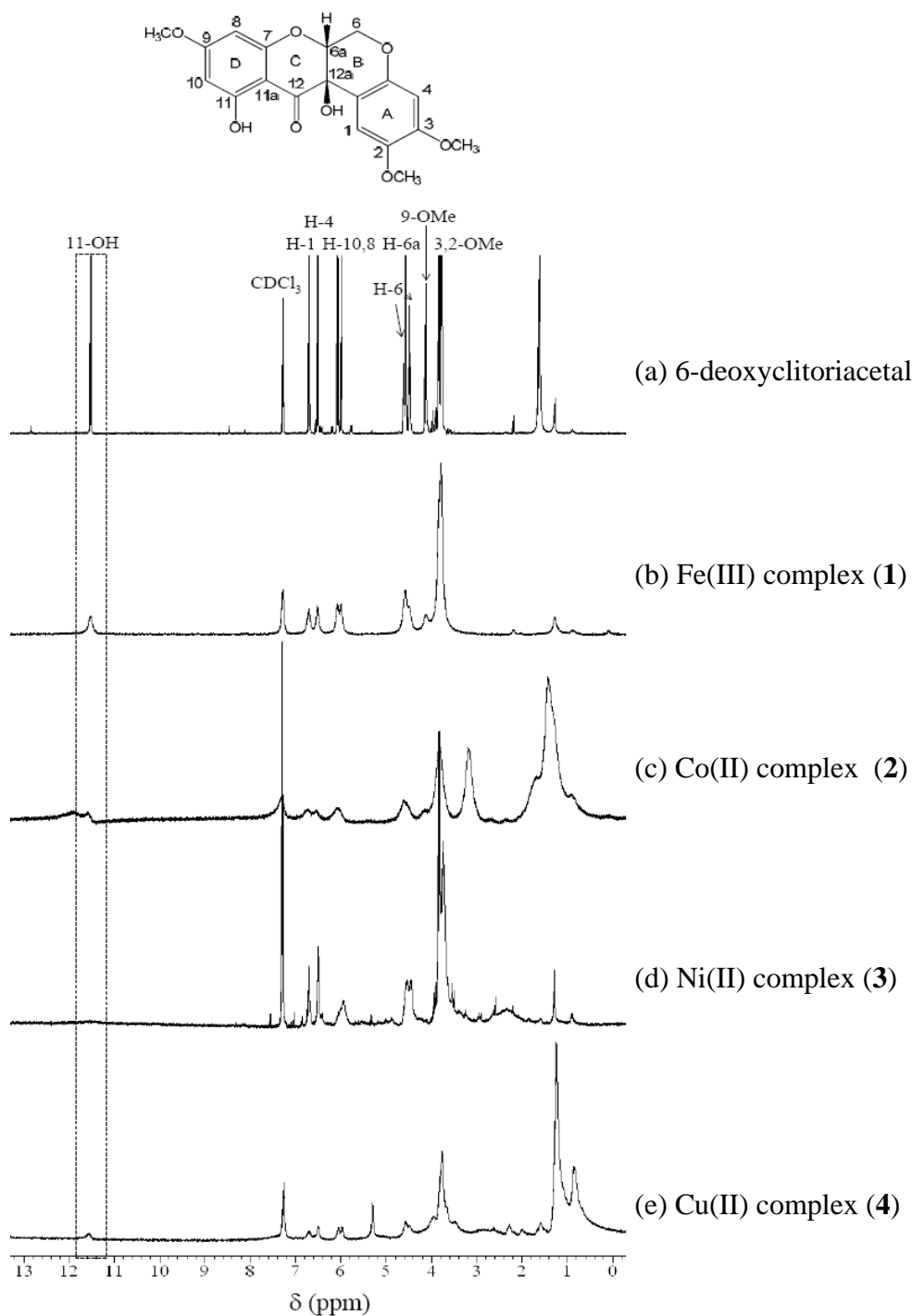


Figure 4.1 ^1H NMR spectra of 6-deoxyclitoriacetal (**L**) (a), Fe complex (**1**) (b), Co(II) complex (**2**) (c), Ni(II) complex (**3**) (d), and Cu(II) complex (**4**) (e)

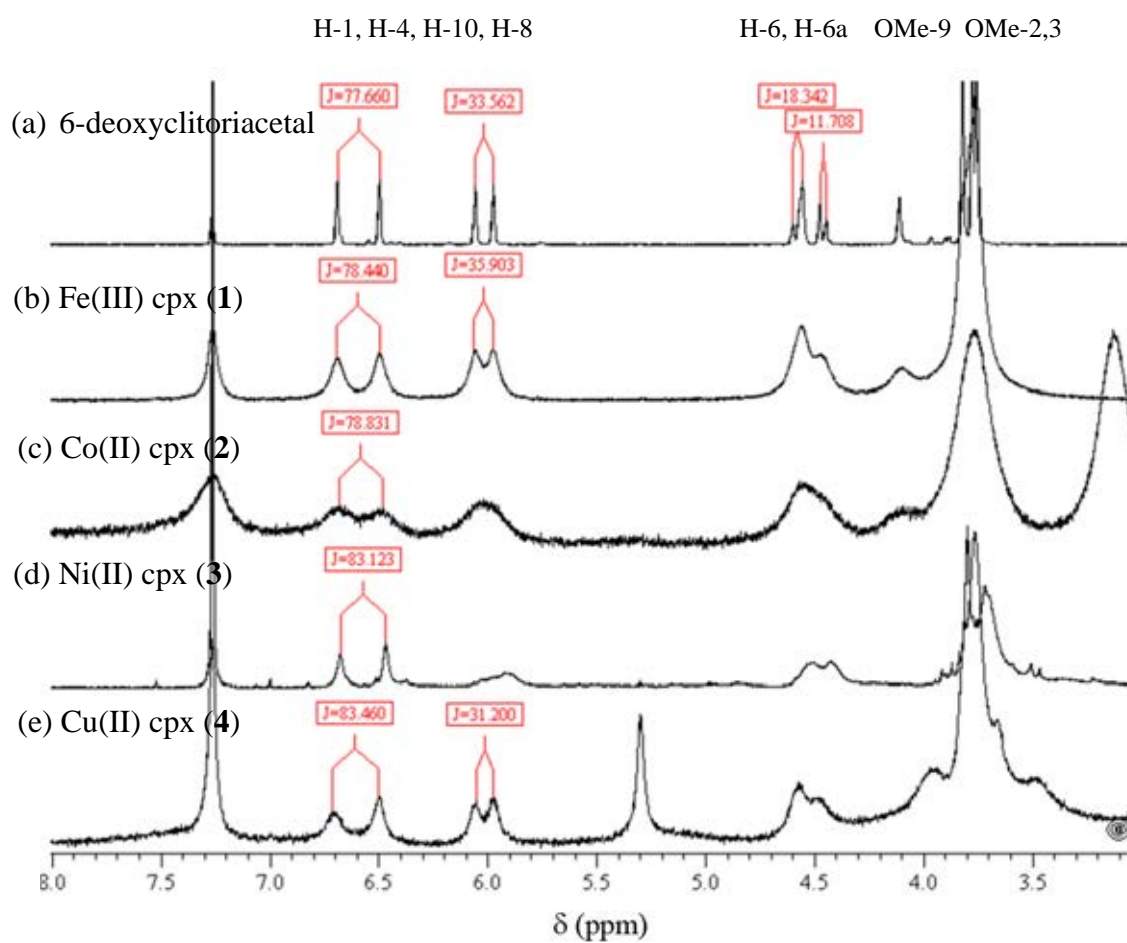


Figure 4.2 Magnified ^1H NMR spectra at 8.00-3.00 ppm for 6-deoxyclitoriacetal (**L**) (a), Fe(III) complex (**1**) (b), Co(II) complex (**2**) (c), Ni(II) complex (**3**) (d), and Cu(II) complex (**4**) (e)

Table 4.1 The selected vibration frequencies of 6-deoxyclitoriacetal and 6-deoxyclitoriacetal-metal complexes.

Complexes	ν_{OH}	$\nu_{\text{C=O}}$	$\nu_{\text{C=C}}$	$\nu_{\text{C-C}}$	$\nu_{\text{C-OH}}$	$\nu_{\text{C-O}}$
L	3477	1635	1510	1453	1351	1225
Fe(III) cpx (1)	3425	1617	1509	1409	1375	1199
Co(II) cpx (2)	3424	1618	1509	1411	1382	1197
Ni(II) cpx (3)	3445	1622	1509	1422	1365	1200
Cu(II) cpx (4)	3420	1618	1508	1420	1377	1200

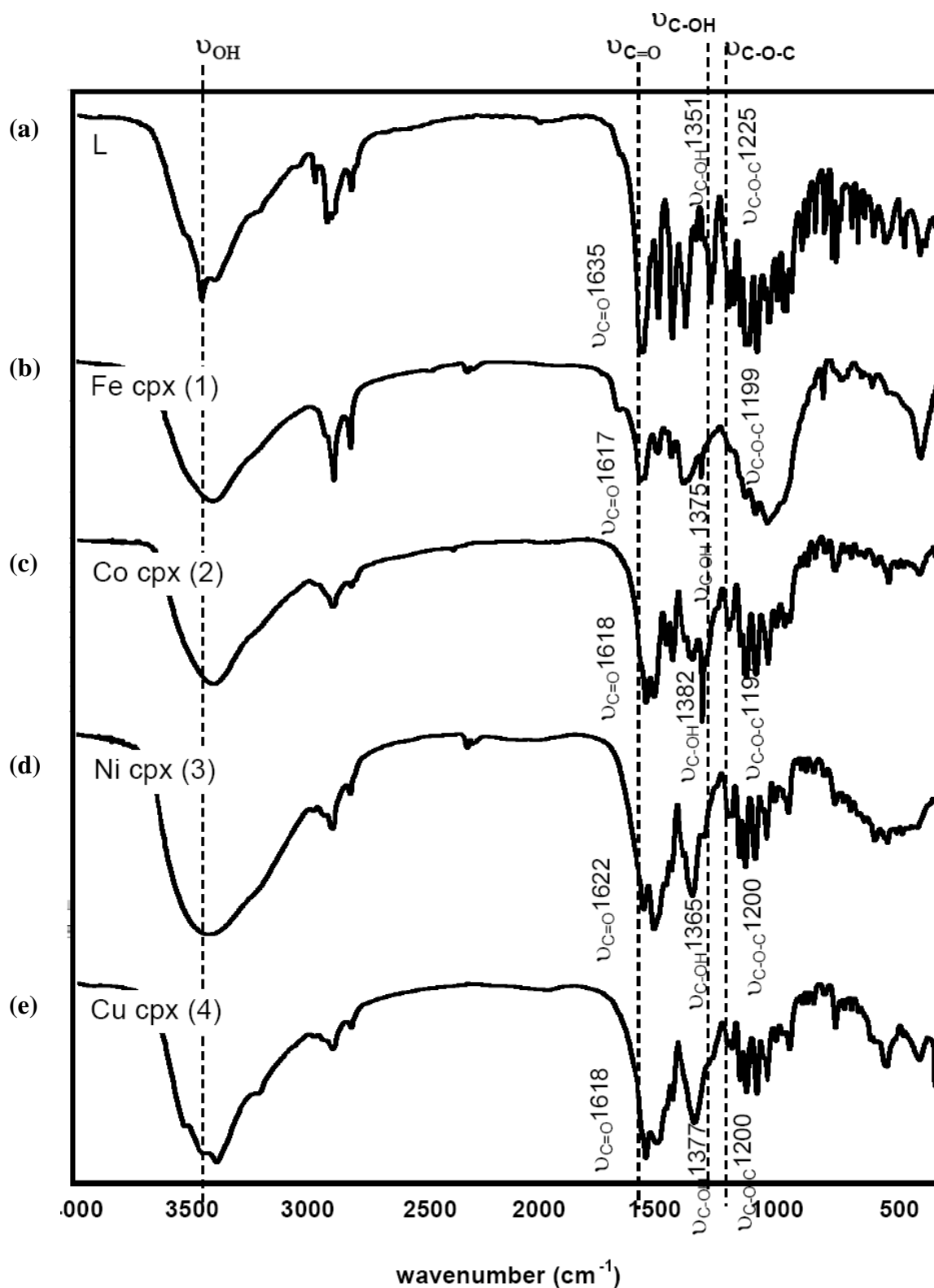


Figure 4.3 IR spectrum of for 6-deoxyclitoriacetal (**L**) (a), Fe(III) complex (**1**) (b), Co(II) complex (**2**) (c), Ni(II) complex (**3**) (d), and Cu(II) complex (**4**) (e)

Table 4.2 Physical properties and percentages of C and H of 6-deoxyclitoriracetal-metal complexes.

Complexes	Molecular Formula	Molecular Weight (g/mol) Found (calc.)	Color	Found (calc.) %	
				C	H
1	$[\text{FeC}_{19}\text{H}_{18}\text{O}_8(\text{H}_2\text{O})_4]\text{Cl}_2$	503.94 (501.04)	Dark orange	45.54 (45.51)	4.98 (5.08)
2	$\text{Co}(\text{C}_{19}\text{H}_{18}\text{O}_8)\text{NO}_3(\text{H}_2\text{O})_2 \cdot 2\text{H}_2\text{O}$	567.07 (566.12)	Dark yellow	40.08 (40.30)	4.93 (4.42)
3	$\text{Ni}(\text{C}_{19}\text{H}_{18}\text{O}_8)\text{CH}_3\text{COO} \cdot 4\text{H}_2\text{O}$	544.78 (544.90)	Light green	43.64 (46.25)	4.77 (5.01)
4	$\text{Cu}(\text{C}_{19}\text{H}_{18}\text{O}_8)_2 \cdot 2\text{H}_2\text{O}$	848.07 (845.88)	Dark green	53.71 (53.90)	4.56 (4.72)

Table 4.3 TGA data of 6-deoxyclitoriacetal-metal complexes.

Complexes	Molecular Formula	MW (g/mol)	T (°C)	Eliminated species	%weight loss	
					Calculated	Found
1	$[\text{FeC}_{19}\text{H}_{18}\text{O}_8(\text{H}_2\text{O})_4]\text{Cl}_2$	501.04	30-300	$4\text{H}_2\text{O}$	14.37	13.00
			300-800	$\text{C}_{19}\text{H}_{17}\text{O}_8^-$	74.45	40.00
2	$\text{Co}(\text{C}_{19}\text{H}_{18}\text{O}_8)\text{NO}_3(\text{H}_2\text{O})_2 \cdot 2\text{H}_2\text{O}$	566.12	30-200	$4\text{H}_2\text{O}$	12.70	11.50
			200-280	NO_3^-	10.95	11.00
3	$\text{Ni}(\text{C}_{19}\text{H}_{18}\text{O}_8)\text{CH}_3\text{COO} \cdot 4\text{H}_2\text{O}$	544.9	280-800	$\text{C}_{19}\text{H}_{17}\text{O}_8^-$	67.07	65.00
			30-200	$4\text{H}_2\text{O}$	10.00	10.00
4	$\text{Cu}(\text{C}_{19}\text{H}_{17}\text{O}_8)_2 \cdot 2\text{H}_2\text{O}$	845.88	200-280	CH_3COO^-	11.00	10.00
			280-800	$\text{C}_{19}\text{H}_{17}\text{O}_8^-$	68.49	70.00
4	$\text{Cu}(\text{C}_{19}\text{H}_{17}\text{O}_8)_2 \cdot 2\text{H}_2\text{O}$	845.88	30-200	$2\text{H}_2\text{O}$	4.25	4.00
			280-800	$\text{C}_{19}\text{H}_{17}\text{O}_8^-$	88.00	45.00

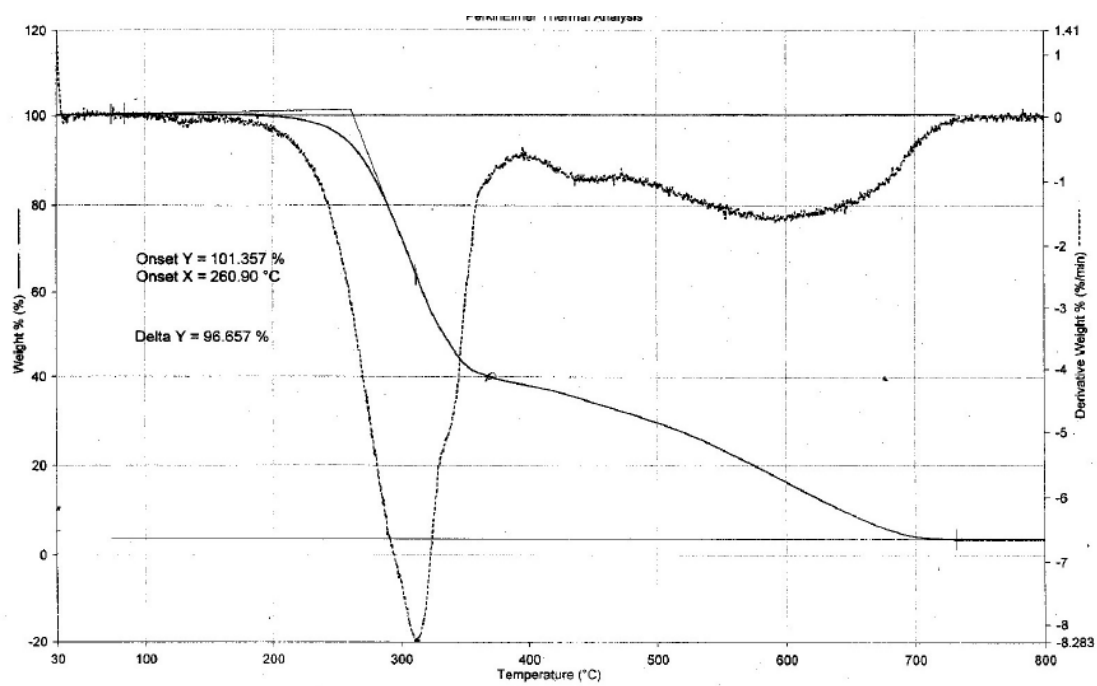


Figure 4.4 TGA thermogram of 6-deoxyclitriacetal.

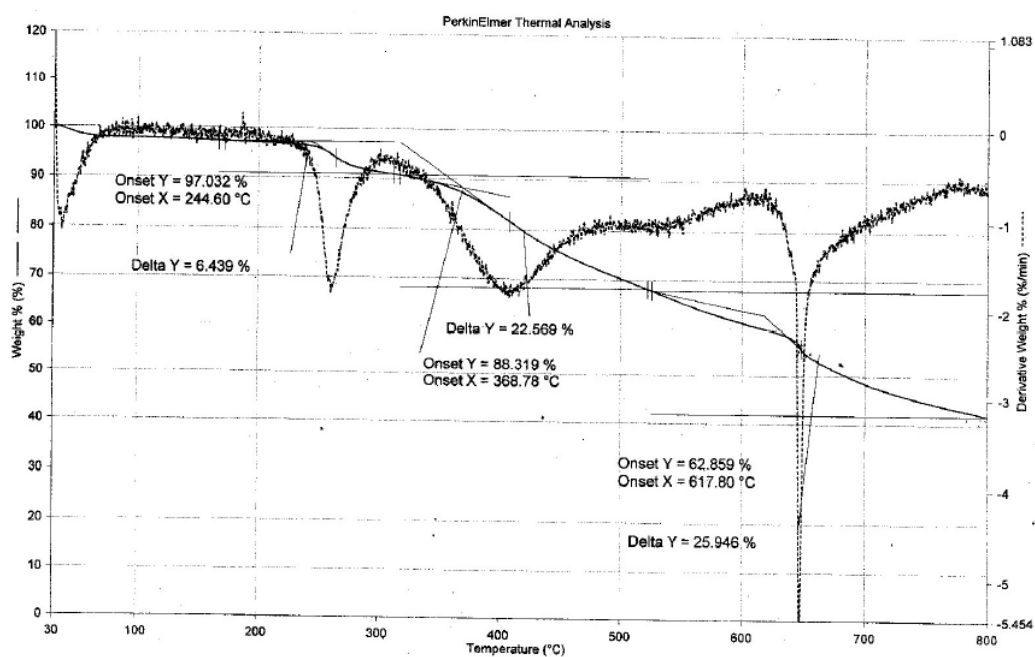
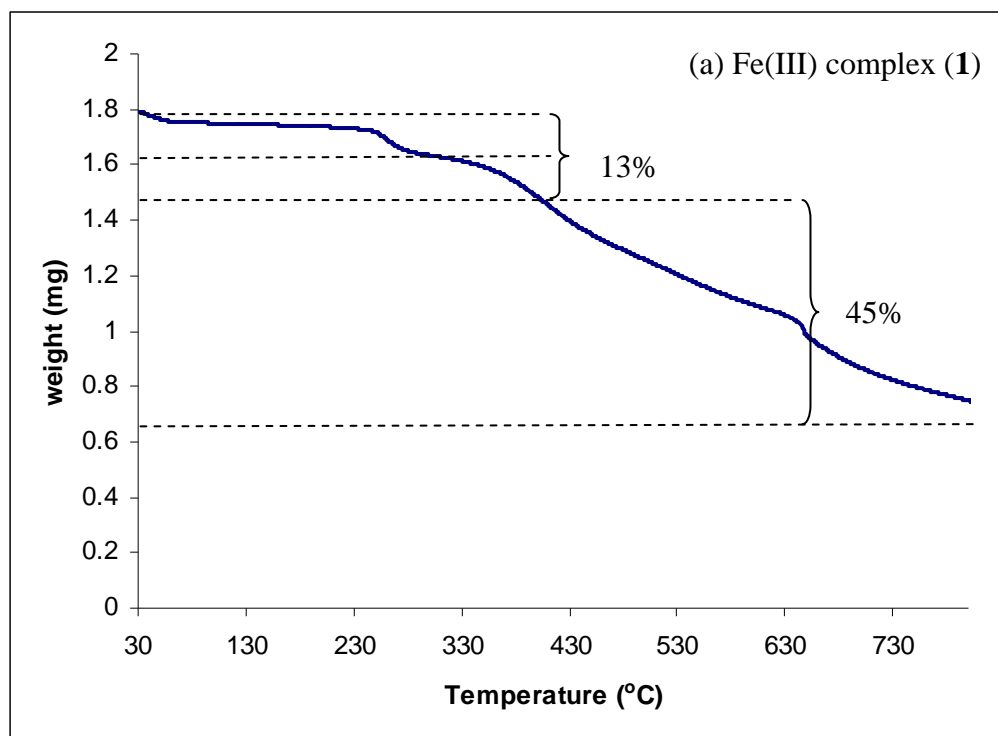


Figure 4.5 TGA thermograms of 6-deoxyclitoriacetal metal complexes of Fe(III) complex (1) (a), Co(II) complex (2) (b), Ni(II) complex (3) (c), and Cu(II) complex (4) (d).

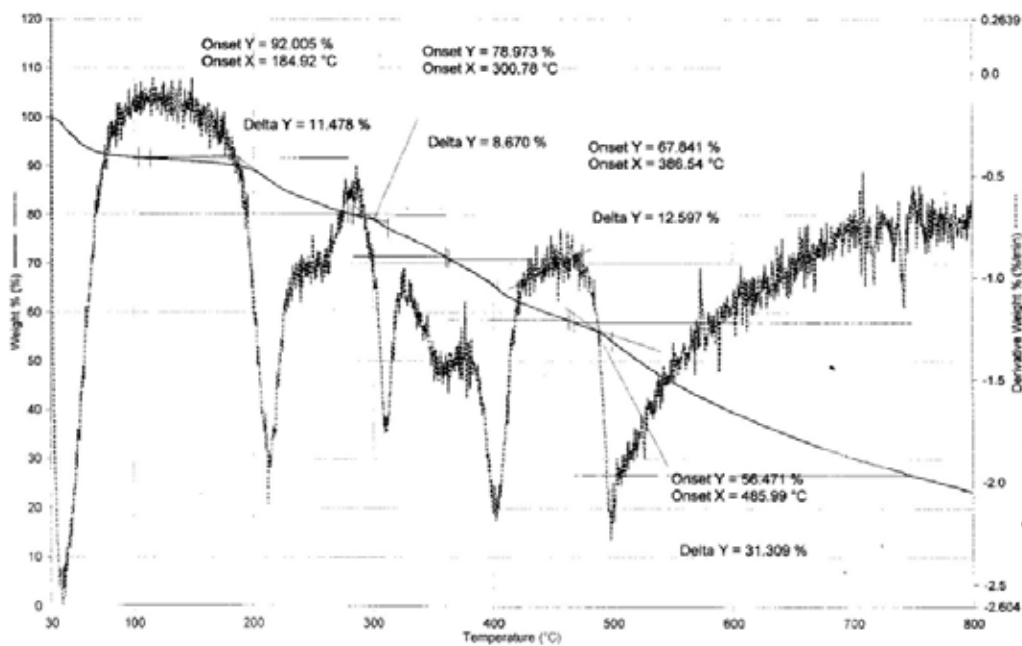
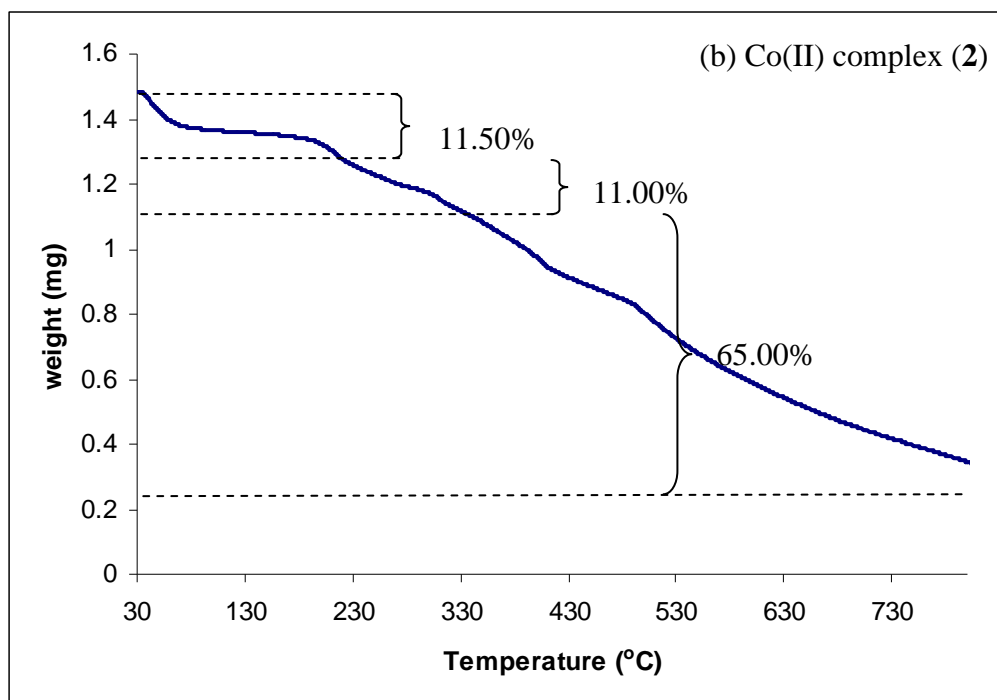


Figure 4.5 con't TGA thermograms of 6-deoxyclitoriacetal metal complexes of Fe(III) complex (1) (a), Co(II) complex (2) (b), Ni(II) complex (3) (c), and Cu(II) complex (4) (d).

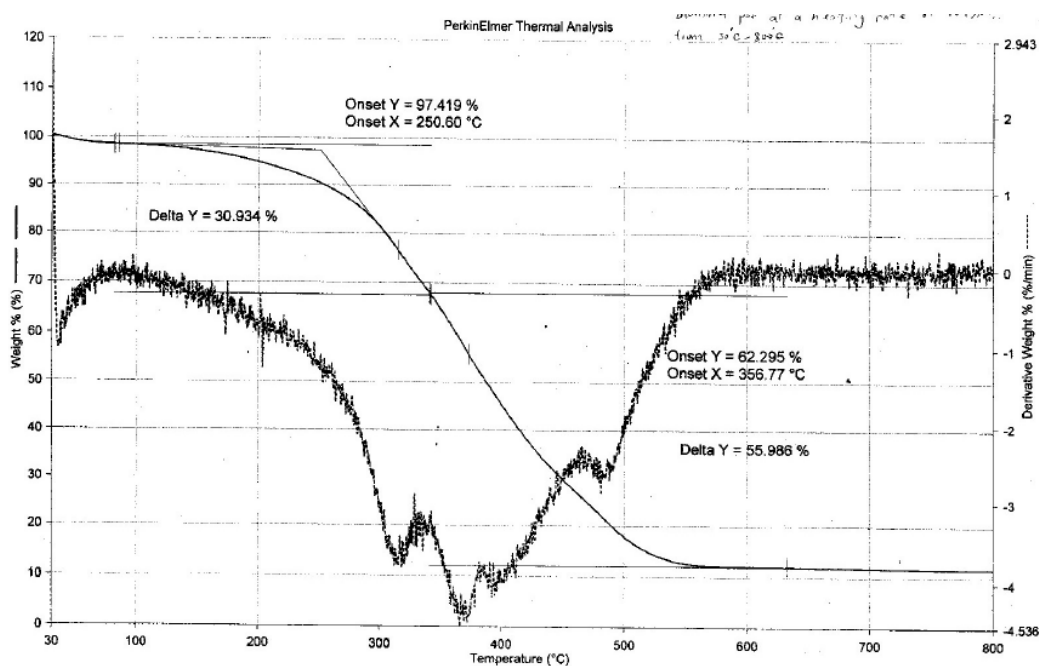
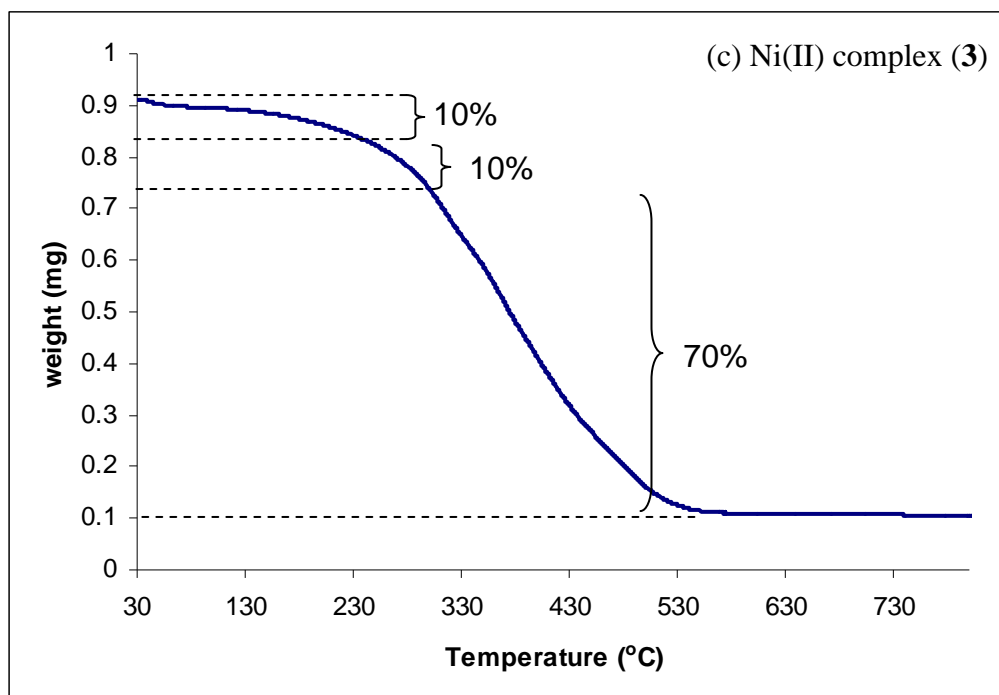


Figure 4.5 con't TGA thermograms of 6-deoxyclitriacetal metal complexes of Fe(III) complex (1) (a), Co(II) complex (2) (b), Ni(II) complex (3) (c), and Cu(II) complex (4) (d).

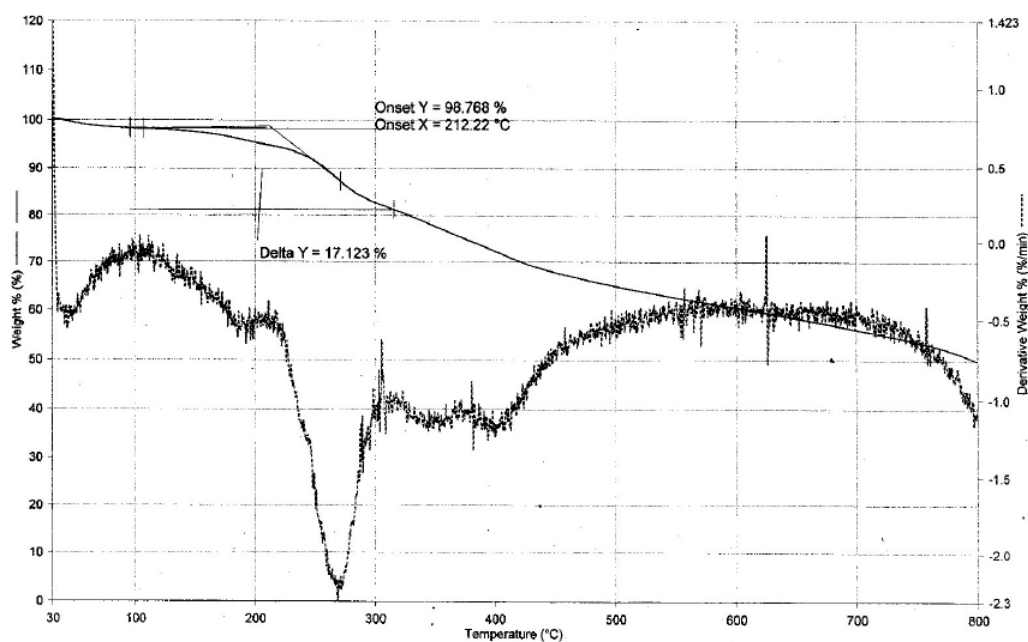
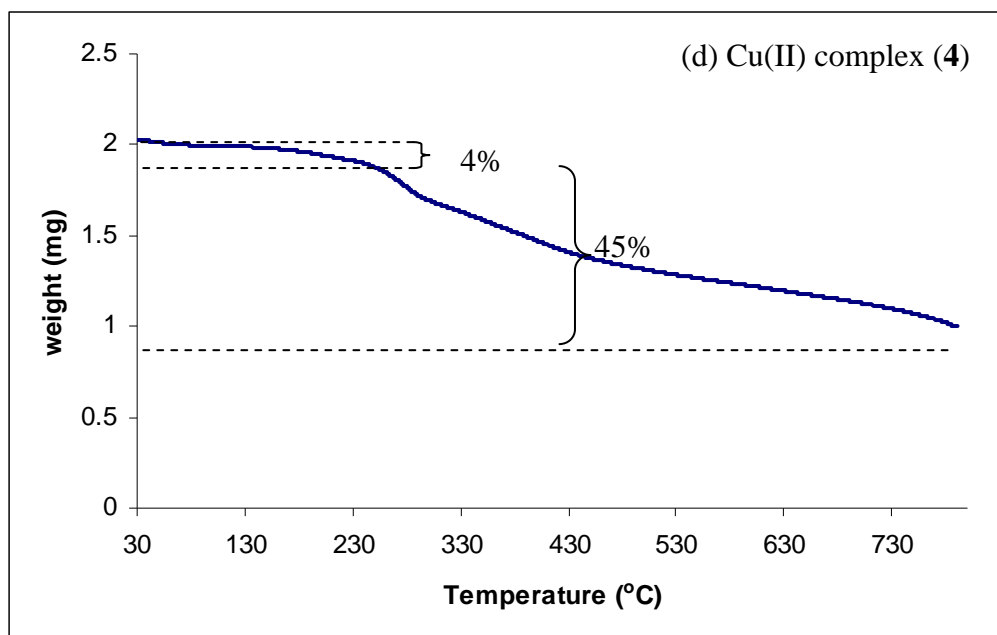


Figure 4.5' cont TGA thermograms of 6-deoxyclitriacetal metal complexes of Fe(III) complex (1) (a), Co(II) complex (2) (b), Ni(II) complex (3) (c), and Cu(II) complex (4) (d).

1.6 Stoichiometric study (Job's Plot)

Complex formation was studied in solutions to obtain the molar ratio of the ligand to metal ion (L: M) using methanol solvents. A series of solutions containing constant concentration of the ligand (10 μM) were treated with increasing amounts of the metal salt (0-10 μM). The results of (L:M) ratio were obtained by plotting absorbance of solution mixtures at detected λ_{max} against $[\text{M}]/[\text{M}+\text{L}]$ (Fig. 4.6).

The maximum absorbance of 6-deoxyclitoriacetal is at 292 nm. The absorbance was decrease when adding the solution of $\text{FeCl}_3 \cdot 6\text{H}_2\text{O}$ to the solution of 6-deoxyclitoriacetal and the characteristic absorbance shift to 296 nm. The decrease of intensity and the red shift occurred because of the coordination between 6-deoxyclitoriacetal and Fe(III) ion. The lowest absorbance found at the fraction $[\text{Fe}]/[\text{Fe} + 6\text{D}]$ of 0.5. This confirms that the stoichiometric ratio for complex of Fe(III) and 6- deoxyclitoriacetal is 1:1.

For 6-deoxyclitoriacetal when added with Co(II) ion showed the similar results as when added with Ni(II) ion. The spectra intensity at 292 nm of 6-deoxyclitoriacetal was increase to the highest absorbance at the fraction $[\text{M}]/[\text{M} + 6\text{D}]$ of 0.5. This confirms that the stoichiometric ratio for complex of Co(II) and Ni(II) to 6- deoxyclitoriacetal is 1:1.

For 6-deoxyclitoriacetal when added with Cu(II) ion, the spectral intensity at 292 nm was decrease to the lowest absorbance at the fraction $[\text{Cu}]/[\text{Cu} + 6\text{D}]$ of 0.3. This confirms that the stoichiometric ratio for complex of Cu(II) and 6-deoxyclitoriacetal is 1:2. From this study, it can be conclude that M:L ratio when M = Fe(III), Co(II), and Ni(II) to L = 6-deoxyclitoriacetal are 1:1. While M = Cu(II), the M:L ratio is 1:2.

From the results of characterization by spectroscopic method, EA, and TGA, the proposed formula of Fe(III), Co(II), Ni(II), and Cu(II) complexes are $[\text{FeC}_{19}\text{H}_{18}\text{O}_8(\text{H}_2\text{O})_4]\text{Cl}_2$, $\text{Co}(\text{C}_{19}\text{H}_{18}\text{O}_8)\text{NO}_3(\text{H}_2\text{O})_2 \cdot 2\text{H}_2\text{O}$, $\text{Ni}(\text{C}_{19}\text{H}_{18}\text{O}_8)\text{CH}_3\text{COO} \cdot 4\text{H}_2\text{O}$, and $\text{Cu}(\text{C}_{19}\text{H}_{18}\text{O}_8)_2 \cdot 2\text{H}_2\text{O}$, respectively.

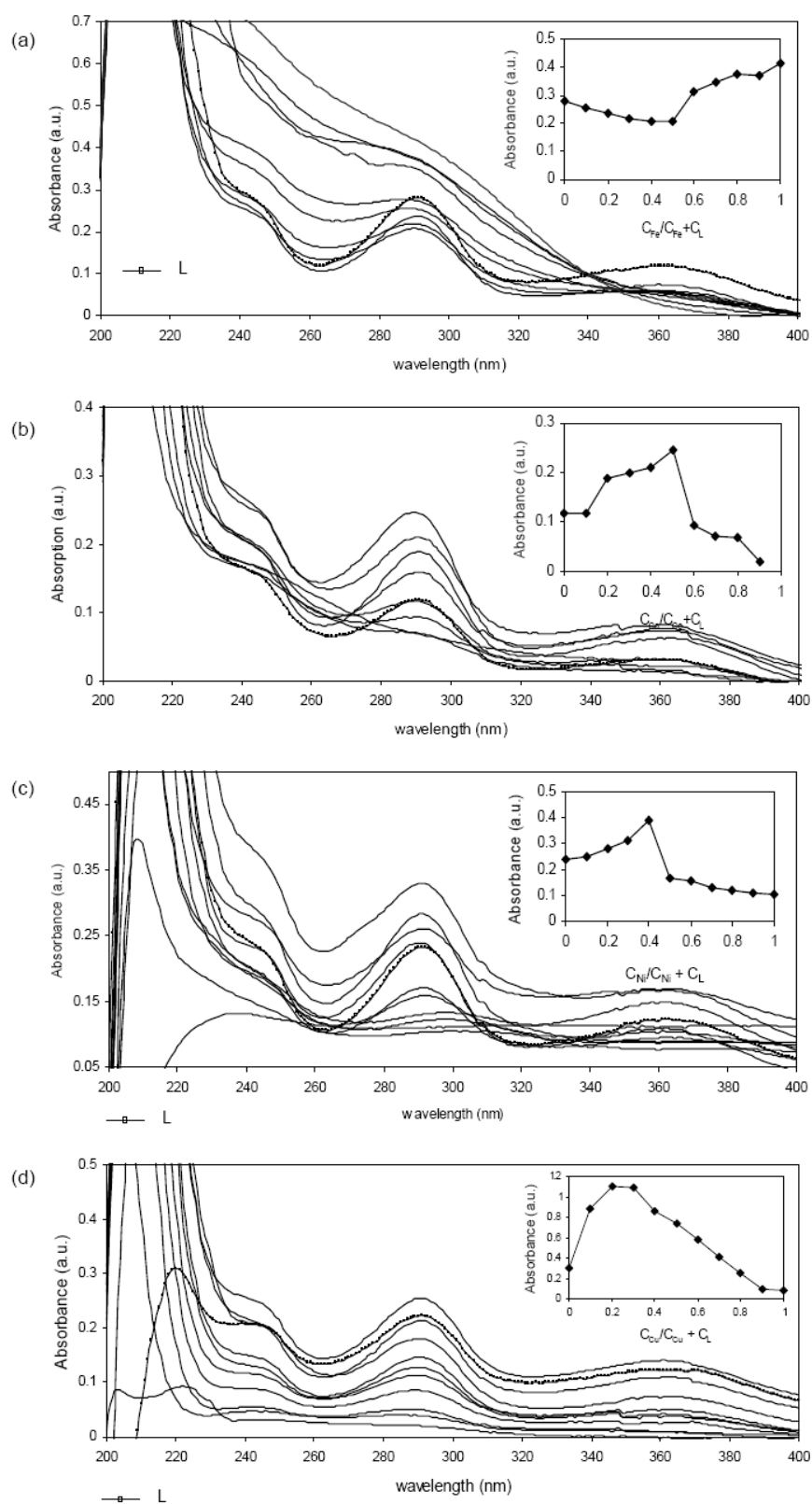


Figure 4.6 Job's plot of the complex formation of ligand (L) with metal ions of Fe(III) (a), Co(II) (b), Ni(II) (c), and Cu(II) (d) monitored by UV-Vis spectrophotometer.

1.7 Summary of molecular structures

From the characterization of 6-deoxyclitoriacetal-metal complexes using Mass, ^1H NMR, and IR spectroscopic method including EA, TGA, and Job's plot, the molecular structure and reaction mechanism of metal complexes can be proposed as the following equations (Fig. 4.7).

Molecular geometries of 6-deoxyclitoriacetal-metal complexes

The 3d metal like Fe(III) always be found in octahedral geometry, while Co(II), Ni(II), and Cu(II) can form different geometries: octahedral, tetrahedral, and square planar. In order to propose the molecular structures of 6-deoxyclitoriacetal-metal complexes the geometry optimizations using MM2 CS Chem office version 11.0 molecular modeling program was carried out. Total energy and the theoretical physical parameters are calculated. 1,3 van der Waals interactions are used to compute the energy of angles around atoms with more than 4 coordinate bonds. The calculated geometries of the lowest energy conformers were used in subsequent frequency calculation and vibrational analysis. The geometry optimization for the compounds was carried out without constraints. Total calculated energies of the prepared metal complexes are in Table 4.4.

In general, Cobalt(II) forms both tetrahedral and octahedral complexes; square planar complexes are very rare. As a $3d^7$ system, cobalt(II) complexes have 3 unpaired electrons. With moderate to strong-field ligands, cobalt(II) complexes tend to be easily oxidized to cobalt(III). As 6-deoxyclitoriacetal is a weak field ligand, Cobalt(II) complexes tend to be found in a high-spin octahedral complex. The optimization geometry and energy are shown in Table 4.4b.

Nickel(II) commonly forms complexes with three different geometries: octahedral, tetrahedral, and square planar. Some five-coordinate complexes are known but are rare. Nickel(II) is a $3d^8$ system so octahedral and tetrahedral complexes will have 2 unpaired electrons and square planar complexes usually will have none. Octahedral complexes can be prepared from both strong field and weak field ligands (or a mixture of both). Among four-coordinate nickel(II) complexes, those with strong field ligands tend to be square planar and those with weak field ligands tend to be tetrahedral. The optimization tetrahedral geometry of Ni(II) complex is proposed in Table 4.4d. The stabilization energy of tetrahedral geometry is lower than octahedral geometry. This indicated that Ni(II) complex of 6-dexyclitriacetal prefer to form tetrahedral geometry.

Copper(II) $3d^9$ system commonly forms complexes with three different geometries: octahedral, tetrahedral, and square planar. The optimization octahedral and tetrahedral geometry of Cu(II) complex are proposed in Table 4.4e-f. The stabilization energy of tetrahedral geometry is lower than octahedral geometry. This indicated that Cu(II) complex of 6-dexyclitriacetal prefer to form tetrahedral geometry.

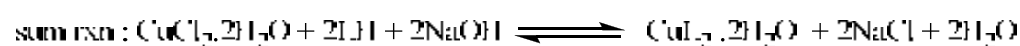
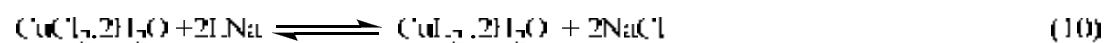
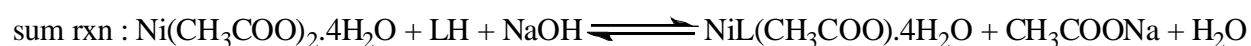
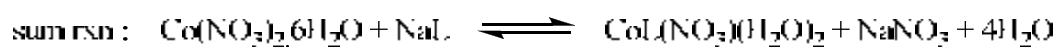
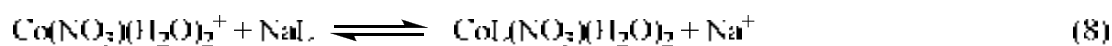
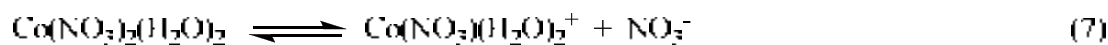
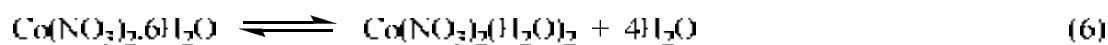
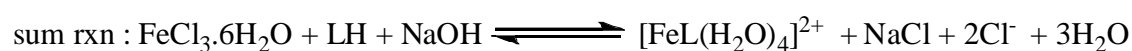
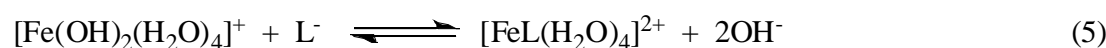
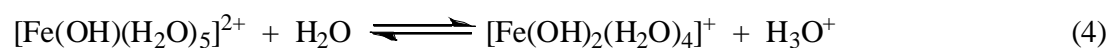


Figure 4.7 Propose reaction mechanisms of 6-deoxyclitoriacetal-metal complexes.

Table 4.4 The proposed molecular structure, optimized geometry and MM2 minimization energy of 6-deoxyclitoriacetal-metal complexes.

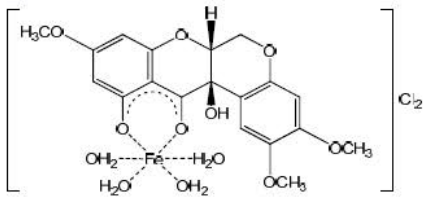


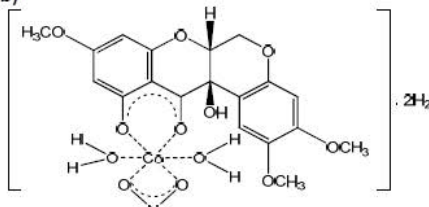
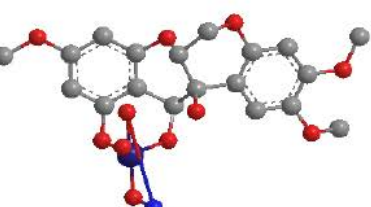
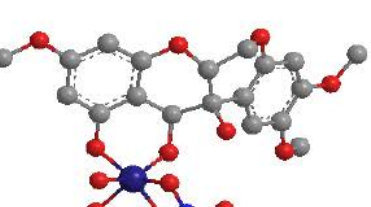
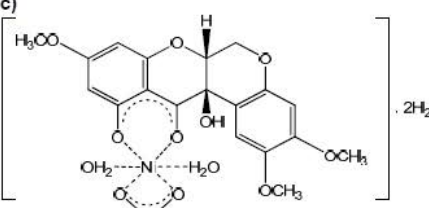

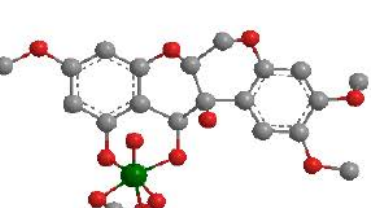
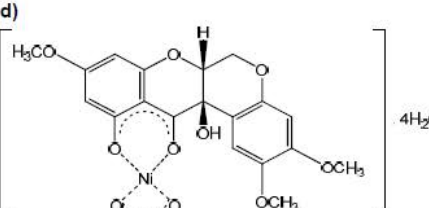
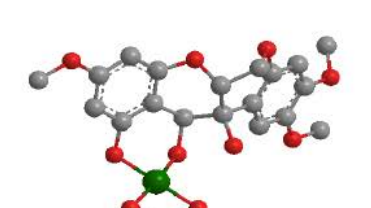
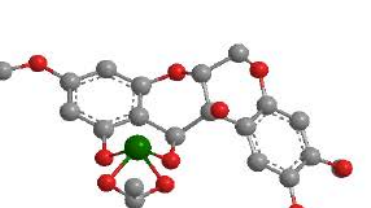
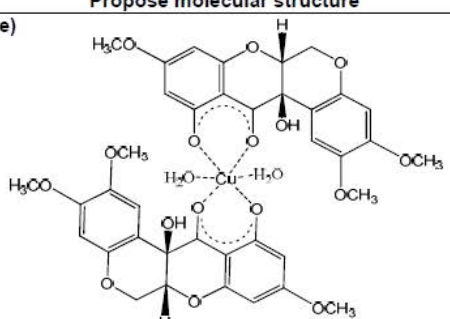
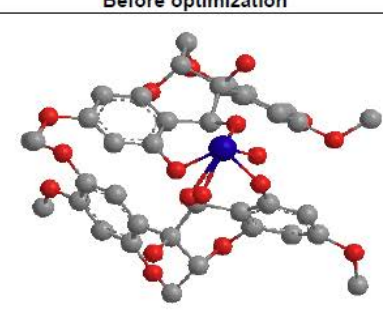
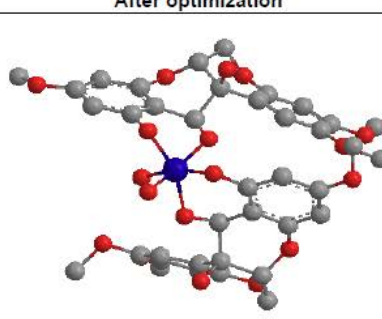
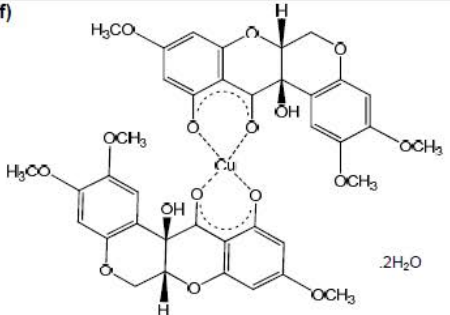
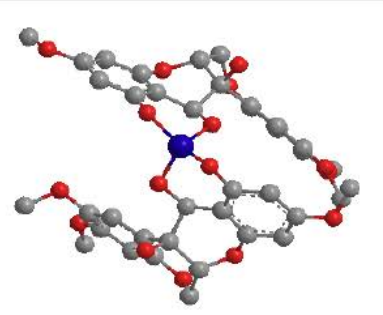
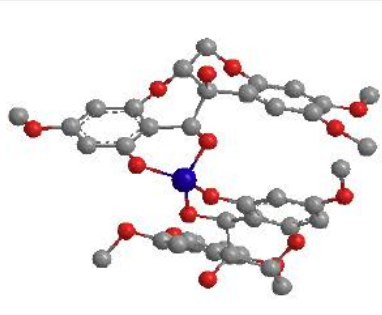
Propose molecular structure	Before optimization	After optimization	MM2 Minimization
<p>(a)</p>  <p>Cl_2</p>			Stretch 27.8093 Bend 109.2484 Stretch-Bend 0.3579 Torsion -6.9526 Non-1,4 VDW -11.5058 1,4 VDW 15.3588 Dipole/Dipole -16.5619 Total Energy 117.7541 kcal/mol
<p>(b)</p>  <p>$\cdot 2\text{H}_2\text{O}$</p>			Stretch 34.618 Bend 118.2814 Stretch-Bend 0.2939 Torsion -10.3216 Non-1,4 VDW -16.5064 1,4 VDW 27.8537 Dipole/Dipole 4.7233 Total Energy 158.9422 kcal/mol
<p>(c)</p>  <p>$\cdot 2\text{H}_2\text{O}$</p>			Stretch 31.1503 Bend 111.8644 Stretch-Bend 0.0091 Torsion -6.1114 Non-1,4 VDW -14.6434 1,4 VDW 25.7955 Dipole/Dipole -1.1249 Total Energy 146.9395 kcal/mol
<p>(d)</p>  <p>$4\text{H}_2\text{O}$</p>			Stretch 3.0795 Bend 50.6806 Stretch-Bend 0.01 Torsion -5.8574 Non-1,4 VDW -11.1407 1,4 VDW 36.1034 Dipole/Dipole 6.3597 Total Energy 79.2350 kcal/mol

Table 4.4'cont The proposed molecular structure, optimized geometry and MM2 minimization energy of 6-deoxyclitoriacetal-metal complexes.

	Propose molecular structure	Before optimization	After optimization	MM2 Minimization																
(e)	 <p>Proposed molecular structure of a copper complex coordinated to two water molecules (H_2O).</p>			<table border="0"> <tr><td>Stretch</td><td>32.3256</td></tr> <tr><td>Bend</td><td>112.1365</td></tr> <tr><td>Stretch-Bend</td><td>0.7662</td></tr> <tr><td>Torsion</td><td>-13.8256</td></tr> <tr><td>Non-1,4 VDW</td><td>-36.112</td></tr> <tr><td>1,4 VDW</td><td>56.1369</td></tr> <tr><td>Dipole/Dipole</td><td>1.1397</td></tr> <tr><td>Total Energy</td><td>152.5673 kcal/mol</td></tr> </table>	Stretch	32.3256	Bend	112.1365	Stretch-Bend	0.7662	Torsion	-13.8256	Non-1,4 VDW	-36.112	1,4 VDW	56.1369	Dipole/Dipole	1.1397	Total Energy	152.5673 kcal/mol
Stretch	32.3256																			
Bend	112.1365																			
Stretch-Bend	0.7662																			
Torsion	-13.8256																			
Non-1,4 VDW	-36.112																			
1,4 VDW	56.1369																			
Dipole/Dipole	1.1397																			
Total Energy	152.5673 kcal/mol																			
(f)	 <p>Proposed molecular structure of a copper complex coordinated to two water molecules (H_2O).</p>			<table border="0"> <tr><td>Stretch</td><td>5.4737</td></tr> <tr><td>Bend</td><td>30.8636</td></tr> <tr><td>Stretch-Bend</td><td>0.4843</td></tr> <tr><td>Torsion</td><td>-14.5835</td></tr> <tr><td>Non-1,4 VDW</td><td>-23.6928</td></tr> <tr><td>1,4 VDW</td><td>58.351</td></tr> <tr><td>Dipole/Dipole</td><td>4.7468</td></tr> <tr><td>Total Energy</td><td>61.6432 kcal/mol</td></tr> </table>	Stretch	5.4737	Bend	30.8636	Stretch-Bend	0.4843	Torsion	-14.5835	Non-1,4 VDW	-23.6928	1,4 VDW	58.351	Dipole/Dipole	4.7468	Total Energy	61.6432 kcal/mol
Stretch	5.4737																			
Bend	30.8636																			
Stretch-Bend	0.4843																			
Torsion	-14.5835																			
Non-1,4 VDW	-23.6928																			
1,4 VDW	58.351																			
Dipole/Dipole	4.7468																			
Total Energy	61.6432 kcal/mol																			

2. Bioassay

The cytotoxic activity was conducted by the MTT assay with human cancer cell lines of; lung carcinoma (CHAGO), hepato carcinoma (Hep-G2), gastric carcinoma (KATO3), colon carcinoma (SW620), and human breast carcinoma (BT474). The inhibition of cell growth (IC_{50}) values, defined as a dose of compound that inhibits cell growth by 50%, were calculated from concentration-response curves (see Appendix A). The IC_{50} values are distinguished into 3 groups i) strong ($IC_{50} = 0.00 - 0.20 \mu\text{M}$), ii) moderate ($IC_{50} = 0.21 - 0.50 \mu\text{M}$), and iii) weak ($IC_{50} > 0.50 \mu\text{M}$). The IC_{50} values are shown in Table 4.5.

For **L**, it exhibited the strongest activity against BT474 tested cell lines ($2.67 \times 10^{-3} \mu\text{M}$). It is also show strong activity against HEP-G2 ($0.163 \mu\text{M}$), which is stronger than **2** ($0.21 \mu\text{M}$) and **3** ($0.21 \mu\text{M}$). The moderate activity found against KB, NCI-H187 and MCF7.

For Fe(III) complex (**1**), it showed the strongest activity against KB ($IC_{50} 5.33 \times 10^{-3} \mu\text{M}$), while moderate cytotoxicity against another cell lines.

For Co(II) complex (**2**), it is strongly active to NCI-H187, CHAGO, and SW620 with $IC_{50} 5.56 \times 10^{-3} \mu\text{M}$, $6.90 \times 10^{-3} \mu\text{M}$, and $0.07 \mu\text{M}$, respectively, which are stronger than the activity of doxorubicin and cisplatin to these cell lines.

For Ni(II) complex (**3**), the strong activity has found against KATO3 and BT474 with $IC_{50} 2.00 \times 10^{-3} \mu\text{M}$, $4.33 \times 10^{-2} \mu\text{M}$, respectively, which are stronger than the activity of doxorubicin and cisplatin to these cell lines.

For Cu(II) complex (**4**), it showed the strong activity against most tested cell lines but it is inactive to KB and it has stronger cytotoxicity than **L** and cisplatin

against all tested cell lines. Moreover, its cytotoxicity is stronger than doxorubicin for KATO3 and BT474.

From these results, it is noticed that the different metal center showed the different potent cytotoxic activity against the tested cell lines. Furthermore, these compounds are non-toxicity to normal cell lines CCD and HS27.

Compare the cytotoxic activity of these compounds to doxorubicin and cisplatin which are commercial drugs, Cu(II) complex (**4**) of 6-deoxyclitoriacetal shows stronger activity against many cell lines (KATO3, BT474, Hep-G2, SW620). Fe(III) complex (**1**) have stronger activity against KATO3, BT474, Hep-G2, and KB. Co(II) and Ni(II) complex (**2** and **3**) also have stronger cytotoxic activity to various cellines (Table 4.5). The stronger cytotoxic activities than doxorubicin and cisplatin of these metal complexes and its non-toxicity properties to normal cell displayed that these novel compounds can be new alternative anticancer agents.

Table 4.5 Inhibition of cell growth and toxicity to normal cell lines of 6-deoxyclitoriacetal and metal complexes.

	IC50 (μM)							Normal Cell ⁱⁱⁱ		
	CHAGO	KATO3	BT474	Hep-G2	SW620	KB ⁱ	NCI-H187 ⁱ	MCF7 ⁱ	CCD	HS27
Doxorubicin	6.13E-02	9.60E-02	0.15	8.83E-02	4.26E-02	0.28	0.16	7.83E-02	Toxic	Toxic
Cisplatin	0.18	0.22	0.29	0.25	0.24	- ⁱⁱ	- ⁱⁱ	- ⁱⁱ	Toxic	Toxic
L	0.22	0.14	2.67E-03	0.14	0.20	0.76	0.66	0.65	Non-toxic	Non-toxic
1	0.27	0.15	0.12	0.19	0.17	5.33E-03	0.27	0.39	Non-toxic	Non-toxic
2	6.90E-03	0.37	0.14	0.21	7.10E-02	inactive ^{iv}	5.56E-03	0.22	Non-toxic	Non-toxic
3	0.21	2.00E-03	4.33E-02	0.21	0.13	inactive ^{iv}	0.41	0.14	Non-toxic	Non-toxic
4	0.15	9.30E-02	7.40E-02	9.80E-02	6.00E-02	inactive ^{iv}	0.24	0.15	Non-toxic	Non-toxic

ⁱ Tested by the National Center for Genetic Engineering and Biotechnology (BIOTEC), National Science and Technology Development Agency (NSTDA), Bangkok, Thailand.

ⁱⁱ Not tested

ⁱⁱⁱ Test at 100 $\mu\text{g}/\text{mL}$

^{iv} IC50 > 100 μM

3. DNA binding studies

DNA is the primary intracellular target of anticancer drugs because the interaction between small molecules and it can cause DNA damage in cancer cells, blocking the division of cancer cells and resulting in cell death [12]. Understanding of the binding properties is needed in developing new potential DNA targeting antitumor drugs. Metal complexes generally interact with double helix DNA in either non-covalent or covalent interaction. The non-covalent way includes intercalation, groove binding and external static electronic effects. The intercalation is one of the most important DNA binding modes. It was reported that the intercalating ability appeared to increase with the planarity of ligands [14-15]. In the case of covalent binding, the labile ligand of the complexes is replaced by a nitrogen base of DNA such as guanine N7. In addition, the coordination geometry and ligand donor atom type also play the key roles in determining the binding extent of complexes to DNA [16, 17]. The metal ion type and its flexible valence, which are responsible for the geometry of complexes, also affect the intercalating ability of metal complexes to DNA [18].

In order to study the interaction between drugs and DNA, titration by UV-Vis spectroscopic method, ethidium bromide displacement by fluorescence spectroscopic method, and the thermal denaturation study of CT-DNA (T_m) have been widely performed.

3.1 DNA-binding study by UV-Vis spectroscopic method

Titration with UV absorption spectroscopy is an effective method to examine the binding mode of DNA with metal complexes [19]. In the intercalative binding mode, the π^* orbital of the intercalating ligand can couple with the π orbital of the

DNA base pairs, thus, decreasing $\pi \rightarrow \pi^*$ transition energy and resulting in the bathochromism. On the other hand, the coupling π orbital is partially filled by electrons, thus, decreasing the transition probabilities and concomitantly resulting in hypochromic [20].

In order to study the binding ability of the compounds with DNA quantitatively, the fixed concentration and volume of complexes were titrated with increasing amount of CT-DNA (Fig.4.8). The behavior of these compounds is quite similar. The absorption spectra showed a $\pi \rightarrow \pi^*$ transition band at 290-292 nm. When increasing amount of DNA, hypochromic peak were at 290 nm of all compounds and presented the red shift. This hypochromism and red shift indicated that the compounds probably interact with CT-DNA by intercalation mode, involving a strong π -stacking between aromatic rings of the compounds and DNA base pairs [21]. In addition, the absorption intensity at 258-260 nm is increased because of the strong binding of the compound to DNA

The following equation was used to calculate for K_b in order to compare the binding ability quantitatively,

$$[DNA]/(\varepsilon_a - \varepsilon_f) = [DNA]/(\varepsilon_b - \varepsilon_f) + 1/K_b(\varepsilon_b - \varepsilon_f)$$

Where ε_a , ε_f , and ε_b are the apparent extinction coefficient, the extinction coefficient for free compound, and the extinction coefficient for compound fully bound to DNA, respectively. The binding constant (K_b) has been determined using the plots of $[DNA]/(\varepsilon_a - \varepsilon_f)$ versus $[DNA]$. From the plots of $[DNA]/(\varepsilon_a - \varepsilon_f)$ versus $[DNA]$, shown in Fig. 4.8, the binding constants (K_b) are given by the ratio of the

slope to the intercept. The intrinsic binding constant (K_b) of 6-deoxyclitoriacetal and metal complexes are shown in Table 4.6.

The intrinsic binding constant (K_b) of metal complexes (**1**, **2**, and **4**) showed the stronger binding affinity than **L** ($1.53 \times 10^6 \text{ M}^{-1}$). **1** have the strongest binding to DNA ($2.21 \times 10^6 \text{ M}^{-1}$) follow by **4** ($2.13 \times 10^6 \text{ M}^{-1}$), **2** ($1.68 \times 10^6 \text{ M}^{-1}$), and **3** ($1.13 \times 10^6 \text{ M}^{-1}$). From the high intrinsic binding constant (K_b) of these compounds (more than $1 \times 10^6 \text{ M}^{-1}$) including the change in absorption spectra (hypochromism and red shift), it indicated that L and metal complexes bind to DNA with intercalation.

To confirm the intercalation binding mode of these compounds, the further study using fluorescent was performed. The study of *Ethidium bromide* (EB) displacement by fluorescence spectroscopy is one of the techniques to investigate the intercalation of binding mode of compound to DNA. This method can be used to confirm the binding mechanism between complexes and DNA. Because *Ethidium bromide* (EB) is an intercalating agent commonly used as a model intercalating compound because EB can strongly intercalate to DNA. If the question compound can replace the EB-DNA complex, this means that the binding mode of compound to DNA is the intercalation mode.

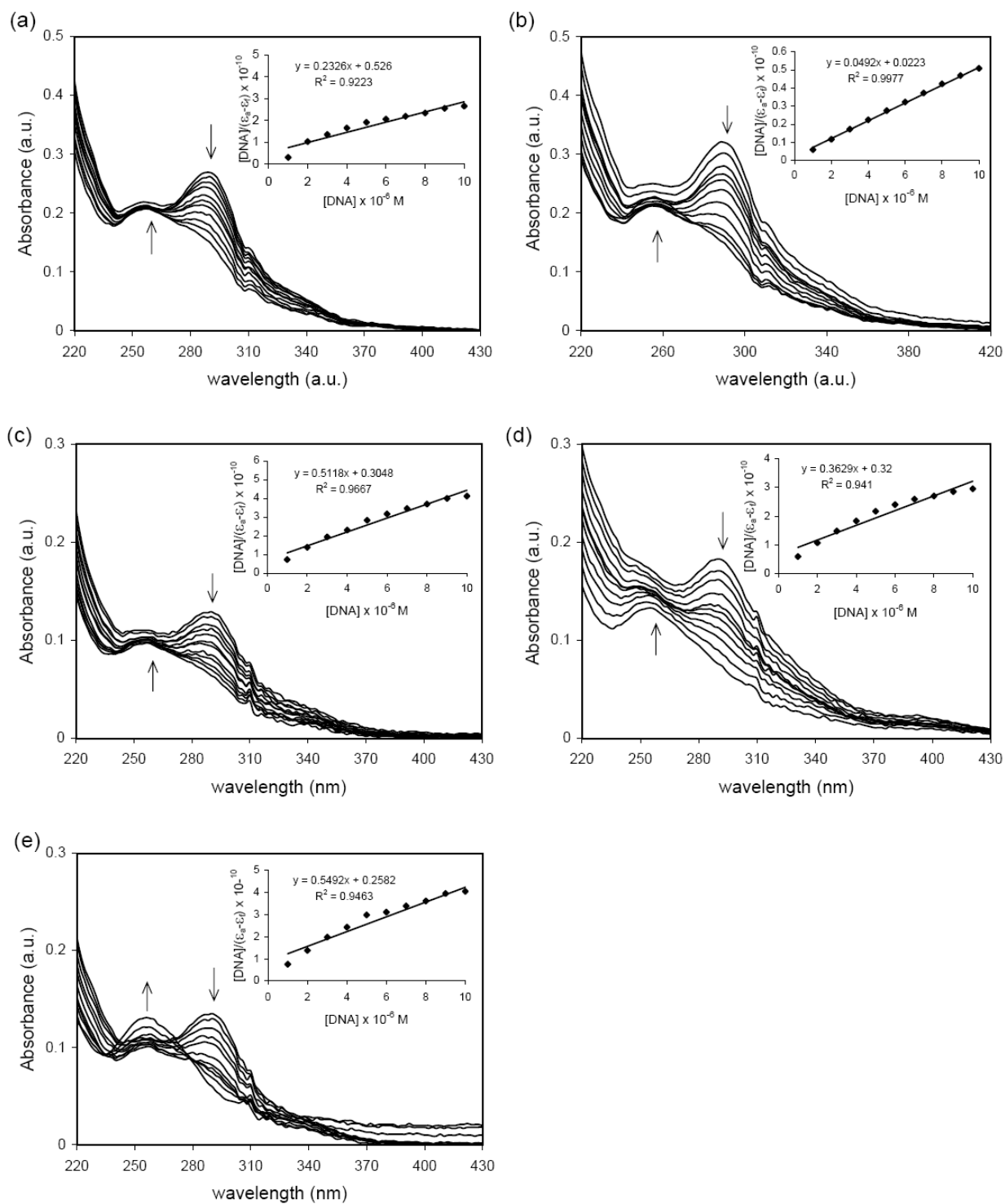


Figure 4.8 Electronic absorption spectra for DNA binding study of **L** (a), **1** (b), **2** (c), **3** (d), **4** (e).

Table 4.6 The binding constant (K_b) and the change of absorption spectra

Compounds	$K_b \times 10^6$ (M^{-1})	Monitored at λ (nm)	Absorption Intensity (%)	Absorption Shift (nm)
Doxorubicin	1.00	485	hypochromism (45)	red shift (7)
Ethidiumbromide	1.32	480	hypochromism (26)	red shift (5)
L	1.53	290	hypochromism (41)	red shift (2)
1	2.21	292	hypochromism (53)	red shift (2)
2	1.68	292	hypochromism (44)	red shift (2)
3	1.13	292	hypochromism (49)	red shift (2)
4	2.13	292	hypochromism (50)	red shift (2)

3.2 Ethidium bromide (EB) displacement study by fluorescence spectroscopic method

The binding of the complexes to calf thymus DNA (CT-DNA) has been studied by fluorescence. Competitive binding studies by measuring the emission of ethidium bromide (EB) bound to DNA show the enhanced emission intensity due to intercalative binding to DNA [22]. Competitive binding of 6-deoxyclitoriacetal metals complexes to DNA reduces the emission intensity of EB with either a displacement of the bound EB from the bound to the free state or the bound complex quenching the emission with a reduction of the emission intensity due to fluorescence quenching of free EB [23].

The concentration of DNA, used for this binding experiments, was determined by measuring the absorption intensity at 260nm with the molar extinction coefficient value of $6600 M^{-1} cm^{-1}$ in 10 mM Tris-HCl–50 mM NaCl buffer (pH 7.4) [24]. The interaction of complexes with DNA was investigated using fluorescence. The fluorescence spectra ($\lambda_{ex} = 346$ nm, $\lambda_{em} = 595$ nm) were recorded at room temperature. In DNA-binding experiment, aliquot of complexes were added to the

samples of EB-DNA mixture. In general, EB does not show emission in the Tris-buffer medium due to fluorescence quenching by solvent. After the mixtures were incubated for 5 min, their fluorescence-emission intensity had been measured after each addition. The fluorescent emission of EB bound to DNA in the presence of complexes (Fig. 4.9) showed the decrease of emission intensity of EB on addition of each complex into the EB-DNA solution. Also, the fluorescence intensities were plotted against complexes' concentration to get a slope that gave the relative extent of binding of each complex to DNA in Fig. 4.9. It is apparent from the plot that EB-bound DNA was efficiently quenched by **L**, **3** and **4** about 20-50%, in which displacement occurred, while with **1** and **2** is about 10-20%. This is indicating that **L**, **3** and **4** exhibited higher DNA-intercalating ability than **1** and **2** at the same conditions. Because **3** and **4** have a nearly square-planar structure when coordinated water dissociates, which is easy to intercalate with DNA. On the other hand, the positively charged of metal complexes may more easily bind to the negatively charged phosphodiester backbone of DNA. Combining structure with the DNA-binding result, its binding mechanism may be explained mainly by intercalation.

To investigate the ability to intercalate with DNA, the Stern-Volmer equation was used.

$$I_0/I = 1 + K_{sv}[Q]$$

I_0 and I represent the emission intensity at the absence and presence of complex, respectively. K_{sv} is a linear Stern-Volmer quenching constant. $[Q]$ is the concentration of compound. The plot between I_0/I versus $[Q]$ for each complex is present in Fig 4.9. From the Stern-Volmer equation, K_{sv} was given from the slope. From Table 4.7, the K_{sv} values of **L** ($1.99 \times 10^5 \text{ M}^{-1}$) is higher than **3** ($6.04 \times 10^4 \text{ M}^{-1}$) and **4** ($6.46 \times 10^4 \text{ M}^{-1}$) about 0.3 times, than **1** ($4.96 \times 10^4 \text{ M}^{-1}$) and **2** ($3.44 \times 10^4 \text{ M}^{-1}$)

about 0.5-0.4 times indicating that the mixture of EB-DNA can be quenched by **L** more than by metal complexes.

Moreover, to determine the binding ability at 50% of EB concentration, the apparent binding constant (K_{app}) of complexes can be calculated as the following equation

$$K_{app}[\text{complex}] = K_{EB}[\text{EB}]$$

Since K_{EB} is DNA binding constant of EB ($1 \times 10^7 \text{ M}^{-1}$), [EB] is EB concentration, and [complex] is complex concentration at 50% fluorescence

The results of K_{app} is in Table 4.7. Like K_{sv} , it is clearly showed that K_{app} of **L** ($3.99 \times 10^7 \text{ M}^{-1}$), **3** ($1.21 \times 10^7 \text{ M}^{-1}$) and **4** ($1.29 \times 10^7 \text{ M}^{-1}$) are higher than K_{app} of EB ($1 \times 10^7 \text{ M}^{-1}$). This confirmed that the intercalation binding can occur between **L**, **3** and **4** to DNA. K_{app} of compound **1** ($0.97 \times 10^7 \text{ M}^{-1}$) and **2** ($0.69 \times 10^7 \text{ M}^{-1}$) are less than K_{app} of EB, indicating that these compounds can less compete with EB at EB-DNA binding site. However, from absorption and emission spectra, it indicated that **1** and **2** bind to DNA with intercalation. For all above results it can be concluded that one possible anticancer mechanism of these compounds use to bind with CT-DNA is the intercalation binding mode.

The effect of electrostatic was investigated in EB-DNA system by vary NaCl concentration at 1, 5, and 10 mM (Fig.4.10). The ability of **1-4** to quench EB at EB-DNA sites are decrease when the concentration of NaCl increase. The effect of ionic strength on quenching constant showed that there is electrostatic force between complexes to DNA.

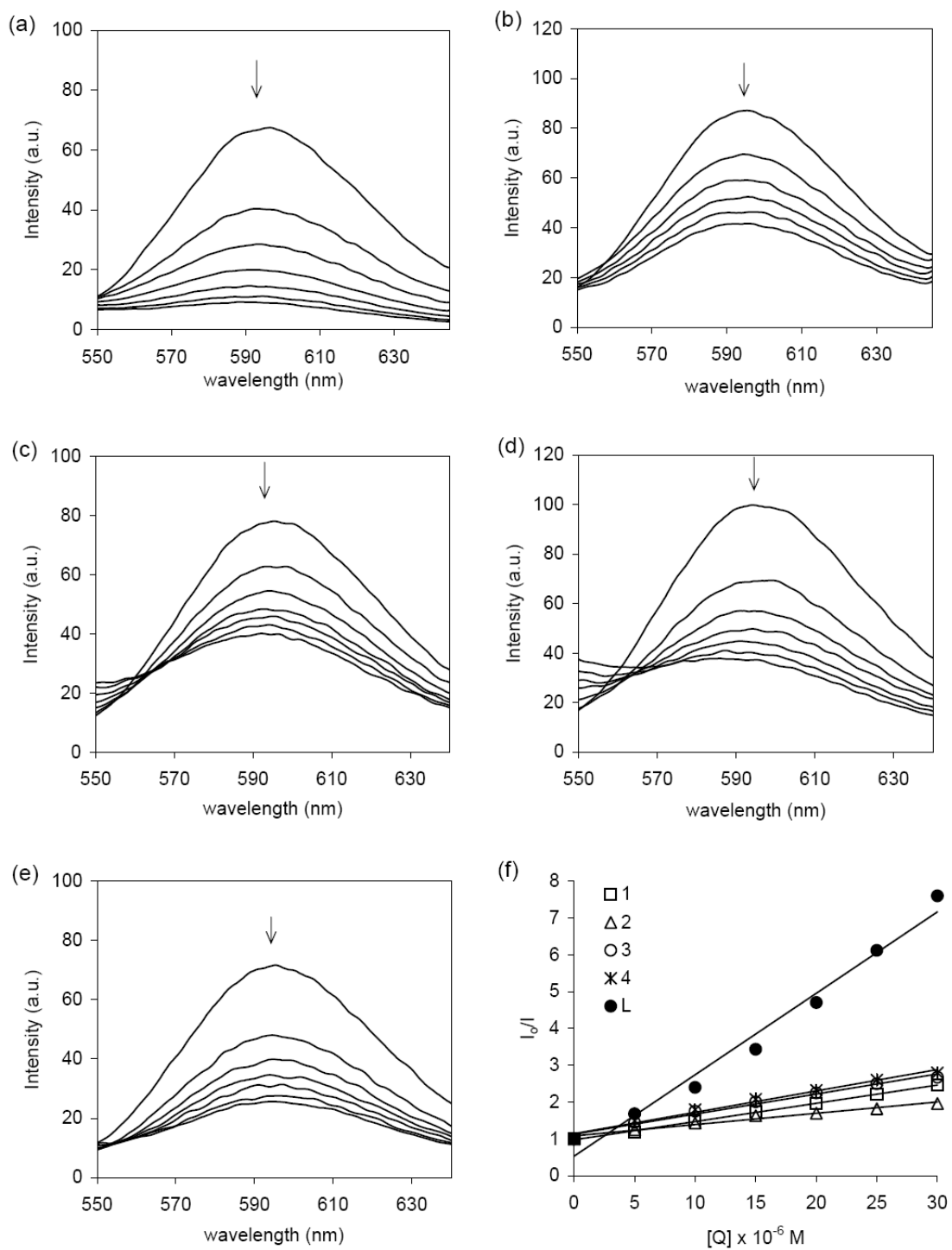


Figure 4.9 Emission spectra of (a) **L**, (b) **1**, (c) **2**, (d) **3**, (e) **4**, (f) Stern-Volmer plot of **L** and metal complexes (**1-4**).

Table 4.7 The Stern-Volmer quenching constant (K_{sv}), the apparent binding constant (K_{app}), and DNA melting temperature (T_m)

Compounds	Stern-Volmer equation	$K_{sv} \times 10^5$ (M^{-1})	$K_{app} \times 10^6$ (M^{-1})	T_m ($^{\circ}C$)	ΔT_m ($^{\circ}C$)
CT DNA	-	-	-	52	0
L	$y = 0.1995x + 1$	1.99	3.01	54	2
1	$y = 0.0484x + 1$	0.48	0.97	63	11
2	$y = 0.0344x + 1$	0.34	0.67	58	6
3	$y = 0.0604x + 1$	0.60	1.25	55	3
4	$y = 0.0646x + 1$	0.65	1.35	60	8

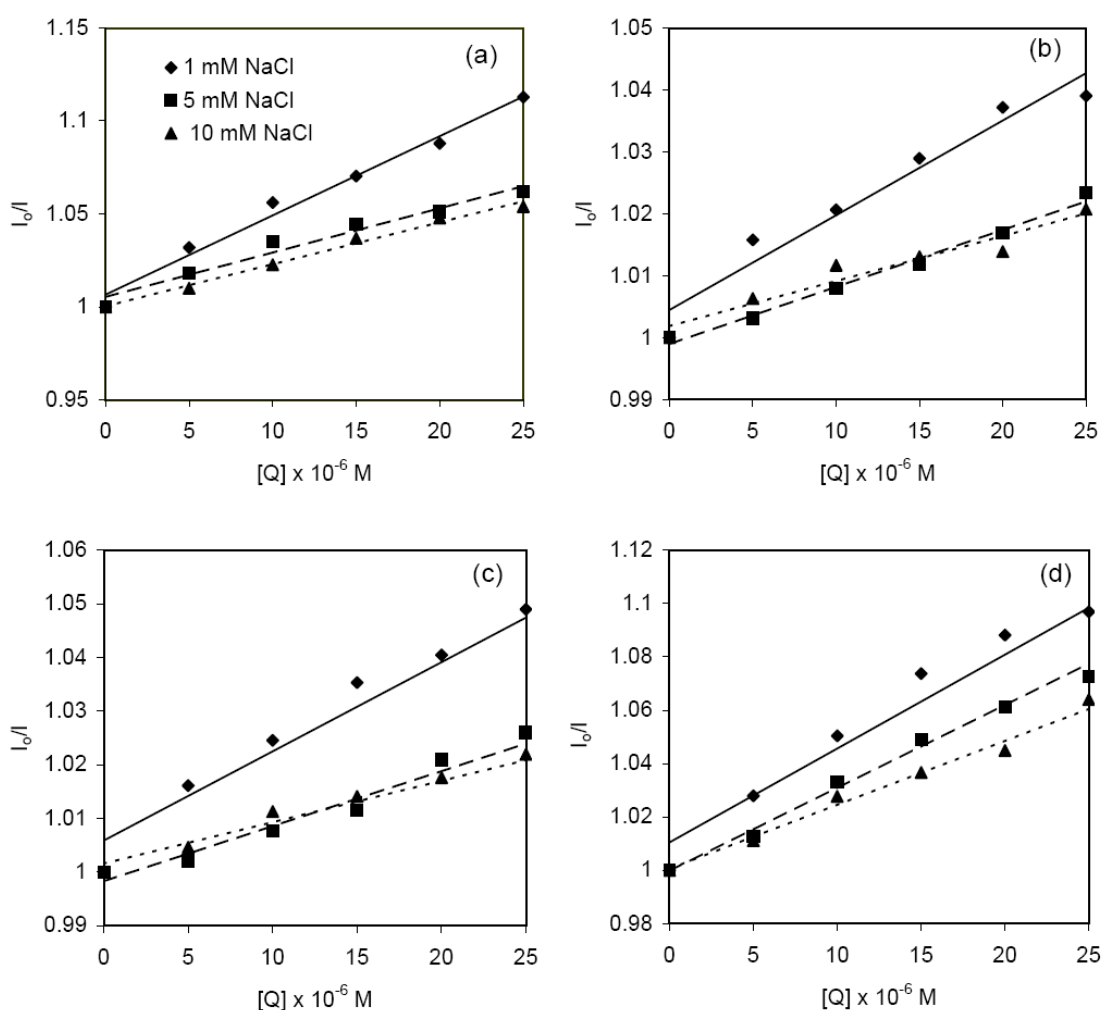


Figure 4.10 Stern-Volmer plot of metal complexes (1-4) with the electrostatic effect test using EB-DNA systems.

3.3 DNA melting temperature

Thermal denaturation studies of CT-DNA are useful method in determining the ability of the present compound to stabilize the double stranded DNA. The interaction of molecules into the double helix has been known to increase the DNA melting temperature (T_m). The melting temperature (T_m) of DNA characterizes the transition from double-stranded to single standard nucleic acid [25]. It was carried out in Tris-HCl buffer containing 40 μM of CT-DNA and 10 μM of the compounds. Melting curves were recorded at 260 nm. The melting curves (T_m) and the table of melting temperature are in Fig. 4.11. From the T_m curve exhibits the melting temperature of CT-DNA at 51°C while the melting temperature of CT-DNA bound with complexes of **L**, **1**, **2**, **3**, and **4** are 54, 63, 60, 55 and 58°C, respectively. The melting temperature of CT-DNA bound with each complex showed the higher T_m indicated that **L** and metal complexes can stabilize CT-DNA. Beside, T_m of the metal complexes are greater than that of **L** this indicated that metal complexes bind to CT DNA stronger than **L**. Therefore, the double stranded DNA can be more stabilized by metal complexes than by **L**.

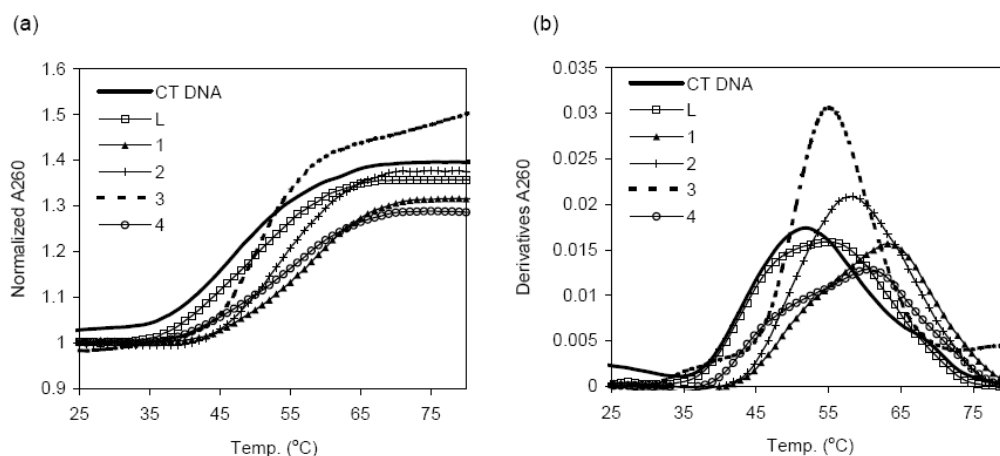


Figure 4.11 Normalized melting temperature curve (T_m) (a) and derivatives melting temperature curve (b).

4. DNA cleavage activity

The DNA cleavage activities have been determined by gel electrophoresis based on qualification of the conversion of supercoiled (SC) pUC19 DNA to nicked circular and linearised. Incubation of DNA with H₂O₂ and compounds (100 μM) irradiated under UV-A light at 365 nm in the dark for 15 min resulted in cleavage activity of pUC19 as can be seen in Fig. 4.12. The irradiation by UV-A results in the formation of reactive singlet oxygen species and/or superoxide radical which can be reduced to H₂O₂ and hydroxyl radical and cause the DNA strands scission [24, 26-30]. **L** (88.41%) exhibited greater cleavage of SC to NC than metal complexes do. Metal complexes **3** cause more cleavage of DNA than **4**, **2** and **1**.

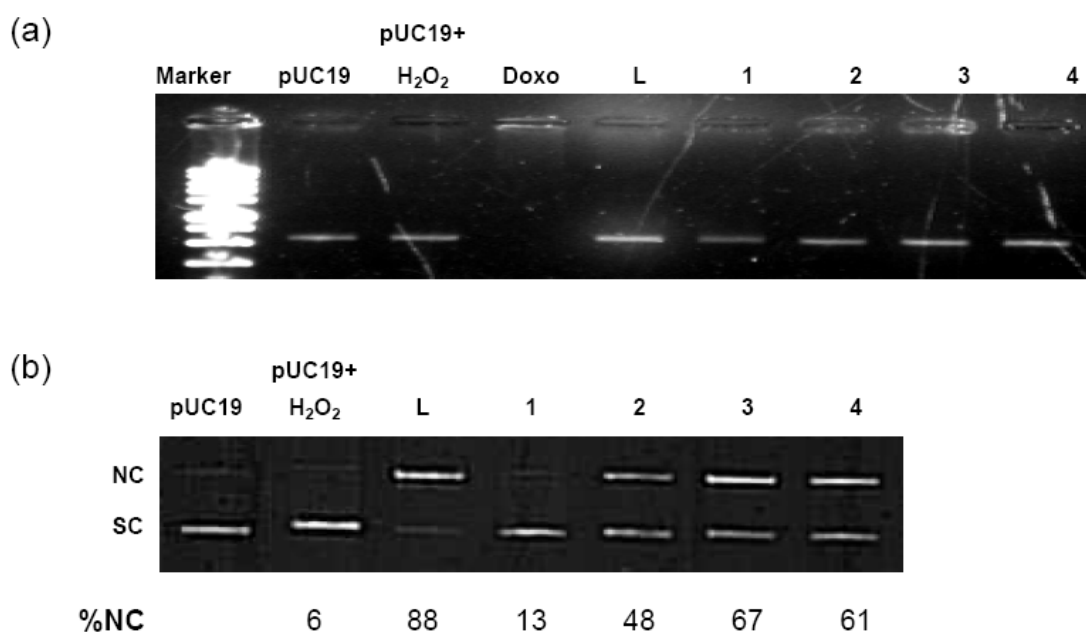


Figure 4.12 Cleavage of pUC19 DNA incubate in the dark (a) lane 1: Marker, lane 2: pUC19 DNA; lane 3: pUC19 DNA + H₂O₂ (250 μM); lane 4: pUC19 DNA + H₂O₂ (250 μM) + Doxorubicin (100 μM); lane 5: pUC19 DNA + H₂O₂ (250 μM) + **L** (100 μM); lane 6: pUC19 DNA + H₂O₂ (250 μM) + **1** (100 μM); lane 7: pUC19 DNA + H₂O₂ (250 μM) + **2** (100 μM); lane 8: pUC19 DNA + H₂O₂ (250 μM) + **3** (100 μM); lane 9: pUC19 DNA + H₂O₂ (250 μM) + **4** (100 μM).

+ **2** (100 μM); lane 8: pUC19 DNA + H_2O_2 (250 μM) + **3** (100 μM); lane 9: pUC19 DNA + H_2O_2 (250 μM) + **4** (100 μM). Under UV-A (b) lane 1: pUC19 DNA; lane 2: pUC19 DNA + H_2O_2 (250 μM); lane 3: pUC19 DNA + H_2O_2 (250 μM) + **L** (100 μM); lane 4: pUC19 DNA + H_2O_2 (250 μM) + **1** (100 μM); lane 5: pUC19 DNA + H_2O_2 (250 μM) + **2** (100 μM); lane 6: pUC19 DNA + H_2O_2 (250 μM) + **3** (100 μM); lane 7: pUC19 DNA + H_2O_2 (250 μM) + **4** (100 μM).

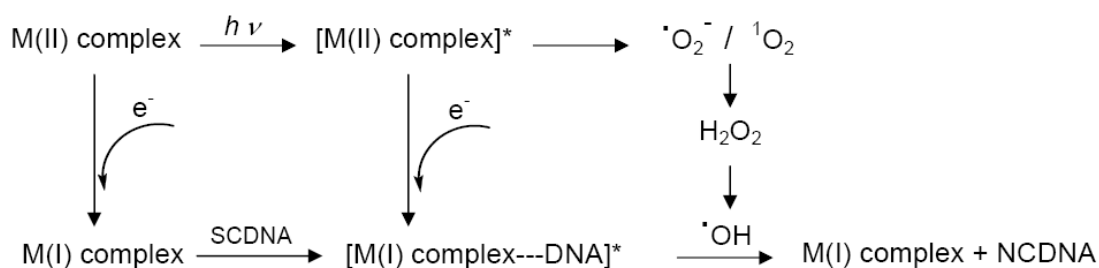


Figure 4.13 Propose mechanistic pathway for the photo-induced nuclease activity of the complexes.

PART II Metal complexes of Schiff base 2-[(4-chlorobenzylimino)-methyl]-phenol and 2-[(4-methoxybenzylimino)-methyl]-phenol

1. Crystal Structures

The crystal structures of complexes **A1**, **A2**, and **A3** are shown in Fig. 4.14. The selected bond distances and bond angles are displayed in Table 4.9. The crystal structure of Ni(II) complexes (**A1**) is square planar geometry (Fig. 4.14a). The two bidentate ligands are chelated around Ni(II) atom. The coordination environment around Ni(II) atom consist of 2 nitrogen atoms (N1, N1#1) and two oxygen atoms (O1, O1#1). The Ni(II) atom lies in the plane of N1, N1#1, O1, O1#1. There is no deviation of four atoms (N1, N1#1, O1, O1#1) from the least-squares. The Ni-N distances are 1.922(2) Å. The Ni-O distances are 1.831(2) Å. The Ni-N and Ni-O distance are in the normal range of Ni-N and Ni-O bond length of other Ni(II) Schiff base complexes that have been reported [47-48]. The distortion occurs from the different size of the atoms coordinated and to the straints of the chelating group which subtend angles around Ni(II) of 87.95° and 92.05°.

The crystal structure of Cu(II) complexes (**A2**) is displayed in Fig. 4.14b. The crystal system of **A2** is monoclinic with space group $P2_1/c$. The Cu(II) environment are hydroxyl oxygen atoms (O1, O1#) and imine nitrogen atoms (N1, N1#). The Cu-N and Cu-O bond distance for **A2** are 2.024(3) Å and 1.887(3) Å, respectively. There is no deviation of four atoms (N1, N1#1, O1, O1#1) from the least-squares plane. The O-Cu-N for is 88.44(13)° and O1#-Cu-N for **A2** is 91.56(13)° which is found to be

deviated from the ideal square planar 90° [48]. Therefore, the structure of **A2** adopted in the distorted square planar geometry.

The crystal structure of Zn(II) complexes (**A3**) displayed in Fig. 4.14c is adopted tetrahedral geometry which is distorted by a small O(1)-Zn-N(1) angle being $96.37(11)^\circ$. The N(1)-Zn-N(1)#1 is $113.96(13)^\circ$. The angle of O(1)#1-Zn-N(1) $122.44(13)^\circ$ is larger than the average tetrahedral value. The Zn-N distance ranging from $2.024(3) \text{ \AA}$ and the Zn-O distance of $1.939(3) \text{ \AA}$ are considered agree well with normal Zn-N and Zn-O bond distances [52].

The crystal structures of complexes **B1**, **B2**, and **B4** are shown in Fig. 4.14d-f. The selected bond distances and bond angles are displayed in Table 4.9. The crystal structure of Ni(II) complexes (**B1**) is square planar geometry (Fig. 4.14d). The two bidentate ligands are chelated around Ni(II) atom. The coordination environment around Ni(II) atom consist of 2 nitrogen atoms (N1, N1#1) and two oxygen atoms (O1, O1#1). The Ni(II) atom lies in the plane of N1, N1#1, O1, O1#1. There is no deviation of four atoms (N1, N1#1, O1, O1#1) from the least-squares. The Ni-N and Ni-O distance for **B1** is 1.924 \AA and 1.843 \AA , respectively. The Ni-N and Ni-O distance are in the normal range of Ni-N and Ni-O bond length of other Ni(II) Schiff base complexes that have been reported [49-50]. The distortion occurs from the different size of the atoms coordinated and to the straits of the chelating group which subtend angles around Ni(II) of 87.98° and 92.02° for **B1**.

The crystal structure of Cu(II) complex (**B2**) is shown in Fig. 4.14e. The crystal system of **B2** is triclinic (*P-1*). The molecules of **B2** are exhibited as dimer in an asymmetric unit cell. The Cu(II) environment are hydroxyl oxygen atoms (O1, O1#) and imine nitrogen atoms (N1, N1#). The selected bond distances and bond

angles are listed in Table 4.9. The Cu-N bond distance for **B2** is 2.011(10) Å, and 2.012(11) Å. The Cu-O distance for **B2** is 1.912(9) Å of molecule I which is longer than that of molecule II (1.880(9) Å). There is the deviation of four atoms (N1, N1#1, O1, O1#1) from the least-squares plane for **B2**. The maximum deviation of four atoms (N1, N1#1, O1, O1#1) from the least-squares plane of **B2** for both molecule I and molecule II are 0.001 Å and 0.001 Å, respectively. The O-Cu-N for **B2** (molecule I) is 88.5(4)° which is bigger than that of **3** (molecule II) 88.3(4)°. The O1#-Cu-N for **B2** (molecule I) is 91.5(4)° which is smaller than that of **3** (molecule II) 91.7(4)°. The O-Cu-N for **B2** was found to be deviated from the ideal square planar 90° [51]. Therefore, the structure of **B2** is adopted in the distorted square planar geometry.

The crystal structure of Zn(II) complexe (**B3**) adopted tetrahedral geometry (Fig. 4.14f) which is distorted by a small O(1)-Zn-N(1) angle being 96.47(11)°. The N(1)-Zn-N(1)#1 has opened up to 124.60(13)°. The angle of O(1)#1-Zn-N(1) 116.24(13)° is larger than the average tetrahedral value. The Zn-N distance ranging from 2.0162(3) to 2.0191(3) Å and the Zn-O distance of 1.925(3) to 1.927(3) Å are considered agree well with normal Zn-N and Zn-O bond distances [52].

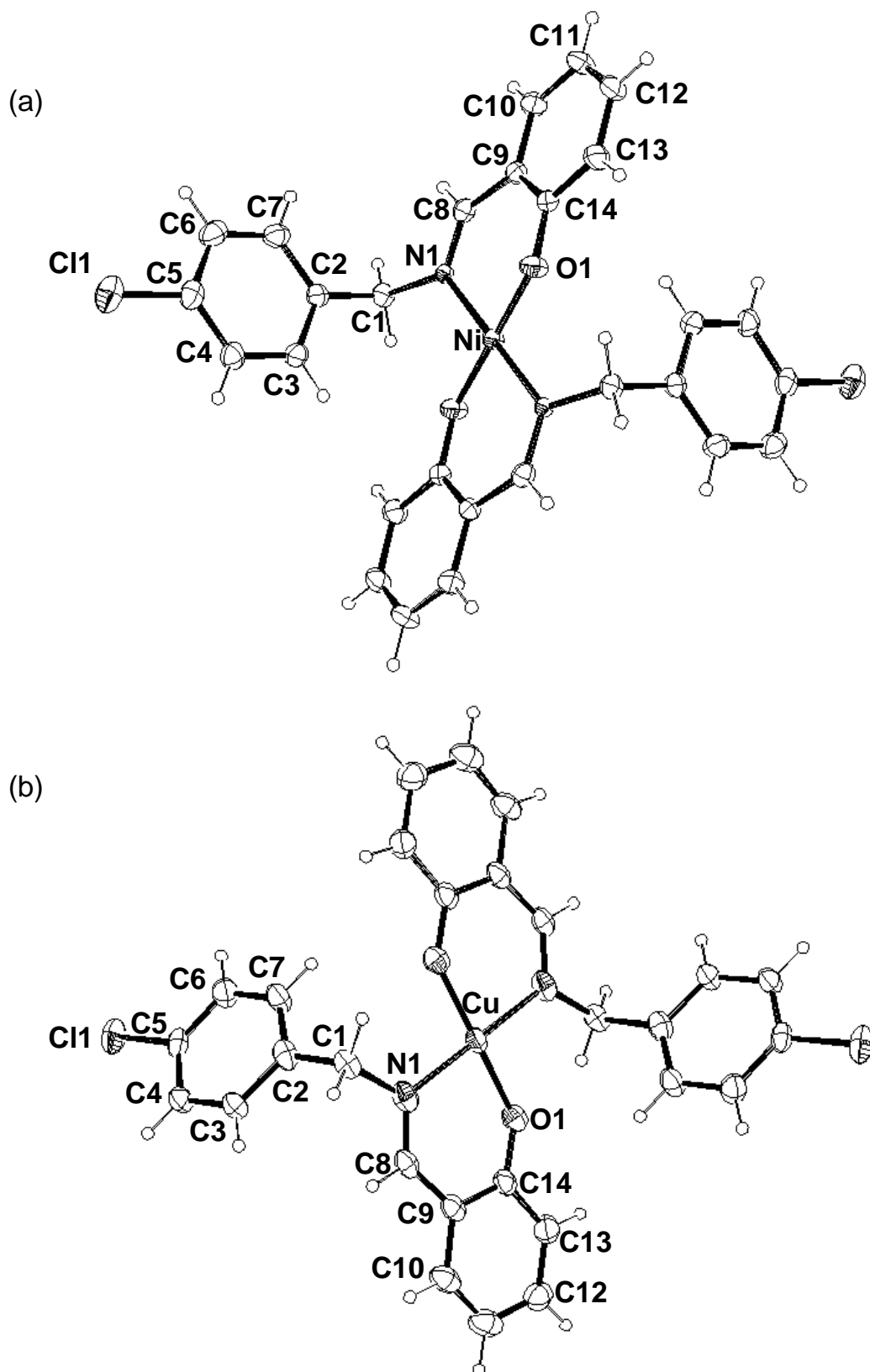


Figure 4.14 Crystal structure of (a) NiA₂ (A1), (b) CuA₂ (A2), (c) ZnA₂ (A3), (d) NiB₂ (B1), (e) CuB₂ (B2), (f) ZnB₂ (B3).

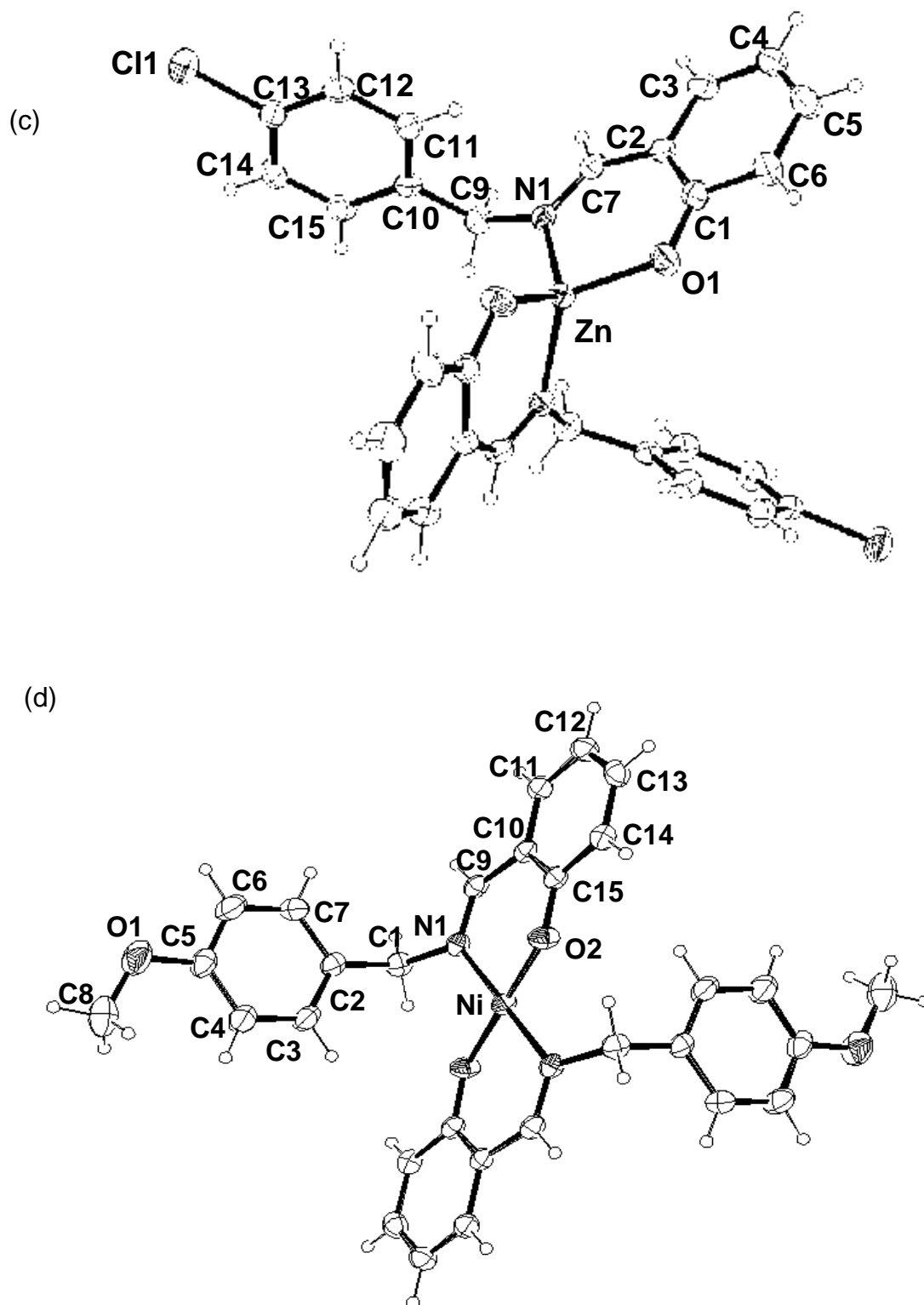


Figure 4.14 cont' Crystal structure of (a) NiA₂ (A1), (b) CuA₂ (A2), (c) ZnA₂ (A3), (d) NiB₂ (B1), (e) CuB₂ (B2), (f) ZnB₂ (B3).

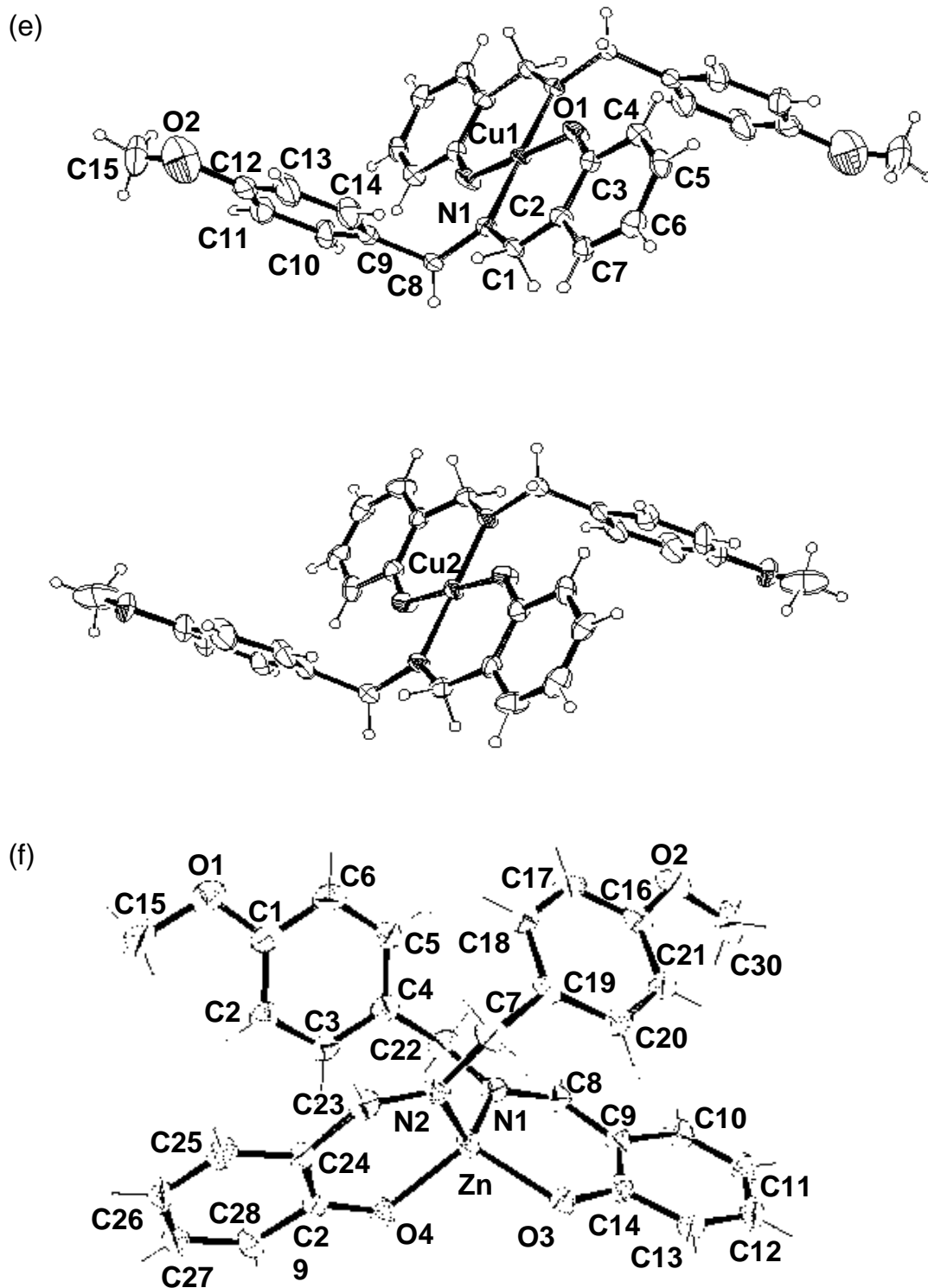


Figure 4.14 cont' Crystal structure of (a) NiA₂ (**A1**), (b) CuA₂ (**A2**), (c) ZnA₂ (**A3**), (d) NiB₂ (**B1**), (e) CuB₂ (**B2**), (f) ZnB₂ (**B3**).

Table 4.8 Crystal data and refinement parameters of Schiff base metal complexes.

Compounds	A	A1	A2	A3	B	B1	B2	B3
Formula	C ₁₄ H ₁₃ NOCl	C ₃₀ H ₂₄ N ₂ O ₂ Cl ₂ Ni	C ₃₀ H ₂₂ N ₂ O ₂ Cl ₂ Ni	C ₃₀ H ₂₂ N ₂ O ₂ Cl ₂ Zn	C ₁₅ H ₁₅ NO ₂	C ₃₀ H ₂₈ N ₂ O ₄ Ni	C ₃₀ H ₂₈ N ₂ O ₄ Cu	C ₂₄ H ₂₈ N ₂ O ₄ Zn
M_r	244	546.1	608.94	555.59	241.28	541.27	544.08	545.93
Crystal system	Orthorhombic	Monoclinic	Monoclinic	Monoclinic	Orthorhombic	Monoclinic	Triclinic	Triclinic
Space group	<i>P</i> 2 ₁ 2 ₁ 2 ₁	<i>P</i> 2 ₁ / <i>c</i>	<i>P</i> 2 ₁ / <i>c</i>	<i>C</i> 2	<i>P</i> 2 ₁ 2 ₁ 2 ₁	<i>P</i> 2 ₁ / <i>c</i>	<i>P</i> -1	<i>P</i> -1
Crystal size (mm)	0.20 x 0.40 x 0.40	0.20 x 0.30 x 0.50	0.20 x 0.40 x 0.40	0.20 x 0.20 x 0.08	0.30 x 0.18 x 0.04	0.50 x 0.04 x 0.04	0.45 x 0.12 x 0.12	0.40 x 0.20 x 0.15
<i>a</i> (Å)	6.2876(2)	11.6480(4)	4.4061(3)	23.2794(12)	5.7190(8)	12.3232(69)	6.5047(6)	9.3685(3)
<i>b</i> (Å)	12.2267(3)	5.8516(2)	11.5669(10)	5.6228(3)	12.7229(19)	5.7403(25)	10.9274(11)	11.5118(3)
<i>c</i> (Å)	16.2664(5)	17.4639(7)	23.7577(16)	12.1418(7)	17.936(3)	17.9303(105)	18.5237(19)	12.2783(4)
α (°)	90	90	90	90	90	90	88.073(4)	77.1480(10)
β (°)	90	91.505(2)	91.821(4)	116.305(2)	90	95.461(18)	79.890(3)	88.861(2)
γ (°)	90	90	90	90	90	90	79.883(2)	80.263(2)
V (Å³)	1250.51(6)	1189.92	1210.20(16)	1424.73	1305.0(3)	1262.61	1276.1(2)	1272.21(7)
Z	4	2	2	2	4	2	2	2
D (g/cm³)	1.241	1.524	1.671	1.297	1.228	1.424	1.416	1.091
θ range (°)	2.08-26.29	1.75-27.46	2.46-30.57	3.25-25.41	2.0-26.5	1.66-28.23	1.12-27.13	1.70-29.13
Goodness of fit on <i>F</i>²	0.820	0.900	0.947	1.053	0.162	0.146	1.351	1.046
R₁ (<i>I</i>>2σ(<i>I</i>))	0.027	0.061	0.082	0.046	0.040	0.039	0.149	0.087
wR₂	0.148	0.0701	0.118	0.148	0.051	0.065	0.372	0.212

Table 4.9 Selected bond length and bond angle of Schiff base metal complexes.

A1							
Bond lengths (Å)				Bond angles (°)			
Ni(1)-O(1)#1	1.831(2)	Cl(1)-C(6)	1.744(3)	O(1)#1-Ni(1)-O(1)	180.000(1)	N(1)-C(9)-C(10)	126.3(2)
Ni(1)-O(1)	1.831(2)	O(1)-C(15)	1.312(3)	O(1)#1-Ni(1)-N(1)	87.95(9)	N(1)-C(2)-C(3)	110.9(2)
Ni(1)-N(1)	1.921(2)	N(1)-C(9)	1.298(4)	O(1)-Ni(1)-N(1)	92.05(9)	O(1)-C(15)-C(14)	119.0(3)
Ni(1)-N(1)#1	1.921(2)	N(1)-C(2)	1.486(3)	O(1)#1-Ni(1)-N(1)#1	92.05(9)	O(1)-C(15)-C(10)	122.8(2)
				O(1)-Ni(1)-N(1)#1	87.95(9)	C(5)-C(6)-Cl(1)	119.2(3)
				N(1)-Ni(1)-N(1)#1	180.000(1)	C(7)-C(6)-Cl(1)	119.6(3)
				C(15)-O(1)-Ni(1)	128.26(18)	C(9)-N(1)-Ni(1)	123.44(18)
				C(9)-N(1)-C(2)	115.4(2)	C(2)-N(1)-Ni(1)	121.15(17)
Symmetry transformations: (#1) -x+2, -y, -z+2							

Table 4.9 con't Selected bond length and bond angle of Schiff base metal complexes.

A2							
Bond lengths (Å)				Bond angles (°)			
Cu(1)-O(2)	1.887(3)	Cl(1)-C(11)	1.753(4)	O(2)-Cu(1)-O(2)#1	180	N(1)-C(1)-C(2)	127.8(3)
Cu(1)-O(2)#1	1.887(3)	N(1)-C(1)	1.291(5)	O(2)-Cu(1)-N(1)	88.44(13)	N(1)-C(8)-C(14)	110.7(3)
Cu(1)-N(1)	2.024(3)	N(1)-C(8)	1.478(5)	O(2)#1-Cu(1)-N(1)	91.56(13)	C(12)-C(11)-Cl(1)	119.5(3)
Cu(1)-N(1)#1	2.024(3)	O(2)-C(3)	1.317(5)	O(2)-Cu(1)-N(1)#1	91.56(13)	C(10)-C(11)-Cl(1)	119.0(3)
				O(2)#1-Cu(1)-N(1)#1	88.44(13)	C(1)-N(1)-Cu(1)	123.3(3)
				N(1)-Cu(1)-N(1)#1	180.000(2)	C(8)-N(1)-Cu(1)	121.6(3)
Symmetry transformations : (#1) -x, -y +1, -z + 1				C(1)-N(1)-C(8)	115.1(3)	C(3)-O(2)-Cu(1)	131.3(3)
A3							
Bond lengths (Å)				Bond angles (°)			
Zn(1)-O(2)	1.9394(5)	Cl(1)-C(13)	1.7692(8)	C(9)-N(1)-C(7)	118.76(6)	N(1)-Zn-O(1)#1	122.44(7)
Zn(1)-O(2)#1	1.9394(5)	N(1)-C(7)	1.2976(1)	C(7)-N(1)-Zn	118.50(7)	N(1)#1-Zn-O(1)#1	96.37(4)
Zn(1)-N(1)	2.0240(8)	N(1)-C(9)	1.4458(6)	C(9)-N(1)-Zn	122.47(9)	N(1)-Zn-O(1)	96.37(4)
Zn(1)-N(1)#1	2.0240(8)	O(1)-C(1)	1.2682(5)	C(1)-O(1)-Zn	124.94(9)	N(1)#1-Zn-O(1)	122.44(7)
Symmetry transformations : (#1) -x+1, y, -z + 1						O(1)-Zn-O(1)#1	107.12(10)

Table 4.9 con't Selected bond length and bond angle of Schiff base metal complexes.

B1							
Bond lengths (Å)				Bond angles (°)			
C(1)-N(1)	1.493(3)	N(1)-Ni(1)	1.9241(19)	N(1)-C(9)-C(10)	127.0(2)	C(9)-N(1)-Ni(1)	123.47(17)
C(9)-N(1)	1.298(3)	O(2)-Ni(1)	1.843(2)	N(1)-C(1)-C(2)	110.94(19)	C(1)-N(1)-Ni(1)	121.11(16)
C(5)-O(1)	1.373(3)	Ni(1)-O(2)#1	1.843(2)	O(1)-C(5)-C(6)	116.4(3)	C(15)-O(2)-Ni(1)	129.28(16)
C(8)-O(1)	1.419(5)	Ni(1)-N(1)#1	1.9241(19)	O(1)-C(5)-C(4)	124.5(3)	O(2)-Ni(1)-O(2)#1	180.00(14)
C(15)-O(2)	1.306(3)			O(2)-C(15)-C(14)#1	119.4(2)	O(2)-Ni(1)-N(1)	87.98(8)
				O(2)-C(15)-C(10)#1	122.6(2)	O(2)#1-Ni(1)-N(1)	92.02(8)
				C(5)-O(1)-C(8)	118.4(2)	O(2)-Ni(1)-N(1)#1	92.02(8)
				C(9)-N(1)-C(1)	115.4(2)	O(2)#1-Ni(1)-N(1)#1	87.98(8)
						N(1)-Ni(1)-N(1)#1	180.00(13)
Symmetry transformations : (#1) -x+1, -y, -y -z							

Table 4.9 con't Selected bond length and bond angle of Schiff base metal complexes.

B2							
Bond lengths (Å)				Bond angles (°)			
C(1)-N(1)	1.320(16)	Cu(1)-O(1)#1	1.912(9)	C(1)-N(1)-Cu(1)	123.1(8)	O(1)-C(3)-C(2)	123.5(12)
C(8)-N(1)	1.481(15)	Cu(1)-N(1)#1	2.022(10)	C(8)-N(1)-Cu(1)	120.7(8)	O(1)-C(3)-C(4)	118.4(12)
C(16)-N(3)	1.277(17)	Cu(2)-O(3)#2	1.880(9)	C(16)-N(3)-Cu(2)	123.3(9)	C(13)-C(12)-O(2)	124(3)
C(23)-N(3)	1.463(16)	Cu(2)-N(3)#2	2.012(11)	C(23)-N(3)-Cu(2)	120.7(9)	C(11)-C(12)-O(2)	117(3)
C(12)-O(2)	1.45(3)	N(1)-Cu(1)	2.022(10)	C(3)-O(1)-Cu(1)	129.3(8)	C(15)-O(2)-C(12)	132(4)
C(15)-O(2)	1.24(4)	N(3)-Cu(2)	2.012(11)	C(22)-O(3)-Cu(2)	130.5(9)	C(30)-O(5)-C(27)	102(2)
C(3)-O(1)	1.289(15)	O(1)-Cu(1)	1.912(9)	O(3)-Cu(2)-N(3)	91.7(4)	N(1)-C(1)-C(2)	125.1(12)
C(22)-O(3)	1.319(15)	O(3)-Cu(2)	1.880(9)	O(3)#2-Cu(2)-N(3)	88.3(4)	N(1)-C(8)-C(9)	112.3(10)
C(27)-O(5)	1.398(19)			O(3)-Cu(2)-N(3)#2	88.3(4)	N(3)-C(16)-C(17)	128.4(12)
C(30)-O(5)	1.24(3)			O(3)#2-Cu(2)-N(3)#2	91.7(4)	N(3)-C(23)-C(24)	113.0(12)
				O(1)-Cu(1)-N(1)#1	88.5(4)	C(1)-N(1)-C(8)	115.8(10)
				O(1)#1-Cu(1)-N(1)#1	91.5(4)	C(16)-N(3)-C(23)	115.8(12)
				O(1)-Cu(1)-N(1)	91.5(4)	O(1)-Cu(1)-O(1)#1	180.000(3)
				O(1)#1-Cu(1)-N(1)	88.5(4)	O(3)-Cu(2)-O(3)#2	180.000(2)
				N(1)#1-Cu(1)-N(1)	180.0(4)	N(3)-Cu(2)-N(3)#2	180.0(5)

Symmetry transformations : (#1) -x+1, -y + 1, -z + 2 (#2) -x, -y+1, -z+1

Table 4.9 con't Selected bond length and bond angle of Schiff base metal complexes.

B3							
Bond lengths (Å)				Bond angles (°)			
Zn(1)-O(3)	1.9279(5)	N(1)-C(7)	1.4841(8)	C(22)-N(2)-C(23)	117.19(32)	N(2)-Zn-O(4)	96.03(11)
Zn(1)-O(4)	1.9247(5)	N(1)-C(8)	1.2909(3)	C(22)-N(2)-Zn	122.86(23)	N(1)-Zn-O(4)	116.24(13)
Zn(1)-N(1)	2.0191(30)	N(1)-C(22)	1.4871(6)	C(23)-N(2)-Zn	119.86(26)	N(2)-Zn-O(3)	114.53(12)
Zn(1)-N(2)	2.0162(30)	N(1)-C(23)	1.2859(4)	C(7)-N(2)-C(8)	116.07(32)	N(1)-Zn-O(3)	96.47(11)
		O(2)-C(16)	1.3672(0)	C(7)-N(2)-Zn	124.53(24)	N(1)-Zn-O(2)	124.60(13)
		O(3)-C(14)	1.3046(1)	C(8)-N(2)-Zn	119.33(26)	O(3)-Zn-O(4)	109.33(12)
		O(4)-C(29)	1.3124(0)	C(14)-O(3)-Zn	124.55(25)		
				C(29)-O(4)-Zn	124.25(23)		

2. Bioassay

The cytotoxic activity was conducted by the MTT assay with five cancer cell lines; lung carcinoma (CHAGO), hepato carcinoma (Hep G2), gastric carcinoma (KATO 3), colon carcinoma (SW 620), and human breast carcinoma (BT 474) and REMA assays with oral cavity carcinoma (KB), small cell lung carcinoma (NCI H187), human breast carcinoma (MCF7). The IC_{50} values are shown in Table 4.10. The screen test of Schiff base, and its Cu and Zn complexes exhibited cytotoxic activities against various cell lines while Ni complexes did not have cytotoxic activity because Ni complexes (**A1**, **B1**) cause the cell growth as seen from %cell viability over 50% for all tested cancer cell lines (Appendix B). Cu complexes of both new Schiff bases (**A2** and **B2**) and Zn complex (**A3**) are not toxic to all tested normal cells, while Zn complexes (**B3**) is toxic to CCD and HS27. Moreover, Cu and Zn complexes were found to be more cytotoxic compared with their parent Schiff base ligand against all tested cancer cell (Table 4.10). The increase in cytotoxic activity of the Cu and Zn complexes may be due to the effect of the metal ion on the normal cell process, considered as Tweedy's chelation theory [53]. When metal coordinated with ligands, polarity of the metal ion is reduced because of partial sharing of its positive charge with the donor group and possible-electron delocalization within the whole chelate ring system. This chelation increase the hydrophobic character and liposolubility of the metal complexes favoring its permeation through the lipid layers of the cell membrane and inhibit activity of cellular enzymes, which play a vital role in metabolic pathways of the tested cells. Furthermore, the formation of hydrogen bond through the azomethine nitrogen atom with the active centers of cell constituents, resulting in interference with the cancer cell process. [54]. Moreover, **A3** showed

stronger cytotoxicity than **A2**. This may cause of the electron withdrawing group (Cl-) in Schiff base (**A**) can be more stabilized by zinc which is more reactive than copper. The stronger Zn–A bond can increase the lipophilic character of Zn complex (**A3**). On the other hand, the electron donating group (OMe-) in Schiff base (**B**) can be more stabilized by copper and cause stronger Cu–B bond which increases the lipophilic character of Cu complex (**B2**) and lead to stronger cytotoxicity of **B2** than **B3**.

In comparison with other researches, cytotoxicity against MCF7 of copper(II) complex **B2** (11.98 μM) is stronger than copper(II) complex of 6-(2-chlorobenzylamino)purine and 6-(3-chlorobenzylamino)purine (24 μM and 54 μM) [55]. For Hep2, the inhibition of cell growth of **B2** is 0.86 μM which is stronger than copper(II) complex of 2-aminomethylthiophenyl-4-bromosalicylaldehyde (ATS) (1.24 μM) [56] and copper(II) complex of 2-((2-((benzo[d]oxazol-2-yl)methoxy) phenoxy) methyl) benzoxazole (20.05 μM) [57].

Moreover, in this work copper(II) complex **B2** has shown efficient cytotoxic activity against KATO3 (2.47×10^{-2} μM) and BT474 (1.45×10^{-3} μM). It can be considered to be a novel effective anticancer agent.

Table 4.10 Toxicity test against normal cell lines and the inhibition of cell growth (IC₅₀) against cancer cell lines.

Compounds	Structure	IC ₅₀ (μM)								Normal Cells		
		CHAGO	HEP G2	KATO 3	SW 620	BT 474	KB	NCI H187	MCF7	Vero	CCD	H27
Cisplatin		0.18	0.25	0.22	0.24	0.29	*	*	0.24 **	*	toxic	toxic
A		> 100	16.60	15.25	25.20	14.96	> 100	inactive	inactive	non-toxic	non-toxic	toxic
A2		29.64	8.77	9.94	15.33	5.03	inactive	inactive	inactive	non-toxic	non-toxic	non-toxic
A3		9.94	7.42	7.27	11.28	6.91	65.14	67.51	68.01	non-toxic	non-toxic	non-toxic
B		> 100	43.52	38.54	51.39	43.73	inactive	inactive	inactive	non-toxic	toxic	toxic
B2		0.86	0.86	2.47E-02	0.49	1.45E-03	16.12	32.31	11.98	non-toxic	non-tox	non-tox
B3		42.57	34.22	28.26	27.52	10.28	inactive	inactive	inactive	non-toxic	toxic	toxic

3. DNA binding experiments

The DNA binding of Schiff base and their metal complexes have been studied by using UV-Vis and fluorescence spectroscopy.

3.1 Titration with UV absorption spectroscopy

The electronic absorption spectra are well known to be the method for determining the binding mode and the binding constant between the complexes and CT DNA [58]. The strong interaction between aromatic ring in Schiff base complexes and the base pairs of DNA lead to the intercalative binding mode [58]. The electronic spectra of the complexes, which its concentration is constant at 20 μM titrated with increasing amount of CT DNA from 2-20 μM , are shown in Fig. 4.15.

The absorption spectra of **A**, **A2**, **A3**, **B**, **B2**, and **B3** showed both increase and decrease intensity characteristic with different % absorption intensity change (see Table 4.11) increase of intensity at 255, and decrease at 277 nm and 385 nm (10% and 16%) (Fig.4.15c).The absorption spectra of **A3** are similar to **A**. The intensity increase at 255 nm (39%) and 323 nm increase after DNA concentration added above 4 μM (115.60%). Moreover, there are decrease of intensity at 276 nm and 387 nm (40% and 81%) for **A3** (Fig. 4.15d).

The absorption spectra of **B**, **B1**, **B2**, and **B3** are in Fig. 4.15e-h. The absorption spectra of **B** showed hypochromism at 270 nm and 393 nm (18% and 78%) and hyperchromism at 257 nm and 325 nm (10% and 64%) (Fig. 4.15e). There are 4 isobestic points shown for **A** at 247, 262, 300, and 347 nm which indicated that there is the equilibrium between DNA and **B**. The absorption intensity is decrease when increasing amount of DNA to **B2** (Fig. 4.15g). Hypochromism appeared for **B2**

absorption spectra at 263 and 385 nm (3% and 23%). The absorption spectra of **B3** are similar to **B** (Fig. 4.15h). The hypochromism founded at 268 nm (14%) and 378 nm (58%). Moreover, there are hyperchromism at 257 nm (3%) after added DNA above 10 μ M.

The absorption spectra of **A**, **A2**, **A3**, **B**, **B2**, and **B3** exhibited hypochromism and red shift which cause of electrons in π^* orbital of ligand can couple with the π orbital of the base pairs of DNA. This also lead to the π - π^* transition energy decrease. From the results of hypochromism and red shift, these refer to **A**, **A2**, **A3**, **B**, **B2**, and **B3** bind with DNA through intercalation binding mode. Moreover, the hyperchromism occurred in the absorption spectra of **A**, **A2**, **A3**, **B**, and **B3** indicated that there is hydrogen bonding between complex and DNA.

The absorption spectra of **A1** and **B1** showed only hyperchromism at 259 nm and 268 nm, and found slightly blue shift (3 nm) for **A1** and strongly blue shift (8 nm) for **B1**. The hyperchromism and blue shift refer to the strong hydrogen bonding between complex and DNA at external contact which can be electrostatic binding or groove binding and lead to the change of DNA conformation [59]. The hyperchromic effect and blue shift can be elaborated as the following reasons. The complexes which consisted of planar aromatic chromophore can partially insert between DNA base pair. The present of metal ion in complexes can lead to the limitation of ion-paired formation between cationic and DNA. After complex fully bound with DNA, an amount of DNA increasing later preferably bind at the groove. This results in the change and damage of DNA double helix [60].

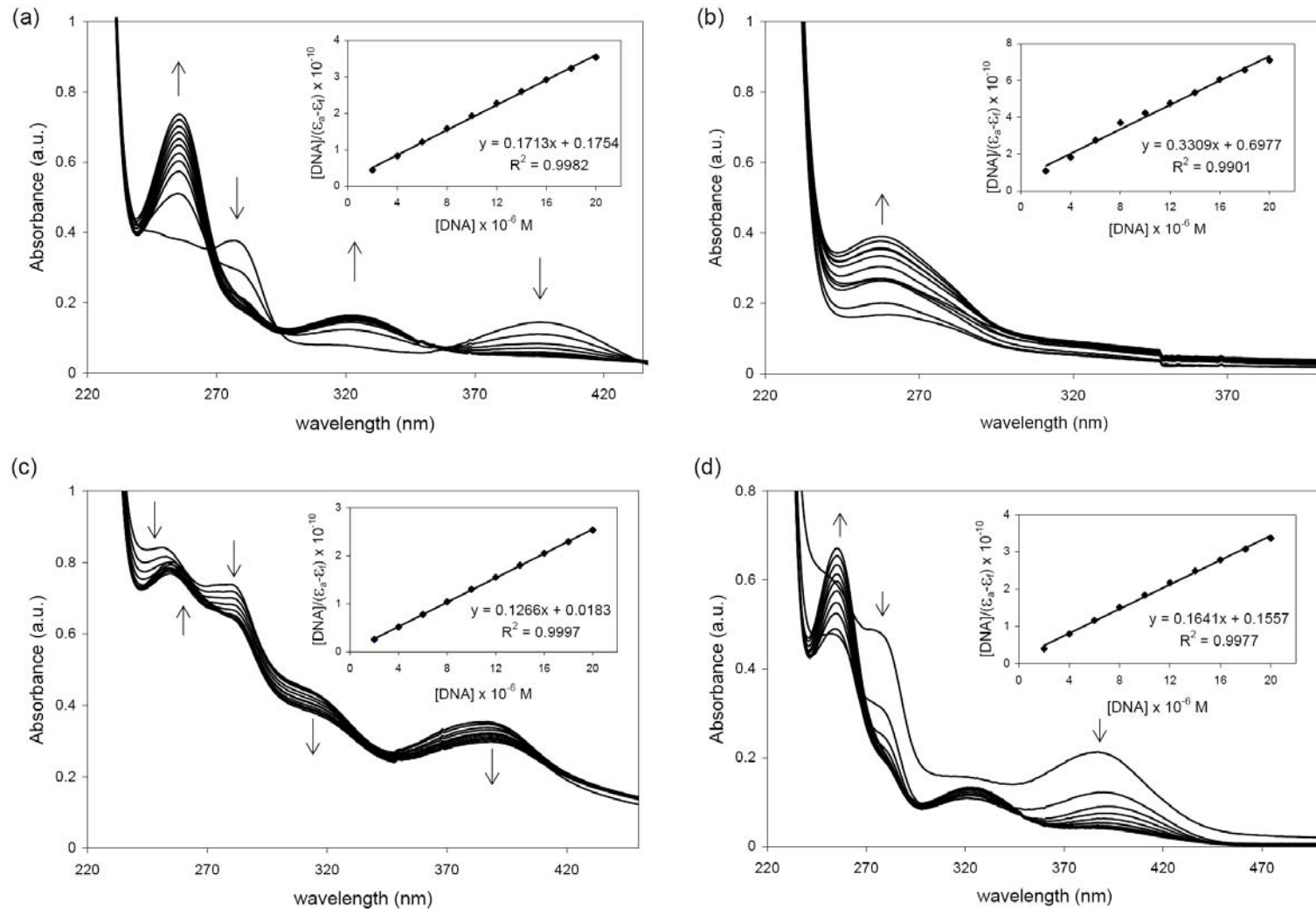


Figure 4.15 Electronic absorption spectra of (a) 4Cl-BMP (**A**), (b) NiA₂ (**A1**), (c) CuA₂ (**A2**), (d) ZnA₂ (**A3**), (e) 4OMe-BMP (**B**), (f) NiB₂ (**B1**), (g) CuB₂ (**B2**), (h) ZnB₂ (**B3**).

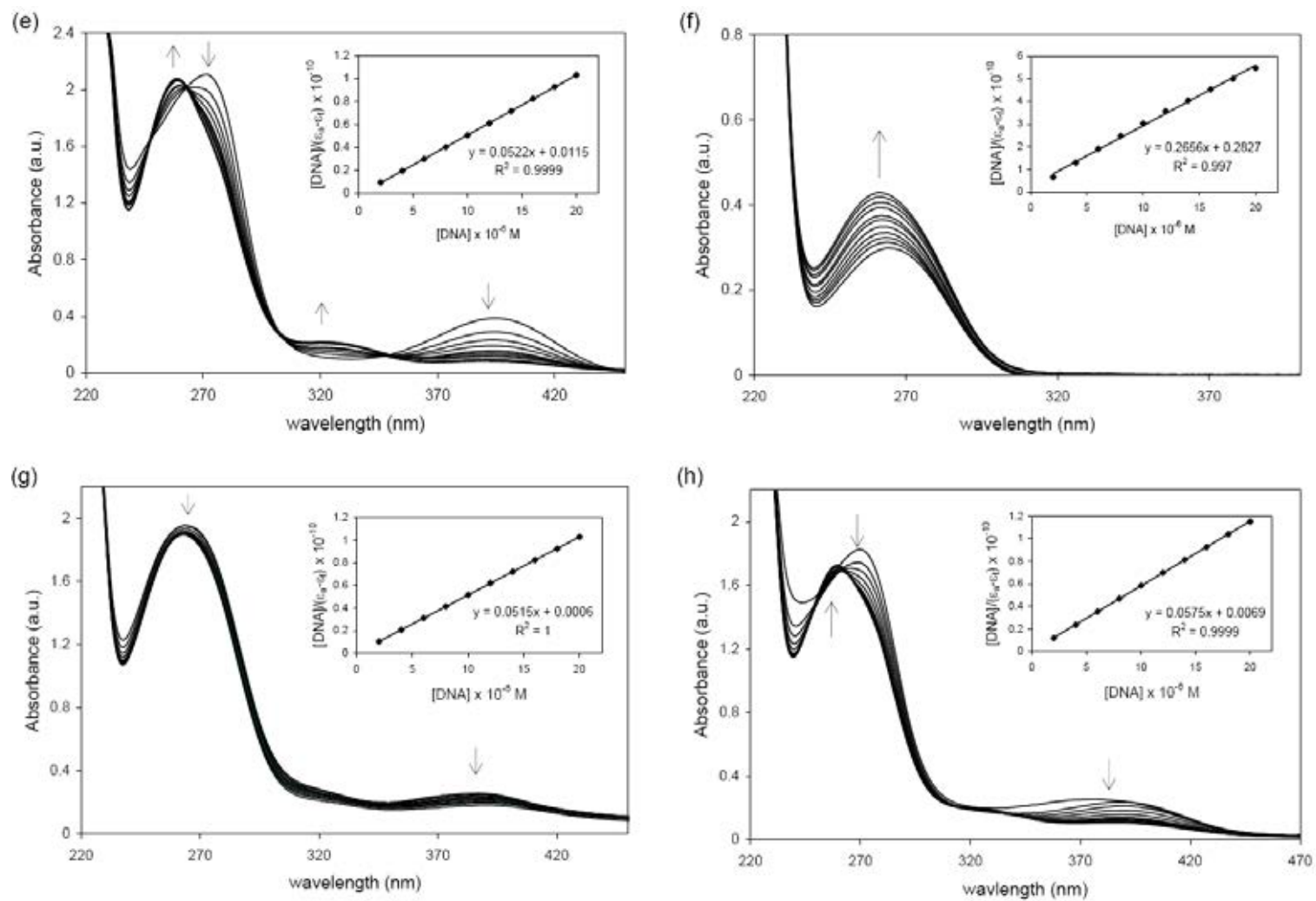


Figure 4.15 cont' Electronic absorption spectra of (a) 4Cl-BMP (A), (b) NiA₂ (A1), (c) CuA₂ (A2), (d) ZnA₂ (A3), (e) 4OMe-BMP (B), (f) NiB₂ (B1), (g) CuB₂ (B2), (h) ZnB₂ (B3).

In order to compare the binding ability quantitatively, we used the following equation to calculate the binding constant (K_b)

$$\frac{[\text{DNA}]}{\varepsilon_a - \varepsilon_f} = \frac{[\text{DNA}]}{\varepsilon_b - \varepsilon_f} + \frac{1}{K_b(\varepsilon_b - \varepsilon_f)}$$

Where ε_a , ε_f , and ε_b are the apparent extinction coefficient, the extinction coefficient for free compound, and the extinction coefficient for compound fully bound to DNA, respectively. The plots of $[\text{DNA}]/(\varepsilon_a - \varepsilon_f)$ versus $[\text{DNA}]$ are shown in Fig. 4.15. The K_b can be calculated from the ratio of the slope to the intercept. The calculated K_b are shown in table 4.11.

Table 4.11 The binding constant (K_b) and the absorption spectra change.

Compounds	$K_b \times 10^6$ (M^{-1})	Monitored at λ (nm)	Absorption Intensity (%)	Absorption Shift (nm)
Doxorubicin	1.00	485	hypochromism (45)	red shift (7)
Ethidiumbromide	1.32	480	hypochromism (26)	red shift (5)
4Cl-BMP (A)	0.98	394	hypochromism (67)	red shift (3)
NiA ₂ (A1)	0.47	259	hyperchromism (57)	blue shift (3)
CuA ₂ (A2)	6.92	383	hypochromism (14)	red shift (4)
ZnA ₂ (A3)	1.36	386	hypochromism (82)	red shift (8)
4OMe-BMP (B)	4.54	392	hypochromism (77)	red shift (2)
NiB ₂ (B1)	0.94	268	hyperchromism (29)	blue shift (8)
CuB ₂ (B2)	8.58	385	hypochromism (23)	red shift (9)
ZnB ₂ (B3)	8.33	378	hypochromism (58)	red shift (10)

The relative different in K_b values could be due to the different binding mode of complexes to DNA. K_b was used to distinguish the binding mode. From literature, if it ranges from $1 \times 10^4 - 1 \times 10^6 \text{ M}^{-1}$ refers to groove binding or electrostatic and K_b over $1 \times 10^6 \text{ M}^{-1}$ refers to intercalating [60]. Among these compounds, copper complexes have shown highly K_b values and the greatest K_b values has found for **B2** ($85.83 \times 10^6 \text{ M}^{-1}$). This is because Cu(II) ion (d^9), in generally, can be found to be 4, 5, and 6 coordinated complexes. **A2** and **B2** formed 4-coordinated square planar complexes which there are more reactive space for interact between DNA bases pair. Moreover, Cu(II) complexes prefer to bind with N7 of guanine, which can form 3 hydrogen bonds, and Zn(II) complexes with N3 of thymidine, which can form 2 hydrogen bonds. This results in Cu(II) complexes bind strongly to DNA. The order of binding ability are **B2** > **B3** > **A2** > **B** > **A3** > **A** > **B1** > **A1**. It indicated that Cu(II) complexes bind to CT DNA stronger than Zn and Ni complexes. This supported the stability order $\text{Zn}^{2+} < \text{Cu}^{2+} > \text{Ni}^{2+}$ in accordance with Irving-Willium's order for divalent metal of 3d series.

Moreover, the binding affinity of doxorubicin and ethidiumbromide were determined. It is obviously show that Schiff base **B**, copper and zinc complexes (**A2**, **A3**, **B2**, and **B3**) have stronger binding ability than doxorubicin and ethidiumbromide. It indicated that **A**, **A2**, **A3**, **B**, **B2**, and **B3** bind to DNA with the intercalation mode while **A1** and **B1**, which have less binding ability than doxorubicin and ethidiumbromide, bind to DNA with the groove binding mode. To further investigate the binding mechanism between complexes and DNA, EB displacement studies by fluorescence spectroscopy were also studied.

3.2 Fluorescence Emission spectra

In order to investigate the intercalation binding mode of CT DNA and the complexes, the fluorescence spectroscopy was used by observing the emission intensity of EB-DNA mixture when added with Schiff base compounds. Excitation of EB-DNA mixture at 346 nm, the emission intensity was observed ranging from 550-650 nm. The Schiff base compounds were added to EB-DNA, the emission intensity observed at 592 nm of EB-DNA was decrease as shown in Fig 4.16. This can be implied that the complex can displace EB at EB-DNA binding sites [61]

According to the Stern-Volmer equation

$$\frac{I_0}{I} = 1 + K_{sq} [Q]$$

where I_0 and I represent the emission intensity at the absence and presence of complex, respectively. K_{sq} is a linear Stern-Volmer quenching constant. $[Q]$ is the concentration of complex/[DNA]. The plot between I_0/I versus $[Q]$ for each complex is present in Fig 4.16. From the Stern-Volmer equation, K_{sq} is given from slope. K_{sq} values (Table 4.12) for Schiff base complexes are in order of Zn > Cu > Ni. The higher K_{sq} values refer to the higher quenching ability of complex and the stronger binding interaction between complex and DNA. The Stern-Volmer constants of these complexes are consistence with the binding ability from UV titration. This indicated that Schiff base ligands, copper and zinc complexes can interact with DNA by intercalating, whereas nickel complex bind to DNA at the groove binding.

For nickel complex, even it can quench EB at EB-DNA binding site but the binding strength is less than other complexes. This may contributed to the inactive cytotoxicity of nickel complex to all tested cell lines. This result exhibited that the binding strength between complexes and DNA including the mode of binding have an important role to the cytotoxic activity.

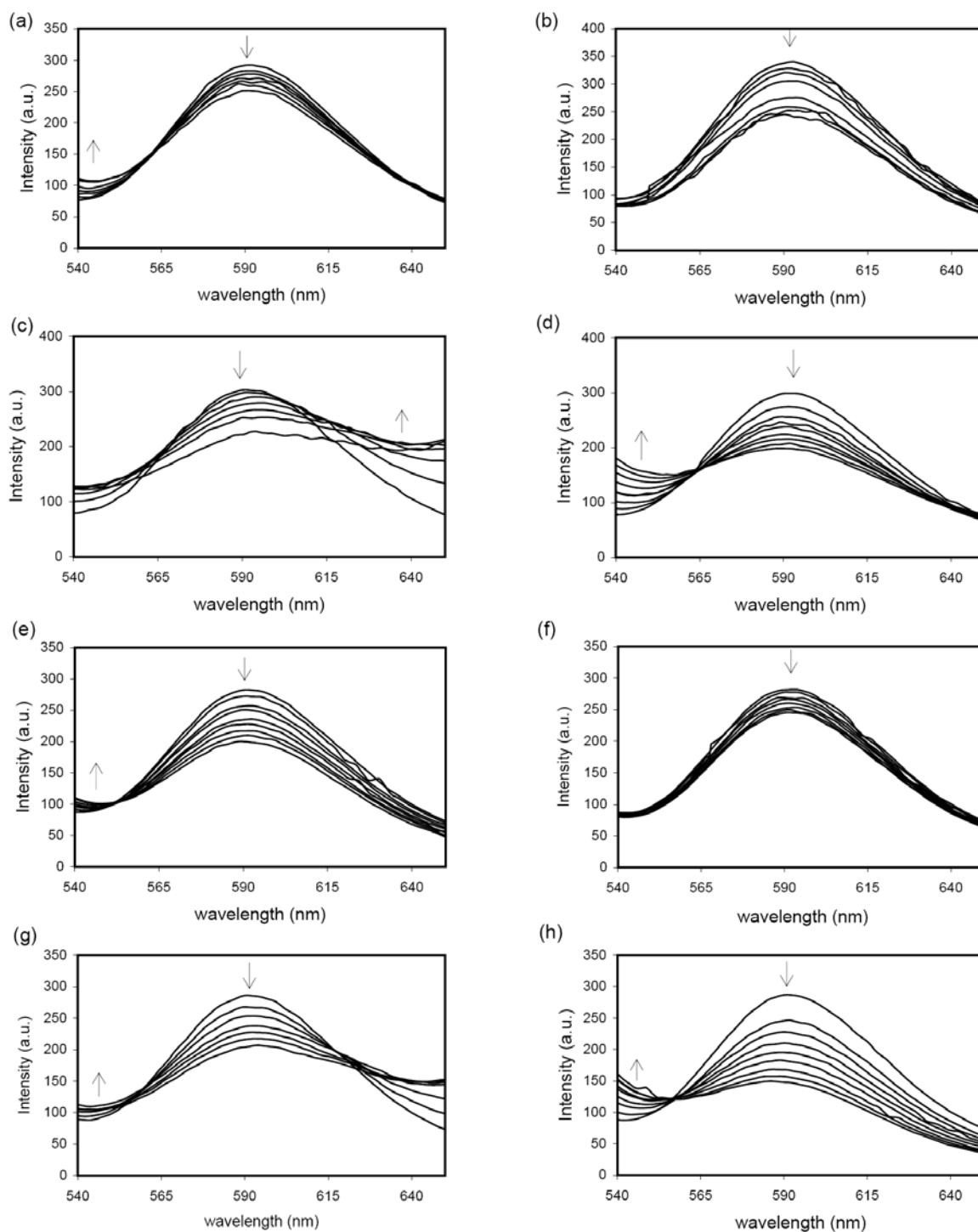


Figure 4.16 Emission spectra of (a) 4Cl-BMP (**A**), (b) NiA₂ (**A1**), (c) CuA₂ (**A2**), (d) ZnA₂ (**A3**), (e) 4OMe-BMP (**B**), (f) NiB₂ (**B1**), (g) CuB₂ (**B2**), (h) ZnB₂ (**B3**).

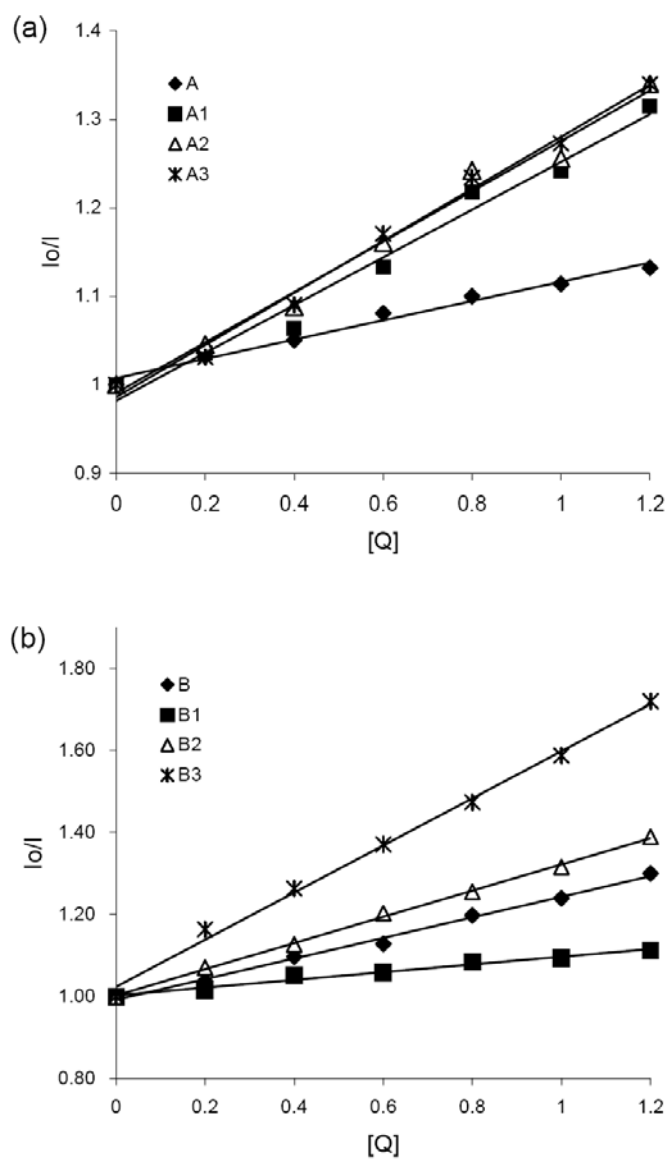


Figure 4.17 Stern-Volmer plot of (a) Schiff base (**A**) and metal complexes (**A1-3**), (b) Schiff base (**B**) and metal complexes (**B1-3**)

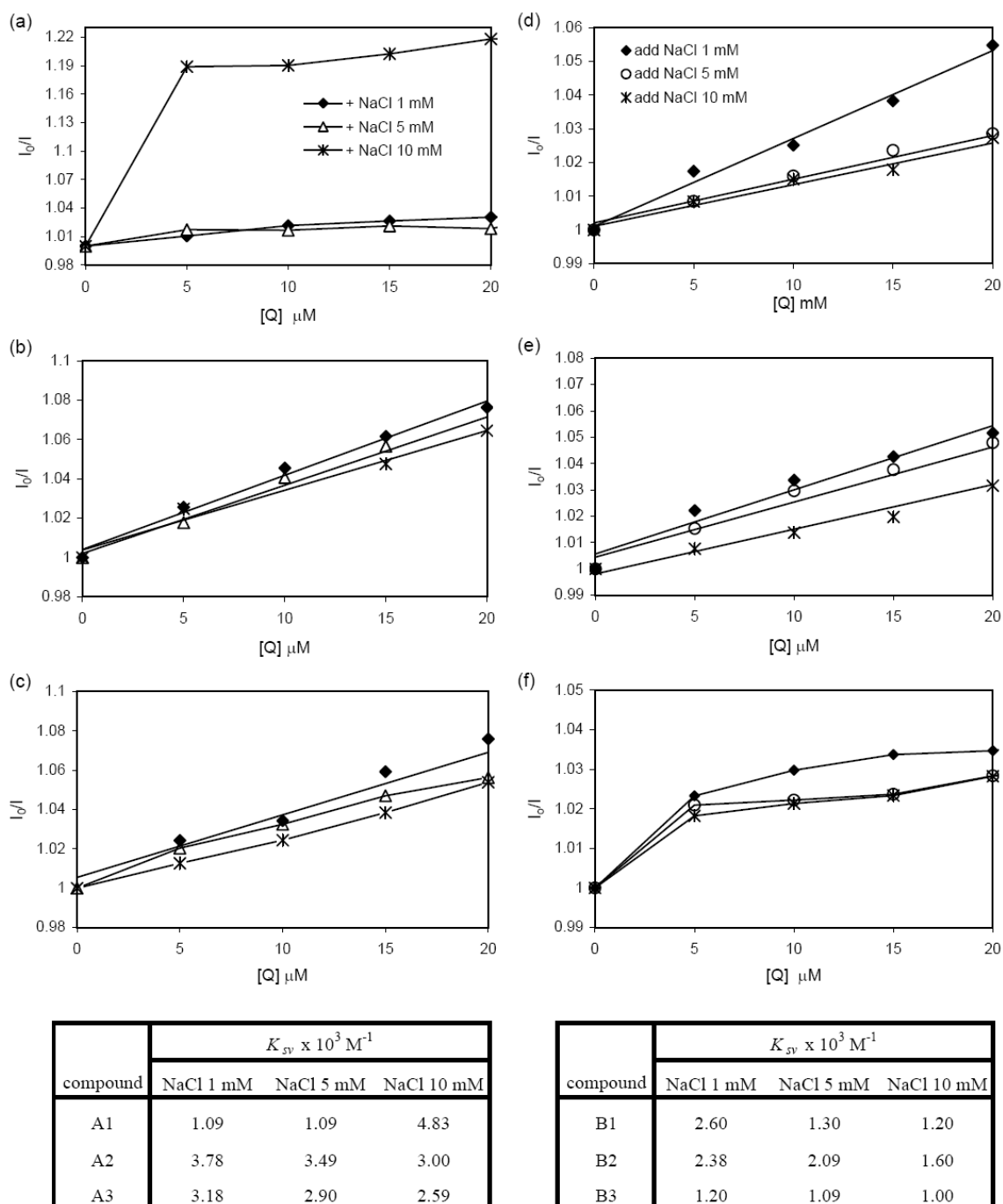


Figure 4.18 Stern-Volmer plot of metal complexes with the electrostatic effect test using EB-DNA systems (a) NiA₂ (**A1**), (b) CuA₂ (**A2**), (c) ZnA₂ (**A3**), (d) NiB₂ (**B1**), (e) CuB₂ (**B2**), (f) ZnB₂ (**B3**).

Table 4.12 Stern-Volmer quenching constant (K_{sv}), the apparent binding constant (K_{app}), and DNA melting temperature (T_m)

Compounds	Stern-Volmer equation (R^2)	K_{sq} (M^{-1})	$K_{app} \times 10^5$ (M^{-1})	T_m ($^{\circ}C$)	ΔT_m ($^{\circ}C$)
CT DNA	-	-	-	49	0
4Cl-BMP (A)	$y = 0.1089x + 1.0074$ (0.985)	1.09	2.19	55	6
NiA ₂ (A1)	$y = 0.2698x + 0.982$ (0.9796)	2.75	5.30	53	4
CuA ₂ (A2)	$y = 0.2848x + 0.9907$ (0.9851)	2.85	5.64	74	25
ZnA ₂ (A3)	$y = 0.294x + 0.9862$ (0.9913)	2.98	5.80	74	25
4OMe-BMP (B)	$y = 0.2507x + 0.9925$ (0.9946)	2.51	4.98	50	1
NiB ₂ (B1)	$y = 0.0941x + 1.003$ (0.9771)	0.94	1.89	64	15
CuB ₂ (B2)	$y = 0.3191x + 1.0029$ (0.9985)	3.19	6.40	67	18
ZnB ₂ (B3)	$y = 0.5743x + 1.0238$ (0.9958)	5.74	11.80	70	21

The effect of electrostatic was also investigated in EB-DNA system by vary NaCl concentration at 1, 5, and 10 mM (Fig. 4.18). In general as the present of metal ion, it is not only bind to DNA at amine groups of DNA bases but also the phosphate backbones. The negatively charges of phosphate backbones must be neutralised by complexing with metal ions. This external binding ability depends on metal ion concentration. The higher metal ions concentration, the higher the duplex stability. Monovalent cations such as sodium or potassium can complex with the phosphates to stabilise the duplex. Therefore, if there are electrostatic interactions between

complexes and DNA, the higher concentration of NaCl will cause the less binding ability of complexes to DNA. From this study, the ability of compounds to quench EB at EB-DNA sites are decrease when the concentration of NaCl increase for most complexes except **A1**. The effect of ionic strength on quenching constant showed that there is electrostatic force between complexes (**A2-B3**) to DNA. Complex **A1** (Fig. 4.18a) showed the opposite result as the quenching constant increase while increasing NaCl concentration. This is because of the phosphates are considered to be hard ligand that prefer hard metals like Ni(II).

The results in this part supported the hypothesis that metal complexes of Schiff base can improve the ability to displace EB in EB-DNA binding sites and prove that the mechanism which copper and zinc complexes bind with CT DNA is the intercalation binding mode and there is electrostatic effect, while nickel complexes can bind to DNA with groove binding with strong electrostatic force.

3.3 DNA melting temperature

Melting temperature (T_m) is a temperature at which 50% of DNA is degraded. Thermal denature studies were carried out in TBE buffer containing 60 μM of CT DNA and 20 μM of the compounds. Melting curves were recorded at 260 nm. The melting curves (T_m) and the table of melting temperature are in Fig. 4.19 and table 4.12. T_m curve exhibited the melting temperature of CT DNA at 49°C, while the melting temperature of CT DNA bound with compounds are increase. Metal complexes showed higher melting temperature than Schiff base ligands. This indicated that the metal complexes can stabilize DNA double strand and bind strongly to CT DNA more than Schiff bases do.

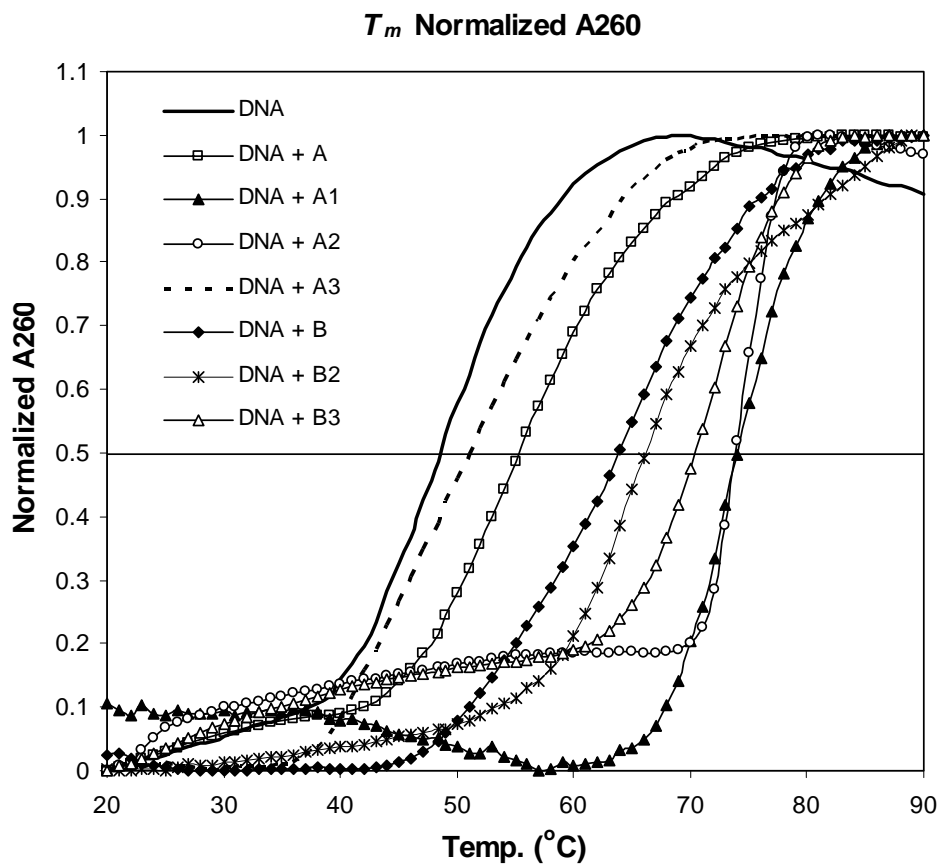


Figure 4.19 Normalized melting temperature curve (T_m).

4. DNA cleavage activity

The DNA cleavage activity of Schiff base metal complexes has been determined by gel electrophoresis based on qualification of the conversion of supercoiled (SC) pUC19 DNA to nicked circular and linearised. Incubation of DNA with compounds (100 μ M) but without addition of any reductant, irradiated under UV-A light at 365 nm in the dark for 15 min resulted in cleavage activity of pUC19 (Fig. 4.20b) while incubation without exposure to UV-A did not show cleavage of DNA (Fig. 4.20a). This phenomenon indicated that all compounds performed direct strand scission, especially copper complex (**B2**). The high ability of DNA strand scission by **B2** supported the results of strong inhibition of cancer cell growth in previous section. This complex is suited for particularly therapeutic applications in cancer chemotherapy. The propose mechanism is shown in Fig. 4.21. The irradiation by UV-A results in the formation of reactive singlet oxygen species and/or superoxide radical that can be reduced to H_2O_2 and hydroxyl radical which cause the DNA strands scission [62-66].

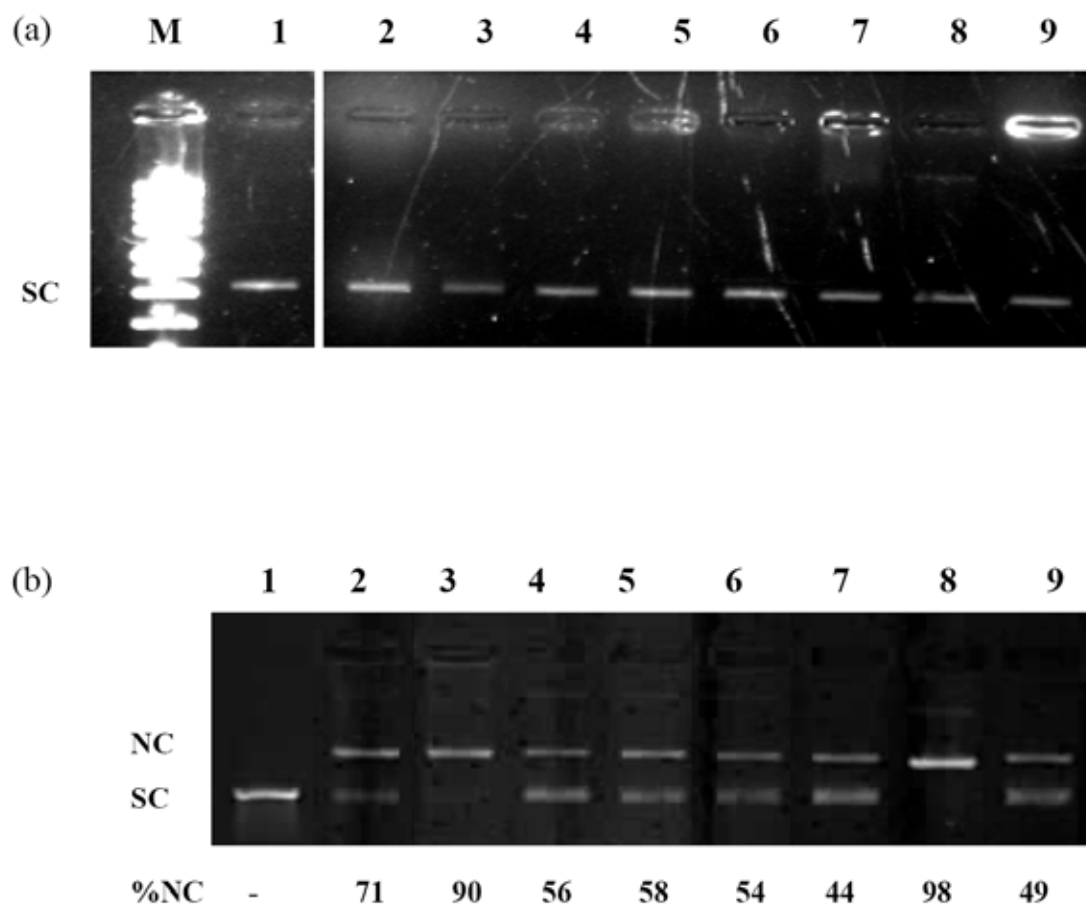


Figure 4.20 Cleavage of pUC19 DNA incubation in the dark (a) and 15 min irradiated under UV-A 365 nm (b) lane 1: pUC19 DNA; lane 2: pUC19 DNA + **A** (100 μ M); lane 3: pUC19 DNA + **A1** (100 μ M); lane 4: pUC19 DNA + **A2** (100 μ M); lane 5: pUC19 DNA + **A3** (100 μ M); lane 6: pUC19 DNA + **B** (100 μ M); lane 7: pUC19 DNA + **B1** (100 μ M); lane 8: pUC19 DNA + **B2** (100 μ M); lane 9: pUC19 DNA + **B3** (100 μ M);

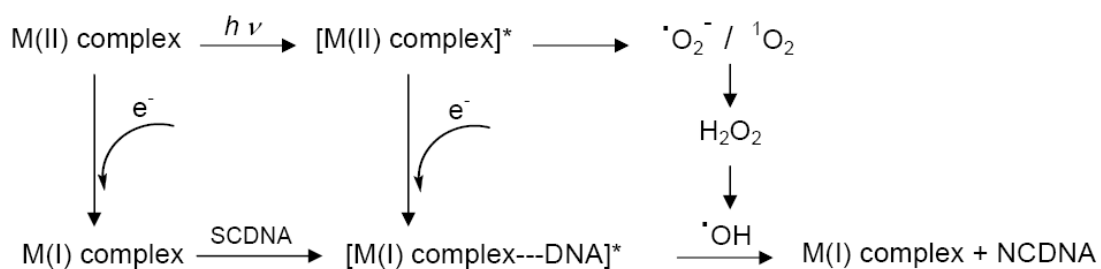


Figure 4.21 Propose mechanistic pathway for the photo-induced nuclease activity of the complexes.

Table 4.13 DNA cleavage reaction conditions and %NC.

Lane	Reaction condition	%NC
1	pUC19	-
2	pUC19 + A (100 μM)	71
3	pUC19 + A1 (100 μM)	90
4	pUC19 + A2 (100 μM)	56
5	pUC19 + A3 (100 μM)	58
6	pUC19 + B (100 μM)	54
7	pUC19 + B1 (100 μM)	44
8	pUC19 + B2 (100 μM)	98
9	pUC19 + B3 (100 μM)	49

CHAPTER IV

CONCLUSION

In this dissertation, the transition metal complexes of 6-deoxyclitoriacetal and Schiff base of 2-[(4-chlorobenzylimino)-methyl]-phenol and 2-[(4-methoxybenzylimino)-methyl]-phenol have been synthesized in order to be new anticancer drugs candidate and their anticancer mechanism have been investigated.

Part I; metal complexes of Fe(III), Co(II), Ni(II), and Cu(II) of 6-deoxyclitoriacetal (**L**) have been synthesized. The proposed molecular structures are FeL(H₂O)₄Cl₂ (**1**), CoL(NO₃)(H₂O)₂.2H₂O (**2**), NiL(CH₃COO).4H₂O (**3**), and CuL₂.2H₂O (**4**). The toxicity test for normal cell line of CH, CCD and HS27 using MTT assay resulted in non-cytotoxic for all complexes. The effective cytotoxic activities have shown for **L** to BT474 (IC₅₀ 0.003 μM), for **1** to KB with IC₅₀ 0.005 μM, for **2** to CHAGO (IC₅₀ 0.007 μM) and NCI-H187 (IC₅₀ 0.005 μM) and for **3** to KATO (IC₅₀ 0.002 μM), while, **4** strongly active to all tested cell except KB. The DNA binding ability performed using UV-Vis gave the binding constant (K_b) of complex **1** ($2.21 \times 10^6 \text{ M}^{-1}$) and **4** ($2.13 \times 10^6 \text{ M}^{-1}$) are greater than **2** ($1.68 \times 10^6 \text{ M}^{-1}$) and **3** ($1.13 \times 10^6 \text{ M}^{-1}$). Hypochromism and red shift observed in absorption spectra for all compounds indicated that these compounds bind to DNA with intercalation binding mode. Intercalating mode was confirmed using EB displacement by fluorescence spectroscopy. It exhibited that **L** and metal complexes bind with the intercalation mode to DNA.

Part II; transition metal complexes of Ni(II), Cu(II) and Zn(II) have been synthesized from Schiff base 2-[(4-chlorobenzylimino)-methyl]-phenol (**A**) and 2-[(4-methoxybenzylimino)-methyl]-phenol (**B**). The X-ray crystal structures of Ni(II) and Cu(II) complexes **A1**, **A2**, **B1**, and **B2** are square planar, while Zn(II) complexes (complex **A3** and **B3**) showed tetrahedral geometry. All compounds are non-cytotoxic to normal cell line of vero cell. The potent cytotoxic activities evaluated using MTT assays have shown for Cu(II) and Zn(II) complexes against all tested cancer cell lines, especially Cu(II) complexes (**B2**) against KATO3 (IC_{50} 0.025 μ M) and BT474 (IC_{50} 1.45 nM). DNA binding studies revealed the strong binding constant (K_b) of Cu(II) and Zn(II) complexes. The binding mode was confirmed to be intercalation by the phenomenon of hypochromic and bathochromic found in absorption spectra including EB displacement examined by fluorescence spectroscopy. However, Ni(II) complexes are inactive to all tested cancer cells and were found to bind with DNA by groove binding mode.

REFERENCES

- [1] Krogsgaard-Larsen, P.; Liljefors, T.; Madsen, U. Textbook of drug design and discovery. Taylor & Francis Inc, New York (2002): 51-58.
- [2] Bergeret, A.; Gadelle, D.; Forterre, P. Purification of a DNA topoisomerase II from the hyperthermophilic archaeon *Sulfolobus shibatae*. A thermostable enzyme with both bacterial and eucaryal features. J. Biol. Chem. 269 (1994): 27663-27669.
- [3] Crombie, L.; Whiting, D. A. Review article number 135 biosynthesis in the rotenoid group of natural products: applications of isotope methodology. Phytochemistry 49 (6) (1998): 1479-1507.
- [4] Zurowska, B.; Erxleben, A.; Glinka, L.; Łeczycka, M.; Zyner, B. E.; Ochocki, J. Synthesis, spectroscopy and magnetism of novel metal complexes of 3-aminoflavone (3-af). X-ray crystal structure of 3-af and $[\text{Cu}(\text{3-af})_2(\text{NO}_3)_2]$. Inorg. Chim. Acta. 362 (2009): 739-744.
- [5] Wang, D. B.; Yang, Y. Z.; L, H. M.; Hai, J.; Wang, Q.; Chen, N. Z. Synthesis, characterization, cytotoxic activity and DNA binding Ni(II) complex with the 6-hydroxy chromone-3-carbaldehyde thiosemicarbazone. J. Organomet. Chem. (2009): 4069-4075.
- [6] Kosmider, B.; Zawlik, I.; Liberski, P.; Osiecka, R.; Zyner, E.; Ochocki., P.; Bartkowiak, J. Evaluation of *P53* and *BAX* gene expression and induction of apoptosis and necrosis by the *cis*-Pt(II) complex of 3-aminoflavone in comparison with *cis*-diamminedichloroplatinum(II) (*cis*-DDP) in human lymphocytes. Mutat. Res. 604 (2006): 28-35.

- [7] Roengsumran, S.; Khorphueng, P.; Chaichit, N.; Muangsin, N.; Petsom, A. Crystal structure of 6-deoxyclitoriacetal, C₁₉H₁₈O₈. Z Kristallogr. NCS. 218 (2003) 105-106.
- [8] Kumar, S.; Qing H.; Reno, J. L. 186 K operation of terahertz quantum-cascade lasers based on a diagonal design. Appl. Phys. Lett. 94 (2009): 105-131.
- [9] Lippard, S. J. Bioinorganic Chemistry, 2nd Edition, University Science Books Millvalley (1994): 505-508.
- [10] Bleomink, M. J.; Reedi, J. K. Metal Ions in Biological Systems, 3rd Edition. Mercel Dekker Inc. New York (1996): 641-644.
- [11] Chakravarti, A.; Noll, E.; Black, P. McL.; Finkelstein, D. F.; Dyson, N. J.; Loeffler, J. S., Quantitatively Determined Survivin Expression Levels Are of Prognostic Value in Human Gliomas. J. Clinical Oncology. 20 (2002): 1063-1068.
- [12] Gao, N.; Ding, M.; Zheng, J. Z.; Zhang, Z.; Leonard, S. S.; Liu, K. J.; Shi, X.; Jiang, B.-H. Vanadate-induced Expression of Hypoxia-inducible Factor 1 α and Vascular Endothelial Growth Factor through Phosphatidylinositol 3-Kinase/Akt Pathway and Reactive Oxygen Species. J. Bio. Chem. 277 (2002): 31963-31971.
- [13] Hanna, W.; Moawad, G. Synthesis, characterization and antimicrobial activity of cobalt(II), nickel(II) and copper(II) complexes with new asymmetrical Schiff base ligands derived from 7-formylanil-substituted diamine-sulphoxine and acetylacetone. Transition Met. Chem. 26 (2001): 644-651.
- [14] Keypour, H.; Salehzadeh, S.; Parish, P. V. Synthesis of Two Potentially

- Heptadentate (N₄O₃) Schiff-base Ligands Derived from Condensation of Tris(3-aminopropyl)-amine and Salicylaldehyde or 4-Hydroxysalicylaldehyde Nickel(II) and Copper(II) Complexes of the Former Ligand. Molecules 7 (2002): 140-144.
- [15] Bruce, A.; Johnson, A.; Lewis, J.; Raff, M.; Roberts, K.; Walters, P. Molecular Biology of the Cell. 4th edition. New York and London: Garland Science (2002).
- [16] Hurley, L.H. DNA and its associated processes as targets for cancer therapy. Nature 2 (2002): 188-200.
- [17] Close, P.; D'Angio G. J.; Sinniah, D.; Meadows, A.T. Basic principles of chemotherapy. Practical pediatric oncology. New York: Wiley-Liss (1992): 155-63.
- [18] Balis FM, Holcenberg JS, Poplack DG. General principles of chemotherapy. Principles and practice of pediatric oncology. 2nd ed. Philadelphia: JB Lippincott (1993): 197-245.
- [19] Krogsgaard-Larsen, P.; Liljefors, T.; Madsen, U. Textbook of drug design and discovery, Taylor & Francis Inc, New York, (2002): 51-58.
- [20] Goodwin, K.D.; Lewis, M.A.; Long, E.C.; Georgiadis, M.M. Crystal structure of DNA-bound Co(III)-bleomycin B₂: insights on intercalation and minor groove binding. P. Natl. Acad. Sci., USA. 105 (2008): 5052-5056.
- [21] Wang, A. Interactions between an anthracycline antibiotic and DNA: molecular structure of daunomycin complexed to d(CpGpTpApCpG) at 1.2° resolution. Biochemistry 26 (1987): 1152-1163.

- [22] Karaliota, A.; Kretsi, O.; Tzougraki, C., Synthesis and characterization of a binuclear coumarin-3-carboxylate copper(II) complex. J. Inorg. Biochem. 84 (1–2) (2001): 33-37.
- [23] Budzisz, E.; Keppler, B.K.; Giester, G.; Woźniczka, M.; Kufelnicki, A.; Nawrot, B. Synthesis, crystal structure and biological characterization of a novel palladium(II) complex with a coumarin-derived ligand. Eur. J. Inorg. Chem. (2004): 4412-4419.
- [24] Kostova, I.; Manolov, I.; Karaivanova, M. Synthesis, physicochemical characterization and cytotoxic screening of new zirconium complexes with coumarin derivatives. Arch. Pharm., Pharm. Chem. 334 (2001): 157-162.
- [25] Creaven, B. S.; Egan, D. A.; Kavanagh, K.; McCann, M.; Mahon, M.; Noble, A.; Thati, B.; Walsh, M. Synthesis and antimicrobial activity of copper(II) and silver(I) complexes of hydroxynitrocoumarins: X-ray crystal structures of $[\text{Cu}(\text{hnc})_2(\text{H}_2\text{O})_2] \cdot 2\text{H}_2\text{O}$ and $[\text{Ag}(\text{hnc})](\text{hncH}=4\text{-hydroxy-3-nitro-2H-chromen-2-one})$. Polyhedron. 24 (2005): 949-957.
- [26] Grazul, M.; Budzisz, E. Biological activity of metal ions complexes of chromones, coumarins and flavones. Coordin. Chem. Rev. 253 (2009): 2588-2598.
- [27] Kostova, I. Synthetic and natural coumarins as cytotoxic agents. Curr. Med. Chem-Anti Cancer Agents. 5 (2005): 29-46.
- [28] Kostova, I.; Momekov, G. New zirconium(IV) complexes of coumarins with cytotoxic activity. Eur. J. Med. Chem. 41 (2006): 717-726.
- [29] Kostova, I.; Momekov, G. Synthesis, characterization and cytotoxicity evaluation of new cerium (III), lanthanum(III) and neodymium (III) complexes. Bioorg. Chem. 21 (2007): 226-233.

- [30] Bergeret, A.; Gabelle, D.; Forterre, P. Purification of a DNA topoisomerase II from the hyperthermophilic archaeon *Sulfolobus shibatae*. a thermostable enzyme with both bacterial and eucaryal features. J. Biol. Chem. 269 (1994) 27663-27669.
- [31] Kosmider, B.; Zawlik, I.; Liberski, P. P.; Osiecka, R.; Zyner, E.; Ochocki, J.; Bartkowiak, J. Evaluation of *P53* and *BAX* gene expression and induction of apoptosis and necrosis by the *cis*-Pt(II) complex of 3-aminoflavone in comparison with *cis*-diamminedichloroplatinum(II) (*cis*-DDP) in human lymphocytes. Mutat. Res. 604 (2006): 28–35.
- [32] Zurowska, B.; Erxleben, A.; Glinka, L.; Łeczycka, M.; Zyner, B. E.; Ochocki, J. Synthesis, spectroscopy and magnetism of novel metal complexes of 3-aminoflavone (3-af). X-ray crystal structure of 3-af and [Cu(3-af)₂(NO₃)₂]. Inorg. Chim. Acta, 362 (2009): 739–744.
- [33] Marmur, J., A procedure for the isolation of deoxyribonucleic acid from microorganisms. J. Mol. Bio. 3 (2) (1961): 208-218.
- [34] Chimsook, P. Structure-activity relationship on cytotoxicity of rotenoid compounds, Doctoral dissertation, Department of Biotechnology, Science, Chulalongkorn University, 2008.
- [35] Bhattacharyya, P.; Parr, J.; Ross, A.T., First synthesis of a unique dilead Schiff base complex. J. Chem. Soc. Dalto. (1998): 3149.
- [36] Kumar, S., Dhar, D. N., Saxena, P. N. Applications of metal complexes of Schiff bases-A review. J. of Scientific & Industrial Research 68 (2009): 181-187.
- [37] Basolo, F., Johnson, R. C. Coordination Chemistry: The Chemistry of Metal Complexes. W. A. Benjamin, inc. (1869): 8.

- [38] Ettling, C. Untersuchungen über das ätherische Oel der Spiraea Ulmaria und die salicylige Säure. Ann. Chem Pharm. 35 (1840): 241-276.
- [39] Djebbar-Sid, S.; Benali-Baitich, O.; Deloume, J. P., Synthesis, characterization and electrochemical behaviour of some copper(II) complexes with linear and tripodal tetradentate ligands derived from Schiff bases. Polyhedron 16 13 (1997): 2175-2182.
- [40] Rahman, M., Mridha, M., Ali, M. A. Transition metal complexes of the Schiff base derived from *S*-methyldithiocarbamate with 2-aminobenzaldehyde. Trans. Met. Chem. 19 (1994): 237-240.
- [41] Clerk, A. J.; Jones, K., Evidence on the Nature of Cobalt-mediated Aryl- radical Cyclization. Tetrahedral Letters. 30 (1989): 5485-5489.
- [42] Clerk, A. J.; Filik, R. P.; Thomas, G. H.; Wongtap, H. Generation and Cyclization of Homogeneous and Solid Supported Copper (II) Schiff Base Complexes. J. Am. Chem. Soc. 1 (1998): 216, 743.
- [43] Xishi, T.; Xian, H. Y.; Qiang, C.; Minyu, T. Synthesis of Some Transition Metal Complexes of a Novel Schiff Base Ligand Derived from 2, 2' – Bis(*p*-Methoxy Phenylamine) and Salicylic Aldehyde. Molecules 8 (2003): 439-443.
- [44] Zhong, X.; Wei, H-L.; Liu, W-S.; Wang, D-Q.; Wang, X. The Crystal Structures of copper(II), manganese(II), and nickel(II) complexes of a (*Z*)-2-hydroxy-*N*'-(2-oxoindolin-3-ylidene) benzohydrazide-potential antitumor agents. Bioorg & Med. Chem. Lett. 17 (2007): 3774-3777.
- [45] Elzahany, E. A.; Hegab, K. H.; Khalil, S. K. H.; Youssef, N. S. Synthesis, Characterization and Biological Activity of Some Transition Metal Complexes with Schiff Bases Derived from 2-Formylindole, Salicylaldehyde, and *N*-amino Rhodanine. Aust. J. Basic & Appl. Sci. 2 (2) (2008): 210-220.

- [46] Shaker, S. A.; Farina, Y.; Salleh, A. A. Synthesis and Characterization of Mixed Ligand Complexes of 8-Hydroxyquinoline and o-hydroxybenzylidene-1-phenyl-2,3-dimethyl-4-amino-3-pyrazolin-5-one with Fe(II), Co(II), Ni(II) and Cu(II) ions. Eur. J. Sci. Research 33 (4) (2009): 703-709.
- [47] Bruce, A.; Johnson, A.; Lewis, J., Raff, M.; Roberts, K., Walters, P. Molecular Biology of the Cell. 4th ed. New York and London: Garland Science (2002).
- [48] Hurley, L.H. DNA and its associated processes as targets for cancer therapy. Nature 2 (2002): 188-200.
- [49] Bleckburn, G.M.; Gait, M.N. Nucleic Acids in Chemistry and Biology. New York: IRL Press (1990): 297-322..
- [50] Pourquier, P.; Pommier, Y. Topoisomerase I-mediated DNA damage. Adv. Cancer Res. 80 (2001): 189-216.
- [51] Nitiss, J. L. Investigating the biological functions of DNA topoisomerases in eukaryotic cells. Biochim. Biophys. Acta Gene Struct. Exp. 1400 (1-3) (1998): 63-81.
- [52] Chaires, J.B. Drug-DNA interactions. Curr. Opin. Struct. Biol. 8 (1998): 314-320.
- [53] Temperini, C.; Messori, L.; Orioli, P.; Bugno, C.D.; Animati, F.; Ughetto, G., The crystal structure of the complex between a disaccharide anthracycline and the DNA hexamer d(CGATCG) reveals two different binding sites involving two DNA duplexes. Nucl. Acids Res. 31 (5) (2003): 1464-1469.
- [54] Bostock-Smith, C.E.; Embrey, K. J.; Searle, M.S. Enhanced binding of a cyclic amidine analogue of Hoechst 33258 to the minor groove of DNA: ¹H NMR and UV melting studies with the decamer duplexed (GGTAATTACC)₂. J. Chem. Soc. Chem. Commun. (1997): 121-122.

- [55] Martinez, R.; Chacon-Garcia, L. The search of DNA-intercalators as antitumoral drugs: what it worked and what did not work. Curr. Med. Chem. 12 (2005): 127-151.
- [56] Liu, L. F. DNA Topoisomerase poisons as antitumor drugs. Annu. Rev. Biochem. 58 (1989): 351.
- [57] Garbett, N. C.; Graves, D. E. Extending Nature's Leads: The Anticancer Agent Ellipticine. Curr. Med. Chem. 4 (2004): 149-172.
- [58] Li, V. S.; Choi, D.; Wang, Z.; Jimenez, L.S.; Tang, M. S.; Kohn, H. Role of the C-10 substituent in Mitomycin C-1-DNA bonding. J. Am. Chem. Soc. 118 (1996): 2326– 2331.
- [59] Zuber, G.; Quada, J. C., Jr; Hecht, S. M. Sequence selective cleavage of a DNA octanucleotide by chlorinated bithiazoles and bleomycins. J. Am. Chem. Soc. 120 (1998): 9368–9369.
- [60] Hecht, S.M. Bleomycin: new perspectives on the mechanism of action. J. Nat. Prod. 63 (2000): 158–168.
- [61] Erkkila, K.E.; Odom, D.T.; Barton, J.K. Recognition and Reaction of Metallointercalators with DNA. Chem. Rev. 99 (1999) 2777–2796.
- [62] Metcalfe, C.; Thomas, J.A. Kinetically inert transition metal complexes that reversibly bind to DNA. Chem. Soc. Rev. 32 (2003): 215–224.
- [63] Haq, I.; Lincoln, P.; Suh, D.; Norden, B.; Choedhry, B.Z.; Chaires, J.B. Interaction of .DELTA.- and .LAMBDA.-[Ru(phen)2DPPZ]2+ with DNA: A Calorimetric and Equilibrium Binding Study. J. Am. Chem. Soc. 117 (1995): 4788–4796.

- [64] Arturo, S.; Giampaolo, B.; Giuseppe, R.; Maria, L.G.; Salvatore, T. The interaction of native DNA with Iron (III)-*N*, *N'*-ethylene-bis(salicylideneiminato)-chloride. J. Inorg. Biochem. 98 (2004): 589-594.
- [65] Maribel, N.; Efren, C.F.; Anßbal, S.; Mercedes, F.M.; Pedro, S.; Dwight, A.; Edgar, M. Design of copper DNA intercalators with leishmanicidal activity. J. Biol. Inorg. Chem. 8 (2003): 401-408.
- [66] Catherine, H.; Marguerite, P.; Michael, R.; Heinz, G.; Stephanie, S.; Bernard, M. Preparation, characterization and crystal structures of manganese (II), iron (III) and copper (II) complexes of the bis[di-1,1-(2-pyridyl) ethyl] amine (BDPEA) ligand; evaluation of their DNA cleavage activities. J. Biol. Inorg. Chem. 6 (2001): 14-22.
- [67] Kumar, C.V.; Barton, J.K.; Turro, N.J. Photophysics of Ruthenium Complexes Bound to Double Helical DNA. J. Am. Chem. Soc. 107 (1985): 5518-5523.
- [68] Xu, H.; Zheng, K.C.; Deng, H.; Lin, L.J.; Zhang, Q.L.; Ji, L.N. Effects of ligand planarity on the interaction of polypyridyl Ru (II) complexes with DNA. Dalton. Trans. 3 (2003): 2260-2268.
- [69] Mahadevan, S.; Palaniandavar, M. Electrochemical study of the enantioselective interaction of Tris(phen)Ru (II) with calf thymus DNA. Inorg. Chim. Acta. 254 (1997): 291-302.
- [70] Xu, H.; Zheng, K.C.; Deng, H.; Lin, L.J.; Zhang, Q.L.; Ji, L.N. Interaction of Ru(II) Complex with Yeast tRNA Studied by Isothermal Clarometry. New J. Chem. 27 (2003): 1255-1263.
- [71] Mozaffar, A.; Elham, S.; Bijan, R.; Leila, H. Thermodynamic and spectroscopic study on the binding of cationic Zn(II) and Co(II) tetrapyridinoporphyrazines

- to calf thymus DNA: the role of the central metal in binding parameters. New J. Chem. 28 (2004): 1227-1234.
- [72] Chaires, J.B. Energetics of drug-DNA binding. Biopolymers 44 (1998): 201-215.
- [73] Zhang, H.; Liu, C.-S.; Bu, X.-H.; Yang, M. Synthesis, crystal structure, cytotoxic activity and DNA-binding properties of the copper (II) and zinc (II) complexes with 1-[3-(2-pyridyl) pyrazol-1-ylmethyl] naphthalene. J. Inorg. Biochem. 99 (2005): 1119-1125.
- [74] Shnulin, A.N.; Nadzhatov, G.N.; Amiraslanov, I.R.; Usubaliyev, B.T.; Mamedov, K.S. Diaquabis (*N, N*-diethylnicotinamide-*N*1)bis(2-hydroxybenzoato-*O*) cobalt(II). Koordinatsionnaya Khimiya 7 (1981): 1409.
- [75] Wang, X-L.; Chao, H.; Li, H.; Hang, X-L.; Liu, Y-J.; Tan, L-F.; Ji, L-N. DNA Interactions of Cobalt (III) Mixed-Polyridyl Complexes Containing Asymmetric Ligands. J. Inorg. Biochem. 98 (2004): 1143-1150.
- [76] Hossain, Z.; Huq, F. Studies on the Interaction Between Ag⁺ and DNA. J. Inorg. Biochem. 91 (2002): 398-404.
- [77] Jiang, J.-Y. Clinical Study of Mild Hypothermia Treatment for Severe Traumatic Brain Injury. J. Neurotrauma. 26 (3) (2009): 399-406.
- [78] Stern, V. O.; Volmer, M. On the quenching-time of Fluorescence. Z. Phys. 20 (1919): 183-188.
- [79] Mosmann, T., Rapid colorimetric assay for cellular growth and survival: Application to proliferation and cytotoxicity assays. J. Immunol. Methods. 65 (1-2) (1983): 55-63.
- [80] Buttke, T. M.; McCubrey, J. A.; Owen, T. C., Use of an aqueous soluble tetrazolium/formazan assay to measure viability and proliferation of

- lymphokine-dependent cell lines. J. Immunol. Methods 157 (1–2) (1993): 233-240.
- [81] "Water Soluble Tetrazolium Salts (WSTs)" Interchim. <http://www.interchim.fr/ft/F/F98881.pdf>. Retrieved 2010-11-19.
- [82] Wilson, Anne P.; John, R. W. Chapter 7: Cytotoxicity and viability, In Masters, Animal Cell Culture: A Practical Approach. Vol. 1 (3rd ed.). Oxford: Oxford University Press. (2000): ISBN 978-0199637966.
- [83] Bernas, T.; Dobrucki, J. Mitochondrial and nonmitochondrial reduction of MTT: interaction of MTT with TMRE, JC-1, and NAO mitochondrial fluorescent probes. Cytometry 47 (4) (2000): 236–242.
- [84] Wang, J. C. Cellular Roles of DNA Topoisomerases: A molecular Perspective. Nat. Rev. Mol. Cell. Biol. 3 (2002): 430-440.
- [85] Boyer, H. W. DNA Restriction and Modification Mechanisms in Bacteria. Ann. Rev. Microbiol. 25 (1971): 153-176.
- [86] Bickle, T. A.; Krüger, D. H. Biology of DNA restriction. Microbiol. Rev. 57 (1993): 434-450.
- [87] Samejima, K.; Earnshaw, W. C. Trashing the genome: the role of nucleases during apoptosis. Nat. Rev. Mol. Cell. Biol. 6 (2005): 677-688.
- [88] Chen, J.; Stubbe, J. Bleomycins: towards better therapeutics. Nat. Rev. Cancer, 5 (2005): 102-112.
- [89] Hengartner, M. O. The Biochemistry of Apoptosis. Nature 407 (2000): 770-776.
- [90] Rich, T.; Allen, R. L.; Wyllie, A. H. Defying Death after DNA Damage. Nature 407 (2000): 777-783.

- [91] Wolfenden, R.; Ridgway, C.; Young, G. Spontaneous Hydrolysis of Ionized Phosphate Monoesters and Diesters and the Proficiencies of Phosphohydrolases as Catalysts. J. Am. Chem. Soc. 120 (1998): 833-834.
- [92] Williams, N. H.; Takasaki, B.; Wall, M.; Chin, J. Structure and nuclease activity of simple dinuclear metal complexes: Quantitative dissection of the role of metal ions. Acc. Chem. Res. 32 (1999): 485-493.
- [93] Sträter, N.; Lipscomb, W. N.; Klabunde, T.; Krebs, B. Two-metal ion catalysis in enzymatic acyl- and phosphoryl-transfer reactions. Angew. Chem. Int. Ed. Engl. 35 (1996): 2024-2055.
- [94] Hegg, E. L.; Burstyn, J. N. Toward the development of metal-based synthetic nucleases and peptidases: a rationale and progress report in applying the principles of coordination chemistry. Coordination Chem. Rev. 173 (1) (1998): 133-165.
- [95] Komiyama, M.; Takeda, N.; Shigekawa, H. Hydrolysis of DNA and RNA by lanthanide ions: Mechanistic studies leading to new applications. Chem. Commun. (1999): 1443-1451.
- [96] Mancin, F; Scrimin, P; Tecilla, P.; Tonellato, U. Artificial metallonucleases Chem. Commun. 28 (20) (2005): 2540-2548.
- [97] Wilcox, D.E. Binuclear Metallohydrolases. Chem. Rev. 96 (1996): 2435-2458.
- [98] Cowan, J.A. Metal activation of enzymes in nucleic acid biochemistry. Chem. Rev. 98 (1998): 1067-1087.
- [99] Desai, N.A.; Shankar, V. Single-strand-specific nucleases. FEMS Microbiol. Rev. 26 (2003): 457-491.

- [100] Champoux, J.J. DNA TOPOISOMERASES: Structure, Function, and Mechanism. Annu. Rev. Biochem. 70 (2001): 369-413.
- [101] Changela, A.; Perry, K.; Taneja, B.; Mondragón, A., DNA manipulators: caught in the act. Curr. Opin. Struct. Biol. 13 (1) (2003): 15-22.
- [102] Chin, J. Artificial dinuclear phosphoesterases. Curr. Opin. Chem. Biol. 1 (1997): 514-521.
- [103] Komiyama, M.; Sumaoka, J., Progress towards synthetic enzymes for phosphoester hydrolysis. Curr. Opin. Chem. Biol. 2 (6) (1998): 751-757.
- [104] Ott, R.; Krämer, R. DNA hydrolysis by inorganic catalyts. Appl. Microbiol. Biotechnol. 52 (1999): 761-767.
- [105] Sreedhara, A.; Cowan, J.A. Catalytic hydrolysis of DNA by metal ions and complexes. J. Biol. Inorg. Chem. 6 (2001): 337-347.
- [106] Franklin, S. J. Lanthanide-mediated DNA hydrolysis. Curr. Opin. Chem. Biol. 5 (2) (2001): 201-208.
- [107] Cowan, J. A. Chemical nucleases. Curr. Opin. Chem. Biol. 5 (6) (2001): 634-642.
- [108] Liu, C.; Wang, M.; Zhang, T.; Sun, H. DNA hydrolysis promoted by di- and multi-nuclear metal complexes. Coor. Chem. Rev. 248 (1-2) (2004): 147-168.
- [109] Sinha, R.P.; Häder, D.-P. UV-induced DNA damage and repair: a review. Photochem. Photobiol. Sci. 1 (2002): 225-236.
- [110] Burrows, C.J.; Muller, J.G. Oxidative Nucleobase Modifications Leading to Strand Scission. Chem. Rev. 98 (1998): 1109-1151.
- [112] Saito, I.; Nakatani, K. Design of DNA-Cleaving Agents. Bull. Chem. Soc. Jpn. 69 (1996): 3007-3019.

- [113] Armitage, B. Photocleavage of Nucleic Acids. Chem. Rev. 98 (1998): 1171-1200.
- [114] Da Ros, T.; Spalluto, G.; Boutorine, A.S.; Bensasson, R.V.; Prato, M. DNA-photocleavage agents. Curr. Pharm.Design. 7 (2001) 1781-1821.
- [115] Pogożelski, W.K.; Tullius, T.D. Oxidative strand scission of nucleic acids: Routes initiated by hydrogen abstraction from the sugar moiety. Chem. Rev. 98 (1998): 1089-1107.
- [116] Paillous, N.; Vicendo, P., Mechanisms of photosensitized DNA cleavage. J. Photochem. Photobiol. B: Biol. 20 (2-3) (1993): 203-209.
- [117] Meunier, B.; Pratviel, G.; Bernadou, J. Active Species Involved in Oxidative DNA Cleavage. Bull. Soc. Chim. Fr. 131 (1994): 933-943.
- [118] Sawyer, D.T.; Valentine, J.S. How super is superoxide? Acc. Chem. Res. 14 (1981): 393-400.
- [119] Sheldrick, G. M. SHELXS97 and SHELXL97. University of Göttingen, Germany. (1997).

APPENDICES

APPENDIX A

Figure A1 Mass spectrum 6-deoxyclitoriacetal

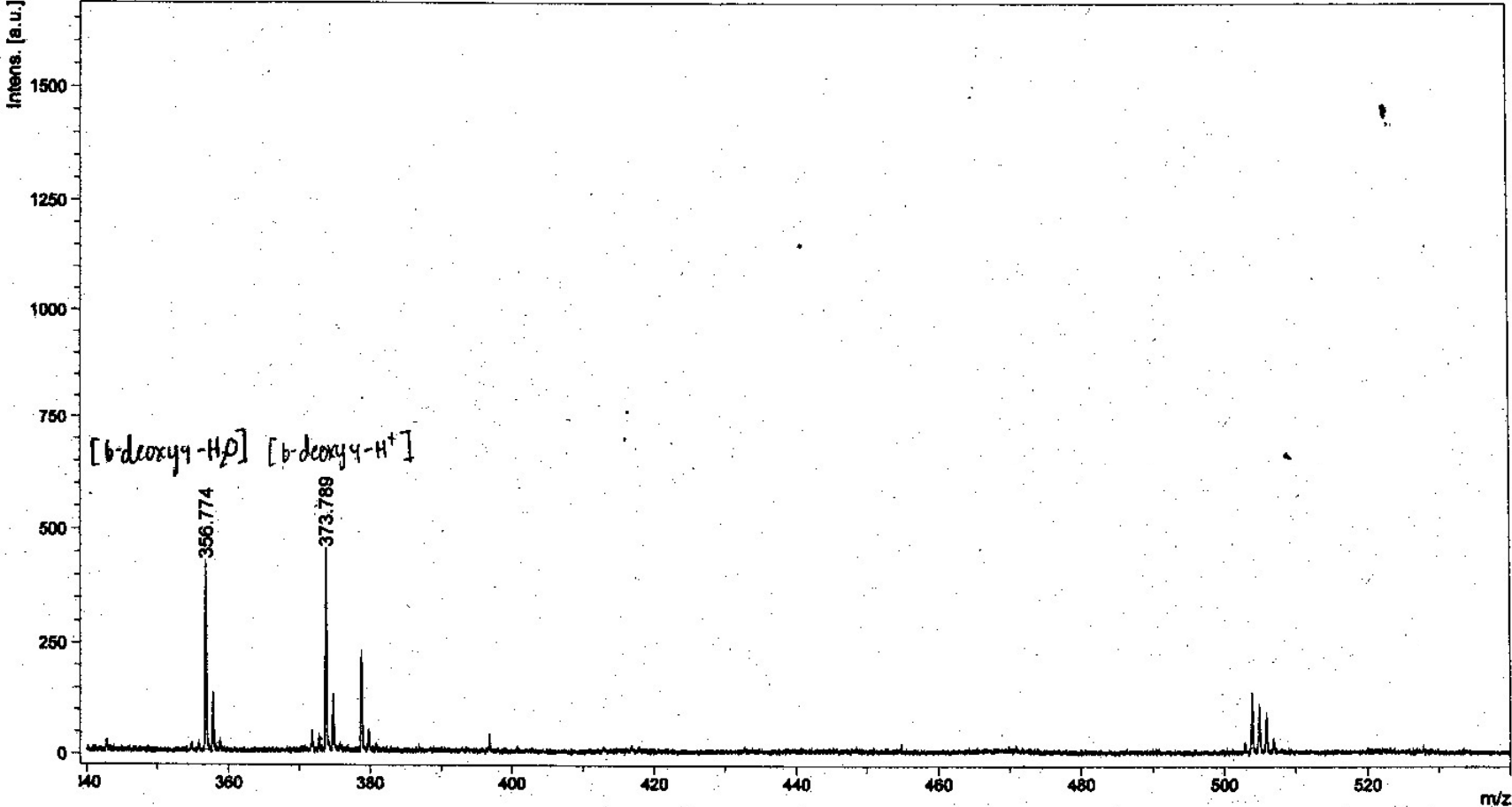


Figure A2 Mass spectrum of 1

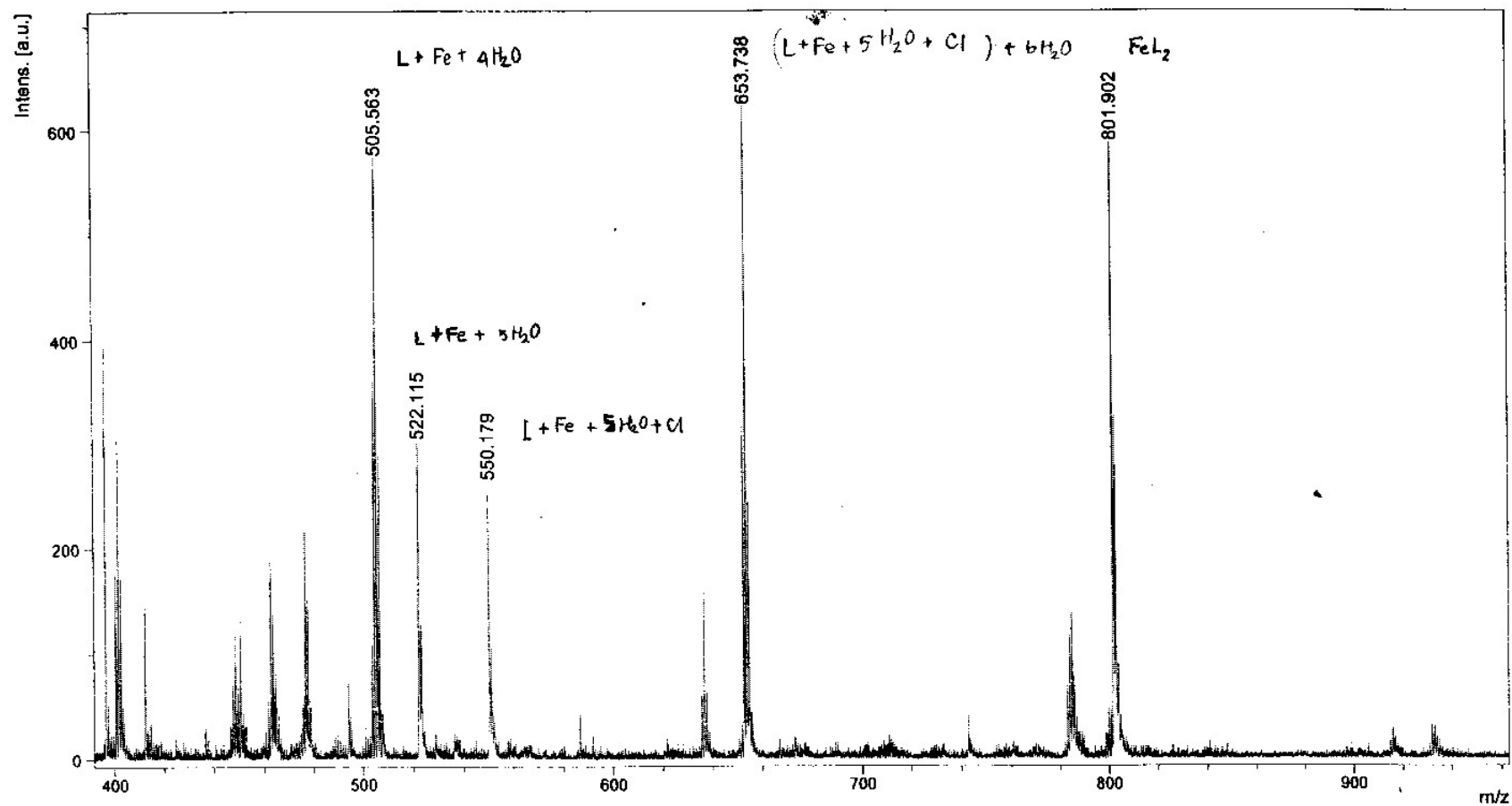
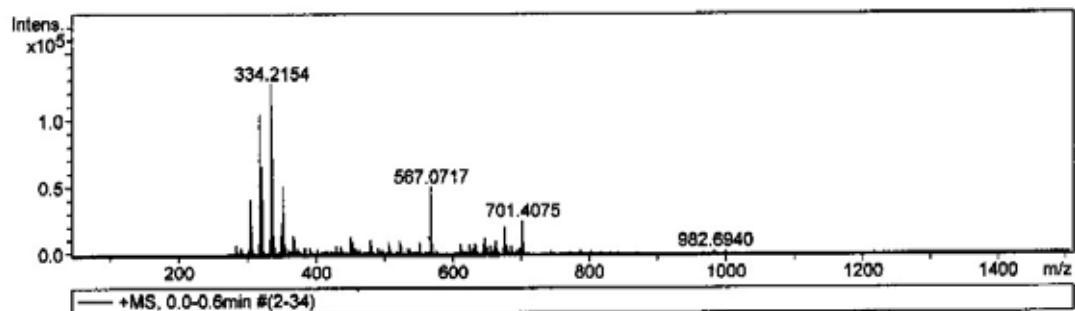


Figure A3 Mass spectrum of 2



#	m/z	Res.	S/N	I	FWHM
1	304.2613	16120	586.5	41719	0.0189
2	318.2405	16904	1302.2	104148	0.0188
3	319.2432	13839	233.8	18877	0.0231
4	320.2505	11422	809.3	65770	0.0280
5	321.2536	11078	162.6	13344	0.0290
6	332.2101	8539	121.8	10861	0.0389
7	334.2154	14828	1408.6	126937	0.0225
8	335.2179	12563	250.2	22740	0.0267
9	336.2310	12724	901.7	82426	0.0264
10	337.2339	12754	179.1	16524	0.0264
11	348.1952	14119	145.9	14488	0.0247
12	350.2121	12677	229.0	23003	0.0276
13	352.2252	14290	496.8	50485	0.0246
14	353.2274	14604	106.3	10914	0.0242
15	366.2053	12854	133.9	14841	0.0285
16	368.2179	14288	118.8	13329	0.0258
17	451.2202	16422	106.9	13780	0.0275
18	453.1731	7137	72.8	9425	0.0835
19	479.2610	10886	86.4	11366	0.0436
20	505.3381	13848	69.6	9247	0.0365
21	522.5947	16130	73.9	9864	0.0324
22	550.6260	15039	67.6	9109	0.0366
23	567.0717	17563	376.8	50398	0.0323
24	568.0737	15572	99.1	13360	0.0365
25	569.0712	15534	72.5	9811	0.0366
26	647.4731	14934	82.6	12286	0.0434
27	663.4683	14935	63.0	9606	0.0444
28	675.2597	17146	128.9	19789	0.0394
29	701.4075	17092	172.6	24816	0.0410
30	702.4113	15636	73.8	10673	0.0449

Figure A4 Mass spectrum of 3

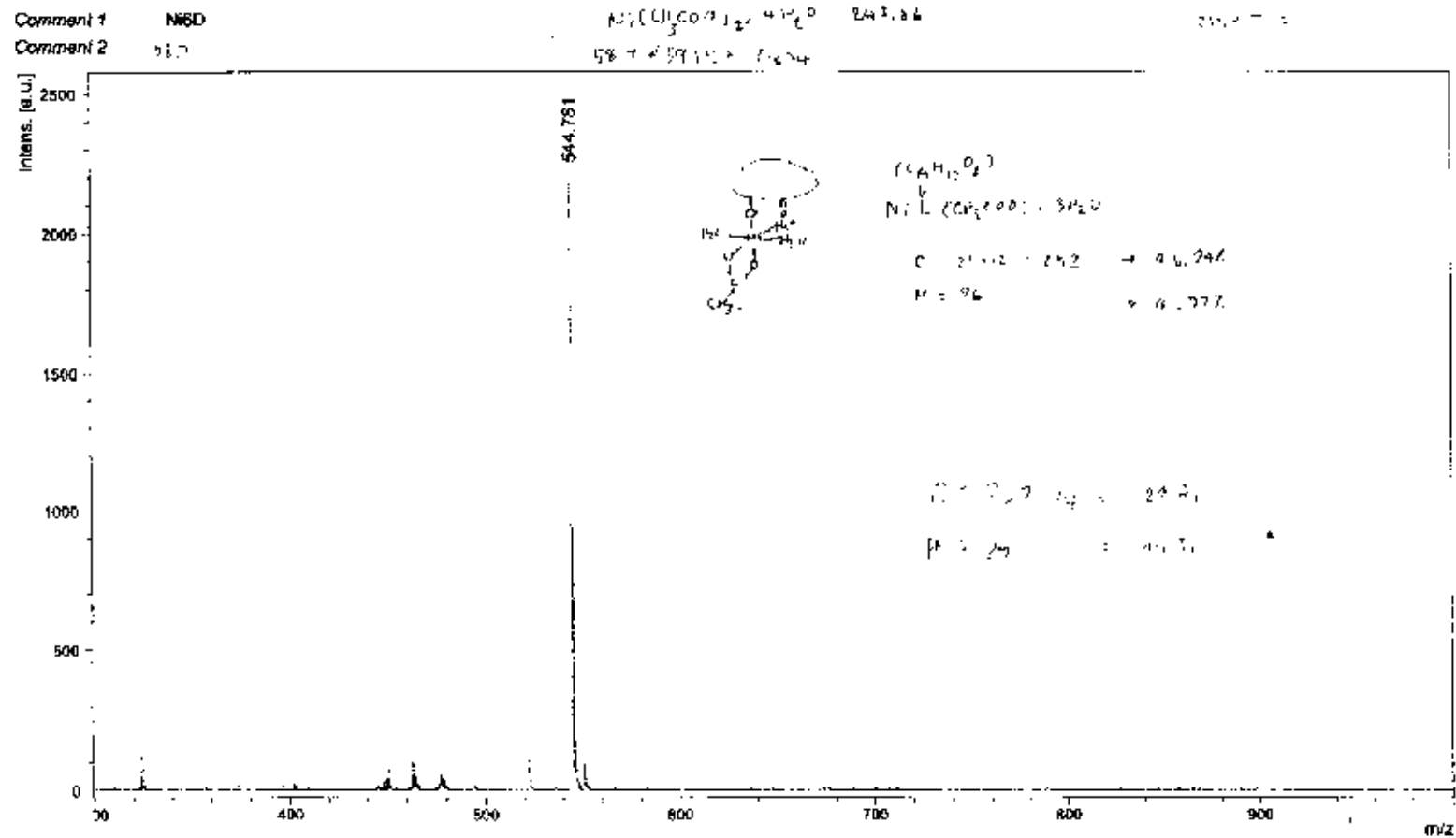
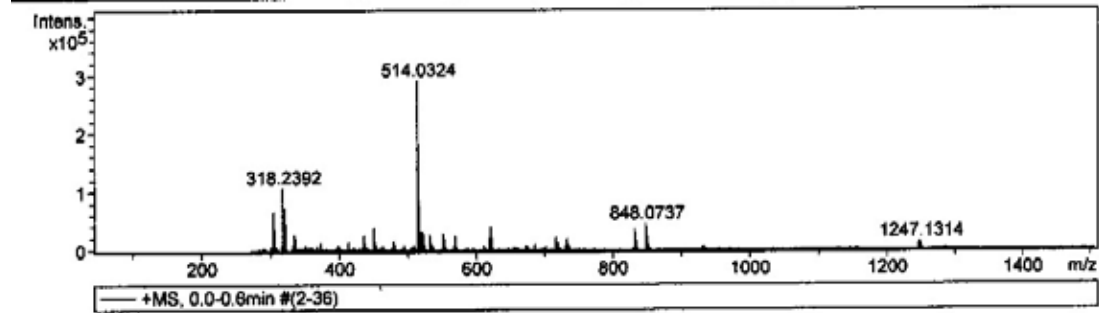


Figure A5 Mass spectrum of 4



#	m/z	Res.	S/N	I	FWHM
1	304.2598	15584	662.5	66311	0.0195
2	318.2392	18178	950.1	107375	0.0175
3	319.2416	12705	151.7	17314	0.0251
4	320.2525	12549	645.8	74194	0.0255
5	321.2551	13370	138.7	16092	0.0240
6	334.2188	10459	218.8	28001	0.0320
7	336.2368	8249	194.6	25270	0.0408
8	435.2411	13881	73.6	17324	0.0314
9	436.0191	16472	105.9	24978	0.0265
10	451.2190	18651	151.4	38377	0.0242
11	479.2549	12937	55.2	15920	0.0370
12	514.0324	23447	1055.3	291414	0.0219
13	515.0353	15784	187.7	51890	0.0326
14	516.0310	16715	442.9	122013	0.0309
15	517.0328	18612	111.9	30907	0.0278
16	518.0240	15176	117.5	32398	0.0341
17	522.5927	17746	117.8	32237	0.0294
18	532.0421	18182	100.0	26898	0.0293
19	550.6244	17096	113.5	29697	0.0322
20	553.1026	15989	87.1	22730	0.0348
21	569.0781	16545	100.4	25485	0.0344
22	620.1176	17320	167.7	40533	0.0358
23	622.1163	16461	86.4	20967	0.0378
24	717.2883	16209	107.4	22792	0.0443
25	733.2785	15891	97.2	19816	0.0467
26	832.0991	17858	222.1	36154	0.0466
27	834.0989	17364	122.9	20050	0.0480
28	848.0737	18152	288.0	45394	0.0467
29	849.0773	16997	120.5	19115	0.0500
30	850.0731	16987	177.6	27993	0.0500

Table A1 ^1H NMR spectral data for **L** and metal complexes.

^1H	δ (ppm)				
	L	1	2	3	4
1	6.67 <i>s</i>	6.68 <i>s</i>	6.67 <i>s</i>	6.68 <i>s</i>	6.70 <i>s</i>
2-Ome	3.75 <i>s</i>	3.76 <i>s</i>	3.76 <i>s</i>	3.72 <i>s</i>	3.66 <i>s</i>
3-Ome	3.77 <i>s</i>	3.76 <i>s</i>	3.76 <i>s</i>	3.72 <i>s</i>	3.76 <i>s</i>
4	6.49 <i>s</i>	6.50 <i>s</i>	6.57 <i>s</i>	6.47 <i>s</i>	6.50 <i>s</i>
6	4.48 <i>d</i> (<i>j</i> = 12)	4.48 <i>s</i>	4.55 <i>s</i>	4.42 <i>s</i>	4.47 <i>s</i>
	4.61 <i>d</i> (<i>j</i> = 18)				
6a	4.58 <i>s</i>	4.57 <i>s</i>	4.55 <i>s</i>	4.50 <i>s</i>	4.57 <i>s</i>
8	5.97 <i>s</i>	5.97 <i>s</i>	6.02 <i>s</i>	5.91 <i>s</i>	5.96 <i>s</i>
9-Ome	3.82 <i>s</i>	4.10 <i>s</i>	4.09 <i>s</i>	3.89 <i>s</i>	3.93 <i>s</i>
10	6.06 <i>s</i>	6.06 <i>s</i>	6.02 <i>s</i>	5.91 <i>s</i>	6.05 <i>s</i>
11-OH	11.50 <i>s</i>	11.53 <i>s</i>	11.53 <i>s</i>	-	11.56 <i>s</i>

Table A2 ^{13}C NMR spectral data for **L** and metal complexes.

^{13}C	δ (ppm)				
	L	1	2	3	4
1	109.29	109.45	109.40	109.39	109.45
1a	108.34	108.40	108.37	108.38	108.42
2	144.42	144.16	144.13	144.14	144.12
2-Ome	56.41	56.46	56.43	56.43	56.42
3	151.39	151.40	151.42	151.43	151.39
3-Ome	55.91	55.90	55.90	55.90	-
4	101.20	101.25	101.22	101.23	101.24
4a	148.36	148.41	148.39	148.39	148.36
6	63.66	63.67	63.66	63.66	63.65
6a	75.61	75.65	75.63	75.63	75.65
7a	161.66	161.68	161.67	161.67	161.66
8	94.57	94.56	94.56	94.56	94.57
9	169.13	169.14	169.12	169.13	169.73
9-Ome	55.82	55.79	55.80	55.90	55.88
10	95.63	95.63	95.63	95.63	95.62
11	164.37	164.39	164.37	164.38	164.37
11a	100.11	100.13	100.13	100.12	100.16
12	195.01	195.02	195.03	195.02	195.05
12a	66.97	66.98	66.98	66.97	66.98

Figure A6 EA of Fe complex (1)

ศูนย์เครื่องมือวิจัยวิทยาศาสตร์และเทคโนโลยี จุฬาลงกรณ์มหาวิทยาลัย
อาคารสถาบัน 3 จุฬาลงกรณ์ ซอย 62 พญาไท กรุงเทพฯ 10330 โทร. 0-2218-8101, 0-2218-8032 โทรสาร (662) 254-0211
SCIENTIFIC AND TECHNOLOGICAL RESEARCH EQUIPMENT CENTRE CHULALONGKORN UNIVERSITY
CHULALONGKORN SOI 62 PHAYA-THAI ROAD BANGKOK 10330 THAILAND TEL. 0-2218-8101, 0-2218-8032 FAX: (662) 254-0211

Report No. 428/2008


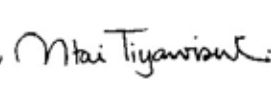
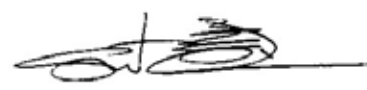
Page 1/1

Analysis Report

Sample Chemical
Request Code No. 511611
Sample owner Miss Benjamat Chailap
Objective To quantitate percentages of C, H and N elements
Instrument CHNS/O ANALYZER (Perkin Elmer PE2400 Series II)
Method Gaseous products freed by pyrolysis in high-purity oxygen were chromatographically separated and quantitatively detected by frontal analysis with thermal conductivity detector.
Analysis date May 23, 2008

Result

Sample Name		%C	%H	%N
J001 (Fe cpx)	(1)	45.554	5.140	-
	(2)	45.660	4.811	-
	(3)	45.404	5.301	-
	average	45.539	5.084	-

  
(Miss Amporn Eongprakornkeaw) (Mr. Utai Tiyawisuttri) (Asst. Prof. Dr. Supongse Nimkulrat)
Analyst Chief Scientist Director

Remark : The results are good only for those samples analyzed.

SS/SN

Figure A7 EA of Co, Ni and Cu complex (2, 3, and 4)

Time = 100 Peak= 260 Calib=1.0200 Btk =0.003	Time = 100 Peak= 17 Calib=1.1722 Btk =0.010	Time = 100 Peak= 4 Calib=1.1113 Btk =0.025	Time = 150 Peak= 6 Calib=1.0490 Btk =0.012
#449 Blank 29 Type	WT=2.000 mg Mst.=0.00	Chan # 1	15:30 Oct-09-4
C = 0.528% H = 0.003% N = -0.017% S = 0.025%			
Time = 100 Peak= 165 Calib=1.0200 Btk =0.003	Time = 100 Peak= 6 Calib=1.1722 Btk =0.010	Time = 100 Peak= 4 Calib=1.1113 Btk =0.025	Time = 150 Peak= 7 Calib=1.0490 Btk =0.012
#450 Blank 30 Type	WT=2.000 mg Mst.=0.00	Chan # 1	15:33 Oct-09-4
C = 0.323% H = 0.014% N = -0.013% S = 0.025%			
Time = 100 Peak= 120 Calib=1.0200 Btk =0.003	Time = 100 Peak= 6 Calib=1.1722 Btk =0.010	Time = 100 Peak= 4 Calib=1.1113 Btk =0.025	Time = 150 Peak= 7 Calib=1.0490 Btk =0.012
#451 [REDACTED] Type	WT=1.911 mg Mst.=0.00	Chan # 1	15:36 Oct-09-4
C = 43.89% H = 4.551% N = 0.021% S = 0.037%			
Time = 117 Peak= 3922 Calib=1.0200 Btk =0.003	Time = 100 Peak= 3914 Calib=1.1722 Btk =0.010	Time = 100 Peak= 29 Calib=1.1113 Btk =0.025	Time = 150 Peak= 10 Calib=1.0490 Btk =0.012
#452 Blank 31 Type	WT=2.000 mg Mst.=0.00	Chan # 1	15:40 Oct-09-4
C = 0.325% H = -0.085% N = -0.018% S = -0.006%			
Time = 100 Peak= 257 Calib=1.0200 Btk =0.003	Time = 100 Peak= 16 Calib=1.1722 Btk =0.010	Time = 100 Peak= 5 Calib=1.1113 Btk =0.025	Time = 150 Peak= 4 Calib=1.0490 Btk =0.012
#453 Blank 32 Type	WT=2.000 mg Mst.=0.00	Chan # 1	15:43 Oct-09-4
C = -0.124% H = -0.009% N = -0.012% S = 0.015%			
Time = 100 Peak= 90 Calib=1.0200 Btk =0.003	Time = 100 Peak= 7 Calib=1.1722 Btk =0.010	Time = 100 Peak= 4 Calib=1.1113 Btk =0.025	Time = 150 Peak= 5 Calib=1.0490 Btk =0.012
#454 Blank 33 Type	WT=2.000 mg Mst.=0.00	Chan # 1	15:46 Oct-09-4
C = 0.005% H = 0.009% N = -0.022% S = 0.007%			
Time = 100 Peak= 22 Calib=1.0200 Btk =0.003	Time = 100 Peak= 7 Calib=1.1722 Btk =0.010	Time = 100 Peak= 5 Calib=1.1113 Btk =0.025	Time = 150 Peak= 5 Calib=1.0490 Btk =0.012
#455 [REDACTED] Type	WT=2.071 mg Mst.=0.00	Chan # 1	15:50 Oct-09-4
C = 52.77% H = 7.169% N = 0.090% S = 0.060%			
Time = 100 Peak=14337 Calib=1.0200 Btk =0.003	Time = 100 Peak= 4567 Calib=1.1722 Btk =0.010	Time = 100 Peak= 72 Calib=1.1113 Btk =0.025	Time = 150 Peak= 20 Calib=1.0490 Btk =0.012
#456 Blank 34 Type	WT=2.000 mg Mst.=0.00	Chan # 1	15:53 Oct-09-4
C = 0.726% H = -0.135% N = -0.014% S = 0.004%			
Time = 100 Peak= 263 Calib=1.0200 Btk =0.003	Time = 100 Peak= 25 Calib=1.1722 Btk =0.010	Time = 100 Peak= 4 Calib=1.1113 Btk =0.025	Time = 150 Peak= 4 Calib=1.0490 Btk =0.012
#457 Blank 35 Type	WT=2.000 mg Mst.=0.00	Chan # 1	15:56 Oct-09-4
C = 0.203% H = -0.028% N = -0.023% S = 0.007%			
Time = 100 Peak= 125 Calib=1.0200 Btk =0.003	Time = 100 Peak= 9 Calib=1.1722 Btk =0.010	Time = 100 Peak= 4 Calib=1.1113 Btk =0.025	Time = 150 Peak= 4 Calib=1.0490 Btk =0.012
#458 Blank 36 Type	WT=2.000 mg Mst.=0.00	Chan # 1	16:00 Oct-09-4
C = -0.015% H = -0.009% N = -0.011% S = 0.007%			
Time = 100 Peak= 30 Calib=1.0200 Btk =0.003	Time = 100 Peak= 6 Calib=1.1722 Btk =0.010	Time = 100 Peak= 5 Calib=1.1113 Btk =0.025	Time = 150 Peak= 5 Calib=1.0490 Btk =0.012
#459 [REDACTED] Type	WT=2.127 mg Mst.=0.00	Chan # 1	16:03 Oct-09-4
C = 47.30% H = 4.708% N = 0.043% S = 0.026%			
Time = 100 Peak=12587 Calib=1.0200 Btk =0.003	Time = 100 Peak= 3886 Calib=1.1722 Btk =0.010	Time = 100 Peak= 30 Calib=1.1113 Btk =0.025	Time = 150 Peak= 8 Calib=1.0490 Btk =0.012
#460 Blank 37 Type	WT=2.000 mg Mst.=0.00	Chan # 1	16:06 Oct-09-4
C = -0.409% H = -0.103% N = -0.006% S = -0.005%			
Time = 100 Peak= 229 Calib=1.0200 Btk =0.003	Time = 100 Peak= 21 Calib=1.1722 Btk =0.010	Time = 100 Peak= 5 Calib=1.1113 Btk =0.025	Time = 150 Peak= 4 Calib=1.0490 Btk =0.012
#461 Blank 38 Type	WT=2.000 mg Mst.=0.00	Chan # 1	16:10 Oct-09-4
C = 0.009% H = -0.009% N = -0.016% S = 0.010%			

Figure A8 TGA thermogram of 6-deoxyclitriacetel (L)

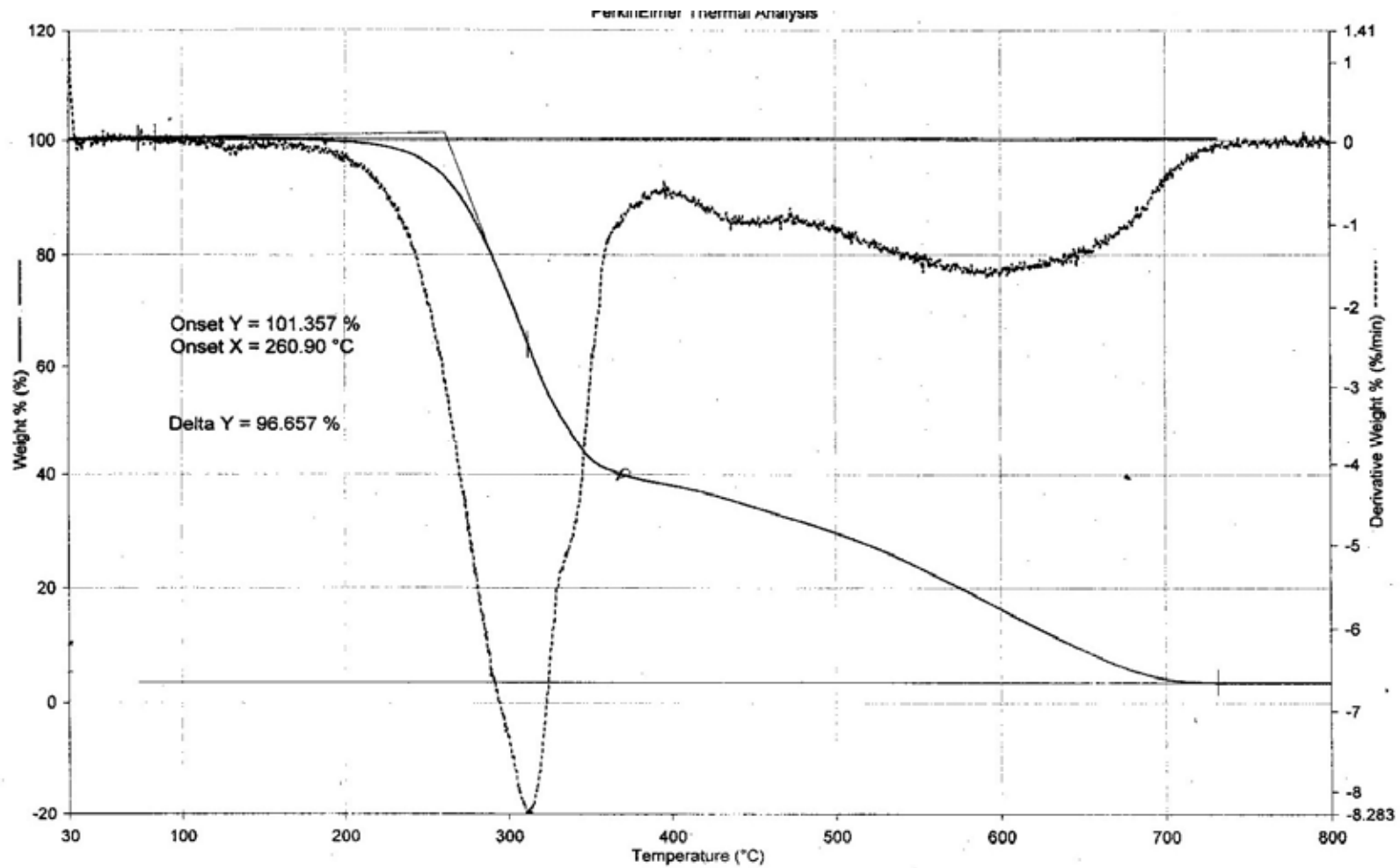


Figure A9 TGA thermogram of Fe(III) 6-deoxyclitoriacetal complex (1)

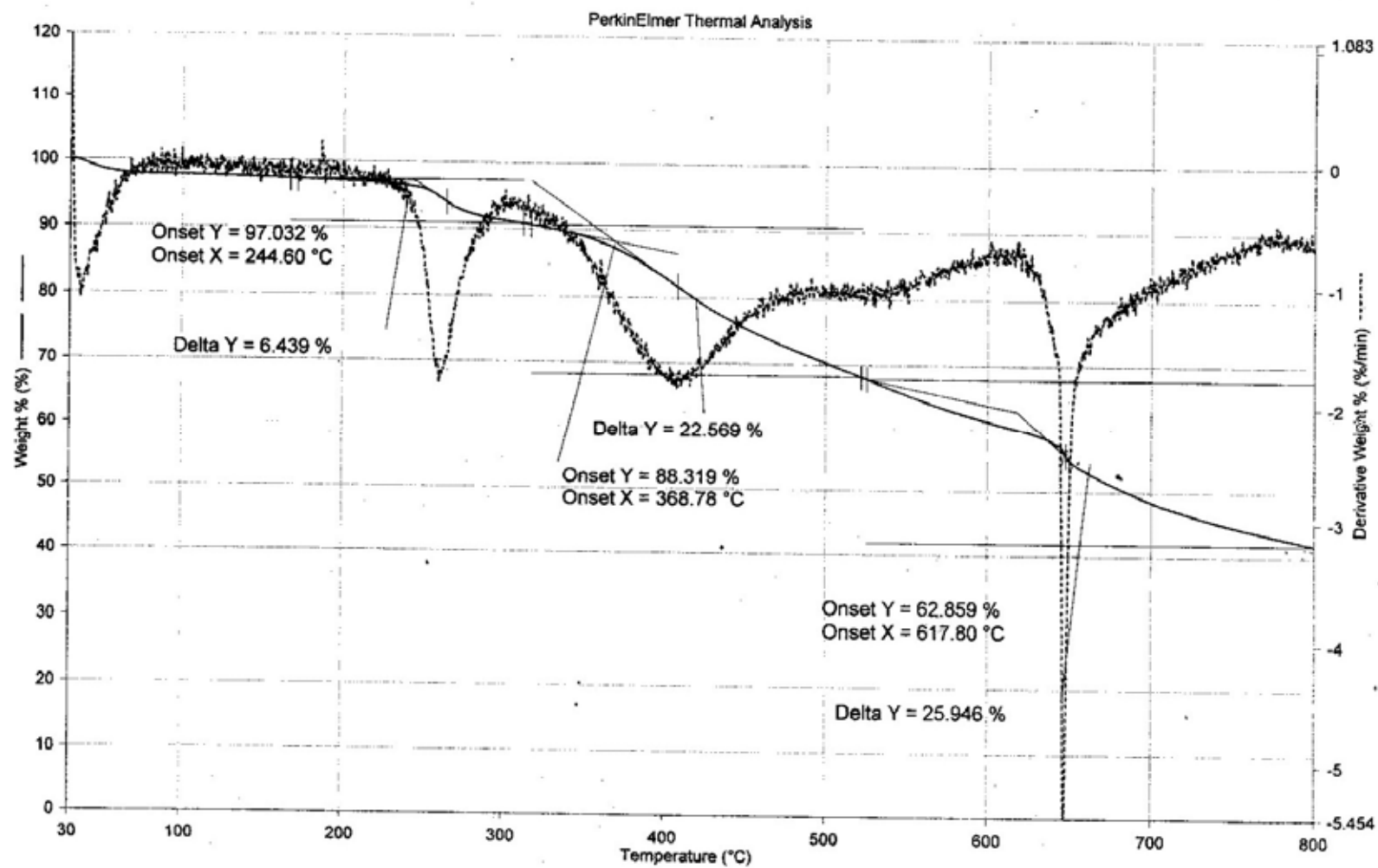


Figure A10 TGA thermogram of Co(II) 6-deoxyclitoriacetal (2)

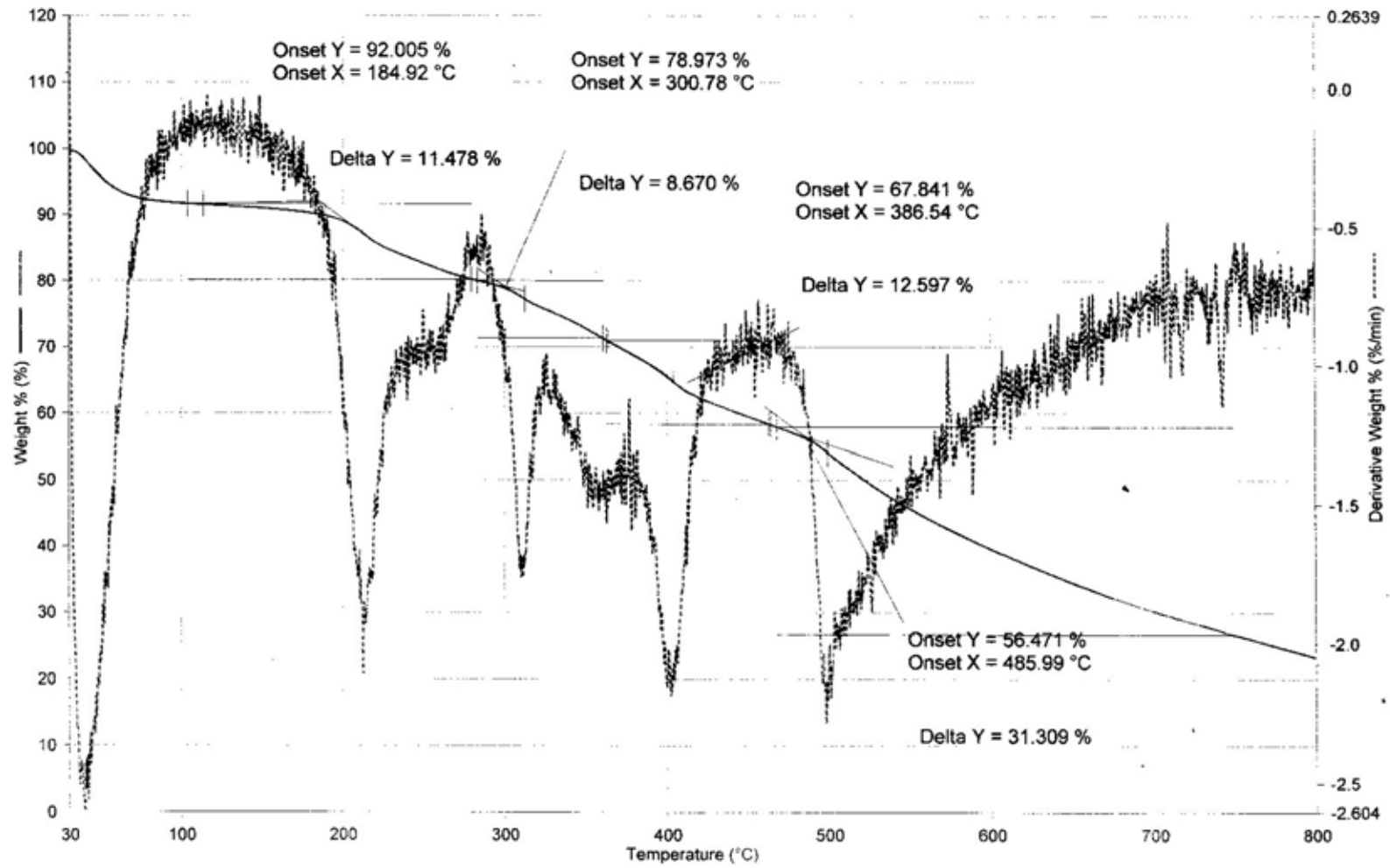


Figure A11 TGA thermogram of Ni(II) 6-deoxyclitoriacetal (3)

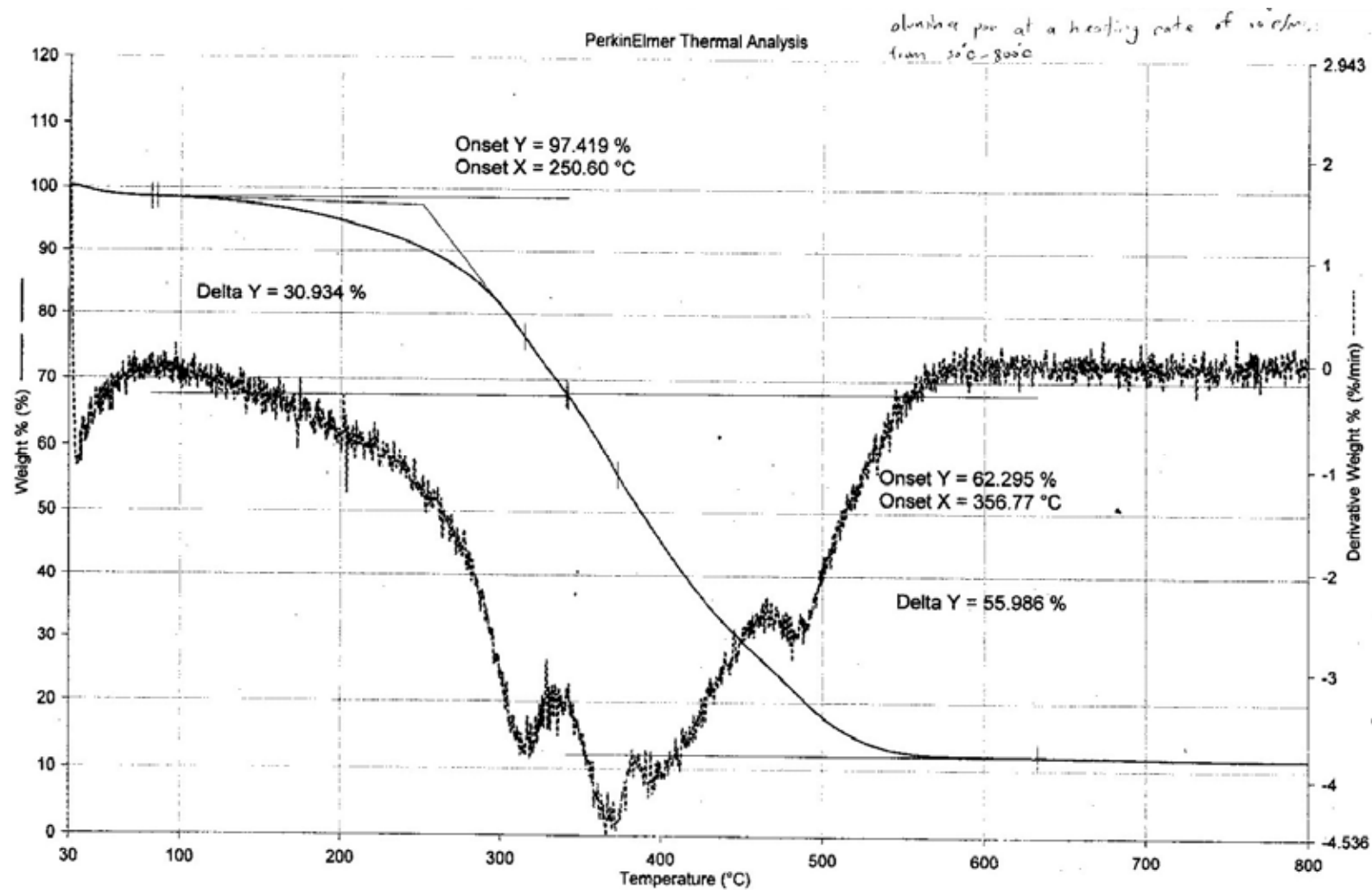


Figure A12 TGA thermogram of Cu(II) 6-deoxyclitoriacetal (4)

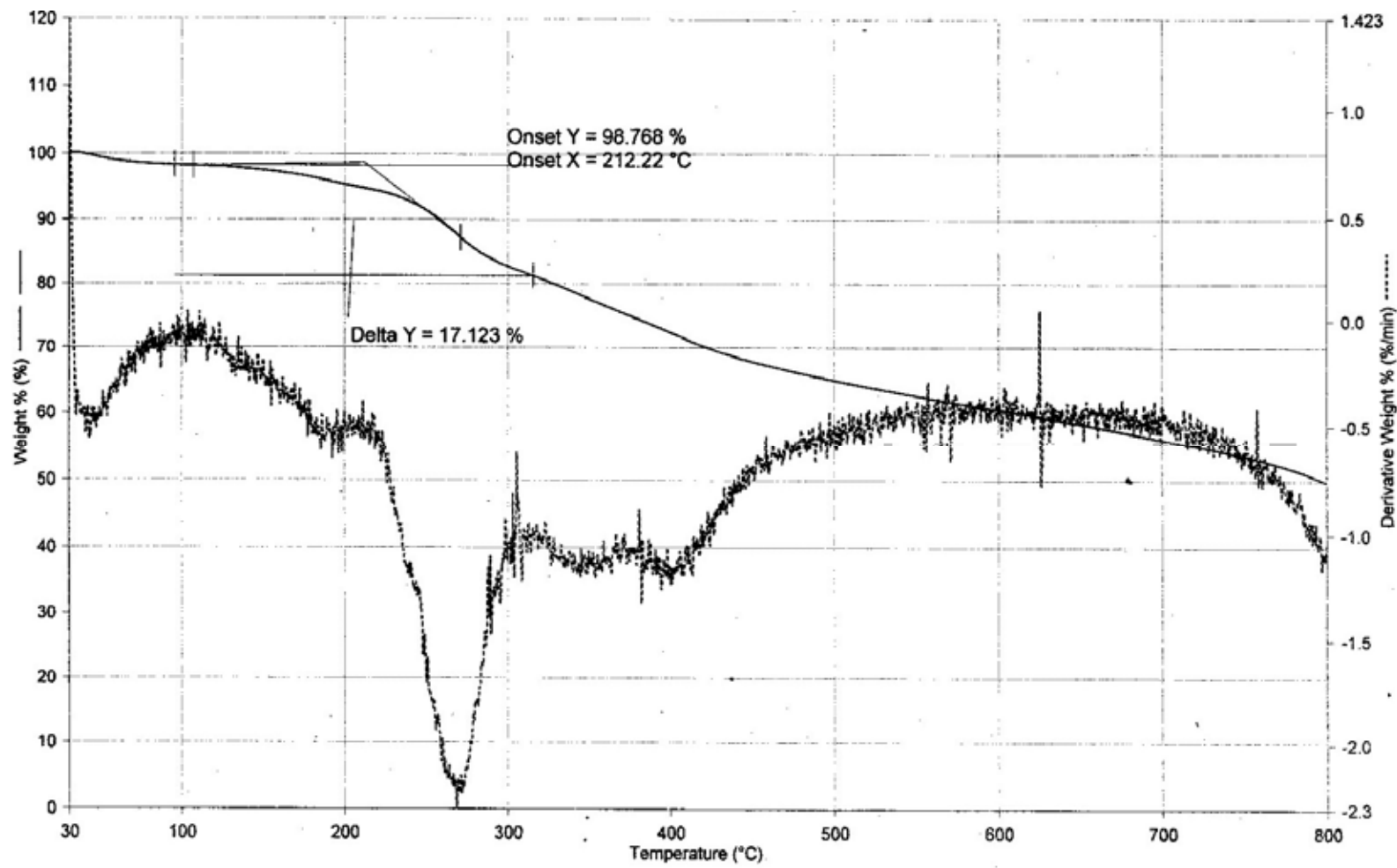


Figure A13 Cell viability test against cancer cell lines for (a) doxorubicin, (b) cisplatin, (c) L, (d) 1, (e) 2, (f) 3, (g) 4.

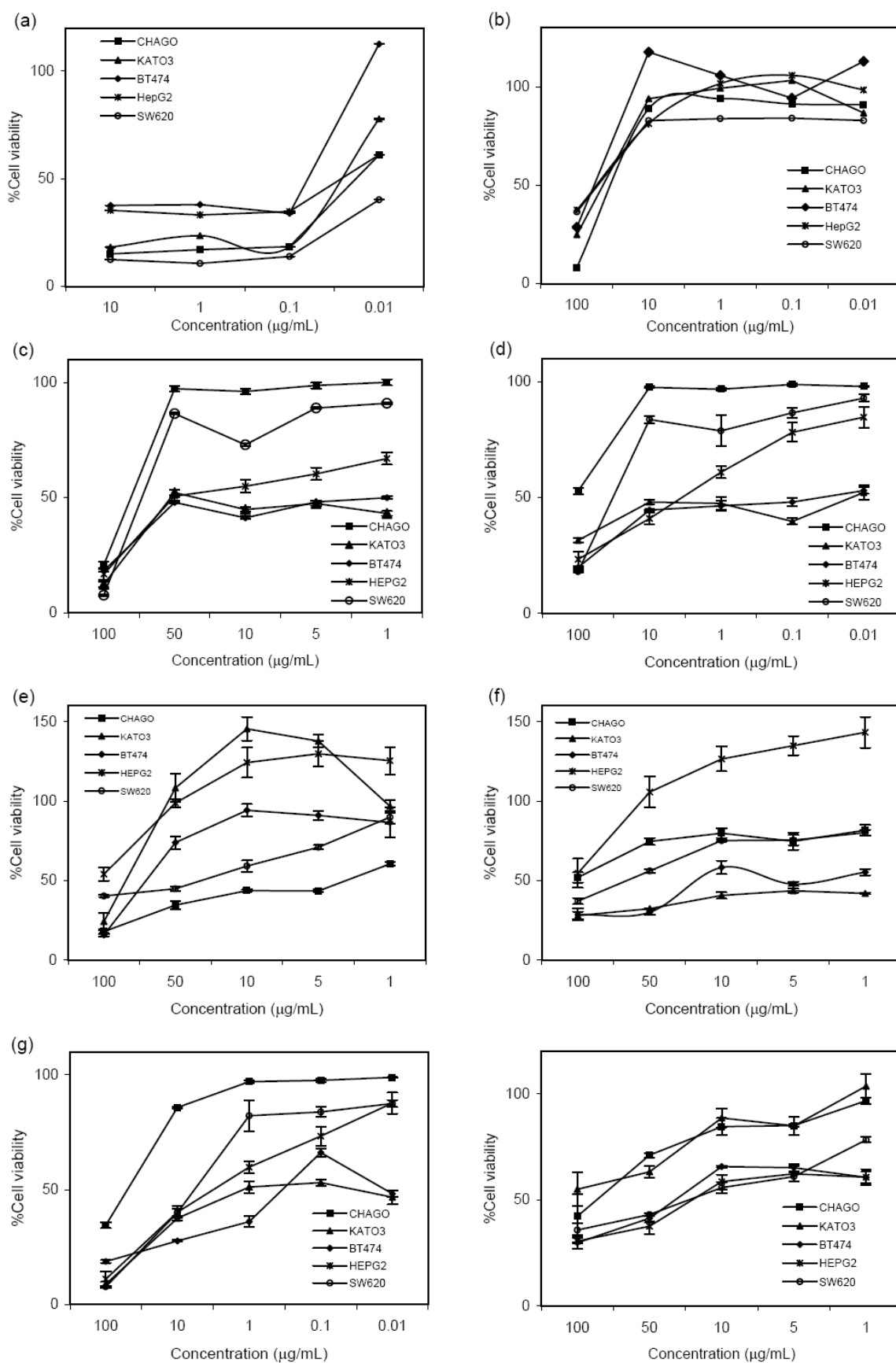
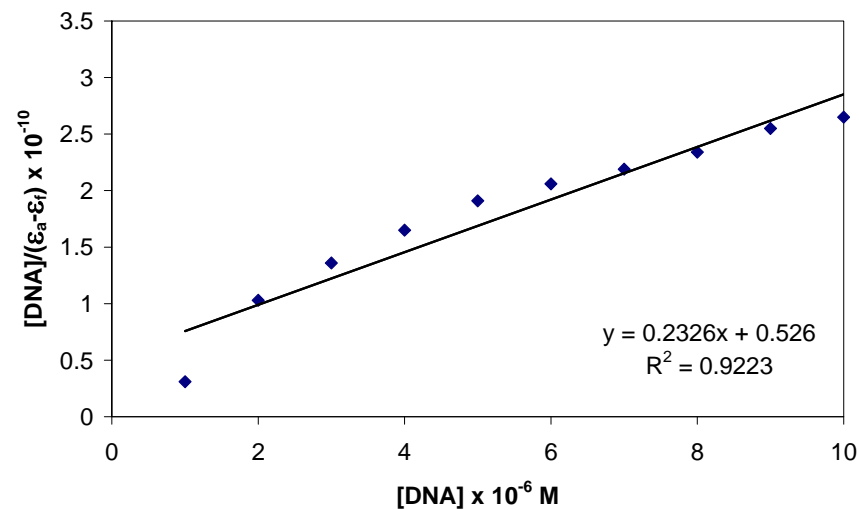
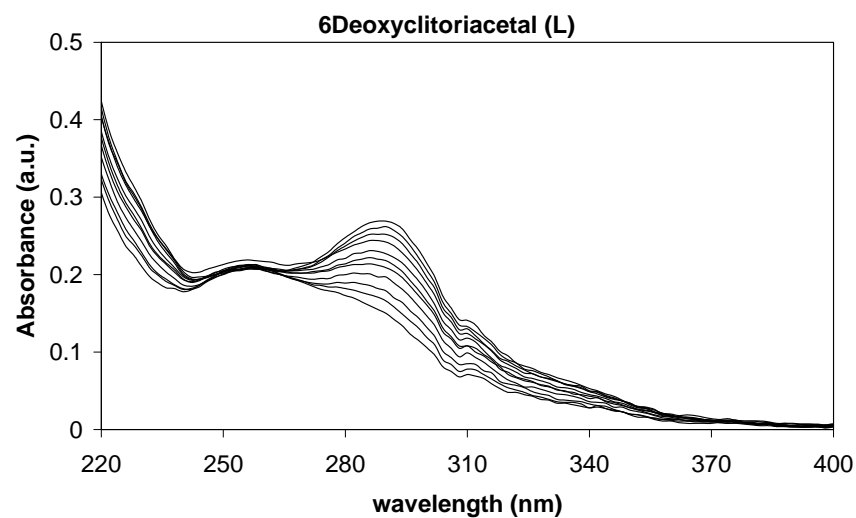
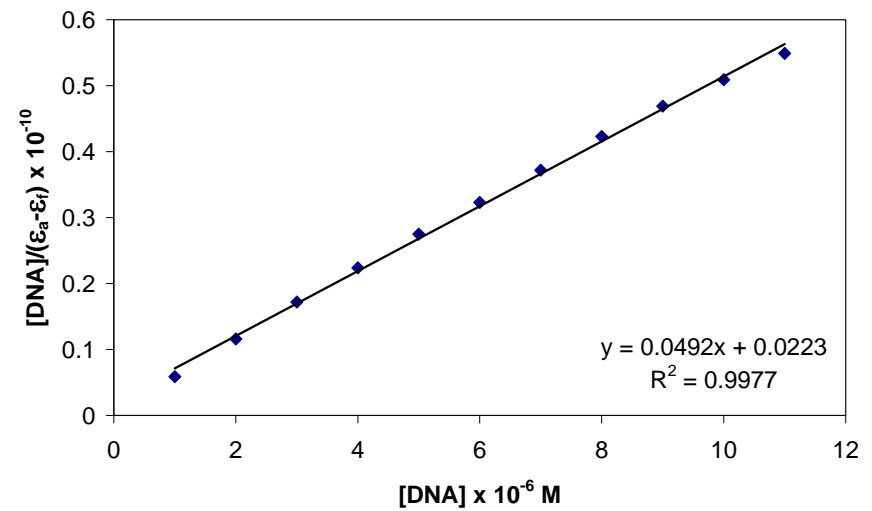
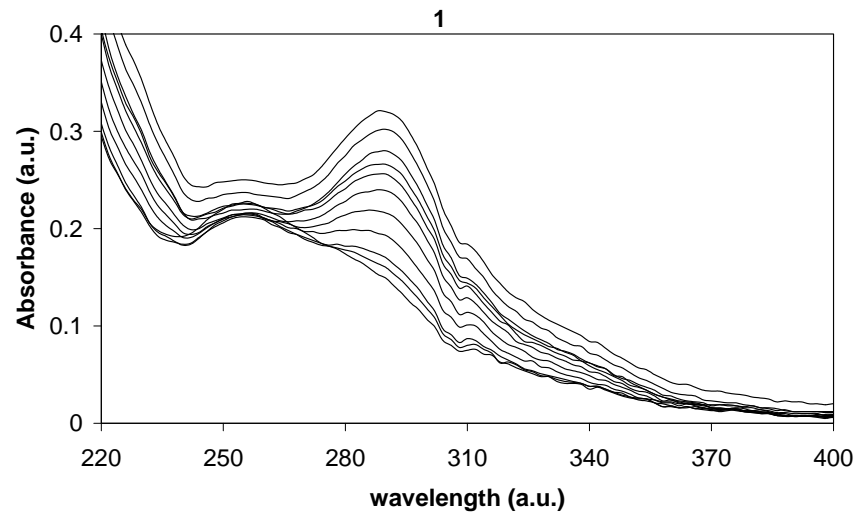


Figure A14 DNA binding experiments

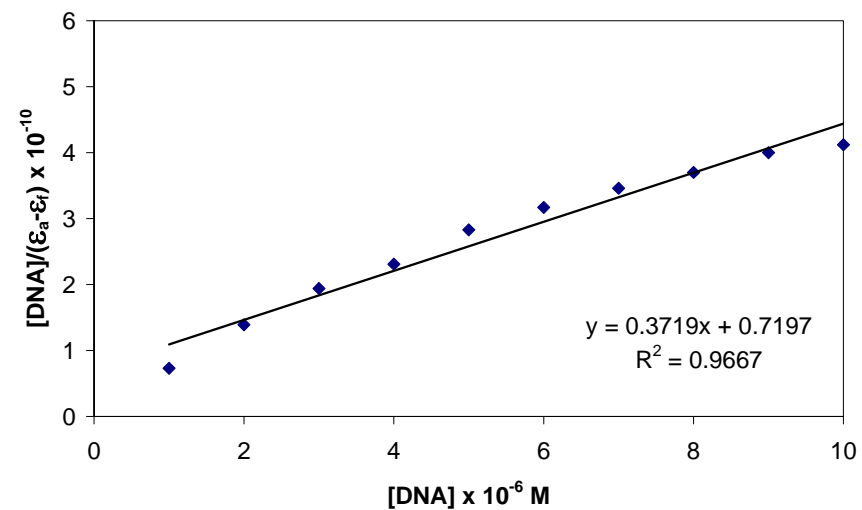
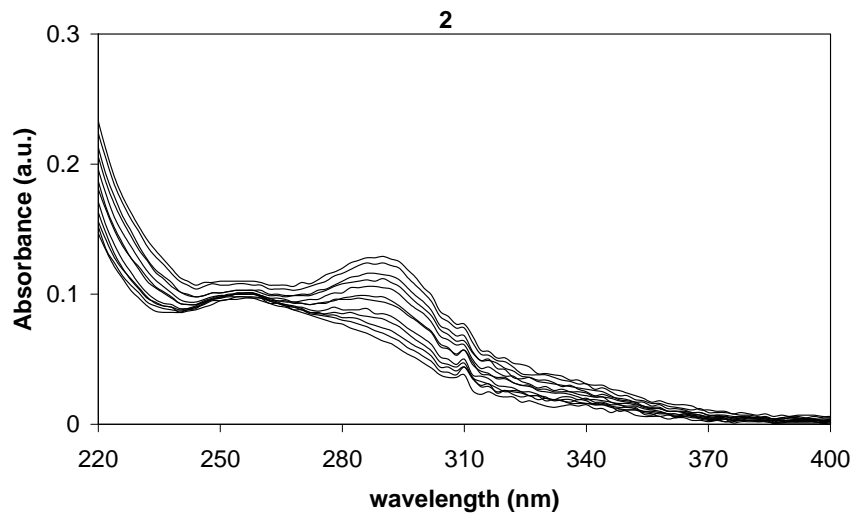
1. Absorption study DNA binding ability



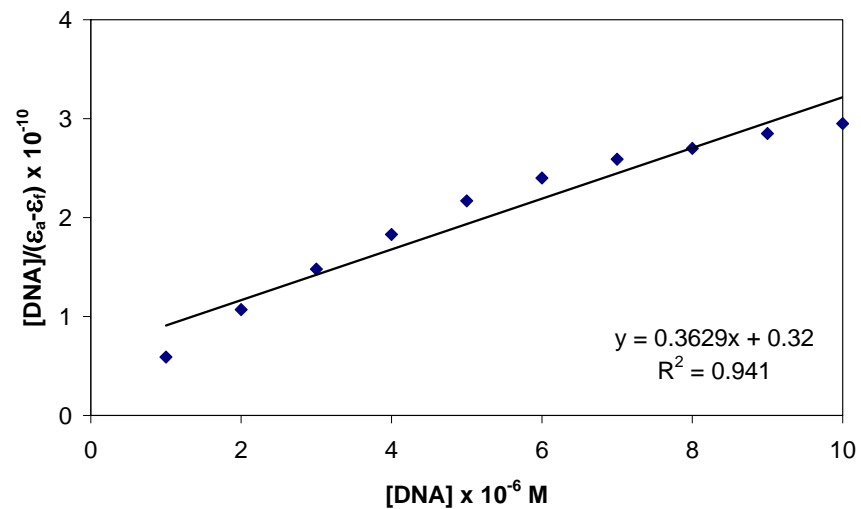
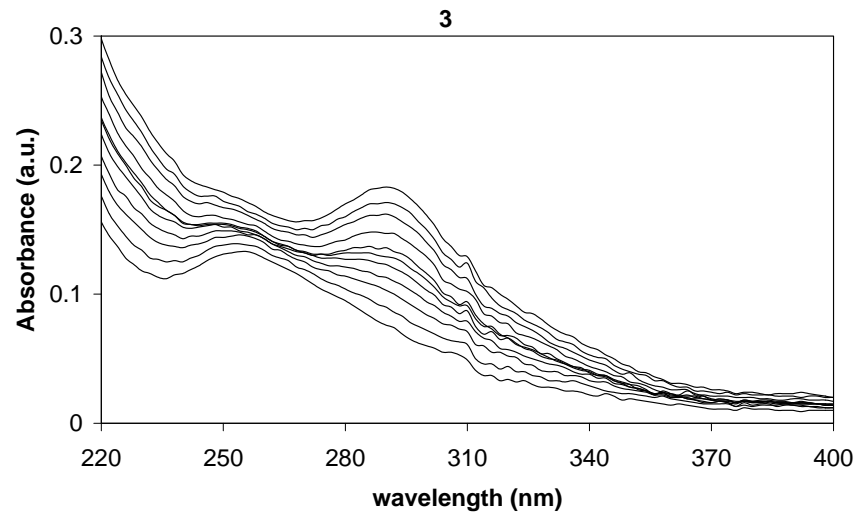
A 290	0.15	0.166	0.179	0.197	0.209	0.218	0.227	0.242	0.251	0.252	0.262	0.269
[DNA] x 10 ⁻⁶ M	0.00	1.00	2.00	3.00	4.00	5.00	6.00	7.00	8.00	9.00	10.00	11.00
[cpd] x 10 ⁻⁶ M	10.00	9.62	9.26	8.93	8.62	8.33	7.81	7.58	7.35	7.14	6.94	6.76
ε _a	15000	17264	19332	22064	24244	26160	29056	31944	34136	35280	37728	39812
ε _a -ε _f	0.00	32264	19332	22064	24244	26160	29056	31944	34136	35280	37728	39812
[DNA]/(ε _a -ε _f)		3.1E-11	1.03E-10	1.36E-10	1.65E-10	1.91E-10	2.06E-10	2.19E-10	2.34E-10	2.55E-10	2.65E-10	2.76E-10



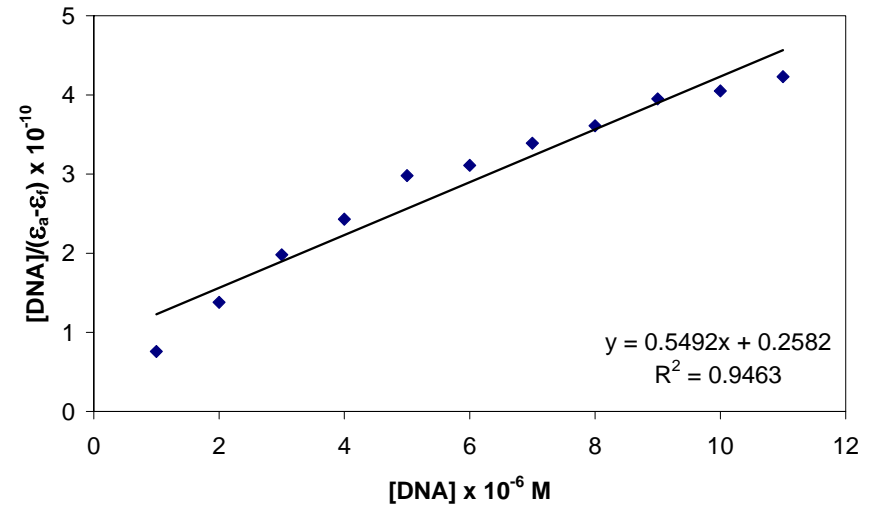
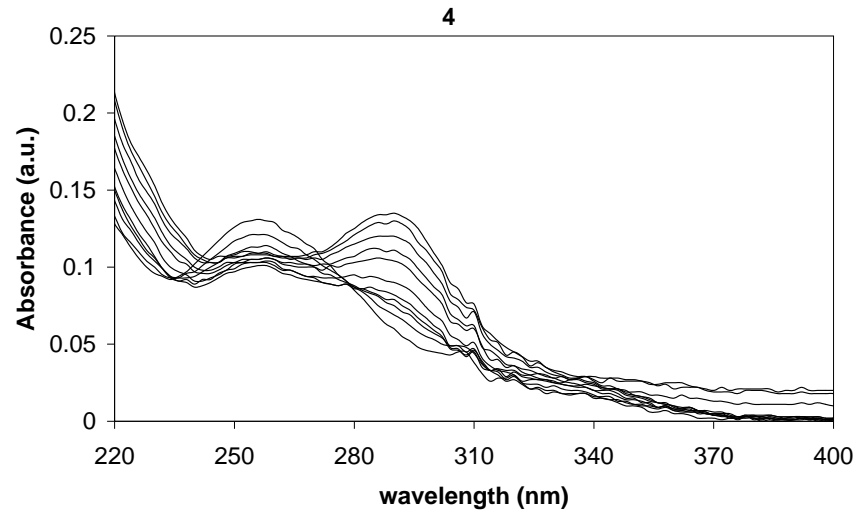
A 290	0.153	0.164	0.174	0.195	0.218	0.24	0.256	0.266	0.267	0.279	0.301	0.321
[DNA] x 10 ⁻⁶ M	0.00	1.00	2.00	3.00	4.00	5.00	6.00	7.00	8.00	9.00	10.00	11.00
[cpd] x 10 ⁻⁶ M	10.00	9.62	9.26	8.93	8.62	8.33	7.81	7.58	7.35	7.14	6.94	6.76
ε _a	15300	17056	18792	21840	25288	28800	32768	35112	36312	39060	43344	47508
ε _a -ε _f	0	170056	171792	174840	178288	181800	185768	188112	189312	192060	196344	200508
[DNA]/(ε _a -ε _f)		5.88E-12	1.16E-11	1.72E-11	2.24E-11	2.75E-11	3.23E-11	3.72E-11	4.23E-11	4.69E-11	5.09E-11	5.49E-11



A 290	0.064	0.07	0.074	0.081	0.094	0.094	0.098	0.105	0.112	0.115	0.124	0.129
$[DNA] \times 10^{-6} \text{ M}$	0.00	1.00	2.00	3.00	4.00	5.00	6.00	7.00	8.00	9.00	10.00	11.00
$[cpd] \times 10^{-6} \text{ M}$	10.00	9.62	9.26	8.93	8.62	8.33	7.81	7.58	7.35	7.14	6.94	6.76
ϵ_a	6400.00	7280.00	7992.00	9072.00	10904.00	11280.00	12544.00	13860.00	15232.00	16100.00	17856.00	19092.00
$\epsilon_a - \epsilon_f$	0.00	13680.0	14392.0	15472.0	17304.0	17680.0	18944.0	20260.0	21632.0	22500.0	24256.0	25492.0
$[DNA]/(\epsilon_a - \epsilon_f)$		7.31E-11	1.39E-10	1.94E-10	2.31E-10	2.83E-10	3.17E-10	3.46E-10	3.7E-10	4E-10	4.12E-10	4.32E-10

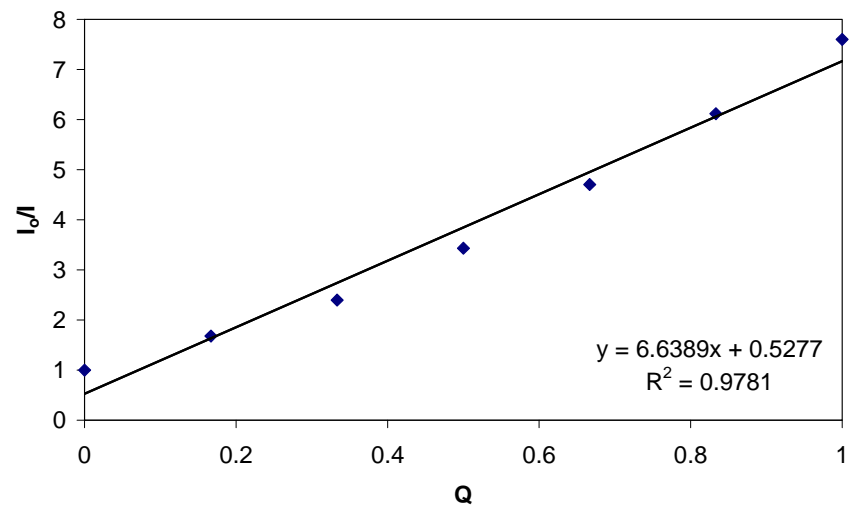
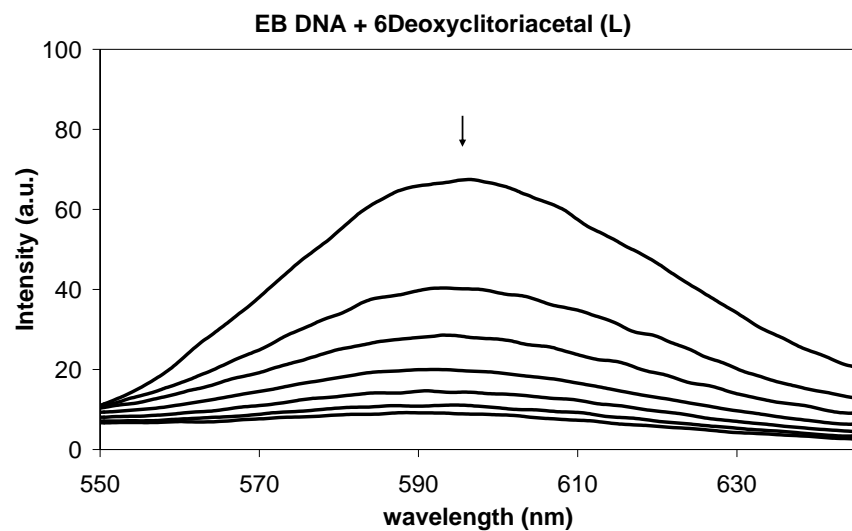


A 290	0.076	0.09	0.103	0.113	0.123	0.129	0.136	0.147	0.162	0.171	0.183
[DNA] x 10 ⁻⁶ M	0.00	1.00	2.00	3.00	4.00	5.00	6.00	7.00	8.00	9.00	10.00
[cpd] x 10 ⁻⁶ M	10.00	9.62	9.26	8.93	8.62	8.33	7.81	7.58	7.35	7.14	6.94
ϵ_a	7600.00	9360.00	11124.00	12656.00	14268.00	15480.00	17408.00	19404.00	22032.00	23940.00	26352.00
$\epsilon_a - \epsilon_f$	0.00	16960.0	18724.0	20256.0	21868.0	23080.0	25008.0	27004.0	29632.0	31540.0	33952.0
[DNA]/($\epsilon_a - \epsilon_f$)		5.9E-11	1.07E-10	1.48E-10	1.83E-10	2.17E-10	2.4E-10	2.59E-10	2.7E-10	2.85E-10	2.95E-10

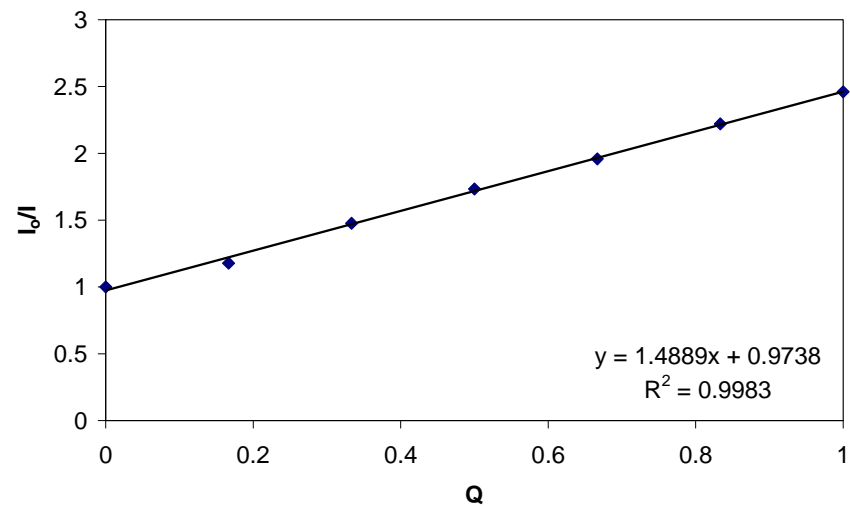
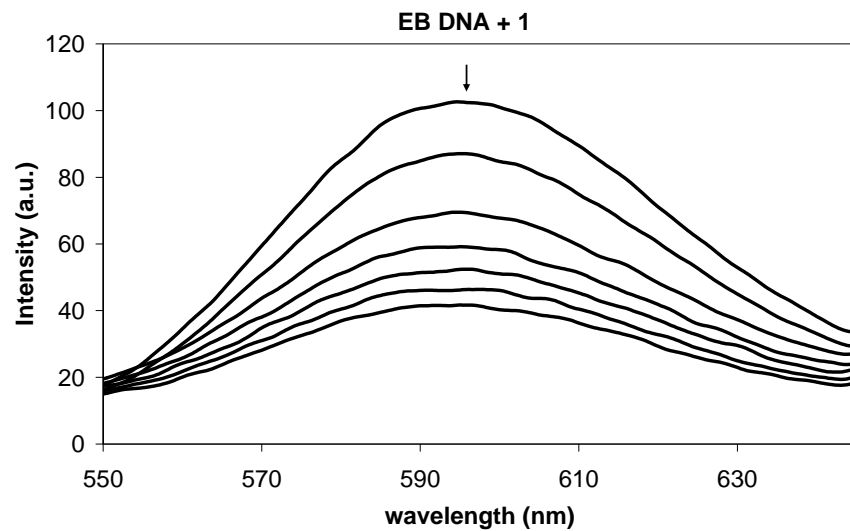


A 290	0.06	0.069	0.079	0.082	0.09	0.09	0.104	0.111	0.119	0.12	0.13	0.135
$[DNA] \times 10^{-6} \text{ M}$	0.00	1.00	2.00	3.00	4.00	5.00	6.00	7.00	8.00	9.00	10.00	11.00
$[cpd] \times 10^{-6} \text{ M}$	10.00	9.62	9.26	8.93	8.62	8.33	7.81	7.58	7.35	7.14	6.94	6.76
ϵ_a	6000	7176	8532	9184	10440	10800	13312	14652	16184	16800	18720	19980
$\epsilon_a - \epsilon_f$	0	13176	14532	15184	16440	16800	19312	20652	22184	22800	24720	25980
$[DNA]/(\epsilon_a - \epsilon_f)$		7.59E-11	1.38E-10	1.98E-10	2.43E-10	2.98E-10	3.11E-10	3.39E-10	3.61E-10	3.95E-10	4.05E-10	4.23E-10

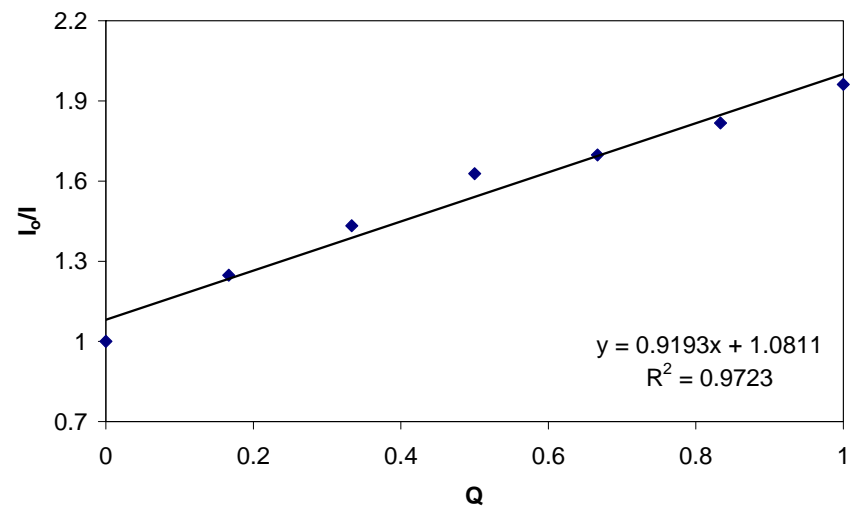
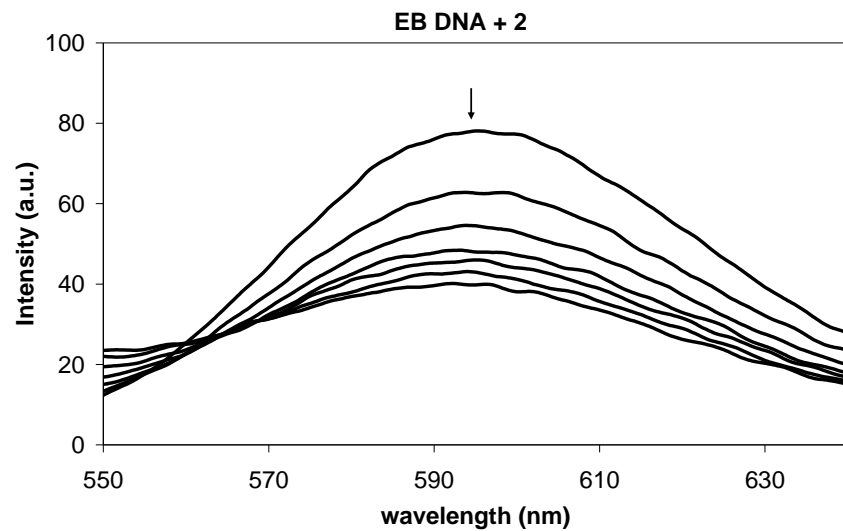
Figure A15 EB displacement study by fluorescent spectroscopy



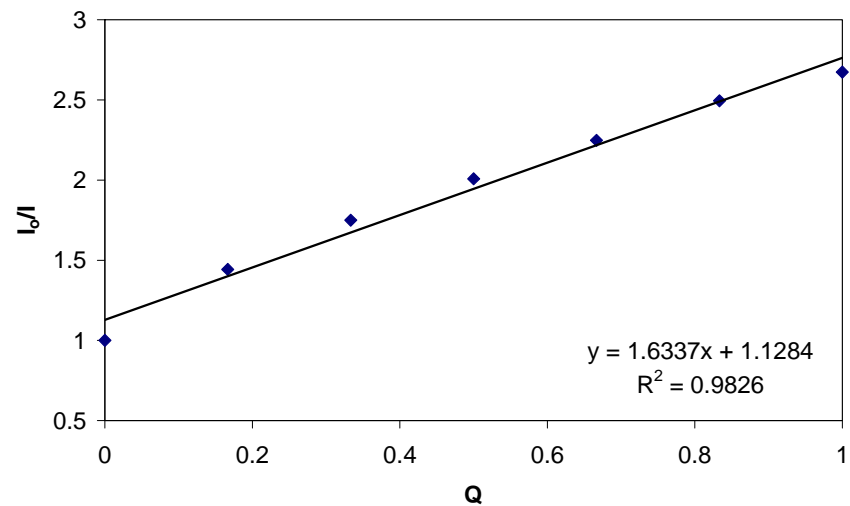
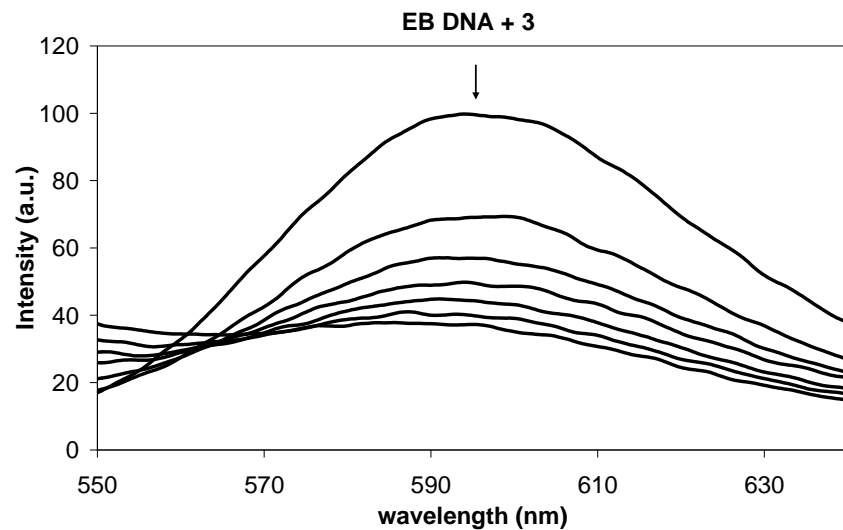
EB DNA added with	-	6D 5 uM	6D 10 uM	6D 15 uM	6D 20 uM	6D 25 uM	6D 30 uM
I at 595 nm	67.437	40.143	28.137	19.646	14.339	11.023	8.874
I ₀	67.437						
I ₀ /I	1.000	1.680	2.397	3.433	4.703	6.118	7.600
[Q]x10 ⁻⁶ M	0	5	10	15	20	25	30
[Q]/[DNA]	0	0.167	0.333	0.500	0.667	0.833	1.000
K _{sq}	6.64						



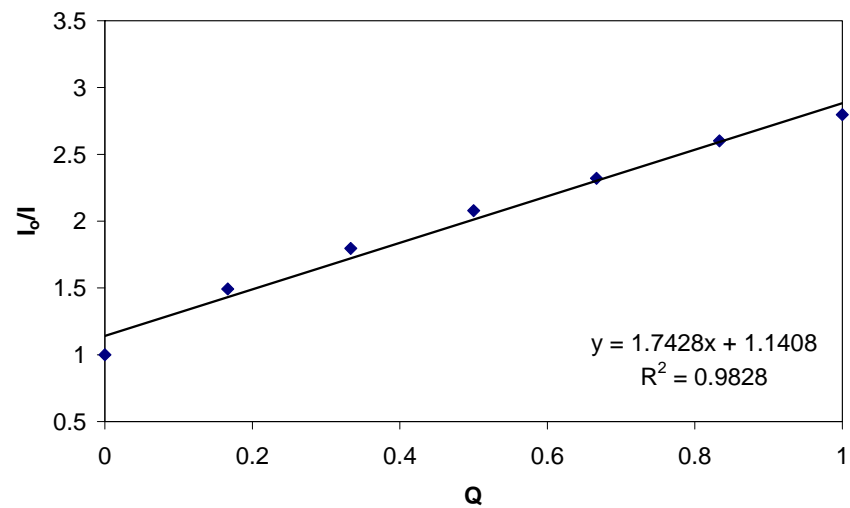
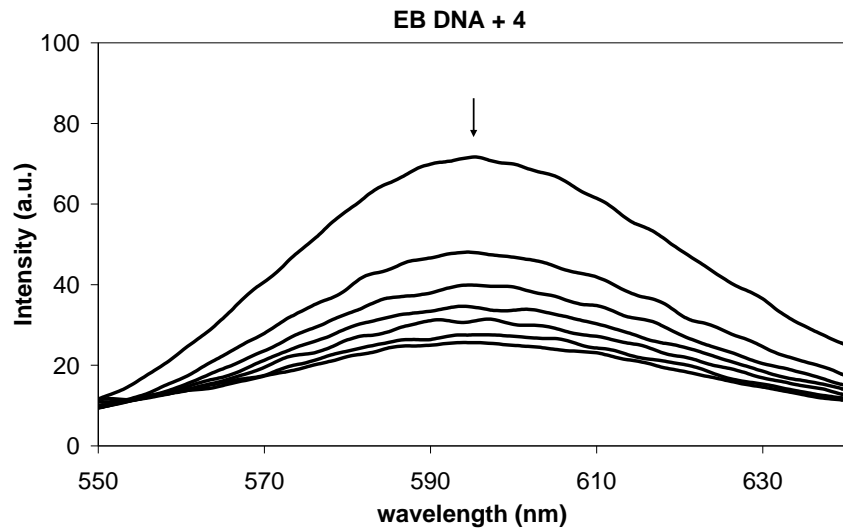
EB DNA added with	-	Fe6D 5 uM	Fe6D 10 uM	Fe6D 15 uM	Fe6D 20 uM	Fe6D 25 uM	Fe6D 30 uM
[Q]x10 ⁻⁶ M	0.000	5.000	10.000	15.000	20.000	25.000	30.000
[Q]/[DNA]	0.000	0.167	0.333	0.500	0.667	0.833	1.000
I at 595nm	102.592	87.061	69.504	59.175	52.377	46.202	41.696
I ₀ /I	1.000	1.178	1.476	1.734	1.959	2.221	2.460
K _{sq}	1.49						



EB DNA added with	-	Co6D 5 uM	Co6D 10 uM	Co6D 15 uM	Co6D 20 uM	Co6D 25 uM	Co6D 30 uM
I at 595 nm	78.092	62.592	54.502	47.977	45.998	42.967	39.805
[Q]x10 ⁻⁶ M	0.000	5.000	10.000	15.000	20.000	25.000	30.000
[Q]/[DNA]	0.000	0.167	0.333	0.500	0.667	0.833	1.000
I ₀ /I	1.000	1.248	1.433	1.628	1.698	1.817	1.962
K _{sq}	0.92						



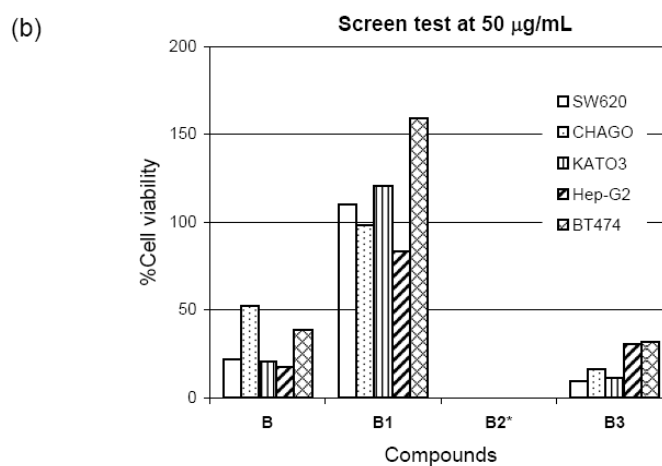
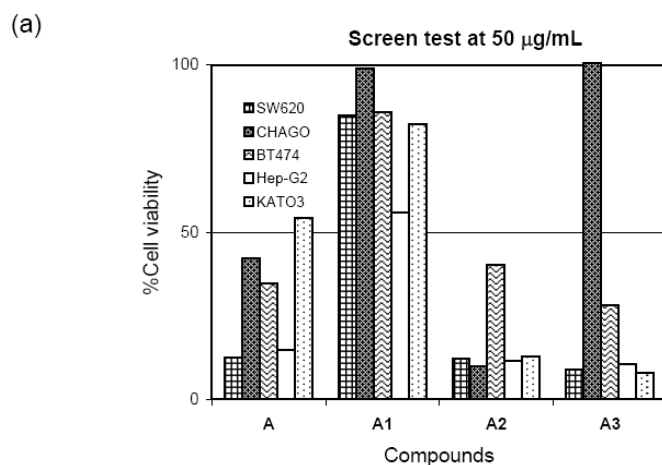
EB DNA added with	-	Ni6D 5 uM	Ni6D 10 uM	Ni6D 15 uM	Ni6D 20 uM	Ni6D 25 uM	Ni6D 30 uM
I at 595nm	99.650	69.076	56.942	49.634	44.331	39.941	37.269
[Q]x10 ⁻⁶ M	0.000	5.000	10.000	15.000	20.000	25.000	30.000
[Q]/[DNA]	0.000	0.167	0.333	0.500	0.667	0.833	1.000
I ₀ /I	1.000	1.443	1.750	2.008	2.248	2.495	2.674
K _{sq}	1.63						



EB DNA added with	-	Cu6D 5 uM	Cu6D 10 uM	Cu6D 15 uM	Cu6D 20 uM	Cu6D 25 uM	Cu6D 30 uM
I at 595 nm	71.654	48.008	39.905	34.469	30.878	27.544	25.620
[Q]x10 ⁻⁶ M	0.000	5.000	10.000	15.000	20.000	25.000	30.000
[Q]/[DNA]	0	0.166666667	0.333333333	0.5	0.666666667	0.833333333	1
I ₀ /I	1.000	1.493	1.796	2.079	2.321	2.601	2.797
K _{sq}	1.74						

APPENDIX B

Figure B1 Screen test of cell viability (a) Schiff base A and metal complexes at 50 $\mu\text{g/mL}$, (b) Schiff base B and metal complexes at 50 $\mu\text{g/mL}$, (c) Schiff base B and metal complexes at 10 $\mu\text{g/mL}$.



*All cell death

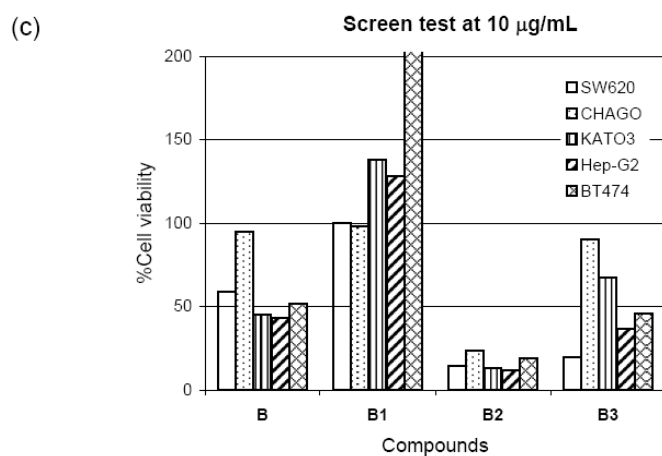


Figure B2 Inhibition of cell growth of different five cancer cell lines test against

(a) A, (b) B, (c) A2, (d) B2, (e) A3, and (f) B3.

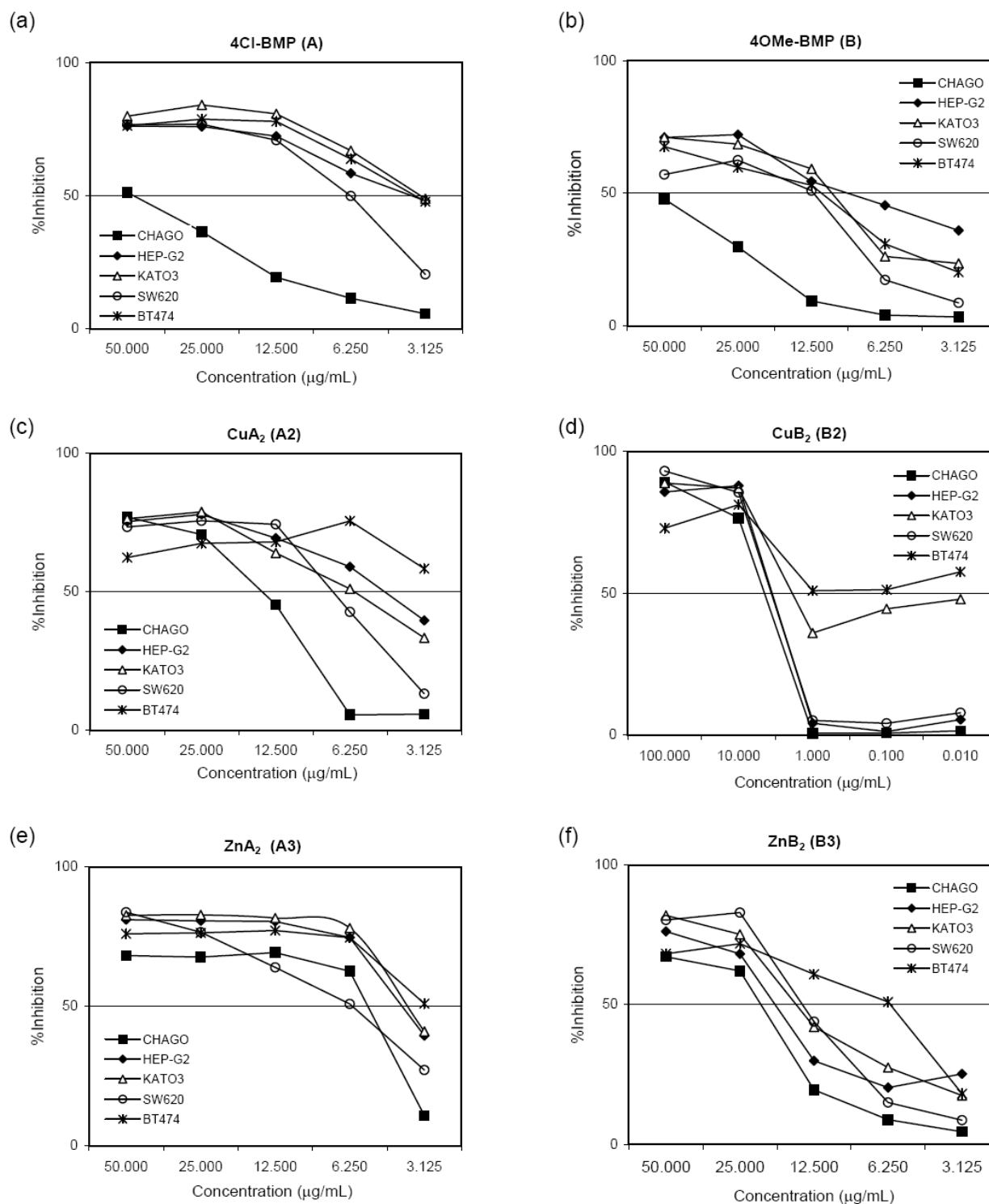


Figure B3 Inhibition of cell growth of different five cancer cell lines test against (a) cisplatin and (b) doxorubicin.

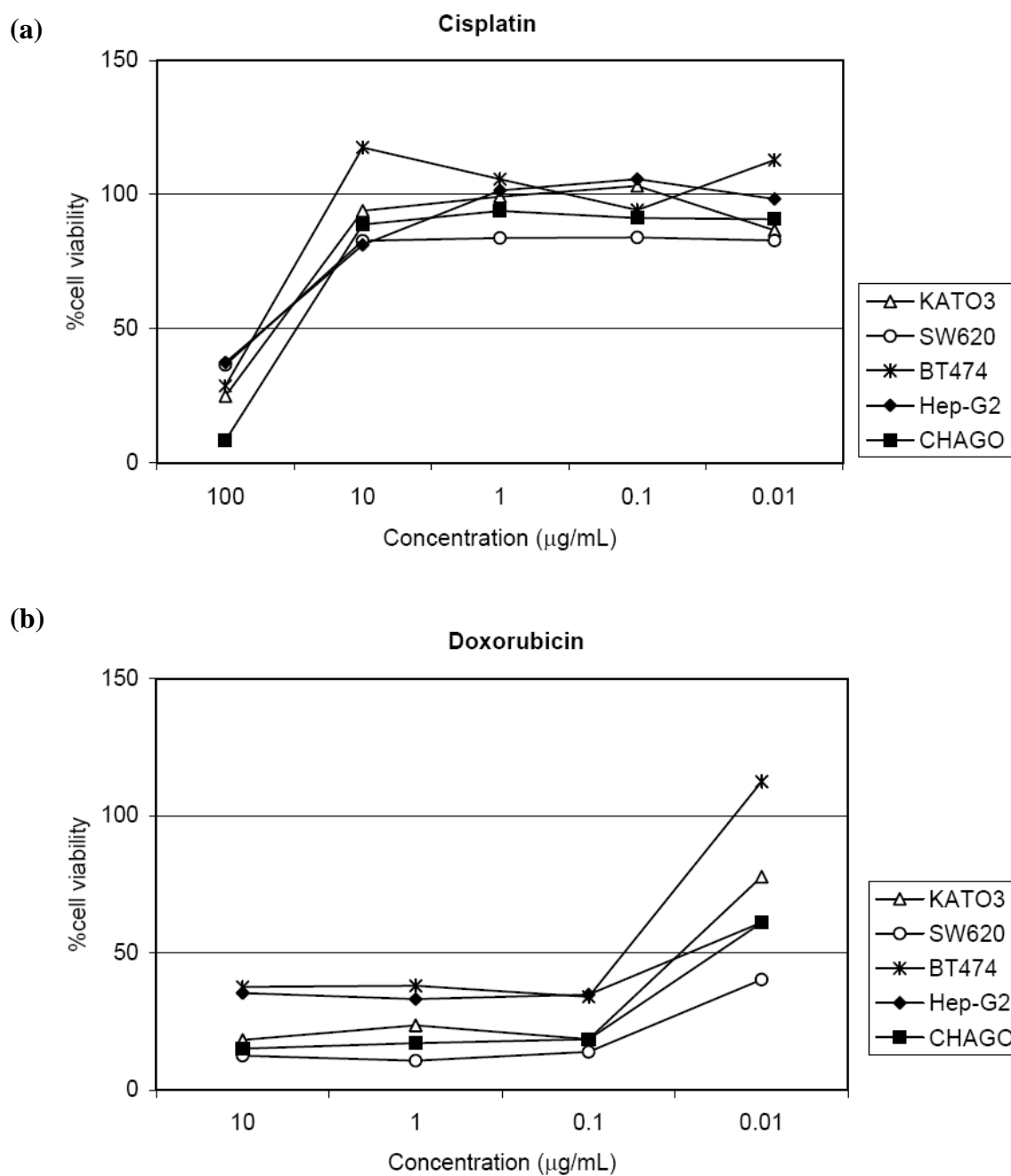
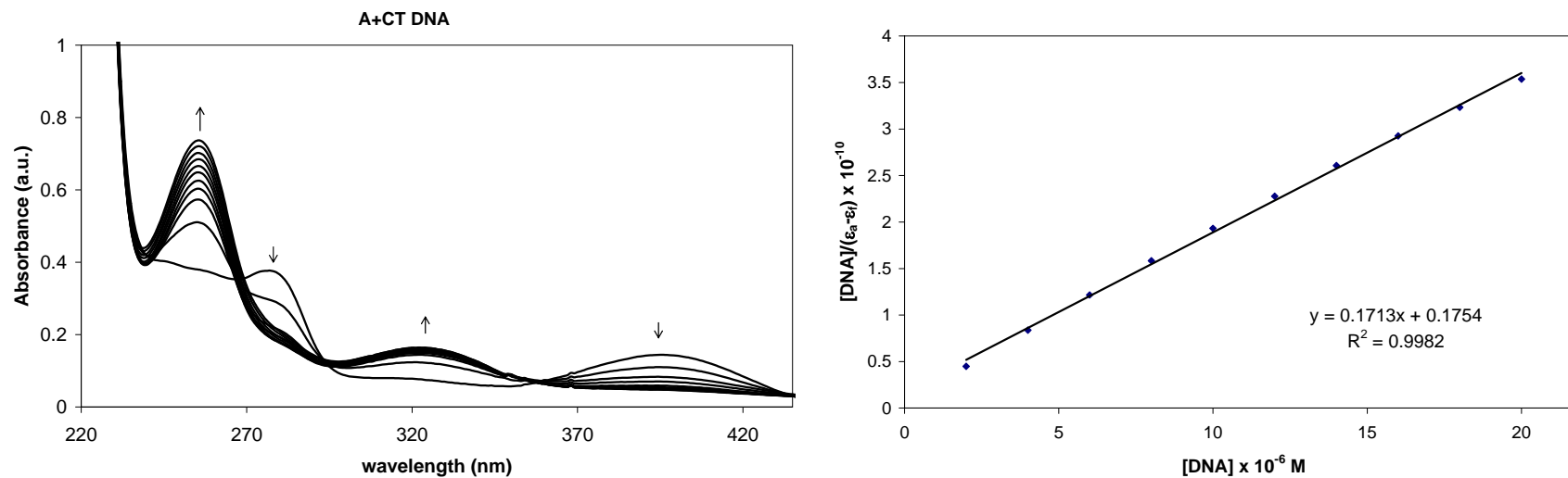


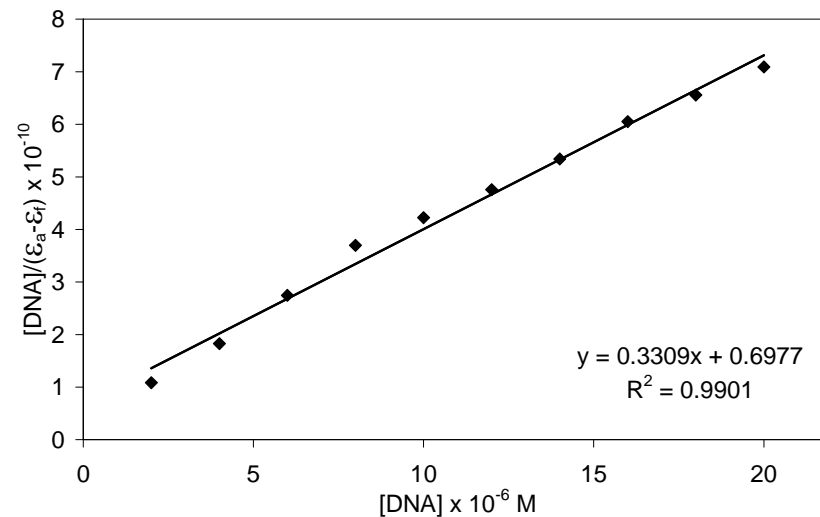
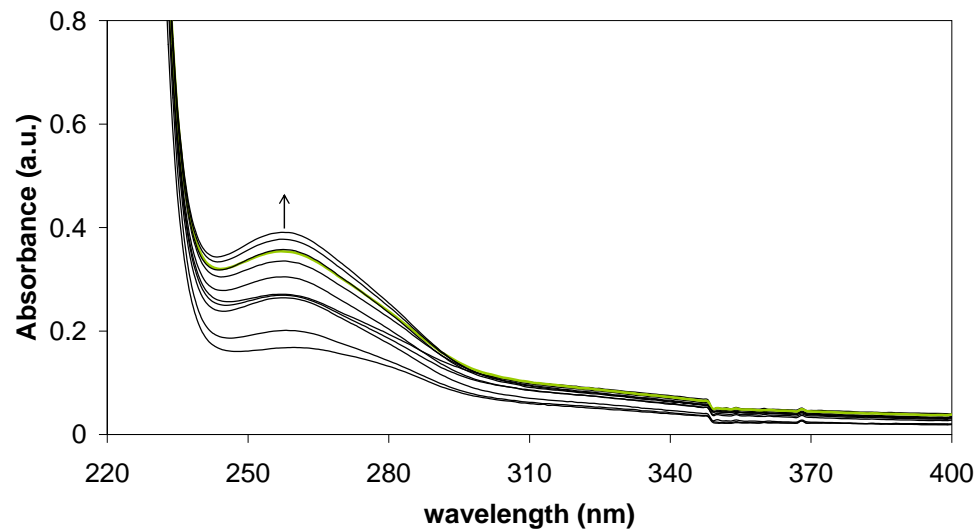
Figure B4 DNA binding experiments

2. Absorption study DNA binding ability

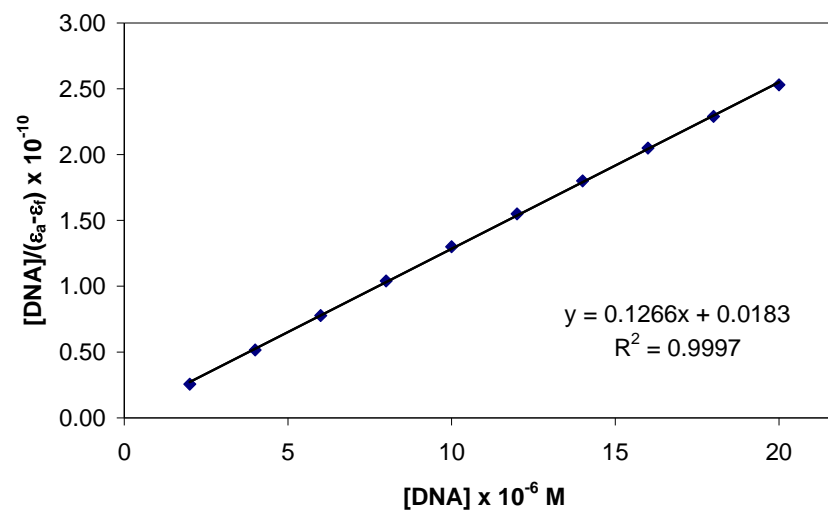
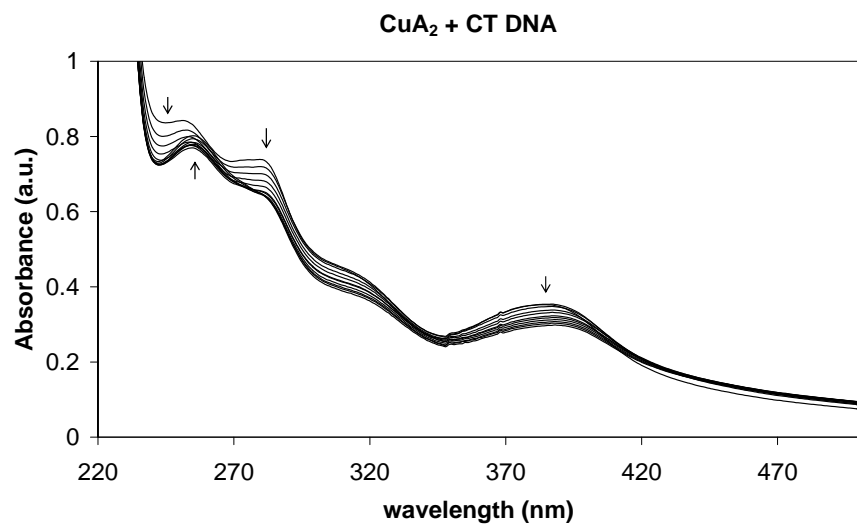


A at 394 nm	0.134	0.100	0.063	0.050	0.039	0.034	0.032	0.031	0.029	0.029	0.028
[DNA] (x 10 ⁻⁶ M)	0.000	2.000	4.000	6.000	8.000	10.000	12.000	14.000	16.000	18.000	20.000
[compound] (x 10 ⁻⁶ M)	20.000	19.960	19.920	19.881	19.841	19.802	19.763	19.724	19.685	19.646	19.608
ϵ_a	6710.120	5021.336	3180.467	2539.759	1967.116	1741.454	1630.695	1555.401	1479.415	1455.394	1424.771
[DNA]/($\epsilon_a - \epsilon_f$)		1.71E-10	4.04E-10	6.48E-10	9.22E-10	1.18E-09	1.44E-09	1.69E-09	1.95E-09	2.20E-09	2.46E-09
K_b (M ⁻¹)	976624										

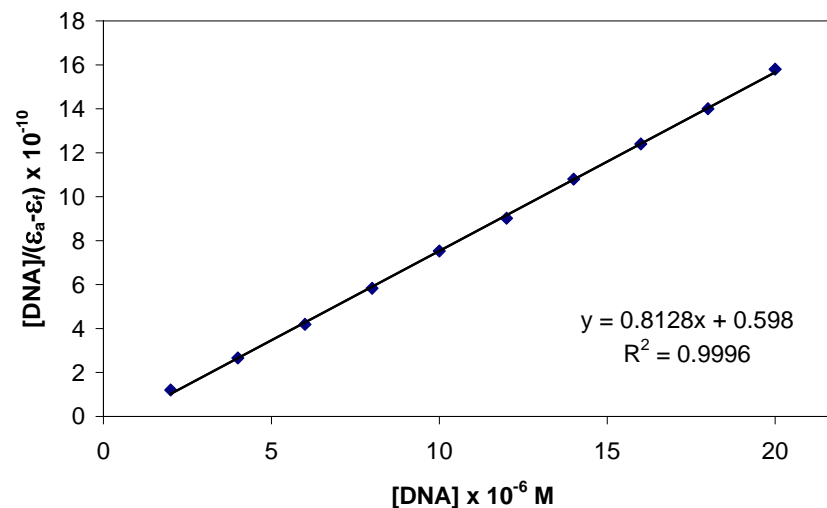
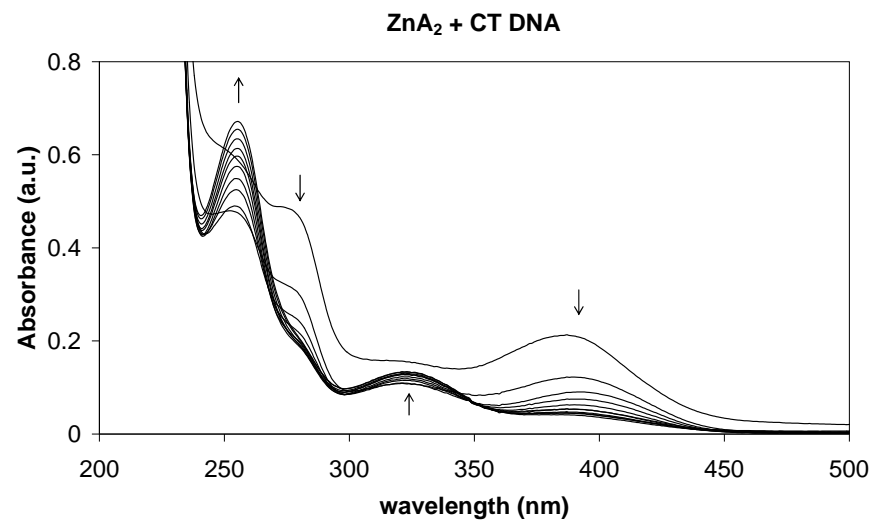
NiA₂ + CT DNA



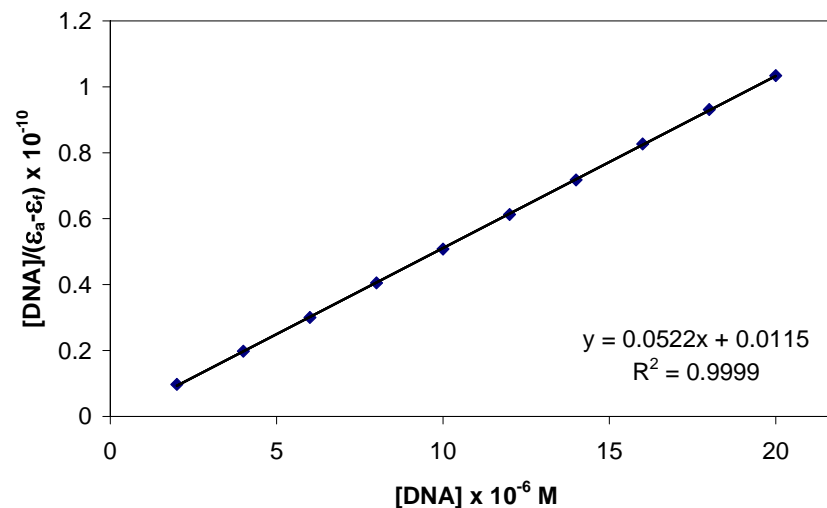
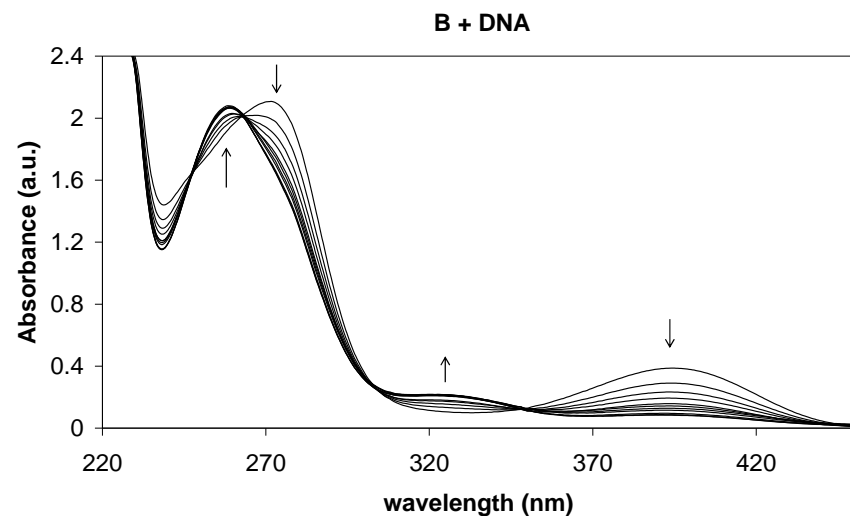
A at 260 nm	0.17	0.20	0.27	0.27	0.28	0.30	0.33	0.35	0.35	0.37	0.39
[DNA] (x 10⁻⁶ M)	0.00	2.00	4.00	6.00	8.00	10.00	12.00	14.00	16.00	18.00	20.00
[compound] (x 10⁻⁶ M)	20.00	19.96	19.92	19.88	19.84	19.80	19.76	19.72	19.69	19.65	19.61
ε_a	8407	10054	13498	13450	14240	15267	16817	17811	18033	19048	19793
[DNA]/(ε_a-ε_f)	0.00	1.08E-10	1.83E-10	2.74E-10	3.53E-10	4.22E-10	4.76E-10	5.34E-10	6.05E-10	6.56E-10	7.09E-10
K_b(M⁻¹)	474272										



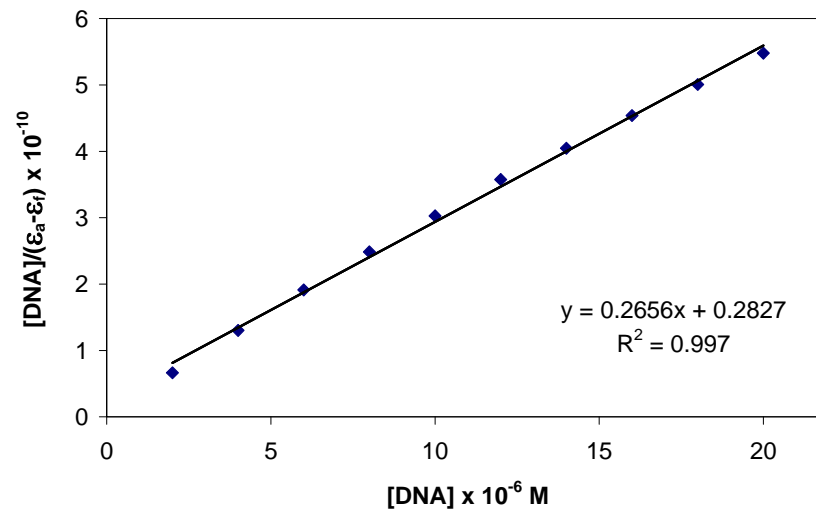
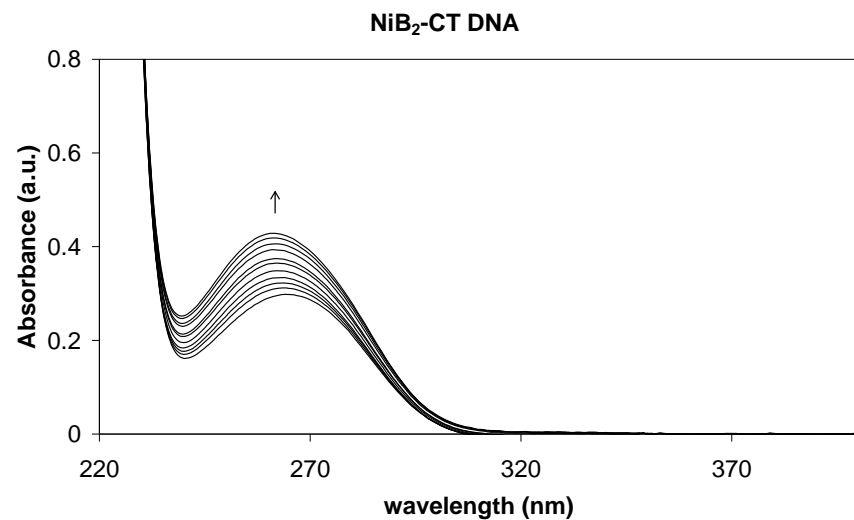
A at 383 nm	0.78	0.77	0.76	0.76	0.75	0.75	0.75	0.76	0.76	0.77	0.78
[DNA] (x 10⁻⁶ M)	0.00	2.00	4.00	6.00	8.00	10.00	12.00	14.00	16.00	18.00	20.00
[compound] (x 10⁻⁶ M)	20.00	19.96	19.92	19.88	19.84	19.80	19.76	19.72	19.69	19.65	19.61
ε_a	39242.40	38795.97	38346.94	37994.57	37755.04	37643.45	38109.29	38349.19	38709.80	39294.99	39786.38
[DNA]/(ε_a-ε_f)		2.56E-11	5.16E-11	7.77E-11	1.04E-10	1.30E-10	1.55E-10	1.80E-10	2.05E-10	2.29E-10	2.53E-10
K_b(M⁻¹)	6918033										



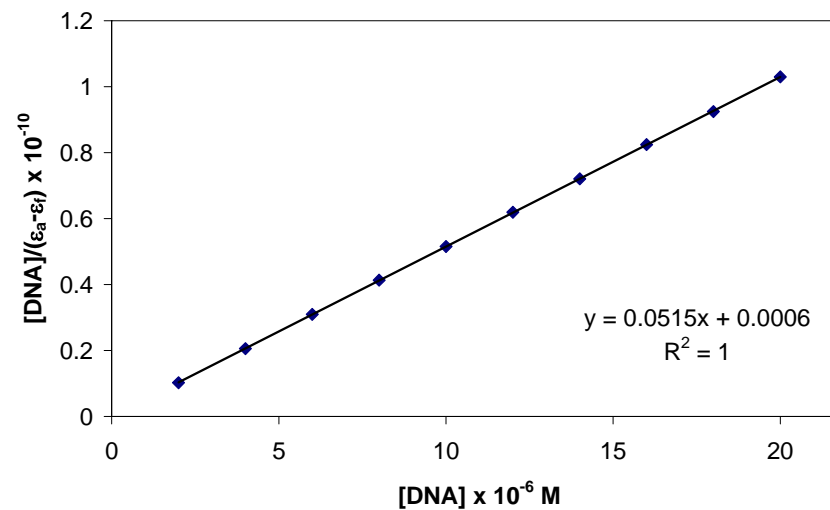
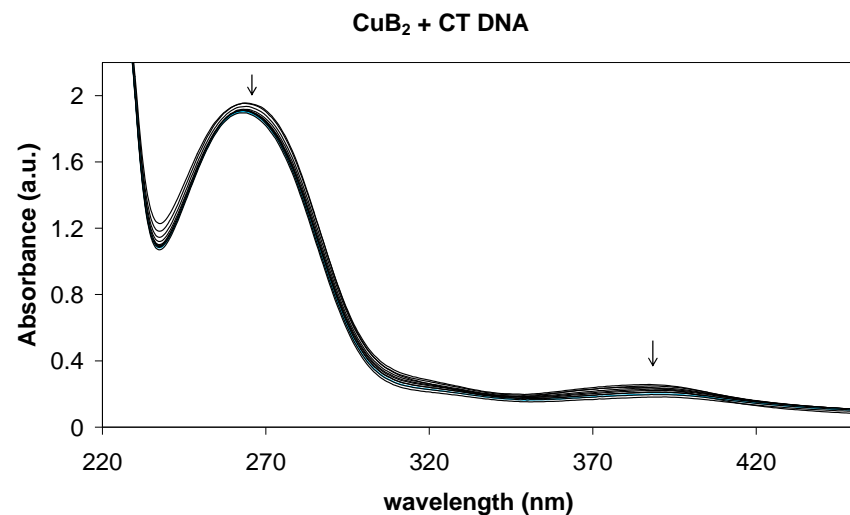
A at 386 nm	0.212	0.121	0.088	0.074	0.062	0.053	0.053	0.047	0.045	0.045	0.041
[DNA] (x 10⁻⁶ M)	0.00	2.00	4.00	6.00	8.00	10.00	12.00	14.00	16.00	18.00	20.00
[compound] (x 10⁻⁶ M)	20.000	19.960	19.920	19.881	19.841	19.802	19.763	19.724	19.685	19.646	19.608
ε_a	10596.77	6064.18	4433.07	3722.25	3135.89	2679.77	2703.09	2397.19	2310.69	2278.11	2100.74
[DNA]/(ε_a-ε_f)		1.20E-10	2.66E-10	4.19E-10	5.83E-10	7.53E-10	9.02E-10	1.08E-09	1.24E-09	1.40E-09	1.58E-09
K_b(M⁻¹)	1359197										



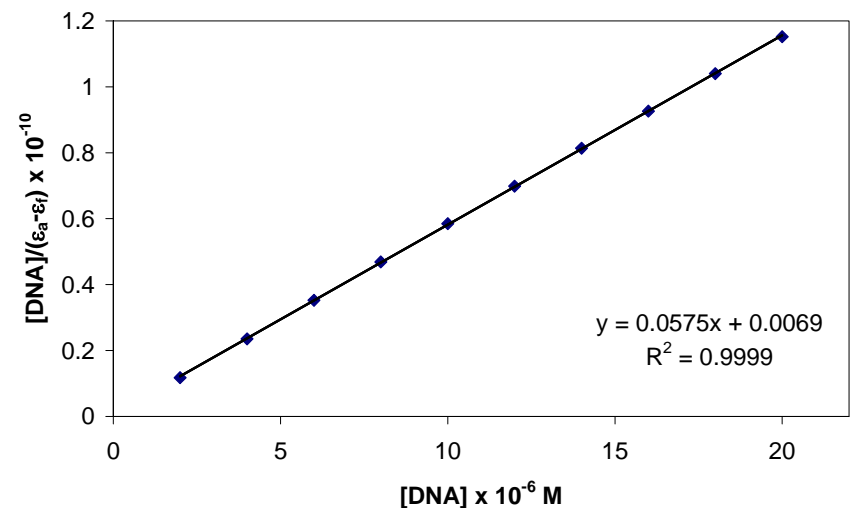
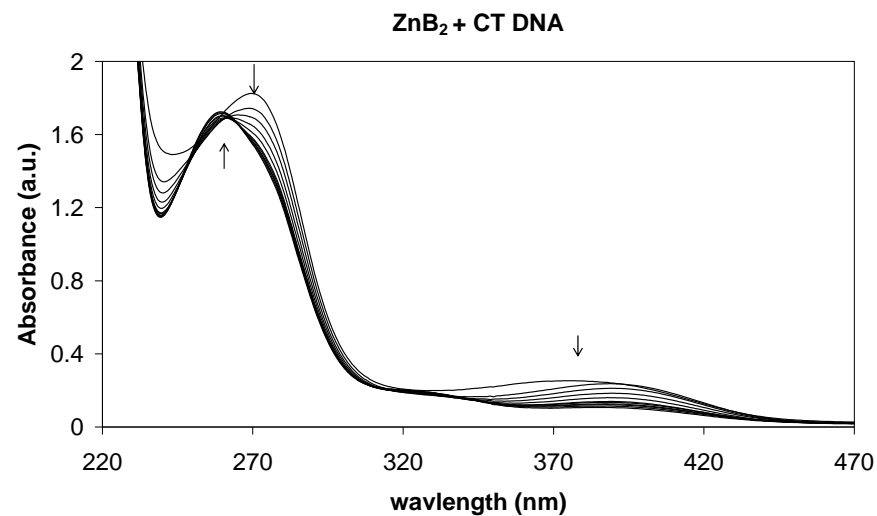
A at 392 nm	2.107	2.002	1.927	1.878	1.827	1.813	1.788	1.770	1.737	1.729	1.726
[DNA] (x 10⁻⁶ M)	0.00	2.00	4.00	6.00	8.00	10.00	12.00	14.00	16.00	18.00	20.00
[compound] (x 10⁻⁶ M)	20.00	19.96	19.92	19.88	19.84	19.80	19.76	19.72	19.69	19.65	19.61
ε_a	105349	100284	96755	94458	92078	91548	90458	89745	88221	88011	88016
[DNA]/(ε_a-ε_f)		9.73E-12	1.98E-11	3.00E-11	4.05E-11	5.08E-11	6.13E-11	7.18E-11	8.27E-11	9.31E-11	1.03E-10
K_b(M⁻¹)	4539130										



A at 261 nm	0.293	0.309	0.320	0.333	0.348	0.364	0.374	0.394	0.406	0.418	0.429
[DNA] (x 10⁻⁶ M)	0.000	2.000	4.000	6.000	8.000	10.000	12.000	14.000	16.000	18.000	20.000
[compound] (x 10⁻⁶ M)	20.00	19.96	19.92	19.88	19.84	19.80	19.76	19.72	19.68	19.64	19.61
ε_a	14648.01	15476.56	16082.08	16735.33	17532.61	18382.46	18921.08	19950.94	20601.75	21299.58	21858.01
[DNA]/(ε_a-ε_f)		6.64E-11	1.30E-10	1.91E-10	2.49E-10	3.03E-10	3.57E-10	4.05E-10	4.54E-10	5.01E-10	5.48E-10
K_b(M⁻¹)	939512										

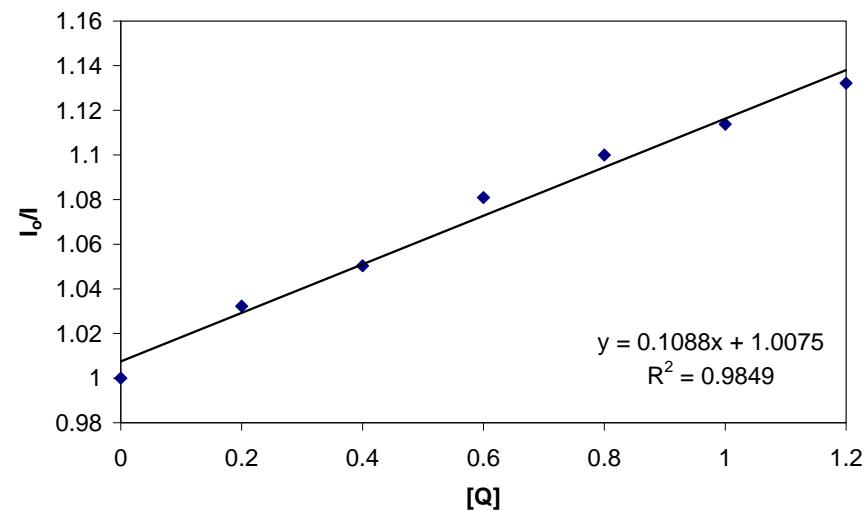
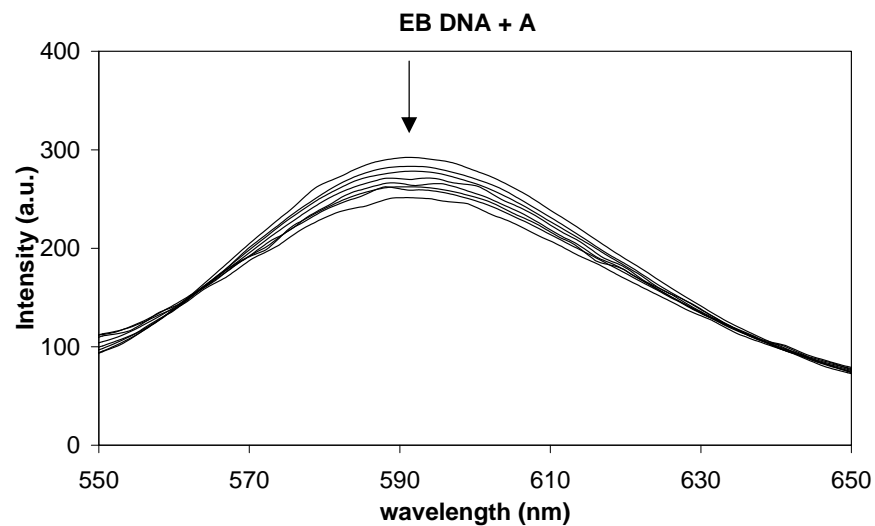


A at 262nm	1.950	1.949	1.931	1.915	1.907	1.910	1.902	1.909	1.900	1.909	1.895
[DNA] (x 10⁻⁶ M)	0.00	2.00	4.00	6.00	8.00	10.00	12.00	14.00	16.00	18.00	20.00
[compound] (x 10⁻⁶ M)	20.00	19.96	19.92	19.88	19.84	19.80	19.76	19.72	19.69	19.65	19.61
ε_a	97487.60	97651.15	96917.20	96326.84	96095.34	96467.89	96252.84	96792.10	96538.11	97149.47	96660.42
[DNA]/(ε_a-ε_f)	0.00	1.02E-11	2.06E-11	3.10E-11	4.13E-11	5.16E-11	6.19E-11	7.21E-11	8.25E-11	9.25E-11	1.03E-10
K_b(M⁻¹)	85833333										

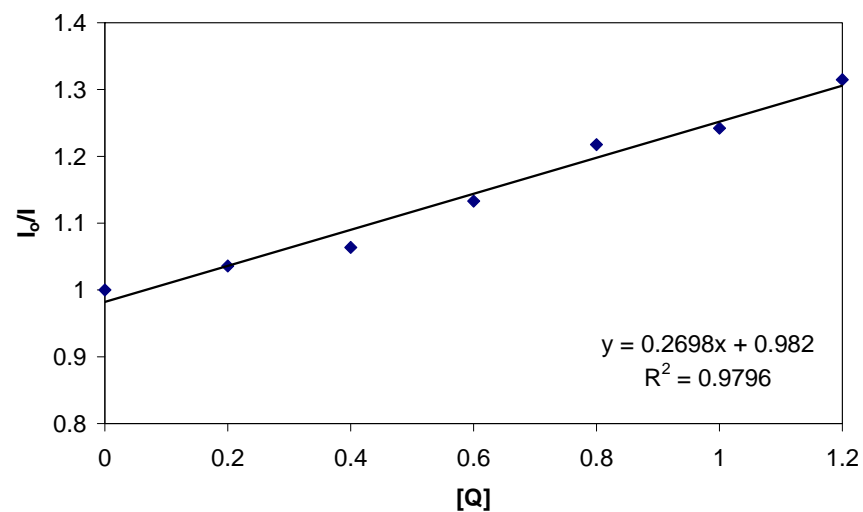
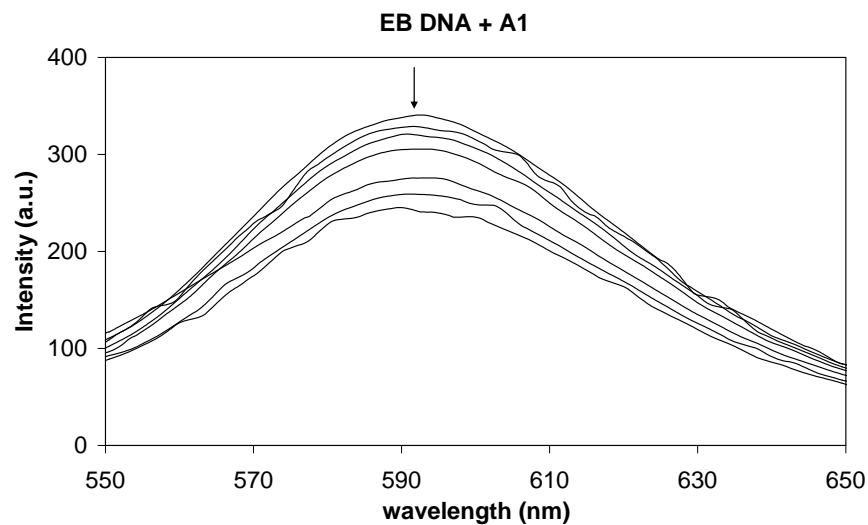


A at 260nm	1.714	1.681	1.681	1.681	1.686	1.690	1.700	1.703	1.714	1.718	1.723
[DNA] (x 10⁻⁶ M)	0.00	2.00	4.00	6.00	8.00	10.00	12.00	14.00	16.00	18.00	20.00
[compound] (x 10⁻⁶ M)	20.00	19.96	19.92	19.88	19.84	19.80	19.76	19.72	19.69	19.65	19.61
ε_a	85688.67	84227.85	84367.30	84559.31	84966.49	85347.59	86030.43	86356.14	87063.52	87449.96	87895.06
[DNA]/(ε_a-ε_f)		1.18E-11	2.35E-11	3.52E-11	4.69E-11	5.85E-11	6.99E-11	8.14E-11	9.26E-11	1.04E-10	1.15E-10
K_b(M⁻¹)	8333333										

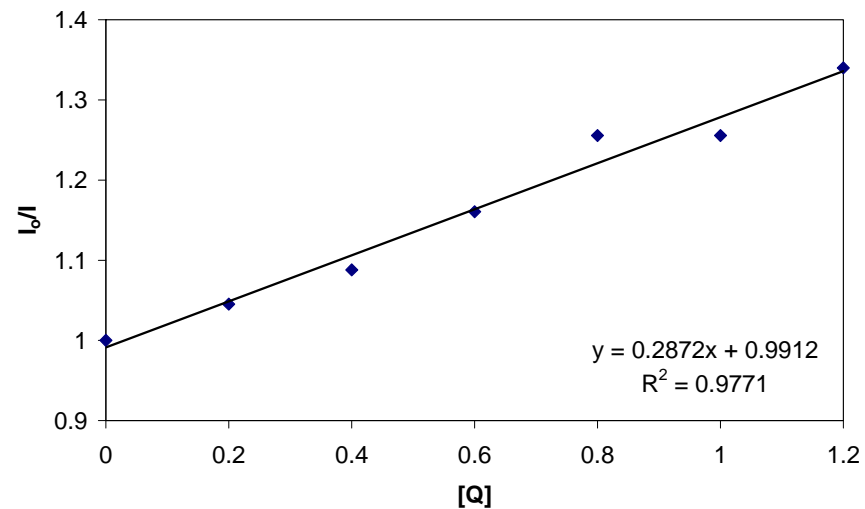
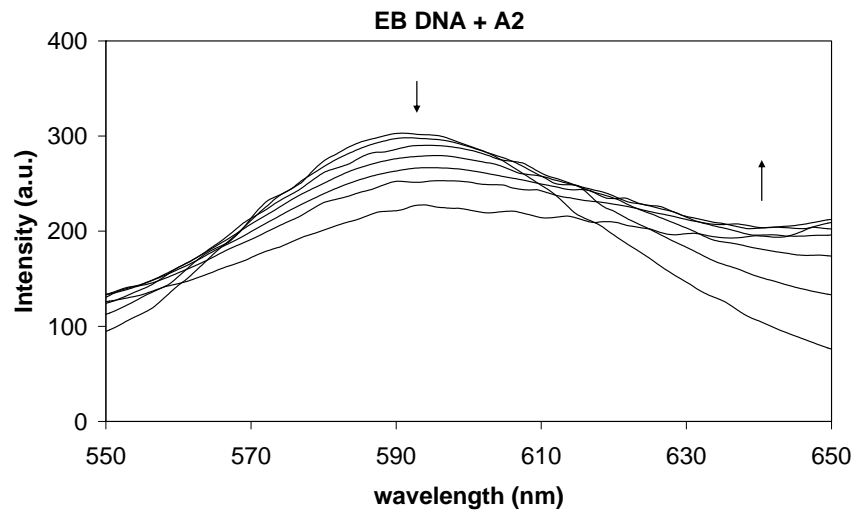
3. EB displacement study by fluorescence spectroscopy



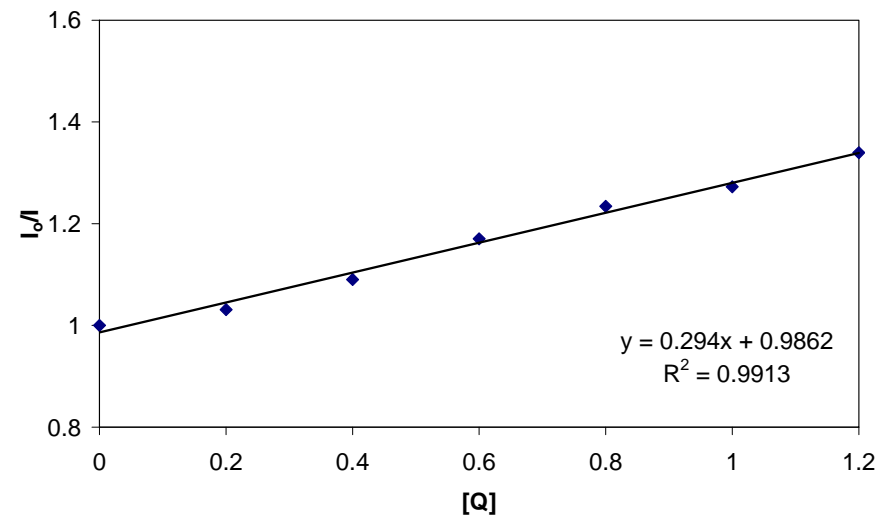
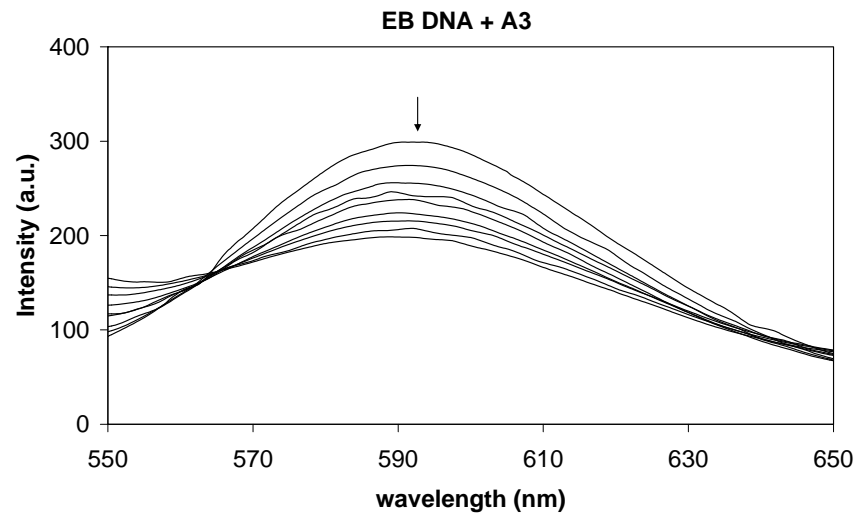
	EB DNA	EB DNA + A 10 μ M	EB DNA + A 20 μ M	EB DNA + A 30 μ M	EB DNA + A 40 μ M	EB DNA + A 50 μ M	EB DNA + A 60 μ M
[Q]x10⁻⁶M	0.000	10.000	20.000	30.000	40.000	50.000	60.000
[Q]/[DNA]	0.000	0.200	0.400	0.600	0.800	1.000	1.200
I at 592 nm	292.192	283.063	278.185	270.317	265.634	262.339	258.094
I_o	292.192						
I_o/I	1.000	1.032	1.050	1.081	1.100	1.114	1.132
K_{sq} x 10⁵ M⁻¹	1.090						



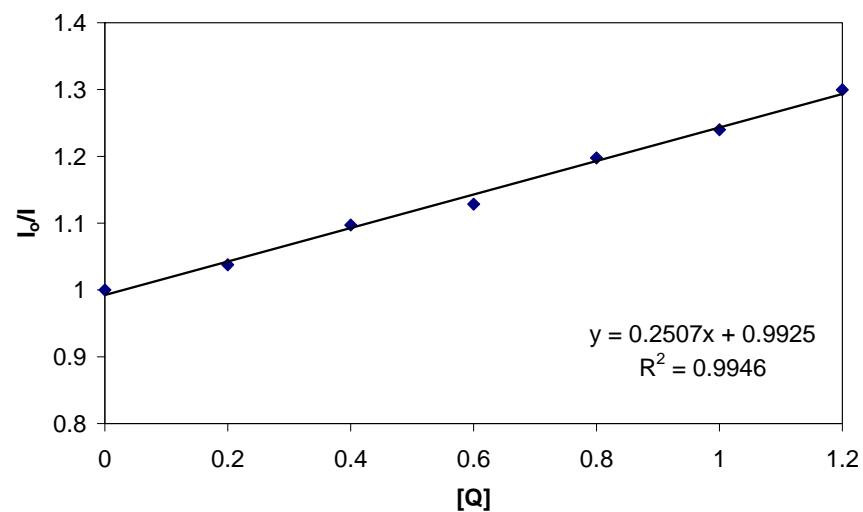
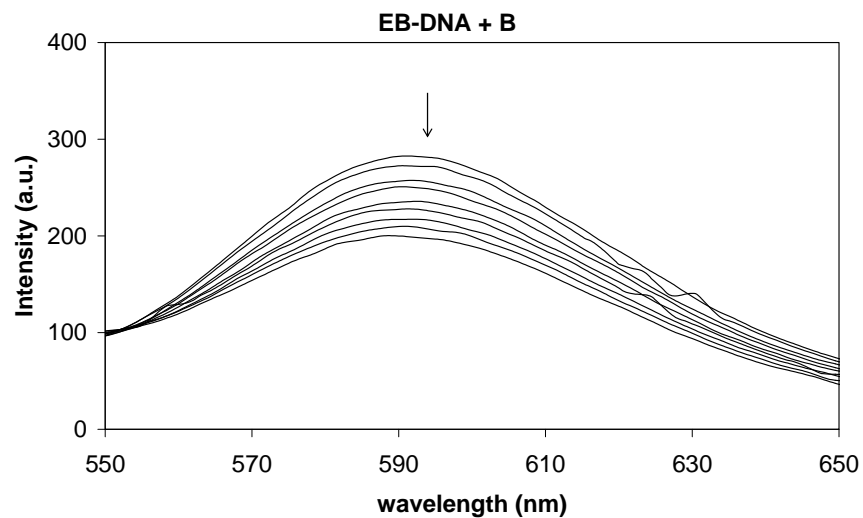
	EB DNA	EB DNA + A1 10 μ M	EB DNA + A1 20 μ M	EB DNA + A1 30 μ M	EB DNA + A1 40 μ M	EB DNA + A1 50 μ M	EB DNA + A1 60 μ M
[Q]$\times 10^{-6}$M	0.000	10.000	20.000	30.000	40.000	50.000	60.000
[Q]/[DNA]	0.000	0.200	0.400	0.600	0.800	1.000	1.200
I at 592 nm	340.438	328.656	320.091	300.462	279.597	274.081	258.930
I_o	340.439						
I_o/I	1.000	1.036	1.064	1.133	1.218	1.242109546	1.315
K_{sq} $\times 10^5$ M⁻¹	2.747						



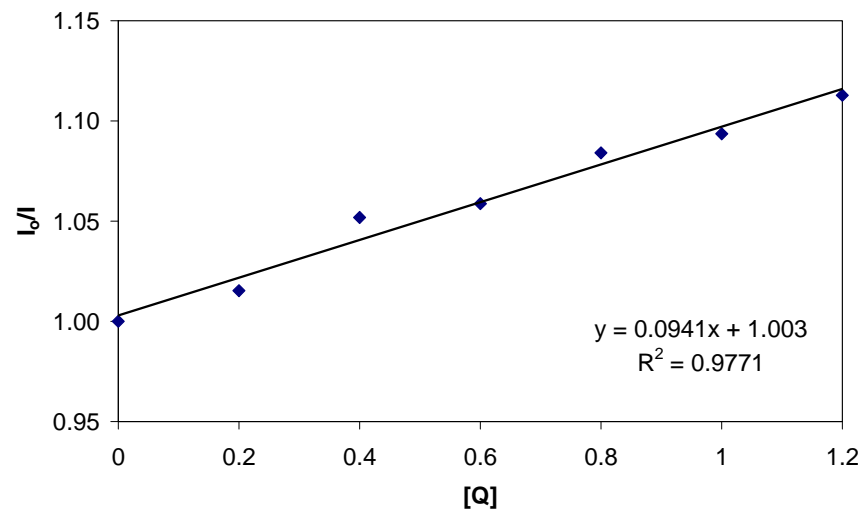
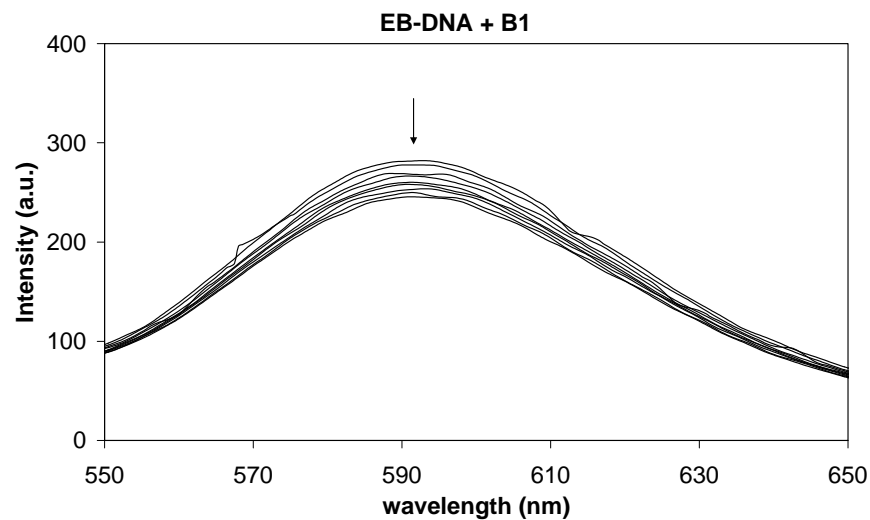
	EB DNA	EB DNA + B3 10 μM	EB DNA + B3 20 μM	EB DNA + B3 30 μM	EB DNA + B3 40 μM	EB DNA + B3 50 μM	EB DNA + B3 60 μM
[Q]x10⁻⁶M	0.000	10.000	20.000	30.000	40.000	50.000	60.000
[Q]/[DNA]	0.000	0.200	0.400	0.600	0.800	1.000	1.200
I at 592 nm	302.524	298.131	289.447	278.071	260.679	240.934	225.771
I_o	302.5244						
I_o/I	1.000	1.045	1.088	1.161	1.256	1.256	1.340
K_{sq} x 10⁵ M⁻¹	2.848						



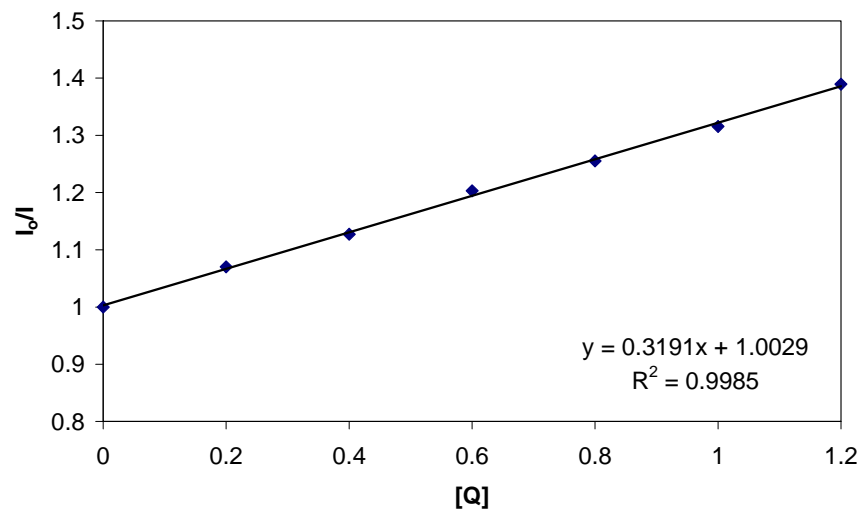
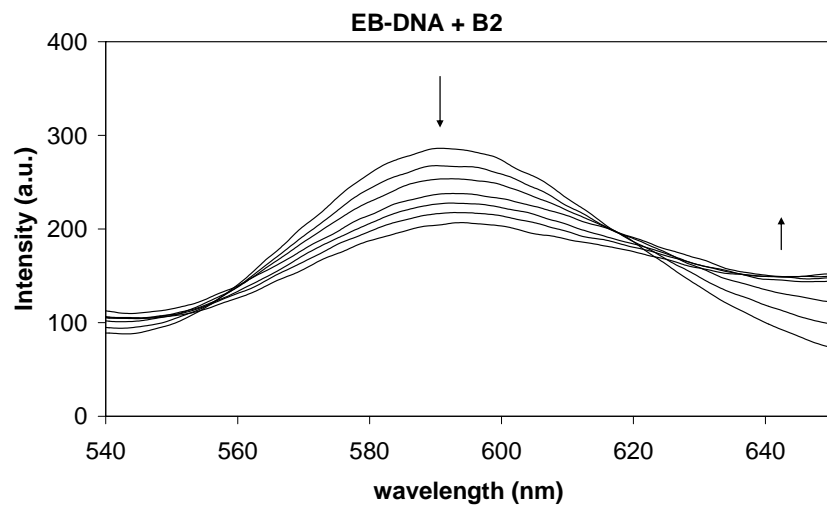
	EB DNA	EB DNA + A3 10 μ M	EB DNA + A3 20 μ M	EB DNA + A3 30 μ M	EB DNA + A3 40 μ M	EB DNA + A3 50 μ M	EB DNA + A3 60 μ M
[Q]x10⁻⁶M	0.000	10.000	20.000	30.000	40.000	50.000	60.000
[Q]/[DNA]	0.000	0.200	0.400	0.600	0.800	1.000	1.200
I at 592 nm	299.034	290.028	274.281	255.501	242.293	234.970	223.209
I₀	299.034						
I₀/I	1.000	1.031	1.090	1.170	1.234	1.273	1.340
K_{sv} x 10⁵ M⁻¹	2.981						



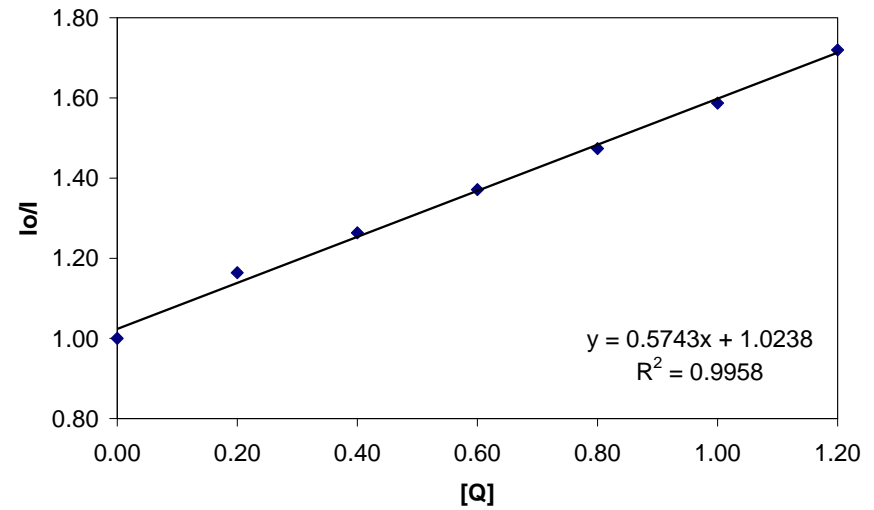
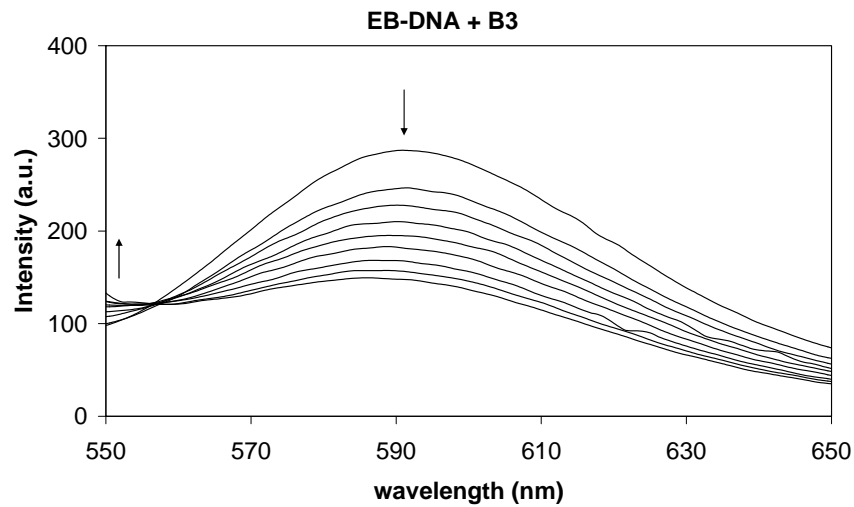
	EB DNA	EB DNA + B 10 μM	EB DNA + B 20 μM	EB DNA + B 30 μM	EB DNA + B 40 μM	EB DNA + B 50 μM	EB DNA + B 60 μM
I at 592 nm	282.374	272.113	257.356	250.230	235.759	227.742	217.265
[Q]$\times 10^{-6}\text{M}$	0.000	10.000	20.000	30.000	40.000	50.000	60.000
[Q]/[DNA]	0.000	0.200	0.400	0.600	0.800	1.000	1.200
I_o	282.374						
I_o/I	1.000	1.038	1.097	1.128	1.198	1.240	1.300
K_{sq} $\times 10^5 \text{M}^{-1}$	2.510						



	EB DNA	EB DNA + B1 10 μM	EB DNA + B1 20 μM	EB DNA + B1 30 μM	EB DNA + B1 40 μM	EB DNA + B1 50 μM	EB DNA + B1 60 μM
I at 592 nm	281.935	277.683	268.043	266.292	260.068	257.805	253.360
[Q] $\times 10^{-6}\text{M}$	0.000	10.000	20.000	30.000	40.000	50.000	60.000
[Q]/[DNA]	0.000	0.200	0.400	0.600	0.800	1.000	1.200
I_0	281.935						
I_0/I	1.000	1.015	1.052	1.059	1.084	1.094	1.113
$K_{sq} \times 10^4 \text{ M}^{-1}$	9.410						



	EB DNA	EB DNA + B2 10 μ M	EB DNA + B2 20 μ M	EB DNA + B2 30 μ M	EB DNA + B2 40 μ M	EB DNA + B2 50 μ M	EB DNA + B2 60 μ M
I at 592 nm	285.822	267.074	253.597	237.577	227.705	217.260	205.725
[Q] $\times 10^{-6}$ M	0.000	10.000	20.000	30.000	40.000	50.000	60.000
[Q]/[DNA]	0.000	0.200	0.400	0.600	0.800	1.000	1.200
I_0	285.822						
I_0/I	1.000	1.070	1.127	1.203	1.255	1.316	1.389
$K_{sq} \times 10^5 \text{ M}^{-1}$	3.191						



	EB DNA	EB DNA + B3 10 μM	EB DNA + B3 20 μM	EB DNA + B3 30 μM	EB DNA + B3 40 μM	EB DNA + B3 50 μM	EB DNA + B3 60 μM
I at 592 nm	286.728	246.356	226.974	209.115	194.572	180.651	166.728
[Q] $\times 10^{-6}\text{M}$	0.000	10.000	20.000	30.000	40.000	50.000	60.000
[Q]/[DNA]	0.000	0.200	0.400	0.600	0.800	1.000	1.200
I_0	286.728						
I_0/I	1.000	1.164	1.263	1.371	1.474	1.587	1.720
$K_{sq} \times 10^5 \text{M}^{-1}$	5.609						

Table B1 Emission intensity for calculate K_{app}

[Q]/[DNA]	I_o/I							
	A	A1	A2	A3	B	B1	B2	B3
0	1.000	1.000	1.000	1.000	1.000	1.000	1.000	1.000
0.2	1.032	1.036	1.045	1.031	1.038	1.015	1.070	1.164
0.4	1.050	1.064	1.088	1.090	1.097	1.052	1.127	1.263
0.6	1.081	1.133	1.161	1.170	1.128	1.059	1.203	1.371
0.8	1.100	1.218		1.234	1.198	1.084	1.255	1.474
1	1.114	1.242	1.256	1.273	1.240	1.094	1.316	1.587
1.2	1.132	1.315	1.340	1.340	1.300	1.113	1.389	1.720
[Q] at 50% I_o	4.56E-04	1.89E-04	1.77E-04	1.72E-04	2.01E-04	5.30E-04	1.56E-04	8.50E-05
Kapp	2.19E+05	5.30E+05	5.64E+05	5.80E+05	4.98E+05	1.89E+05	6.40E+05	1.18E+06
Ksq	1.09E+05	2.70E+05	2.85E+05	2.94E+05	2.51E+05	9.40E+04	3.19E+05	5.74E+05

VITA

Chuttree Phurat was born on June 21, 1982 in Lampang, Thailand. She received Bachelor Degree of Science in Chemistry from Chulalongkorn University in 2003 and graduated with the Master Degree of Science in 2006. Since 2006 she has become a student in Doctor of Philosophy of Chulalongkorn University studying in Program of Chemistry, Faculty of Science, Chulalongkorn University.